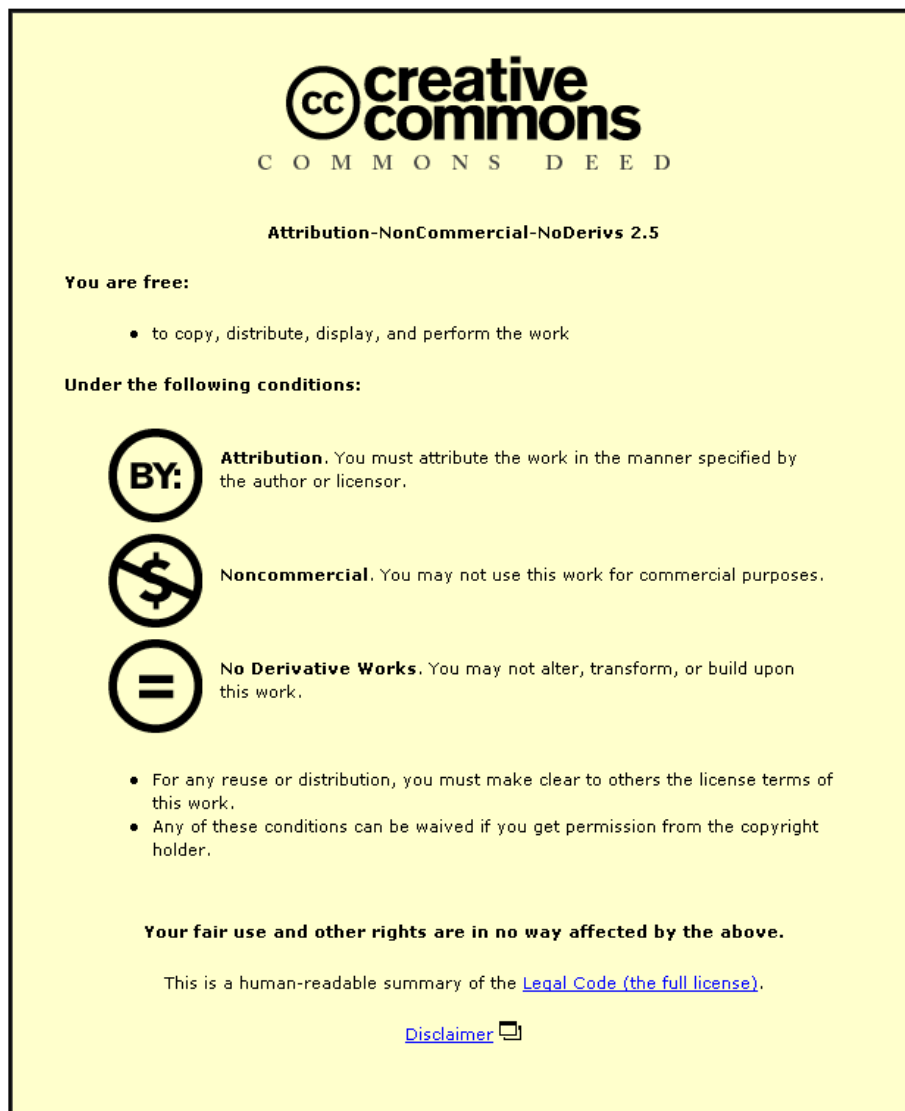


This item was submitted to Loughborough University as a PhD thesis by the author and is made available in the Institutional Repository (<https://dspace.lboro.ac.uk/>) under the following Creative Commons Licence conditions.



For the full text of this licence, please go to:
<http://creativecommons.org/licenses/by-nc-nd/2.5/>



University Library

Author/Filing Title .. REED, JAMES

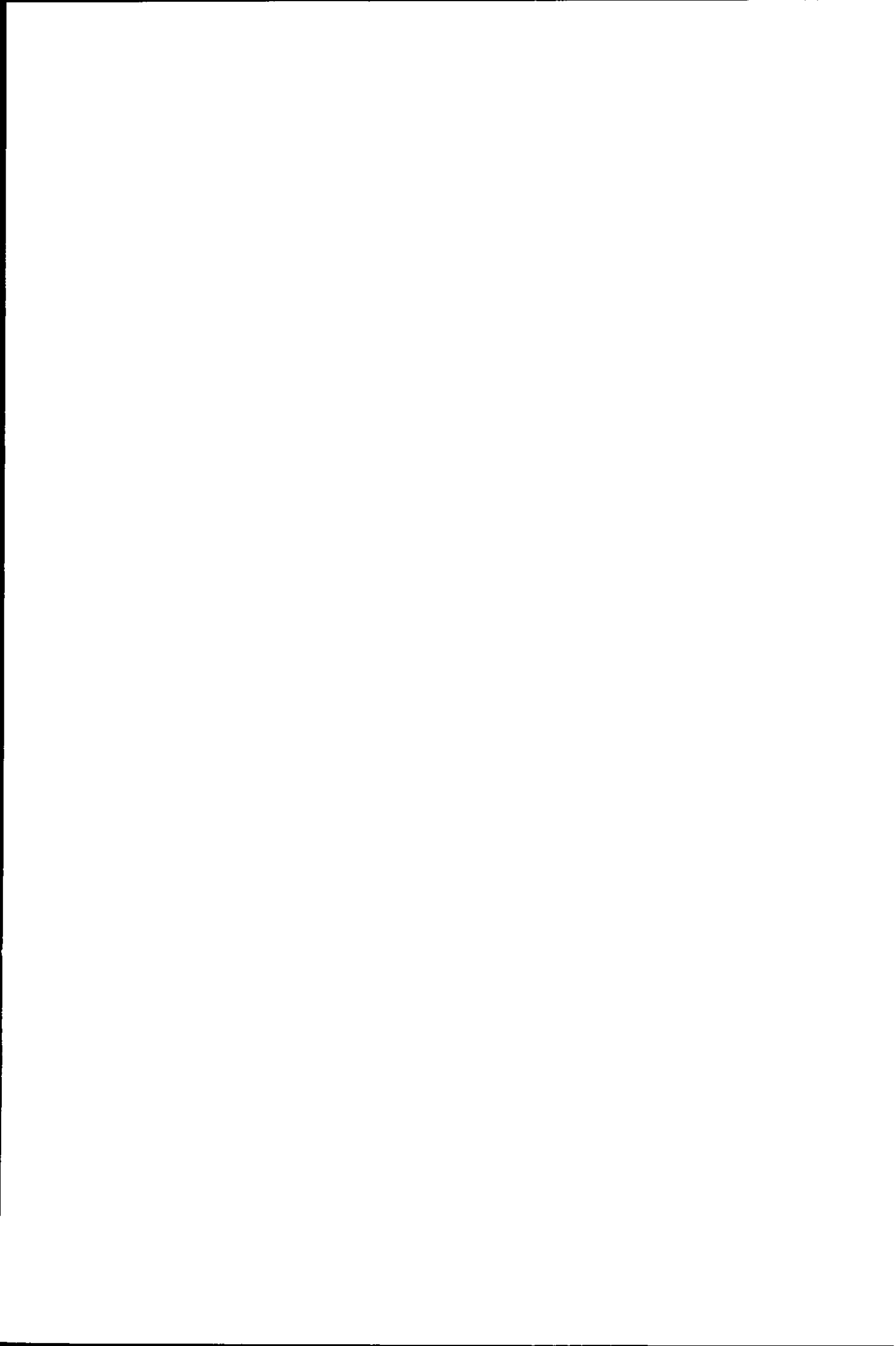
.....
Class Mark .. T

Please note that fines are charged on ALL
overdue items.

FOR REFERENCE ONLY

0403115914





**A Microchannel Sulphur Tolerant
Steam Reformer with Integral Multi-
Zone Catalytic Combustor**

**By
James Reed MEng.**

A Doctoral Thesis
Submitted in partial fulfilment of the requirements
for the award of
Doctor of Philosophy of Loughborough University
10 Nov. 2004

 Loughborough University Pilkington Library
Date <i>SEPTEMBER '05</i>
Class <i>T</i>
Acc No. <i>0403115914</i>

To Mum and Dad

Acknowledgements

I would like to thank the following organisations and people who made this work possible. Loughborough University, Intelligent Energy Ltd., Catal Ltd. Chart Marston Ltd. In particular the following people for their help and support. Chris Dudfield, Paul Adcock, Rui Chen, Alf Mosely, Anne Matthews, Pete Hood, Phil, Mebs Virgi, Root Woods, Jeremy Matcham, and Phil Mitchell. Jude, Marv, and Hux for giving me plenty of opportunities to skive off and indulge my rock star fantasies. Jen and Gid, Dave, Stu, Sim and Caz, Nick, Beccy, Steve, Brum, Dex, Pig, Atkin, Dave N., and those citric aware people for all those other excuses to skive off, partys, festivals, travel, and the pub And lastly my parents for offerng support and a place to go and relax when I needed it.

Contents

FIGURES	X
TABLES	XIII
NOMENCLATURE	XIV
ABSTRACT	XVI
1 INTRODUCTION	1
1 1 THE CASE FOR HYDROGEN	1
1 2 FUEL SOURCE	4
1 2 1 <i>Water</i>	5
1 2 2 <i>Hydrocarbons</i>	5
1 2 3 <i>Biomass</i>	6
1 3 WHAT IS A FUEL CELL?	6
1 4 FUEL CELL APPLICATIONS	11
1 4 1 <i>Stationary Power</i>	11
1 4 1 1 Combined Heat and Power	11
1 4 1 2 Distributed Generation	12
1 4 2 <i>Portable Power</i>	13
1 4 2 1 Man Portable Power	13
1 4 2 2 Transportation	13
1 4 3 <i>Summary</i>	15
1 5 FUEL SUPPLY FOR THE SPFC	16
1 5 1 <i>Pure Hydrogen Storage or Supply</i>	17
1 5 1 1 Pressurised Storage	18
1 5 1 2 Liquid Storage	18
1 5 1 3 Metal Hydride	18
1 5 1 4 Carbon Nanofibres	19
1 5 2 <i>Fuel Processing</i>	19
1 5 3 <i>Fuel Cell Operating Requirements</i>	20
1 5 4 <i>Steam Reforming</i>	22
1 5 5 <i>Partial Oxidation Reforming</i>	24
1 5 6 <i>Autothermal Reforming</i>	25
1 5 7 <i>Other Reforming Methods</i>	26
1 5 7 1 Plasma Reforming	26
1 5 7 2 Biological Reforming	26
1 5 7 3 Membrane Reactors	26
1 5 7 4 Sponge-Iron Reforming	26
1 5 7 5 Non-Catalytic Steam Reforming	26
1 5 8 <i>Balance Of Plant</i>	26

1 5 8 1	Desulphurisation	26
1 5 8 2	Water Gas Shift	26
1 5 8 3	Carbon Monoxide Clean Up	26
1 6	CONCLUSIONS .. .	26
2	SYSTEM SIMULATION.....	26
2 1	OVERVIEW OF ASPEN PLUS.	26
2 2	LIQUID PETROLEUM GAS AND METHANE REFORMING SIMULATION . .	26
2 2 1	<i>Steam Reforming</i>	26
2 2 1 1	Method	26
2 2 1 2	Results	26
2 2 2	<i>Autothermal Reforming</i>	26
2 2 2 1	Method	26
2 2 2 2	Results	26
2 2 3	<i>Conclusions</i>	26
2 3	DETERMINING THE REACTANT FEED REQUIREMENTS	26
2 3 1	<i>Method</i>	26
2 3 2	<i>Results</i>	26
2 3 3	<i>Conclusion</i>	26
2 4	A FUEL CELL SYSTEM SIMULATION	26
2 4 1	<i>Excel Model Description</i>	26
2 4 1 1	Data and Constants	26
2 4 1 2	User Settings	26
2 4 1 3	Reformer Model Description	26
2 4 1 4	Combustor Model Description	26
2 4 1 5	Power Balance	26
2 5	RESULTS	26
3	REACTOR DESIGN AND NOVEL TECHNOLOGY	26
3 1	REACTOR DESIGN	26
3 1 1	<i>Packed Bed Reactors</i>	26
3 1 2	<i>Ceramic Monolith Reactors</i>	26
3 1 3	<i>Microchannel Heat Exchangers</i>	26
3 2	MANUFACTURING METHODS	26
3 3	DESCRIPTION OF THE MICROCHANNEL REACTOR.. . . .	26
3 3 1	<i>Plate Details</i>	26
3 3 2	<i>Function Layer Description</i>	26
3 4	ASSEMBLY DESCRIPTION	26
3 5	REFORMER OUTLET MANIFOLD	26
3 5 1	<i>Gasketed/ Welded Join</i>	26
3 6	CATALYST APPLICATION	26
4	DESCRIPTION OF THE TEST ASSEMBLY.....	26

4 1	TEST ASSEMBLY	26
4 1 1	<i>Test Assembly Safety System</i>	26
4 1 2	<i>Laboratory Safety System</i>	26
4 2	MASS FLOW CONTROLLERS	26
4 3	WATER SUPPLY PUMPS	26
4 3 1	<i>Continuous Flow Syringe Pump</i>	26
4 3 2	<i>Diaphragm Pump</i>	26
4 4	HYDROGEN FEED SOLENOIDS	26
4 5	EXHAUST HEAT EXCHANGERS AND RECOVERY SYSTEM..	26
4 6	ELECTRIC PREHEATERS	26
4 6 1	<i>Combustor Air Preheat</i>	26
4 6 2	<i>Liquid Petroleum Gas and Water Preheat</i>	26
4 7	CONTROL UNITS	26
4 7 1	<i>Hydrogen Fuel Injection Control Unit</i>	26
4 7 2	<i>Air and Hydrogen Control Unit</i>	26
4 7 3	<i>Heater Control Units</i>	26
4 8	GAS SUPPLY NETWORK	26
4 9	ANALYSIS EQUIPMENT	26
4 9 1	<i>Gas Chromatography</i>	26
4 9 1 1	<i>Calibration</i>	26
4 9 2	<i>Online Analysis</i>	26
4 9 3	<i>Pressure Tappings</i>	26
4 9 4	<i>Thermocouples</i>	26
4 10	REFORMER START UP PROCEDURE	26
4 11	REFORMER SHUT DOWN PROCEDURE	26
5	DESIGN AND DEVELOPMENT OF THE CONTROL AND DATA ACQUISITION SOFTWARE.....	26
5 1	SOFTWARE OVERVIEW	26
5 1 1	<i>LabVIEW</i>	26
5 1 2	<i>Delphi</i>	26
5 2	CONTROL SOFTWARE OVERVIEW	26
5 2 1	<i>Controller Design Basics</i>	26
5 2 2	<i>Data Acquisition and Logging</i>	26
5 2 3	<i>Control Strategy – Basic Principle</i>	26
5 2 4	<i>Control Strategy – Details of Operation</i>	26
5 2 5	<i>Development of the Control Strategy</i>	26
5 3	DESCRIPTION OF THE GRAPHICAL USER INTERFACE.	26
5 4	CONTROL SOFTWARE DEVELOPMENT	26
5 4 1	<i>Initial Software Development</i>	26
5 4 2	<i>Calibration of the Hydrogen Solenoid Injectors</i>	26

5 4 3	<i>Solenoid Valve Operating Characteristics</i>	26
5 4 4	<i>Controller Development</i>	26
5 4 5	<i>Look-up Table Generation</i>	26
5 4 6	<i>Development of the Look-up Table</i>	26
5 4 7	<i>Initial Controller Testing</i>	26
5 4 8	<i>Simplification of the Controller</i>	26
5 4 9	<i>Final Controller Development</i>	26
5 5	SYRINGE PUMP SOFTWARE	26
6	MULTI-ZONE COMBUSTOR EVALUATION	26
6 1	INITIAL OPERATION	26
6 1 1	<i>Determination of the Pressure Drop</i>	26
6 2	INITIAL LIGHTING OFF EXPERIMENTS	26
6 2 1	<i>Tests Without Coolant and the Addition of Insulation</i>	26
6 2 2	<i>Operational Failure of the Hydrogen Solenoids</i>	26
6 2 3	<i>Start Up Times of the Microchannel Reactor</i>	26
6 2 4	<i>Internal Reactor Temperature Distribution</i>	26
6 2 5	<i>Effect of Preheating the Air on the Temperature Distribution</i>	26
6 2 6	<i>Effect of Coolant on the Temperature Distribution</i>	26
6 2 7	<i>Effect of Combustor Air Direction on the Temperature Distribution</i>	26
6 2 8	<i>Lighting Off the Combustor Using Methane</i>	26
6 3	INDIVIDUAL COMBUSTION ZONE TESTS.	26
6 4	CLOSED LOOP CONTROL OF THE COMBUSTOR	26
6 5	HEAT TRANSFER PERFORMANCE	26
6 6	CONCLUSION	26
7	SIMULATION OF THE REACTOR	26
7 1	AIMS	26
7.2	SOFTWARE	26
7 3	ASSUMPTIONS...	26
7 4	BRIEF DESCRIPTION OF THE MODEL	26
7 5	SINGLE MODULE DESCRIPTION	26
7 5 1	<i>The BrnExComp Subsystem</i>	26
7 5 2	<i>The H₂Oxidation Subsystem</i>	26
7 5 3	<i>The RfmProdsHeat Subsystem</i>	26
7 5 3 1	<i>The Water Heat Subsystem</i>	26
7 5 3 2	<i>The LPG Heat Subsystem</i>	26
7 5 3 3	<i>The Heat Subsystem</i>	26
7 5 4	<i>The Energy/Burner Reformer Subsystem</i>	26
7 5 5	<i>The Radiative Losses Subsystem</i>	26
7 5 6	<i>The Brn Temp Subsystem</i>	26

7 5 7	<i>Module Subsystem Integration</i>	26
7 5 7 1	Internal Heat Transfer	26
7 5 8	<i>Inter-Module Connectivity</i>	26
7 5 8 1	Conduction	26
7 6	A 4-MODULE REACTOR MODEL	26
7 7	A 16-MODULE REACTOR MODEL	26
7 8	A COMPARISON OF THE MODEL PERFORMANCE TO THAT OF THE REACTOR .	26
7 9	CONCLUSION	26
7 9 1	<i>Further Development of the Model</i>	26
8	SINGLE STAGE SULPHUR TOLERANT STEAM REFORMER.....	26
8 1	EVALUATION OF THE SULPHUR TOLERANT CATALYST USING LIQUID PETROLEUM GAS AS A FEEDSTOCK	26
8 1 1	<i>Results</i>	26
8 1 2	<i>Summary</i>	26
8 2	CONCLUSION	26
9	DUAL-STAGE STEAM REFORMER.....	26
9 1	EVALUATION OF THE DUAL-STAGE REFORMER USING PROPANE, LIQUID PETROLEUM GAS, AND METHANE	26
9 1 1	<i>Evaluation of the Reformer using Propane as a Feedstock</i>	26
9 1 2	<i>Evaluation of the Reformer using Methane as a Feedstock</i>	26
9 1 3	<i>Evaluation of the Reformer using Liquid Petroleum Gas as a Feedstock</i>	26
9 2	SUMMARY..	26
9 3	CONCLUSION	26
10	CONCLUSION	26
11	REFERENCES	26
APPENDIX 1: RESULTS TABLES FOR THE MICROCHANNEL STEAM REFORMER.....		26
APPENDIX 2.1 A MULTI-FUNCTION COMPACT FUEL REFORMING REACTOR FOR FUEL CELL APPLICATIONS		26
APPENDIX 2.2: LPG STEAM REFORMING IN A COMPACT MICROCHANNEL REACTOR USING SULPHUR TOLERANT CATALYST		26
APPENDIX 2.3: A DUAL-CATALYST MULTI-FUEL MICROCHANNEL STEAM REFORMER		26

Figures

FIGURE 1 1 ATMOSPHERIC CARBON DIOXIDE TRENDS [REF M CONTE (2002)]	2
FIGURE 1 2. THE HYDROGEN ECONOMY FOR SUSTAINABILITY	3
FIGURE 1 3 A SCHEMATIC OF A SPFC [REF Y M FERNG (2004)]	9
FIGURE 1 4 A TYPICAL POLARISATION CURVE	10
FIGURE 1 5 A TECHNOLOGY COMPARISON FOR CHP APPLICATIONS	12
FIGURE 1 6 A PROTOTYPE FUEL CELL POWERED BICYCLE [REF L CARDINALI (2002)]	15
FIGURE 1 7 A SCHEMATIC OF A TYPICAL FUEL PROCESSOR	21
FIGURE 1 8 THE IDATECH STEAM REFORMER	23
FIGURE 1 9 A SCHEMATIC OF AN AUTO THERMAL REFORMER [REF. T RAMPE (2000)]	26
FIGURE 1 10 A METHANOL MEMBRANE REACTOR [REF R BUXBAUM (2003)]	26
FIGURE 2 1. THE EFFECT OF TEMPERATURE ON THE DRY PRODUCTS OF STEAM REFORMING OF LPG AT S/C = 3 5	26
FIGURE 2 2 THE EFFECT OF STEAM TO CARBON RATIO ON THE DRY PRODUCTS OF STEAM REFORMING LPG AT 750°C	26
FIGURE 2 3 THE EFFECT OF TEMPERATURE ON THE DRY PRODUCTS OF STEAM REFORMING OF CH ₄ AT S/C = 3 5	26
FIGURE 2 4 THE EFFECT OF STEAM TO CARBON RATIO ON THE DRY PRODUCTS OF STEAM REFORMING CH ₄ AT 700°C	26
FIGURE 2 5. THE HEAT DUTY OF THE ATR OF LPG FOR VARYING INLET AND REFORMER TEMPERATURES AT S/C = 2, O ₂ /C = 0 38	26
FIGURE 2 6 THE EFFECT OF INLET TEMPERATURE ON THE ATR OF LPG AT S/C = 2, O ₂ /C = 0 38	26
FIGURE 2 7 THE REQUIRED H ₂ TO SUPPORT THE STEAM REFORMING REACTION OVER VARYING LPG FLOWRATES AND TEMPERATURES AT S/C = 2 5	26
FIGURE 2 8. THE REQUIRED AIR FEED TO THE COMBUSTOR TO SUPPORT THE STEAM REFORMING REACTION OVER VARYING LPG FLOWRATES AND TEMPERATURES AT S/C = 2 5	26
FIGURE 3 1. SIMPLIFIED MICROCHANNEL SHIMS	26
FIGURE 3.2 SHIM NUMBER KTS10001	26
FIGURE 3.3 SHIM NUMBER KTS10002	26
FIGURE 3 4 SHIM NUMBER KTS10003	26
FIGURE 3 5 SHIM NUMBER KTS10011	26
FIGURE 3 6 SHIM NUMBER KTS10012	26
FIGURE 3 7 SHIM NUMBER KTS10013	26
FIGURE 3 8 SHIM NUMBER KTS10014	26
FIGURE 3 9 SHIM NUMBER KTS10015	26
FIGURE 3 10 SHIM NUMBER KTS10016	26
FIGURE 3.11. SHIM NUMBER KTS10017	26
FIGURE 3 12 SHIM NUMBER KTS10018	26
FIGURE 3 13 THE MICROCHANNEL REACTOR	26
FIGURE 3 14 A CROSS-SECTION OF THE MICROCHANNEL REACTOR	26

FIGURE 3.15 THE REACTOR LAYOUT	26
FIGURE 3.16 THE POSITION OF THE INTERNAL THERMOCOUPLES	26
FIGURE 3.17 REFORMER EXIT MANIFOLD DRAWING	26
FIGURE 3.18 A VIEW OF THE EXIT MANIFOLD SHOWING THE POSITIONING OF THE INTERNAL THERMOCOUPLES	26
FIGURE 3.19. THE FLEXITALLIC GASKET	26
FIGURE 3.20. THE WELDED REFORMER EXIT MANIFOLD	26
FIGURE 3.21 THE REACTOR INSTALLED IN THE TEST RIG	26
FIGURE 4.1 THE TEST RIG	26
FIGURE 4.2 THE GAS LAYOUT FOR THE TEST RIG	26
FIGURE 4.3 THE ELECTRICAL LAYOUT FOR THE TEST RIG.....	26
FIGURE 4.4 A SCHEMATIC OF THE LEE PRODUCTS SOLENOID VALVE	26
FIGURE 4.5 THE EXHAUST PATHS FOR THE TEST RIG	26
FIGURE 4.6 AIR PREHEATER TUBE SHOWING POSITION OF S S POWDER	26
FIGURE 4.7 SOLENOID DRIVER CIRCUIT	26
FIGURE 5.1. LABVIEW CIRCUIT DIAGRAM FOR THE CONTROL AND DATA ACQUISITION SOFTWARE	26
FIGURE 5.2 A SIMPLE CONTROL LOOP	26
FIGURE 5.3 THE CONTROL LAYOUT FOR THE MULTI-ZONE COMBUSTOR	26
FIGURE 5.4 THE GRAPHICAL USER INTERFACE	26
FIGURE 6.1: THE POSITION OF THE INTERNAL THERMOCOUPLES	26
FIGURE 6.2 START UP OF THE COMBUSTOR SHOWING SOLENOID VALVE FAILURE	26
FIGURE 6.3 START UP TIMES AND TEMPERATURE SPREAD OF THE COMBUSTOR	26
FIGURE 6.4 START UP OF THE COMBUSTOR USING CH ₄	26
FIGURE 6.5 THE RATE OF CHANGE OF TEMPERATURE DUE TO H ₂ FED TO ZONE ONE	26
FIGURE 6.6 THE RATE OF CHANGE OF TEMPERATURE DUE TO H ₂ FED TO ZONE TWO	26
FIGURE 6.7 THE RATE OF CHANGE OF TEMPERATURE DUE TO H ₂ FED TO ZONE THREE	26
FIGURE 6.8 THE RATE OF CHANGE OF TEMPERATURE DUE TO H ₂ FED TO ZONE FOUR	26
FIGURE 6.9 CLOSED LOOP CONTROL OF THE COMBUSTOR TEMPERATURE..	26
FIGURE 6.10 A COMPARISON OF TRADITIONAL REFORMER TEMPERATURE CONTROL AND THE MULTI-ZONED APPROACH	26
FIGURE 6.11 THE H ₂ CONVERSION EFFICIENCY W R T COMBUSTOR TEMPERATURE	26
FIGURE 6.12 THE H ₂ CONVERSION EFFICIENCY W R T COOLANT FLOW RATE	26
FIGURE 6.13 HEAT TRANSFER EFFICIENCY AND HEAT FLUX W R T COMBUSTOR TEMPERATURE	26
FIGURE 6.14 TEMPERATURE DIFFERENCE BETWEEN THE COMBUSTOR AND COOLANT EXHAUST W R T COMBUSTOR TEMPERATURE	26
FIGURE 6.15 HEAT TRANSFER EFFICIENCY AND HEAT FLUX W R T COOLANT FLOW RATE	26
FIGURE 6.16 TEMPERATURE DIFFERENCE BETWEEN THE COMBUSTOR AND COOLANT EXHAUST W R T COOLANT FLOW RATE	26
FIGURE 7.1 A SIMPLIFIED SCHEMATIC OF A MODULE	26
FIGURE 7.2 A SCHEMATIC OF A SINGLE MODULE	26

FIGURE 7 3 THE FOUR-MODULE REACTOR MODEL	26
FIGURE 7 4 TEMPERATURE OUTPUT FROM THE FOUR-MODULE REACTOR MODEL WITHOUT COOLANT	26
FIGURE 7 5 TEMPERATURE OUTPUT FROM THE FOUR-MODULE REACTOR MODEL WITH COOLANT	26
FIGURE 7 6 TEMPERATURE OUTPUT FROM THE FOUR-MODULE REACTOR MODEL WITHOUT COOLANT	26
FIGURE 7 7 TEMPERATURE OUTPUT FROM THE FOUR-MODULE REACTOR MODEL WITH COOLANT	26
FIGURE 7 8 THE 16-MODULE REACTOR MODEL	26
FIGURE 7 9 THE TEMPERATURE OUTPUT OF THE 16-MODULE MODEL	26
FIGURE 7 10 THE TEMPERATURE DISTRIBUTION OF THE 16-MODULE MODEL	26
FIGURE 7 11: THE TEMPERATURE DISTRIBUTION OF THE 16-MODULE MODEL WITH 20 SLPM N ₂ AS COOLANT	26
FIGURE 7 12. THE TEMPERATURE DISTRIBUTION OF THE 16-MODULE MODEL	26
FIGURE 7 13 THE TEMPERATURE OUTPUT OF THE 16-MODULE MODEL WITH 20 SLPM N ₂ AS COOLANT	26
FIGURE 7 14 THE TEMPERATURE DISTRIBUTION OF THE REACTOR	26
FIGURE 7 15: THE TEMPERATURE DISTRIBUTION OF THE REACTOR WITH 20 SLPM N ₂ AS COOLANT	26
FIGURE 7 16 THE TEMPERATURE DISTRIBUTION OF THE REACTOR WITH 20 SLPM N ₂ AS COOLANT	26
FIGURE 8 1 DRY REFORMATE COMPOSITION AT VARYING TEMPERATURE...	26
FIGURE 8 2 DRY REFORMATE COMPOSITION WITH VARYING STEAM TO CARBON RATIO	26
FIGURE 8 3. DRY REFORMATE COMPOSITION WITH VARYING REACTANT FLOW-RATE	26
FIGURE 8 4. REFORMER EFFICIENCY AT VARYING REACTANTS FLOW RATE	26
FIGURE 8 5 PREDICTED FUEL CELL POWER OUTPUT AT VARYING REACTANTS FLOW RATE	26
FIGURE 9 1 STEAM REFORMER CATALYST DISTRIBUTION	26
FIGURE 9 2 THE EFFECT OF ZONE 4 TEMPERATURE ON REFORMER PERFORMANCE	26
FIGURE 9 3 THE EFFECT OF STEAM TO CARBON RATIO ON THE REFORMER PERFORMANCE	26
FIGURE 9 4 THE EFFECT OF C ₃ H ₈ FLOW RATE ON THE REFORMER PERFORMANCE	26
FIGURE 9 5 THE EFFECT OF C ₃ H ₈ FLOW RATE ON REFORMER EFFICIENCY	26
FIGURE 9 6 THE EFFECT OF C ₃ H ₈ FLOW RATE ON FUEL CELL POWER OUTPUT	26
FIGURE 9 7 THE EFFECT OF CH ₄ FLOW RATE ON THE REFORMER PERFORMANCE	26
FIGURE 9 8 THE EFFECT OF ZONE 4 TEMPERATURE ON REFORMER PERFORMANCE	26
FIGURE 9 9 THE EFFECT OF STEAM TO CARBON RATIO ON REFORMER PERFORMANCE	26
FIGURE 9 10 THE EFFECT OF CH ₄ FLOW RATE ON REFORMER EFFICIENCY	26
FIGURE 9 11 THE EFFECT OF CH ₄ ON FUEL CELL POWER OUTPUT	26
FIGURE 9 12 THE EFFECT OF LPG FLOW RATE ON REFORMER PERFORMANCE.	26
FIGURE 9 13 THE EFFECT OF ZONE 4 TEMPERATURE ON REFORMER PERFORMANCE.	26
FIGURE 9 14 THE EFFECT OF STEAM TO CARBON RATIO ON REFORMER PERFORMANCE	26
FIGURE 9 15. THE EFFECT OF LPG FLOW RATE ON THE REFORMER EFFICIENCY	26
FIGURE 9 16 THE EFFECT OF THE LPG FLOW RATE ON THE FUEL CELL POWER OUTPUT.	26

Tables

TABLE 1 1· A COMPARISON OF FUEL CELL TECHNOLOGIES	8
TABLE 1 2· A COMPARISON OF HYDROGEN STORAGE METHODS	17
TABLE 2 1· COMPOSITION OF LPG	26
TABLE 2 2· THE REQUIRED FLOW RATE OF LPG AND H ₂ O TO PRODUCE 0.5 kWe AT EQUILIBRIUM	26
TABLE 2 3· THE REQUIRED FLOW RATES OF H ₂ AND AIR REQUIRED TO SUPPORT THE STEAM REFORMING REACTION	26
TABLE 2 4· THE SIZE OF THE MASS FLOW CONTROLLERS	26
TABLE 3 1· A COMPARISON OF MICROCHANNEL WITH OTHER COMPETING TECHNOLOGIES	26
TABLE 3 2· SHIM DESIGNATIONS	26
TABLE 5 1· SCXI CHANNEL ASSIGNMENTS	26
TABLE 6 1· PRESSURE DROP ACROSS THE COMBUSTOR	26
TABLE 6 2· PRESSURE DROP ACROSS THE REFORMER	26
TABLE 7 1· INPUT SETTINGS FOR THE 4-MODULE MODEL TEST 1	26
TABLE 7 2· INPUT SETTINGS FOR THE 4-MODULE MODEL TEST 2	26
TABLE 7 3· INPUT SETTINGS FOR THE 4-MODULE MODEL TEST 3	26
TABLE 7 4· INPUT SETTINGS FOR THE 4-MODULE MODEL TEST 4	26
TABLE 7 5· INPUT SETTINGS FOR THE 16-MODULE MODEL TEST 1	26
TABLE 7 6· INPUT SETTINGS FOR THE 16-MODULE MODEL TEST 2	26
TABLE 7 7· INPUT SETTINGS FOR THE 16-MODULE MODEL TEST 3	26
TABLE 7 8· INPUT SETTINGS FOR THE 16-MODULE MODEL TEST 4	26
TABLE 8.1. RESULTS SUMMARY OF THE SINGLE-STAGE REFORMING	26
TABLE 9.1 A COMPARISON OF REFORMER PERFORMANCE USING DIFFERENT FUELS	26

Nomenclature

μ_A = Fuel Cell Activation Losses /V

μ_O = Fuel Cell ohmic losses /V

μ_C = Fuel Cell concentration losses. /V

η_{HEX} = Heat transfer efficiency.

η = Reformer conversion efficiency.

η_b = The H₂ conversion efficiency of the combustor

η_h = Heater efficiency.

ΔH_f = Enthalpy of Formation

A = Area available for heat transfer /m

C_a = The percentage conversion the LPG

C_n = The carbon ratio per molecule LPG

C_p = Specific heat at constant pressure.

F = The flow rate of hydrogen (dm³/min (STP)) required to produce 1 kWe output from a fuel cell.

H = The flow rate of hydrogen (mol/min) produced at equilibrium by 1 mol/min of LPG for a given steam to carbon ratio

\dot{m} = Mass flow rate /mol.sec⁻¹

n_p = The carbon ratio per molecule of propane

n_{pr} = The carbon ratio per molecule of propylene

n_e = The carbon ratio per molecule of ethane

n_b = The carbon ratio per molecule of butane

n_m = The carbon ratio per molecule of methane

P_{LHV} = The lower heating value of the products of reforming

P_t = Thermal power /kW

q = Heat Flux /kW.m⁻²

R_{LHV} = The lower heating value of the reactants for reforming

T = Temperature /°C

U_p = The % volume of propane in LPG

U_{pr} = The % volume of propylene in LPG

U_e = The % volume of ethane in LPG

U_b = The % volume of butane in LPG

U_m = The % volume of methane in LPG

V_{ACT} = Actual fuel cell voltage /V

V_{MAX} = Theoretical fuel cell voltage /V

Abstract

The aim of this Ph.D. is to develop and evaluate a compact 'fast response' hydrocarbon fuel processor with integrated control software and novel design concepts for use with both stationary and transportation applications using PEM fuel cells. A multi-function compact chemical reactor designed for hydrocarbon steam reforming was evaluated. The reactor design is based on diffusion bonded laminate micro-channel heat exchanger technology. The reactor consists of a combustor layer, which is sandwiched between two steam reforming layers. Between the two function layers, a temperature monitoring and control layer is placed, which is designed to locate the temperature sensors. The combustor layer has four individually controlled combustion zones each connected to a separate fuel supply. The reactor design offers the potential to accurately control the temperature distribution along the length of the reactor using closed loop temperature control. The experimental results show that the variance of temperature along the reactor is negligible. The conversion efficiency of the combustor layer is approximately 90 to 100%. The heat transfer efficiency from combustion layer to reforming layers is 65% to 85% at 600°C and 400°C, respectively. A sulphur tolerant catalyst, designed for use with LPG, was washcoated on to the reforming layers. The reformer was tested over a wide range of reactor temperatures, steam to carbon ratios and fuel flow rates. To increase the reformer performance a second nickel-based catalyst was added to the rear of the reformer. The multi-zoned combustor enabled the two catalysts to be operated at differing temperatures as required. The reformer was tested over a further range of operating temperatures, steam to carbon ratios and feed rates whilst using the fuels, LPG, C_3H_8 and CH_4 . The performance of the reformer whilst using C_3H_8 and LPG showed good agreement suggesting that the performance of the reformer was not adversely affected by the presence of sulphur in the fuel. 98% conversion of C_3H_8 was achieved at a predicted fuel cell power output of 1.98kWe.

1 Introduction

1.1 The Case for Hydrogen

It can be argued that the move from conventional fossil fuels to the wide spread use of hydrogen is inevitable. There are two arguments that lead to this conclusion. Firstly, there is depletion of economically viable fossil fuel sources, and secondly, there are the environmental arguments, particularly the effect of carbon dioxide on the environment [D.S. Scott (2004)]. The first argument concerns itself with finding a renewable energy source coupled with a clean efficient energy-carrying vector. In this case the energy vector is hydrogen. Hydrogen can be produced by electrolysis of water using electricity generated from renewable sources. The second part of the argument concerns the production of CO₂ as by products of human usage of fossil fuels. CO₂ is a greenhouse gas, which if its production is not limited will lead to climate instability that if left unchecked could be catastrophic. Figure 1.1 shows the predicted rate of CO₂ production and the theoretical limit of CO₂ in the atmosphere to minimise climate change as set by the Intergovernmental Panel on Climate Change (IPCC). Stabilisation of the CO₂ content of the atmosphere requires a 50% reduction in emissions by 2050. The current trends of CO₂ emissions coupled with increased energy demands require that a clean energy source be found.

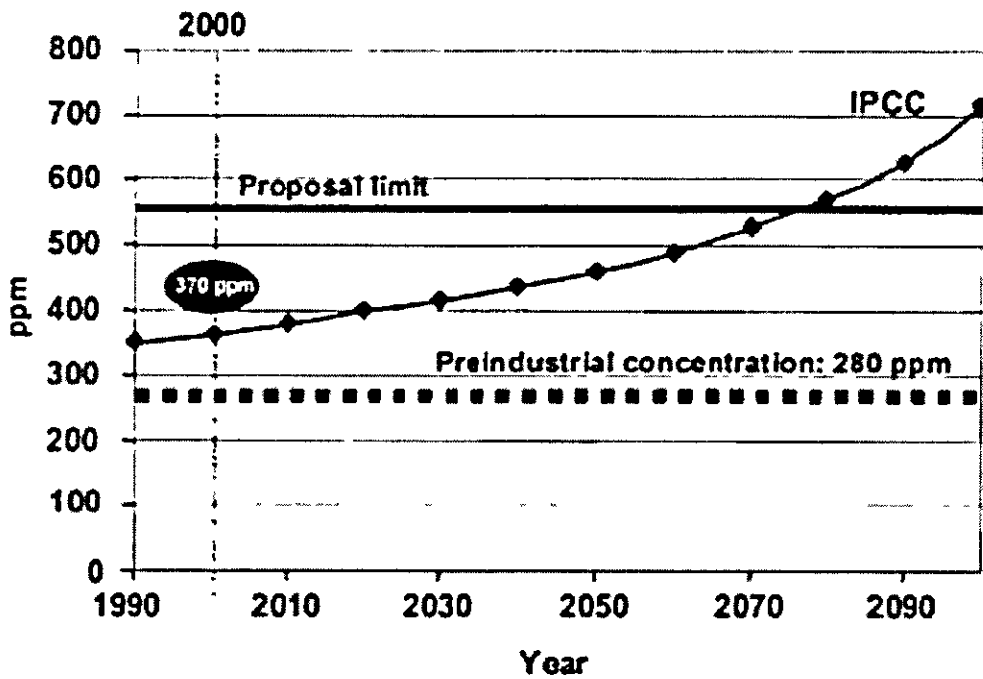


Figure 1.1: Atmospheric Carbon Dioxide Trends [Ref. M. Conte (2002)]

Renewable hydrogen production is free from CO₂ emissions. Additionally, even if it was possible to capture the CO₂ produced at stationary power plants, it would still be necessary to have a clean energy vector, with which to provide energy for mobile applications. Because of this and other political considerations there is a concerted effort to move towards a hydrogen economy.

The idea of the hydrogen economy has been established now for 30 years. The system behind it can be summed up in Figure 1.2 [Ref. T N. Vezirlogu (2000)]

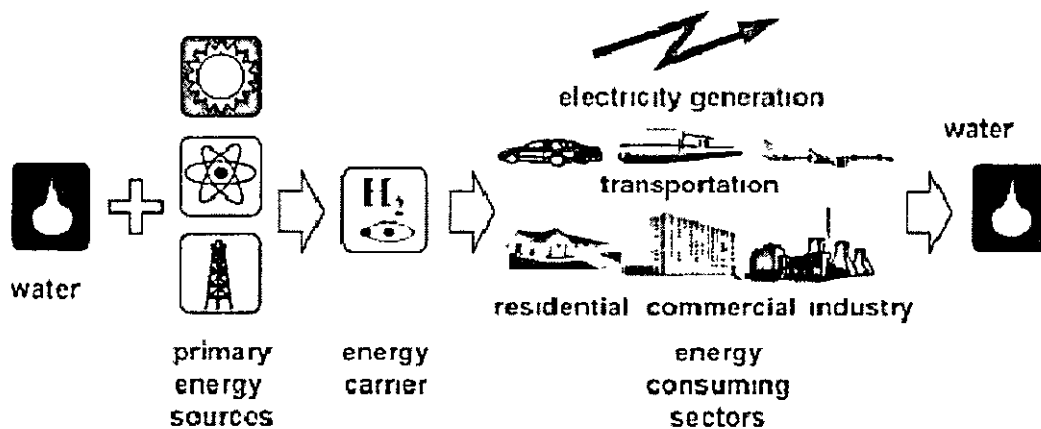


Figure 1.2: The Hydrogen Economy for Sustainability

Figure 1 2 shows a cyclical sustainable process for energy generation based on hydrogen as an energy carrier. Primary energy sources are used to produce hydrogen, a secondary energy source, by electrolysis of water, or reforming of fossil fuels. The hydrogen then acts as an energy carrier, or vector. Hydrogen can be used in two main areas of power generation. It can be used as a fuel for an internal combustion engine (ICE), or as fuel for a fuel cell. In both cases the product of each device is water, though there is the potential for NO_x production by the (ICE). The fuel cell offers higher practical efficiencies than an ICE. This is because a fuel cell does not have to be able to cope with the high combustion temperatures required by a heat engine to run at maximum efficiency. It is not practical, due to material constraints, to build an ICE capable of running at such temperatures [Ref A.E Lutz (2002)]. A fuel cells performance is not constrained in this way.

The goal of a hydrogen economy is closest in Iceland. This is because of the countrys natural geothermal and hydroelectric resources. Approximately 58% of Icelands resources are met in this way, with the remainder being provided by imported fossil fuels. The Icelandic Government supports the goal, and The Icelandic New Energy Company Ltd. has been founded with industrial partners such as DaimlerChrysler AG, Norsk Hydro ASA, and Shell International BV. They envisage a 5 phase plan to produce the worlds first hydrogen economy before 2040 [Ref B Amason (2000)].

Phase 1: A demonstration fuel cell bus project in Reykjavik.

Phase 2: Replacement of Reykjavik bus system with fuel cell buses

Phase 3: Introduction of methanol fuelled solid polymer fuel cell (SPFC) cars.

Phase 4 SPFC vessel demonstration

Phase 5: Replacement of fishing fleet with SPFC vessels.

The importance of Iceland leading the way in this respect is that it sets a standard and shows that the technology is viable. It is an important step in the acceptance of the technology in the eyes of not just the public but other governments

If hydrogen is to be adopted as a fuel by industry successfully, it will need to be accepted by the public who will have to come to terms with the change of routine and technology that such a move would entail. There are three main factors that influence acceptance of a new technology. These are risk, the perception of risk, and satisfaction with the technology. In order to reduce the perception of risk and increase the potential satisfaction of the technology there are three areas that can be worked on. These are education, marketing, and exposure to the product. If the public is well enough informed about the benefits of the technology and convinced that the risk from such technology is no greater than current technology, and allowed access to the technology, the chance of acceptance is more likely [Ref. I. Schulte (2004)].

1.2 Fuel Source

Hydrogen is a secondary fuel. That is to say that it is not naturally occurring and has to be produced using an intermediary process of some kind. There are many available feedstocks for the production of hydrogen. A short description of some of the most common feedstocks shall be attempted here.

1.2.1 Water

Hydrogen is produced from water using electrolysis. This is the opposite process to that which produces electricity inside a fuel cell. The drawback of the electrolysis process is that it requires a source of electricity. Currently the majority of electricity production is from fossil fuels. A study of well to wheel (WTW) costs for SPFC vehicles found that greenhouse gas emissions from direct hydrogen, produced by average US electric vehicles are not significantly less than conventional ICE powered vehicles. In addition they actually consume more energy WTW than ICE powered vehicles [Ref. M. Wang (2002)]. For electrolysis to be of real benefit, renewable sources of electricity need to be employed in the process. Renewable electricity sources include solar energy [Ref. P. Hollmuller (2000)], hydroelectric power [Ref. A.G. Dutton (2000), Z. Yumurtacı (2004)], and wind power [Ref. K. Agbossou (2001)]. These methods use hydrogen as an energy storage method, which can then be utilised with a fuel cell to produce electricity.

1.2.2 Hydrocarbons

Hydrocarbons are attractive as primary fuels because they are readily available. They can be reformed to produce hydrogen rich gas, which can then be utilised by a fuel cell. The issues surrounding the choice of appropriate hydrocarbon for a given fuel cell application are well covered in the literature. The issues include; hydrogen yield, cost, fuel infrastructure and safety [Ref. L.F.Brown (2001)]. The majority of these discussions concern the use of fuel cells in vehicles. This is because there is no current hydrogen supply infrastructure available for vehicle users, and until that time the suitability of the intermediate fuelling option is of importance to make any transfer of technology as smooth as possible. In the case of DaimlerChrysler they are developing a gasoline fuel processor for use in an automobile because the infrastructure for fuel supply is already there [Ref. S. Springmann (2004)]. The use of gasoline also allows the end user to make the switch between technologies smoothly, as he would already be used to filling his car with gasoline. However, it can be argued that the use of gasoline is not a big enough step forwards in terms of the environmental benefits of using a fuel cell. PeugeotCitroen have investigated the

reforming of bio-ethanol, which as will be discussed in section 1.2.3, is CO₂ neutral and therefore a more environmentally favourable choice of fuel [Ref. V. Klous (2002)]

For the stationary fuel cell market, the situation is different. Large-scale plants make use of high temperature fuel cells, which can internally reform hydrocarbons and are not affected by impurities such as CO. At the domestic scale, there is already a natural gas infrastructure that a fuel cell system can make use of. In remote areas where there is not a pipe line infrastructure, fuels such as bottled LPG can be used as a feedstock to provide a remote power source.

1.2.3 Biomass

Biomass is the name given to a substance made of organic components originally produced by fixing carbon dioxide in the atmosphere. One such example are the waste products of the sugar cane refining process [Ref. D. Dellepiane (2003)], bagasse and barbojo. As long as the original biomass species are reintroduced, cyclical flow of carbon dioxide can be attained keeping the concentration of carbon dioxide in the atmosphere constant. For this reason, biomass is likely to play a part in a sustainable energy future [Ref. Y. Matsumura (2004)]. There are different methods that can be employed to produce a hydrogen rich gas from biomass. One such method is by gasification of the biomass [Ref. C.N. Hamelinck (2002)], though the biogas produced requires further refining before it is suitable for use in a SPFC. Another method is through the use of anaerobic bacteria, discussed briefly in section 1.5 7.2.

1.3 What is a Fuel Cell?

The fuel cell concept has been around since 1835. William Grove a physics professor at the London Institute based his experiment on reversing the water electrolysis process. The term fuel cell was coined in 1889 when an attempt was made to make the first practical model. Fuel cells have since been investigated for use in a number of different applications, automotive, combined heat and power (CHP), space flight,

aviation, MW scale generators, and portable battery sized fuel cells. A fuel cell can be seen as analogous to a battery. The major difference is that a battery carries its fuel internally, whilst a fuel cell uses external fuel. This means that provided there is a supply of fuel to the cell, electricity will be produced.

The six most technically advanced types of fuel cells are shown in Table 1.1. These are:

- Solid polymer electrolyte fuel cell (SPFC)
- Alkaline fuel cell (AFC)
- Phosphoric acid fuel cell (PAFC)
- Molten carbonate fuel cell (MCFC)
- Solid oxide fuel cell (SOFC)
- Direct methanol fuel cell (DMFC)

The solid polymer fuel cell utilises H_2 as its fuel, which it combines electrochemically with oxygen (from air) to produce electricity, heat and water [Ref. J. Larminie (2000)]. This can be seen in the equations for the reactions at the anode and cathode below (equation 1.1 – 1.2 respectively).



A simple hydrogen/air fuel cell consists of an electrolyte with a porous anode and cathode on either side (see figure 1.3).

Fuel Cell Type	SPFC	AFC	PAFC	MCFC	SOFC	DMFC
Operating Temperature	40 – 80	80 – 100	200 – 220	600 – 650	800 – 1000	40 – 80
Current Density	High	High	Moderate	Moderate	High	
Charge Carrier	H ⁺	OH ⁻	H ⁺	CO ₃ ⁻	O ⁻	H ⁺
Prime cell components	Carbon based		Graphite based	Stainless Steel	Ceramic	Carbon Based
Catalyst	Platinum		Platinum	Nickel	Perovskites	Platinum/Ruthenium
Product Water Management	Evaporative		Evaporative	Gaseous Product	Gaseous Product	Evaporative
Product Heat Management	Process gas + independent cooling medium		Process gas + independent cooling medium	Internal reforming + process gas	Internal reforming + process gas	Process gas + independent cooling medium
Stage of Development	Prototypes and field demo	Space	Early commercial applications	Field demo	Laboratory demo	Early Prototypes
Likely applications	Electric Utility, portable power and transportation	Military and space	Electric utility and transportation	Electric utility	Electric utility	Portable
Advantages	Low temperature Quick start Solid electrolyte reduces corrosion and management problems	High performance	High efficiency for cogeneration Can use impure fuel	High efficiency Flexibility of fuels	High efficiency Flexibility of fuels Solid electrolyte reduces corrosion and management problems	Low Temperature Solid Electrolyte Liquid fuel
Disadvantages	High sensitivity to fuel impurities Requires expensive catalysts	Expensive removal of CO ₂ from fuel and air supplies	Low current and power Large size and weight	High temperature enhances corrosion and break down of cell components	High temperature enhances corrosion and break down of cell components	Methanol Permeability through Membrane
Prospect for high efficiency	Good	Good	Good	Good	Good	Good
Prospect for low cost	Good	Good	Fair	Fair	Fair - Good	Good

Table 1.1: A Comparison of Fuel Cell Technologies

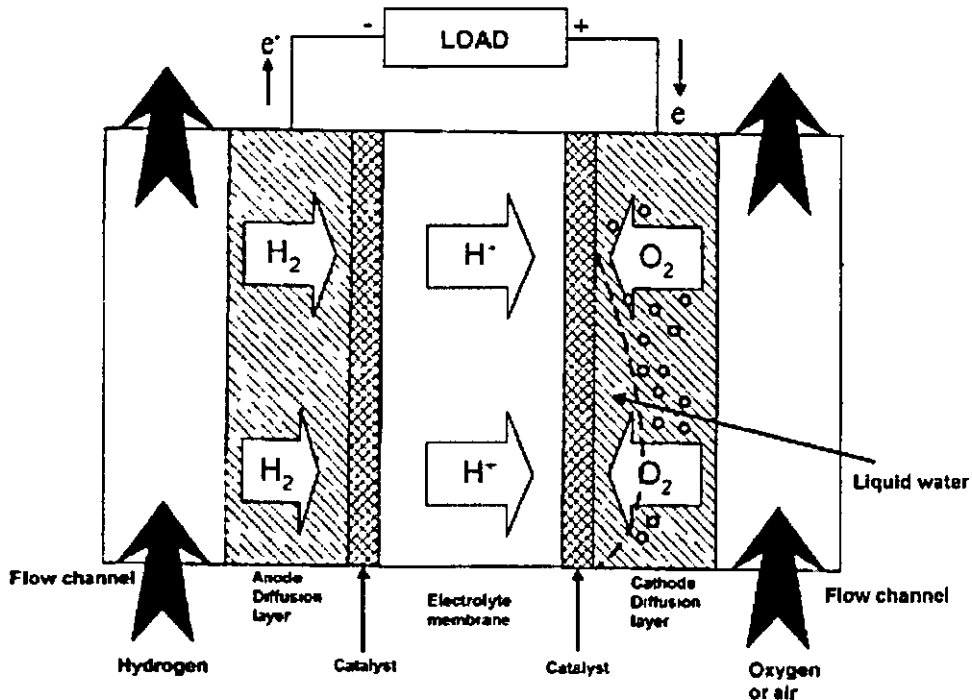


Figure 1.3: A Schematic of a SPFC [Ref. Y.M. Ferng (2004)]

Hydrogen is fed to the anode where it diffuses through the diffusion layer to the catalyst. The hydrogen dissociates to protons and electrons via the reaction shown in Equation 1.1. At the same time oxygen is fed to the cathode where it diffuses through the diffusion layer to the cathode catalyst. The oxygen reacts with the protons via the electrolyte membrane and with the electrons via the external circuit as shown in Equation 1.2. Current will continue to flow for as long as the fuel and oxygen are supplied to the fuel cell and the electrodes are connected across a load. The power generated is a direct result of the chemical energy of the reaction and as there is no combustion, the only chemical product is water

The theoretical operating voltage of a fuel cell is 1.223v. However, fuel cells are typically operated at 0.7v with a theoretical peak efficiency of 80%

The reason for this can be seen by looking at a typical polarisation curve (Figure 1.4).

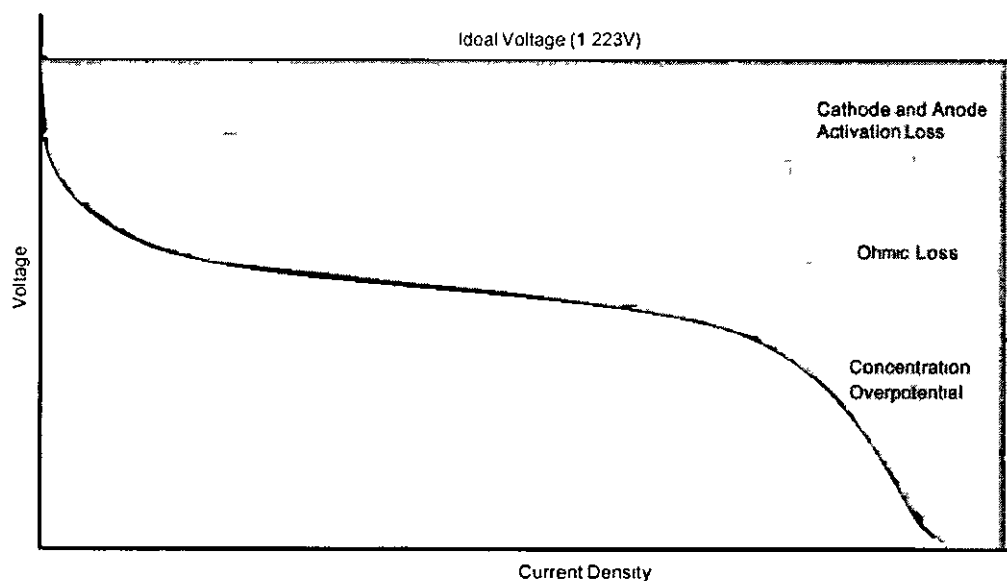


Figure 1.4: A typical polarisation curve

The activation losses are due to the activation energy of the reaction. A high catalyst surface area is important for fuel cell performance here. The ohmic loss is due to resistances in the materials. The main losses here are due to ion conduction in the polymer electrolyte and contact resistances between different fuel cell layers. The concentration overpotential is the region where the reactants can not be supplied to the catalysts at a sufficient rate. Water build up at the cathode can also lead to flooding in this region. This cuts off the supply of oxygen to the cell and reduces the performance. This means that the operating voltage of the cell is determined as shown by Equation 1.3

$$V_{ACT} = V_{MAX} - \mu_A - \mu_O - \mu_C \quad \text{Equation 1.3}$$

Where V_{ACT} = actual cell voltage, V_{MAX} = theoretical cell voltage, μ_A = Activation Losses, μ_O = ohmic losses, and μ_C = concentration losses.

The fuel cell performance can be influenced by various operating factors. These are cell temperature, anode humidification, and operating pressure [Ref. L Wang (2003)]. Developments in membrane technology that allow the SPFC to run at higher temperatures (120°C – 140°C) would allow steam produced by the fuel cell to be

recycled for use in a steam reformer, and would increase the system efficiency. Investigations into membranes capable of operating at up to 200°C are also being investigated but will need an uncertain technological breakthrough to become reliable [Ref. T Kosugi (2004)].

1.4 Fuel Cell Applications

The possible applications of fuel cell technology are varied but they all have the potential for efficient, clean methods of supplying electricity for a variety of needs. The applications of fuel cells can be divided into two main groups; stationary power generation, and portable power generation. Within each of those groups different types of fuel cell technology are implemented so that a wide range of power needs are catered for.

1.4.1 Stationary Power

Stationary power systems can be split into two main groups; Large scale power generation, and smaller scale units for use in homes as combined heat and power (CHP) systems perhaps connected to a distributed grid.

1.4.1.1 Combined Heat and Power

Fuel cells as the basis of combined heat and power (CHP) systems are an interesting alternative to the conventional separate natural gas and electricity supplies commonly employed in homes today. The idea being that given a natural gas supply to the house, the CHP system is used to generate any electricity when required. The “waste” heat from the system can be employed to heat water [Ref T. van der Does (1996)]. SPFC systems are ideally suited to home CHP applications. A comparison of different technologies shows that SPFC (proton exchange membrane, PEM) systems offer the best package overall (Figure 1.5) [Ref. W. Colella (2002)].

		Combined Heat and Power (CHP)					Conventional Generation	
		PEM Fuel Cell	Solid Oxide Fuel Cell	Micro-turbine	Reciprocating Engine (Gas)	Stirling Engine (Gas)	Grid Electric & Boiler	Superior Grid Electric & Boiler
Key Success Factors	Financial	Cost Competitive	High Performance	High Performance	High Performance	High Performance	High Performance	High Performance
		Suitability for Micro-Cogeneration	High Performance	High Performance	High Performance	High Performance	High Performance	High Performance
		Matching Heat to Power Ratio	High Performance	High Performance	High Performance	High Performance	High Performance	High Performance
		High Overall Efficiency	High Performance	High Performance	High Performance	High Performance	High Performance	High Performance
		Advanced Development Stage	High Performance	High Performance	High Performance	High Performance	High Performance	High Performance
	Technical	Long Lifetime	High Performance	High Performance	High Performance	High Performance	High Performance	High Performance
		Straightforward Grid Interconnection	High Performance	High Performance	High Performance	High Performance	High Performance	High Performance
		Low Maintenance Requirements	High Performance	High Performance	High Performance	High Performance	High Performance	High Performance
	Environmental	Low Carbon Dioxide Emissions	High Performance	High Performance	High Performance	High Performance	High Performance	High Performance
		Low SOx, NOx, HC and CO Emissions	High Performance	High Performance	High Performance	High Performance	High Performance	High Performance
		Low Noise Impact	High Performance	High Performance	High Performance	High Performance	High Performance	High Performance

Figure 1.5: A Technology Comparison for CHP Applications

It can be seen that fuel cell solutions out perform the other technologies on an environmental basis. This is important for the reasons given above in section 1.1. Another advantage that a fuel cell system has over other CHP technology options, is potentially better performance when considering the heat to power generation ratio of the system. The heat to power generation ratio is important to consider because the heat to power ratio demands on the system will vary over time. By careful system control it is possible to control the heat to power ratio of a fuel cell system so that the users demands are met in an efficient manner [Ref. E. Entchev (2003)].

1.4.1.2 Distributed Generation

Distributed generation is the decentralised generation of electricity, interconnected to a distribution network. The size of generator can range from large 100 MW systems to small domestic CHP systems in the order of 1-2 kW [Ref. P. Dondi (2002)].

1.4.2 Portable Power

Fuel cell systems are well suited to portable power generation. This is because hydrogen provides an efficient solution to the energy vector problem

1.4.2.1 Man Portable Power

With the advent of ever more complex portable computers, users demand increasing battery life. A miniature fuel cell can provide the extra lifetime between charges that the latest rechargeable battery packs can not. Research into liquid fuelled direct methanol fuel cells for applications such as mobile phones [Ref. C.K. Dyer (2002)] are being investigated, whilst hydrogen fuelled SPFC systems fed by metal hydride storage systems are proposed for larger equipment such as laptops. [Ref. K. Tuber (2003)]

Military applications for portable fuel cell technology include a mobile personal power source for modern infantry [Ref. J.W. Raadschelders (2001)]. This application envisages the use of a direct methanol SPFC to replace the soldiers current battery packs. The idea is to consolidate the soldiers power needs to a single fuel cell source. Another method uses a miniature methanol fuel processor to generate a hydrogen rich gas to feed the fuel cell [D.R. Palo (2002)]. An ambient pressure fuel cell stack is also being developed to be used as a portable generator for recharging the soldiers battery packs. This is seen as an intermediate step between conventional methods of powering the soldier and the use of personal fuel cell power packs. The reason being that there is a lot of work to be done on ruggedising fuel cell technology to make it suitable for the battlefield [Ref. J.M Moore (2002)].

1.4.2.2 Transportation

Vehicle manufacturers have been investing heavily in fuel cell technology to develop fuel cell powered cars or hybrid fuel cell vehicles. The reasoning behind fuel cell

vehicles is that they offer the opportunity to reduce emissions and increase the efficiency of the vehicle.

To decrease its dependence on overseas oil the U.S. Government set up the Partnership for a New Generation of Vehicles (PNGV). It was established in 1993 as a partnership between The Federal Department of Energy (DOE) R&D program and The United States Council for Automotive Research (USCAR) which represents DaimlerChrysler, General Motors, and Ford. The partnerships long-term goal is the production of a six seater family saloon which can achieve 80mpg, whilst matching Government safety and emissions regulations. The PNGV has led to DOE investment into SPFC technology as a means to produce a low to zero emissions vehicle. This is the DOE fuel cells for transportation program [Ref. S.G Chalk (2000)].

Fuel cell hybrid vehicles could use conventional batteries as a secondary power source. The battery would be used to store energy under braking and to supplement the fuel cell under acceleration [Ref. H.S. Lee (2003)]. Depending on the source of the hydrogen used to fuel the fuel cell, such a vehicle could have zero emissions. In the case of a system with an onboard fuel processor, hybridisation can be a solution to the cold start problem, as well as improving the load following of the system, something that is especially important in a vehicle [Ref. G. Pede (2004)]. There has been interest in the public transportation field as well. Buses are well suited to fuel cell implementation. As fleet vehicles they can fill up with hydrogen at a central refuelling station simplifying the question of how to provide the fuel cell with hydrogen [Ref. J.M. Vidueira (2003), A. Folkesson (2003)]

The flexibility of fuel cell technology with regards to transportation applications is demonstrated by a 300W electric bicycle prototype developed at ENEA Casaccia Research Center in Rome, Italy (Figure 1.6)

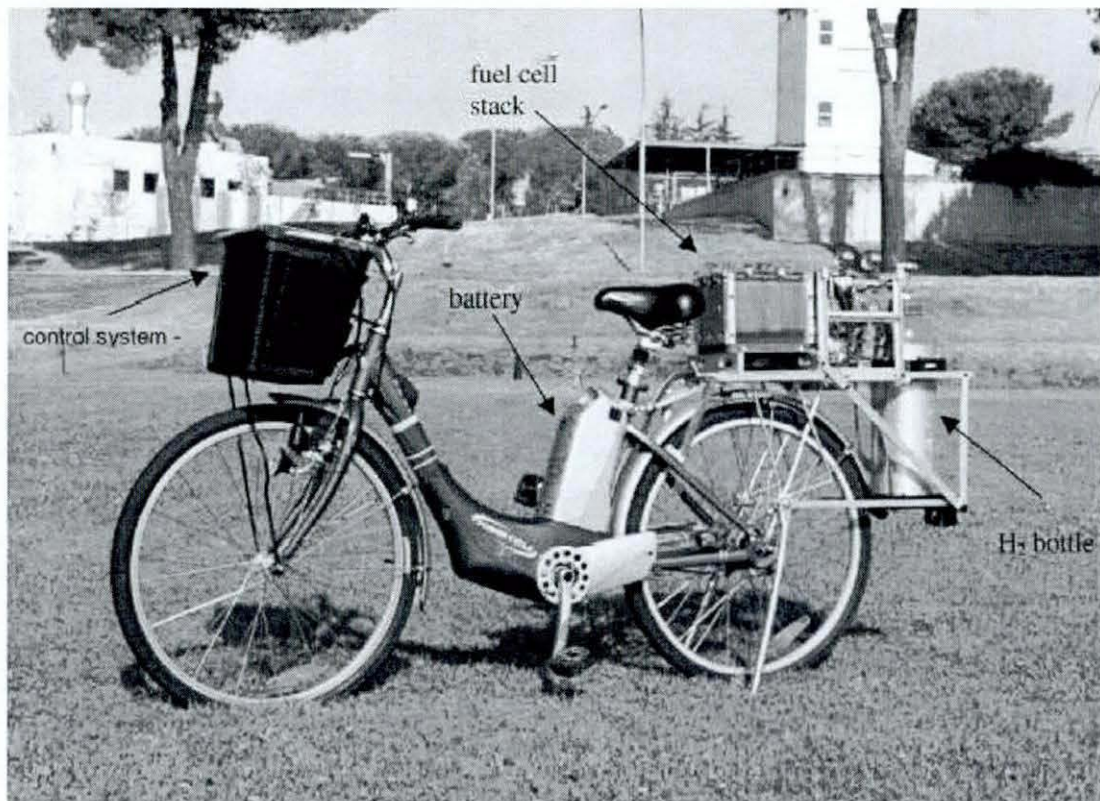


Figure 1.6: A Prototype Fuel Cell Powered Bicycle [Ref. L. Cardinali (2002)]

Other applications include the use of fuel cells to power motorcycles [Ref. J.H. Wang (2002)], and even submarines [Ref. A. Psoma (2002)].

SPFC technology from the 100 W range to the 250 kW range can be used in a variety of transportation applications with the power solution tailored to the application.

1.4.3 Summary

It has been shown that the solid polymer fuel cell (SPFC) is seen as a potential clean power plant for a number of applications. The application that the fuel cell is used for is an example aside from the initial obvious cost issues. Although the automotive sector has invested significantly in the development of SPFC systems over the past decade, technology costs are still at present uncompetitive compared to those for the internal combustion engine (ICE). Near term costs for SPFC systems have been reported to be approximately an order of magnitude greater than the ICE on a \$/kW basis. The current cost of fuel cell technology is running at \$200/kW, the goals of the

PNGV state a \$50/Kw aim. In the long term it may be possible to reduce the cost to \$10/kW [Ref. I Bar-On (2002)].

Whilst a consideration of technology improvements and volume production will assist in reducing SPFC costs in the mid to long term, a more cost competitive market for SPFC technology is now seen as the stationary power market and distributed generation in particular. Stationary systems use the same SPFC stack technology that is used in automotive fuel cell systems. As such they need a hydrogen stream with a high level of purity (low sulphur and CO levels) to operate effectively.

1.5 Fuel Supply for the SPFC

For the SPFC, there are essentially two methods of supplying H₂ to it.

- Direct (pure) H₂ storage and supply
- Storage in the form of hydrocarbon/alcohol carrier using chemical processing to liberate the H₂.

Table 1.2 shows the energy density options for some methods of hydrogen storage.

Fuel	Gravimetric Energy Density of Fuel MJ/m ³ (kWh/l)	Volumetric Energy Density of Fuel and Container (kWh/l)	Gravimetric Energy Density of fuel and Container (kWh/l)
Petroleum (0.8kg/l)	12.2	9.5	11.0
Methanol (0.72kg/l)	6.4	4.4	5.3
Compressed Hydrogen Gas (0.016kg/l)	39.7	1.0	1.6
Liquid Hydrogen	39.7	1.5	4.8
Carbon Nanofibre	30	13.8	13.8
Fe-Ti Hydride (5.8kg/l)	0.84	4.0	0.55
Lead-acid Battery (2.8kg/l)	-	0.06	0.03

Table 1.2: A Comparison of Hydrogen Storage Methods

1.5.1 Pure Hydrogen Storage or Supply

The first option for fuelling the fuel cell is that of pure H₂ storage. The major advantage of this is the fuel cell will be zero emission. This is probably the desirable future for fuel cell technology. But currently, clean H₂ production is costly and inefficient, and there are also drawbacks with storing and handling pure H₂. These drawbacks are seen in the hydrogen embrittlement process [Ref. V. I. Schavchko (2000)]. At high temperature and pressure hydrogen molecules decompose into atoms and small quantities penetrate into the metal. Usually these atoms are able to pass right through the metal and out the other side. However if they build up inside a micro crack, they can accumulate and reform molecules. The molecules can not penetrate the metal and so the partial pressure inside the crack increases and the crack development is promoted. The use of preventative coatings may slow hydrogen permeation down but does not provide a long-term solution, and may exacerbate the

situation in some circumstances [Ref. V.V. Panaysuk (2000)]. Mechanisms for hydrogen embrittlement at lower temperatures have also been proposed [Ref A N Kuzyukov (2002)]

1.5.1.1 Pressurised Storage

The major drawback of this method is the weight penalty incurred by the cylinder. However, for bus applications the cylinders can be stored on the roof using conventional technology. Current research and development in this field is addressing the development of composite cylinders utilising very high pressures to increase energy storage density.

1.5.1.2 Liquid Storage

It can be seen in Table 2:1 that onboard storage of liquid hydrogen produces good vehicle range and gravimetric energy density. The difficulty comes with the cryogenic storage of the liquid. Hydrogen becomes a liquid at -253°C and would have to be maintained at this temperature inside the vehicle. There is also the question of refuelling. Currently BMW and Ford have test liquid hydrogen refuelling stations, with BMWs being open to the public [Ref. K. Pehr (2001), Ref. 6]. These currently require special training and permits to use and have some way to go before they are suitable for wider use.

1.5.1.3 Metal Hydride

Metal Hydrides allow good volumetric energy density but are compromised by their gravimetric energy density. The refuelling process is also more time consuming than the other methods considered here. If used in a vehicle it would be necessary to replace the storage container to refuel the vehicle. Owing to the weight of the metal hydride system this is impractical. However for stationary applications they hold more promise. This is because the weight is less critical. The rate of hydrogen release is

dependent on the heat transferred to the metal hydride [Ref. S. Levesque (2000)] Metal hydride storage methods provide a means of creating a hydrogen buffer inside a fuel processing system that can be activated to help with the transient response of the system.

1.5.1.4 Carbon Nanofibres

Another option is to use carbon nanofibres to store the H₂. Impressive claims have been made for this technology but so far these claims have not been verified [Ref. Yu.S. Nechaev (2003)]. If this technology does become viable in the future it will free up the H₂ economy by allowing compact dense H₂ storage. For this reason there is a lot of ongoing research in this area [Ref. C. Gu (2004), D.V Schur (2003), L Zhou (2004), Q. Zeng (2004), X Chen (2004)]

1.5.2 Fuel Processing

The last option and the one that will be investigated the most thoroughly in this chapter, is the use of hydrocarbon fuels, which can then be reformed to produce a hydrogen rich gas stream. This is an attractive solution to the hydrogen storage problem, because it overcomes some of the difficulties mentioned above and the technology (at a large scale) is well tested.

Firstly, if the hydrocarbon is chosen carefully there is no need to create a new fuel supply infrastructure as the existing infrastructure will already be useable. This is an advantage in a stationary power market as well as the transportation market. Secondly, most hydrocarbons are more easily and efficiently stored than H₂ making them more suitable for transportation applications. Thirdly, the heat generated by the reformer can be thermally integrated with the fuel cell to increase the efficiency of the system. This has benefits for use in the home. The generator needs to have a quick start-up time and follow transients in fuel demand well. Certain applications confer space restraints on the installed system. Therefore a compact fuel processor design coupled with the compactness of SPFC technology can be advantageous

1.5.3 Fuel Cell Operating Requirements

Before discussing the required components of a fuel processor it is necessary to understand the demands of the fuel cell with regards to the output of the fuel processor.

For the purposes of this work I will concentrate on the requirements of the SPFC. This is because the SPFC has particular benefits, which have meant that it has become the favoured fuel cell for a variety of uses. These are transportation, distributed generation and other portable small-scale applications. It has a high current density ($>1 \text{ A/cm}^2$) and a low operating temperature ($<80^\circ\text{C}$). This means that the stack will have fast start up times and be compact enough to be used for mobile applications. Also because it uses a solid electrolyte the fuel cell will operate in any orientation and there is no chance of spillage or corrosion making them safe to handle.

Impurities such as CO, CO₂ and sulphur in the fuel will decrease the fuel cells performance. Small amounts of CO will poison the fuel cell anode by preferentially adsorbing onto the platinum electro-catalyst instead of H₂. Typical reformat contains $>1\%$ CO by volume. This is considerably higher than the fuel cells tolerance of 10ppm (0.001% by vol.) and thus the concentration of CO has to be reduced [Ref. K. Ledjeff-Hey (2000)]. Development of catalysts to produce CO resistant anodes is being investigated [Ref. J-D. Kim (2001)]. CO₂ is significantly less of a problem than CO, although it does affect anode performance slightly through the reaction of CO₂ with adsorbed hydrides on platinum. In an acid electrolyte, such as that used in a SPFC, the CO₂ predominantly acts as a diluent.

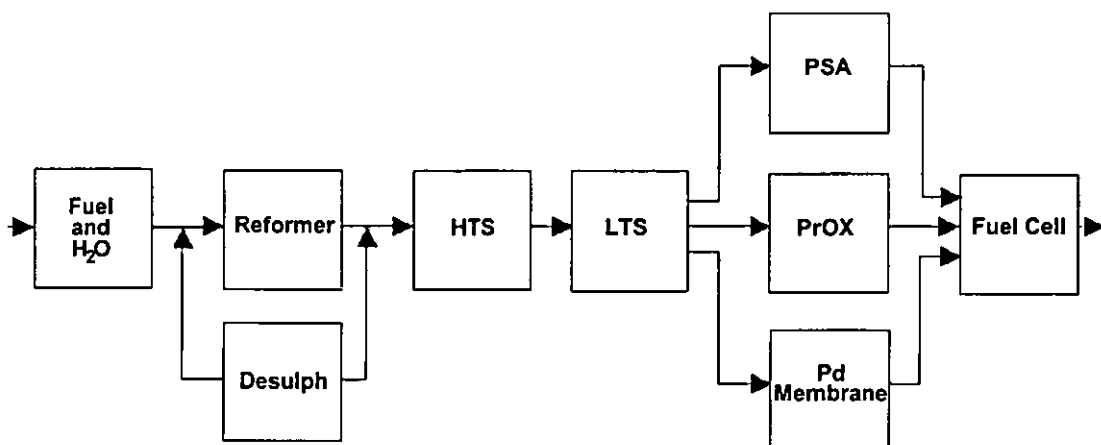


Figure 1.7: A Schematic of a Typical Fuel Processor

Figure 1.7 shows a simplified schematic of a fuel processor system. In order to address the fuel purity requirements of the SPFC the fuel processor is a multi-stage system. Briefly the system can be split into four sections. The desulphurisation reactor, the fuel reformer, the water gas shift reactors, and the CO removal stage. This work is concerned with the reforming stage of the fuel processor, but a brief overview of the balance of the fuel processor will be included, in order that the reformers place in the system is understood, and the implications of reformer design on the remainder of the fuel processor can be seen.

The reforming of hydrocarbons is a well-tested technology at the industrial scale. The difficulties arise in adapting the technology to the constraints of the small scale for use with a SPFC. The fuel processing approach and its incorporation into the fuel cell system has a major effect on the SPFC systems efficiency [Ref. J.M. King (2000)]. The requirements for a fuel processor can be summarised as follows:

- High Hydrogen Yield
- High Level of Product Purity
- Rapid Start Up
- Low Weight and Volume
- Short Transient Response Times

The above constraints mean that several competing technologies are being considered as each fair better on different aspects of the demands. These are:

- Steam Reforming
- Partial Oxidation Reforming
- Autothermal Reforming
- Novel Methods

1.5.4 Steam Reforming

In this process the hydrocarbon fuel is reacted with steam to produce a hydrogen rich product gas. Carbon in the fuel is converted into CO by oxidation with oxygen in the steam. Hydrogen from the fuel and steam is released as a gas. The reaction is endothermic. Below is the theoretical equation (Equation 1.4) that describes the steam reformation of a typical hydrocarbon [Ref. J. Larminie (2000)].



This is an endothermic process and so heat needs to be applied to the reformer to keep it at the required temperature. The temperature is critical because it determines the composition of the reformat. A catalyst is used to increase the reaction kinetics, which will lower the reforming temperature and reduce the reactor size. Because of the endothermic nature of the steam reforming process it is necessary to supply a continuous supply of heat to the reformer. This is usually done by the addition of a combustor to the reformer system. Traditionally steam reformers offer lower transient performance than partial oxidation or autothermal methods of reforming. However, the thermal integration of the combustor and reformer is an area where improvements can be made. A well integrated combustor can decrease transient response times by an order of magnitude [Ref. M. Sundaresan (2003)]. It is possible to utilise unused hydrogen from the fuel cell to partly fuel the combustor. This can recover up to 55% of the LHV of the fuel [W.G. Colella (2003)].

A steam reformer can be seen in figure 1.8. It is made by IdaTech and consists of 15 tubular reactors arranged around a combustor. The tubes receive their heat via radiation from the combustor flame and conduction from the combustor flue gases. The reformer reactants are distributed equally between the tubes by the inlet manifold [Ref D.G. Loffler (2003)].

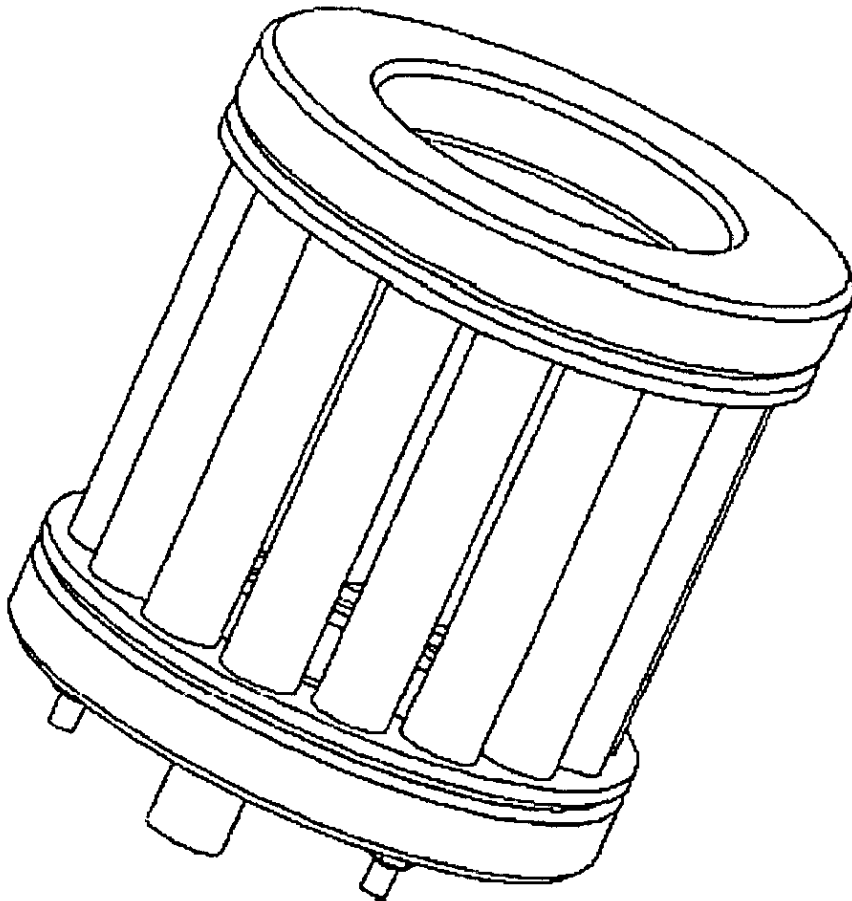


Figure 1.8 The IdaTech Steam Reformer

Carbon in the fuel is converted into CO and so is always present in the reformat. This poses problems for the use of such a fuel with a SPFC as the low temperature of operation (80°C) means that there is competition for electro-catalyst sites in the fuel cell between CO and H₂ molecules. This results in the fuel cell efficiency being drastically reduced. Although this poisoning is reversible, there is still a requirement for treatment of the reformat stream before it reaches the fuel cell.

To reduce the formation of CO it is possible to increase the steam to carbon ratio. This has the effect of suppressing the reverse water gas shift reaction [Ref. J. Agrell

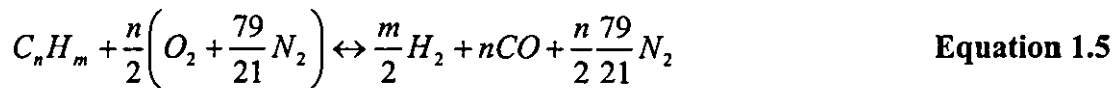
(2002)]. However, the addition of excess water at the reformer stage has to be balanced with the system design. The additional water will quench the reactor and lead to the production of CO_2 via the water gas shift reaction. In addition, although hydrogen production increases with steam to carbon ratio, it is not possible to raise the hydrogen yield above its theoretical limit [Ref. Y. Lwin (2000)]. Adding oxygen to the reactants also suppresses the formation of CO. This leads to autothermal reforming discussed in section 1.5.6. Reducing the required operating temperature of the reactor will also reduce the amount of CO produced. This will however, accompany a reduction in hydrogen yield. To produce the highest possible hydrogen yield from a steam reformer it is necessary to operate at low pressure, high temperature and relatively high steam to carbon ratio [Ref. F. Joensen (2002)].

1.5.5 Partial Oxidation Reforming

There are two types of partial oxidation (POX) reformers, catalytic and non-catalytic: Non-catalytic reforming is described in Equation 1.5. The hydrocarbon is partially oxidised to produce the products of hydrogen and carbon monoxide, although in practice some carbon dioxide is also produced. Catalytic partial oxidation reforming is similar to autothermal reforming except that instead of oxidation taking place in the gas phase, it takes place catalytically and no flame is produced [Ref. D.K. Liguras (2004)].

POX systems rely on the reaction of the fuel in a limited amount of oxygen to prevent complete oxidation. It allows for simpler design by removing the need for external heat and water supplies, such as those required with steam reforming. Also, since no external heat input is required, potentially better transients (start up times and responses to changes in demand) are available. There is also little or no soot produced which allows the use of heavy fuel oils. However, the reaction produces fewer moles of hydrogen for a given fuel than steam reforming. Additionally, the air also has to be pressurised to fuel cell operating pressure, which counts as another loss of energy from the system. Since the reaction is exothermic it is not possible to use unutilised fuel from the fuel cell in the way that it can be used with a steam reformer, and thus lower system efficiencies result. It might also be necessary to externally cool the

reactor to prevent the reaction from running away. In a practical system air is used to provide the oxygen for the reaction. This leads to dilution of the product gas with nitrogen. This has the effect of lowering the partial pressure of the hydrogen at the fuel cell anode, which in turn leads to lowering the efficiency of the fuel cell [Ref. J. Larminie (2000)].



1.5.6 Autothermal Reforming

This is a combination of steam reforming and partial oxidation reforming. It uses the exothermic partial oxidation reaction to supply the heat required to support the endothermic steam reforming reaction. Vaporised hydrocarbon fuel, air and water are fed to the reactor. This allows the system to be started as a POX reformer for fast start up times, before operating in the thermally neutral state to gain the benefits of the higher H_2 production rate of steam reforming. It ideally runs in a thermally neutral state. However in practise a near autothermal operating point is reached [Ref. N. Edwards (1998)]. A schematic of an autothermal reformer (ATR) can be seen in Figure 1.9.

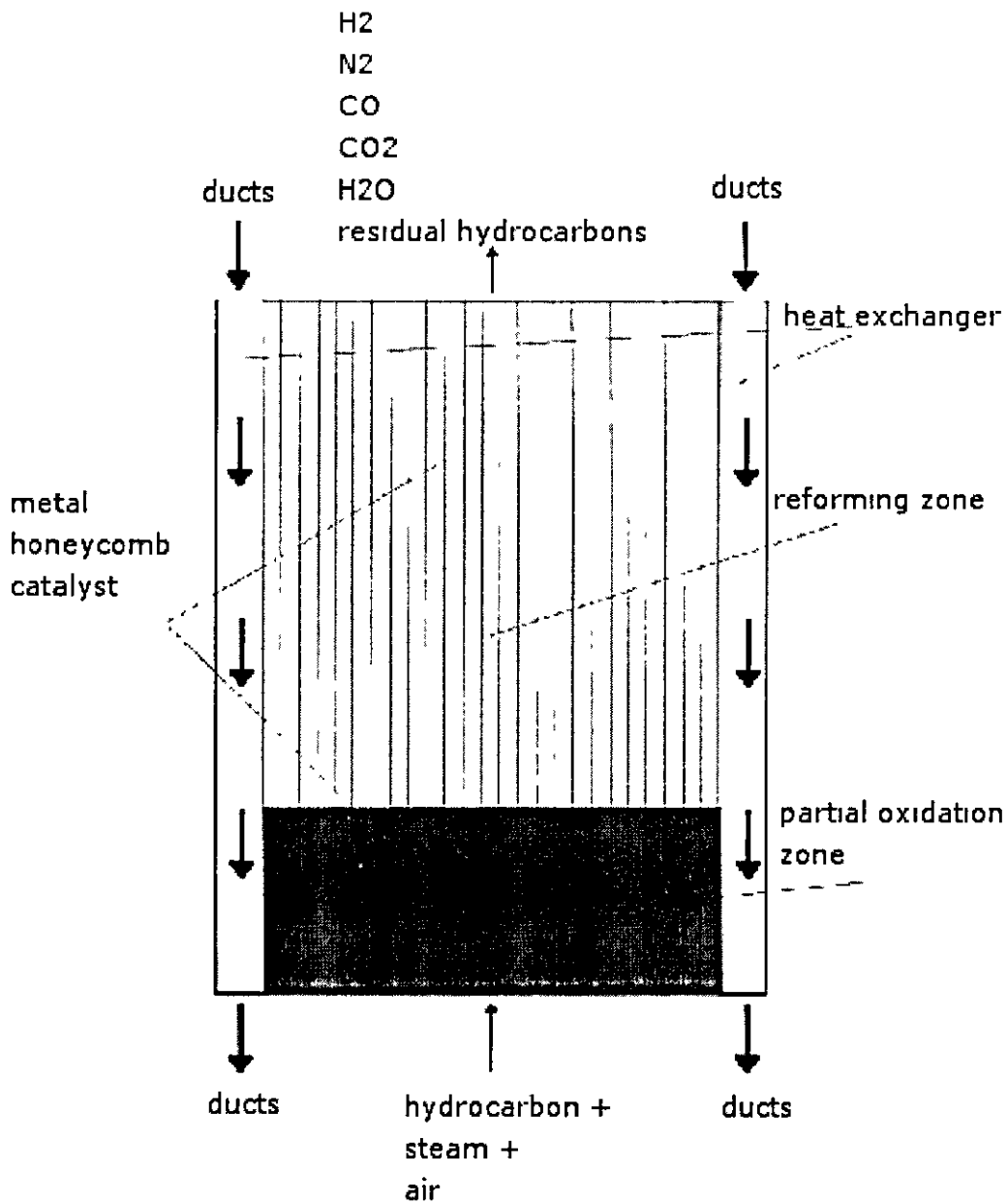


Figure 1.9: A Schematic of an Autothermal Reformer [Ref. T. Rampe (2000)]

In the reactor shown, the catalyst is divided into two areas. This is because of the different reaction rates of the combustion and reforming reaction. In the first zone the oxidation of the hydrocarbon fuel is the dominant reaction. The second zone is used for complete reforming. In this way the catalyst at the reformer inlet is heated by direct heat transfer from the combustion and the second catalyst is heated by the product gases.

It is important to control the steam to carbon and oxygen to carbon ratios in order to maximise the production of hydrogen whilst minimising the production of CO. The values required are dependant on the hydrocarbon fuel used [Ref. A. Ersoz (2003)]. The operating temperature of the reactor is determined by the steam to carbon and oxygen to carbon ratios. By increasing the oxygen flow or decreasing the water flow, the equilibrium temperature of the reactor is reduced and vice-versa [Ref. S.H. Chan (2001)].

As with the steam reforming and partial oxidation techniques, carbon monoxide is a natural by product of the process. ATR also suffers from the same dilution problem that afflicts POX reformers run using air to provide the oxygen. Namely that of dilution of the product gas due to the nitrogen content in air, which in turn lowers the efficiency of the fuel cell.

1.5.7 Other Reforming Methods

Aside from the three most common methods of reforming there are several less common methods under investigation

1.5.7.1 Plasma Reforming

Plasma discharges have been found to be useful in the reforming of hydrocarbons and thermal cracking of natural gas. The high temperature of operation serves as a large load on the system. Non-thermal plasma has been used as a catalyst for partial oxidation and other methods. By altering the electrical parameters of the discharge it is possible to control the reforming process [Ref. M.G. Sobacchi (2002)].

1.5.7.2 Biological Reforming

There is a lot of interest in the use of natural renewable methods of generating hydrogen via the use of anaerobic microfauna to break down biological matter. It has

been shown that under suitable conditions it is possible to culture bacteria that convert carbohydrates into hydrogen and carbon dioxide [Ref. M. Morimoto (2004)]. It is also possible to use bacteria to act as a clean up system for removing CO from syngas produced by the gasification of biomass via conventional means. The bacteria convert CO into CO₂ and H₂ using the water gas shift reaction. It is also possible to use bacteria to sequester CO₂ as biomass [Ref. W. Merida (2004)]. Though promising for long term natural hydrogen production, the biological systems are not suitable for integration into a SPFC system due to the inability of the process to load follow.

1.5.7.3 Membrane Reactors

Membrane reactors, whilst not making use of a novel process, represent a novel way of using existing technologies. Membrane reactors typically consist of a steam reformer directly coupled to a porous membrane that only allows hydrogen to pass through it. In this way an almost pure hydrogen supply for a fuel cell is produced. A typical membrane reactor can be seen in Figure 1.10.

In a study of methane reforming using membrane reactors [Ref. F. Galluci (2004)] it was found that the presence of the membrane pushed the equilibrium of the reaction towards the products. In this way it is possible to produce similar methane conversions to traditional methods but at a lower temperature. This represents an energy saving. This occurs because the extraction of the hydrogen increases the concentration of reactants and increases the residence time so effectively increasing the catalyst activity [Ref. M.E.E. Abashar (2004)]. The best results with a membrane reactor occur when the pressure differential across the membrane is high and the membrane is as thin as possible. Another advantage of using a membrane reactor is that the fuel processor size is reduced, and there is a small efficiency benefit due to not requiring a preferential oxidation (PrOx) step with the accompanying slight loss of H₂ that takes place [Ref. J.R. Lattner (2004)]. The reactor needs to run at 850°C – 950°C to maximise the efficiency. This is at the limit of the palladium membrane technology. The cost of the membrane is also an issue, as is coke formation due to the removal of hydrogen by the membrane. The requirement to pressurise the reactor

places parasitic loads on the overall system, which are not present in a conventional steam reformer system.

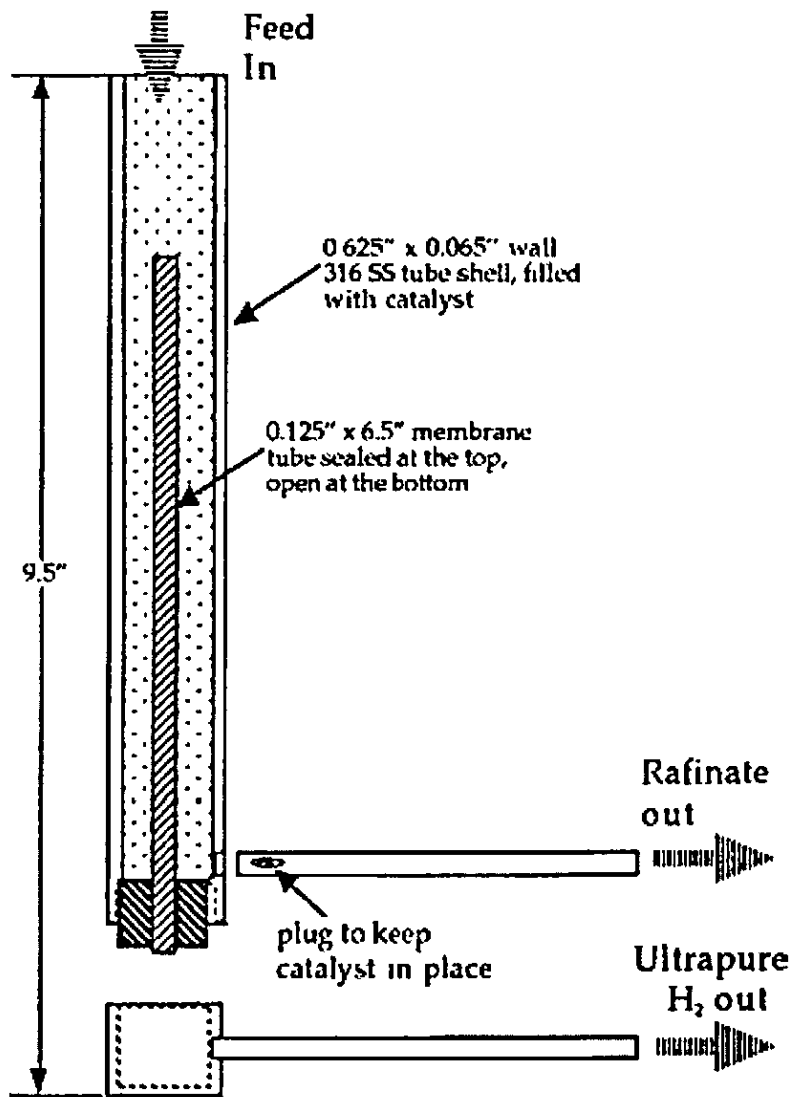


Figure 1.10: A Methanol Membrane Reactor [Ref. R. Buxbaum (2003)]

1.5.7.4 Sponge-Iron Reforming

The sponge-iron process is one method that has been investigated as an alternative or as a complement to more traditional reforming methods. Essentially the process is based on the reduction of a contact mass by a synthesis gas and the oxidation of the same contact mass by steam for the production of pure hydrogen. During the

reduction phase, the synthesis gas reacts with magnetite (Fe_3O_4), which in turn is converted into wuestite (FeO) and finally to iron (Fe). Steam is used as an oxidant and the reaction starts with Fe or FeO . The higher the temperature the higher the production of hydrogen. The process is endothermic and the maximum hydrogen production rate is dependent on the slow reduction step of the process [V. Hacker (2003)]. The technology could be used in such a way so as to provide hydrogen to vehicles. Cassettes loaded with Fe would be packed onto a vehicle and water passed over them to release the hydrogen from the water. The cassettes could then be replaced with fresh ones. The problems with this type of system are the high operating temperature and a decrease in activity of the Fe due to repeated redox cycles [Ref. K. Otsuka (2003)]. The technology is also being investigated as a way of producing hydrogen from biomass [Ref. R. Sime (2003)].

1.5.7.5 Non-Catalytic Steam Reforming

An alternative to catalytic steam reforming is hybrid non-catalytic steam reforming [Ref. P. Marty (2003)]. The reaction combines the fuel with air and steam. This process allows the production of a fuel flexible fuel reformer. It also overcomes the problems associated with catalysts of poisoning and carbon formation. A drawback is that the temperature required to reform the fuel is higher than that required for a catalytic process. This would reduce the efficiency of the system by requiring more heat to be transferred to the reactor. It also doesn't solve the catalyst poisoning problem further down stream of the reactor.

1.5.8 Balance Of Plant

The design of the balance of the fuel processor is no less important than that of the reformer. Careful consideration must be made of the integration, both thermal and chemical, to produce a complete efficient fuel processor system.

1.5.8.1 Desulphurisation

Sulphur levels in the ppb range will irreversibly damage the platinum catalyst of the fuel cells anode. Also sulphur is a poison for most common nickel based reforming catalysts. Since commercial grade LPG (and other fuels) unavoidably contain sulphur as an odorant, the sulphur needs to be removed from the fuel stream before it reaches the reformer catalyst and fuel cell [Ref. D.L King (2000)]. Typically one of two methods of desulphurisation are used. HydroDesulphurisation (HDS) with zinc oxide beds, or absorption techniques utilising activated carbon [Ref. J. Larminie (2000)] HDS is the best suited for SPFC systems as there is an available stream of hydrogen rich gas to promote the hydrogenolysis reaction. The HDS reactor requires heating to around 350 – 400°C for the hydrogenolysis reaction to complete This reduces the efficiency of the fuel processor as well as introducing greater complexity and size.

Sulphur tolerant steam reforming catalysts are being developed that will allow the option of reforming heavier hydrocarbons such as kerosene [Ref T. Suzuki (2000)] They would also allow the steam reforming of fuels such as LPG and natural gas without the need for a desulphurisation stage before the reformer. The use of a sulphur tolerant reforming catalyst allows the movement of the desulphuriser reactor downstream, where the reformat is already at the required temperature. Additionally, if sulphur tolerant water gas shift catalysts are used it needs only a H₂ separation membrane (provided the metal membrane is sulphur tolerant) to be used to strip out the sulphur, along with the other impurities in the reformat stream, before the fuel cell. The sulphur could then be removed by adsorption in the usual way on a zinc oxide bed, or recycled through the steam reformer combustor, without affecting the performance of the fuel processor.

1.5.8.2 Water Gas Shift

This is a two stage process comprising a high temperature shift (HTS) (260-370°C) and low temperature shift (LTS) (200-260°C). In order that the desired reaction takes place the reformat stream needs to be cooled to the correct temperature. This is done

by passing the reformer products through heat exchangers. With careful system design the heat energy extracted can be used elsewhere in the system to increase the overall thermal efficiency. Using these shift reactions, some of the CO present in the reformat can be used to release H₂ from water, increasing the volume of H₂ in the reformat. The water gas shift (WGS) process is well established at large scale. Cu is supported on ZnO and Al₂O₃ and encourages dissociative adsorption of H₂O, which releases H₂ and oxidises the catalyst. The catalyst surface is then reduced by CO, and CO₂ is produced. An associative pathway is also present, where on the Cu sites an intermediate product is formed from the CO and H₂O, which then decomposes into H₂ and H₂O. The WGS reactor is the largest part of the fuel processor due to the required low gas hourly space velocity (GHSV) required for the LTS reaction [Ref. J. Pasel (2004)]. The WGS reaction is relatively slow compared to reforming and is inhibited by thermodynamics at high temperatures. Low CO exit conditions require low temperature and high H₂O /CO ratios. Large variations in CO output from the WGS will adversely affect a downstream PrOx reactors performance causing variation in the CO fed to the fuel cell [Ref. Y. Choi (2003)].

The overall reaction (Equation 1.6) is exothermic.



The copper-based catalysts are pyrophoric so need to be protected from O₂ and water during start up of the fuel processor. Non-pyrophoric catalysts are being developed to address this problem [Ref. W. Ruettinger (2003)].

1.5.8.3 Carbon Monoxide Clean Up

Carbon monoxide concentrations of between 8 and 15% (Figure 2.1) are produced as a thermodynamic function of the reaction temperature and steam to carbon ratios required to achieve acceptable levels of hydrocarbon conversion at acceptable reactor temperatures. This has a detrimental effect on the performance of SPFCs due to competition for electro-catalyst sites in the fuel cell between CO and H₂ molecules.

This results in the fuel cell efficiency being drastically reduced and introduces the need for a H₂ purification system [Ref. C. Qi (2000)] There are several CO removal methods currently used. In addition the use of an air bleed at the anode can increase the tolerance of the fuel cell to CO.

1.5.8.3.1 Preferential Oxidation

This is the preferential oxidation of CO as shown in Equation 1.7. This reaction takes place over a catalyst between 200 and 100°C This means that little in the way of heat exchange is needed between the PrOX reactor and the WGS reactor or fuel cell. Catalytic selectivity is required to prevent the oxidation of H₂.



1.5.8.3.2 Palladium Membrane Separation.

This method of clean up produces almost pure hydrogen. A fine palladium silver alloy membrane is used which only allows hydrogen molecules to pass through it A high pressure differential is required on either side of the membrane in order that the hydrogen molecules are forced through it (typically 20 bars [Ref. J.R. Rostrup-Nielson (2000)]). The generation of the high pressure required, places large parasitic losses on the fuel cell system as a whole, reducing the overall system efficiency. The material cost of the membrane is also high reducing further its practicality. To reduce the costs of the membrane, thinner membranes on a metallic support have been investigated [Ref. S. Tosti (2003)]. This also has the effect of reducing the required pressure differential across the membrane [Ref. R A J Dams (1997)].

The H₂ produced will be at a low pressure whilst the off gas will be at high pressure. In a steam reforming system the advantage of this is that it allows greater flexibility in the combustor design with regards to temperature control systems. A draw back is that

because the H_2 is at low pressure it is not possible to use metal hydride storage devices to help the system cope with transient response

1.5.8.3.3 Methanation

This usually takes place over a heterogeneous catalyst such as nickel or alumina at 600°C [Ref. R A J. Dams (1997)]. A disadvantage of methanation is that it reduces the amount of H_2 in the fuel reformat as shown in equation 1.8. If large amounts of CO are present then the reduction in H_2 can be significant due to the stoichiometry of the reaction.



1.5.8.3.4 Pressure Swing Adsorption.

Pressure swing adsorption (PSA) relies on the fact that under pressure, gases are attracted to solid surfaces. The higher the pressure the more gas is adsorbed. When the pressure is released the gas is released. Because different gases are attracted to different solids more or less strongly than others the PSA process can be used to separate out a mixture of gases [Ref. R.A J. Dams (1997)]. In the case of SPFC applications the CO in the fuel reformat can be separated from the hydrogen and discarded leaving a clean fuel for the SPFC to use. Large adsorbent beds are required however and the technology is better suited to large plant applications than smaller scale ones e.g. automotive. However, fast cycle PSA systems are now being offered at small scale which may open up the technology for the small scale market.

An advantage of this system is that the H_2 remains at high pressure after the reactor. This facilitates the use of metal hydride storage to smooth out the transient response of the fuel cell system. It does mean however that the off gas fed back to the combustor in a steam reforming system is at ambient pressure and this would greatly influence the combustor design and temperature control strategy.

1.6 Conclusions

From the above discussion it is clear that the question of how to supply hydrogen to the SPFC is one that has not been adequately solved. This Ph.D. addresses that issue. It aims to improve the performance of the steam reformer. The reasoning behind the choice of steam reformer is as follows:

A steam reformer can use any unused H_2 from the fuel cell exhaust to partially fuel its combustor. This improves the overall system efficiency. It is not possible to use the unused H_2 in this way when utilising a POX or ATR system. A steam reformer can utilise any unconverted hydrocarbon fuel in the combustor to provide some of the energy required to support the steam reforming reaction. This improves the overall system efficiency. Steam reforming produces the highest amount of H_2 per mole of fuel. This can be clearly seen from equations 1.4 and 1.5. Steam reforming is endothermic so the reaction cannot run away. This is the opposite situation to that of POX and ATR, where if the control system fails there is the possibility that the reaction will run away. This means that in the event of a control failure the steam reforming reaction will halt itself. Steam reforming and POX methods are simpler than ATR to run. POX is the simplest as it doesn't require external water or heat supplies.

It is thought that performance increases can be made in the following ways. Traditional steam reformers control the temperature of the reactor based on the exit temperature of the reformer. This creates a temperature gradient along the length of the reactor introducing inefficiencies into the system. By accurately controlling the reactor temperature along its length it is thought that improvements in efficiency can be achieved. Packed bed reactors are by their nature bulky pieces of equipment. By using novel heat exchanger technology the size of the reformer can be substantially decreased. Because the steam reforming reaction is endothermic it is limited by the rate of heat transfer to the reformer. Because of this traditional steam reformers have had poor transient response capabilities. The use of novel heat exchanger technology coupled with close control of the reactor temperature will rectify that situation. By

incorporating a novel sulphur tolerant reforming catalyst the size of the complete fuel processor will be decreased.

The aim of this Ph.D. is to develop and evaluate a compact 'fast response' hydrocarbon fuel processor with integrated control software and novel design concepts for use with both stationary and transportation applications using PEM fuel cells.

2 System Simulation

In order to understand better the steam reforming process and to develop a test matrix for use with the microchannel reactor, equilibrium modelling was carried out. This modelling was initially carried out using the Aspen Plus software from Aspen Inc. The data gained was later entered in to an Excel spreadsheet so that at-a-glance results could be ascertained for a range of operating conditions.

2.1 Overview of Aspen Plus

The first stage of work to be completed was initial system modelling using the Aspen Plus program. This program allows chemical plants to be simulated quickly so that design decisions can be made.

Aspen Plus (Aplus) is a chemical equilibrium-modelling program from AspenTech. It allows the user to model chemical processes and plants and determines the effect of making changes to the system. There are 6 basic stages that the user has to go through to set up and run a simulation in Aspen.

- **Creating the model:** This is done using a drag and drop method where blocks and streams are placed on the flowsheet in the configuration desired.
- **Defining the stream components:** Before running a simulation it is important to define which components (Chemical species) are going to be used. Once this is done the stream properties (flow rate, mass fraction, temperature and pressure) can be specified
- **Block properties:** Here the operating conditions for the blocks are set. In the case of a Gibbs reactor the outlet temperature and pressure must be set.
- **Sensitivity analysis:** This allows the user to adjust one or more parameter over a user-defined range of values in order that the sensitivity of the system to the change can be determined. The results can then be plotted.

- Running Once the model is complete the simulation can be started Aspen will then report any errors that occurred whilst the simulation was run and warn the user
- Results viewing The results can be viewed as individual block or stream data, or in the case of the sensitivity data as plots.

The operation of Aplus was initially verified against various reaction data

Aplus was used to generate data for the design of the test-rig, such as sizing the MFCs required for the rig operation. It was also used to narrow the focus of the test matrix by providing initial guesses about the optimum operating conditions of the reformer.

2.2 Liquid Petroleum Gas and Methane Reforming Simulation

2.2.1 Steam Reforming

The effects of temperature and steam to carbon ratio on the equilibrium products of the steam reforming of LPG and CH₄ were investigated using Aspen Plus

The LPG mixture used in the following work can be seen in Table 2.1

Component	% Vol
Propane	91.4
Propylene	6.1
Ethane	2
Butane	0.4
Methane	0.1

Table 2.1: Composition of LPG

In order to calculate the amount of water required to make up the correct steam to carbon ratio, the carbon ratio per molecule of LPG first needed to be calculated. It was done as shown in Equation 2.1.

$$C_{LPG} = V_p C_p + V_{pr} C_{pr} + V_e C_e + V_b C_b + V_m C_m \quad \text{Equation 2.1}$$

Where C_{LPG} is the carbon ratio per molecule LPG, $V_p, V_{pr}, V_e, V_b, V_m$ is the % vol of propane, propylene, ethane, butane and methane respectively, and $C_p, C_{pr}, C_e, C_b, C_m$ is the carbon ratio per molecule of propane, propylene, ethane, butane and methane respectively.

2.2.1.1 Method

A simple flow sheet was used which utilised a Gibbs reactor in the place of the reformer. The Gibbs reactor works on the basis of the minimisation of Gibbs free energy when a reaction reaches equilibrium.

The flow rate of LPG and CH_4 were set at 1 mol/min. Because only equilibrium modelling was used here, and the interest was primarily on the percentage composition of the products, the results gained are independent of overall flow rate of the reactants. The steam to carbon ratio was varied from 1 to 3.5 in increments of 0.5. The reformer temperature was varied from 300 to 1000°C in increments of 50°C. The results were plotted as % composition against reformer temperature and as % composition against steam to carbon ratio (Figures 2.1, 2.2).

2.2.1.2 Results

For these simulations the effects of steam to carbon ratio and reformer operating temperature were examined.

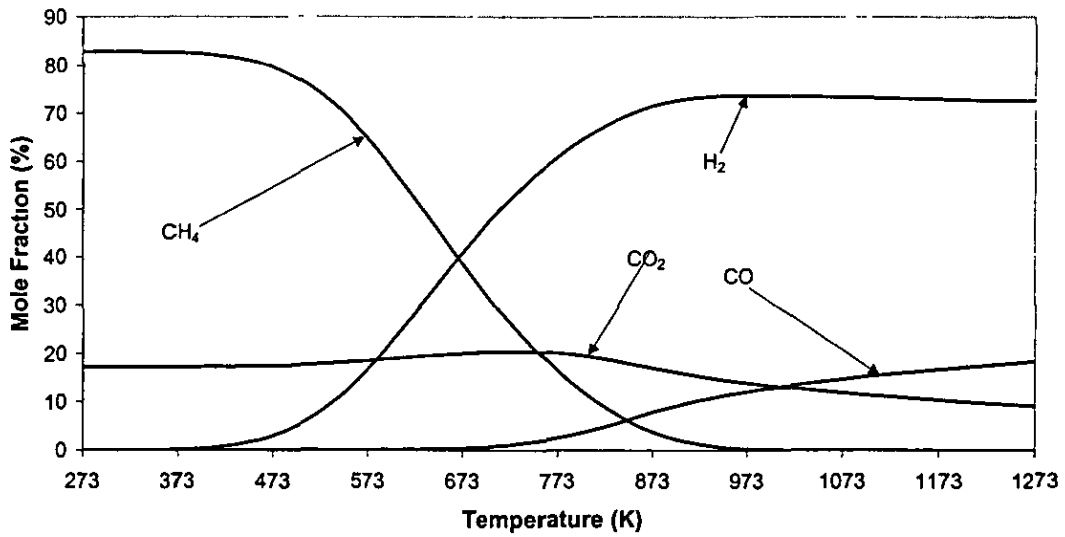


Figure 2.1: The Effect of Temperature on the Dry Products of Steam Reforming of LPG at S/C = 3.5

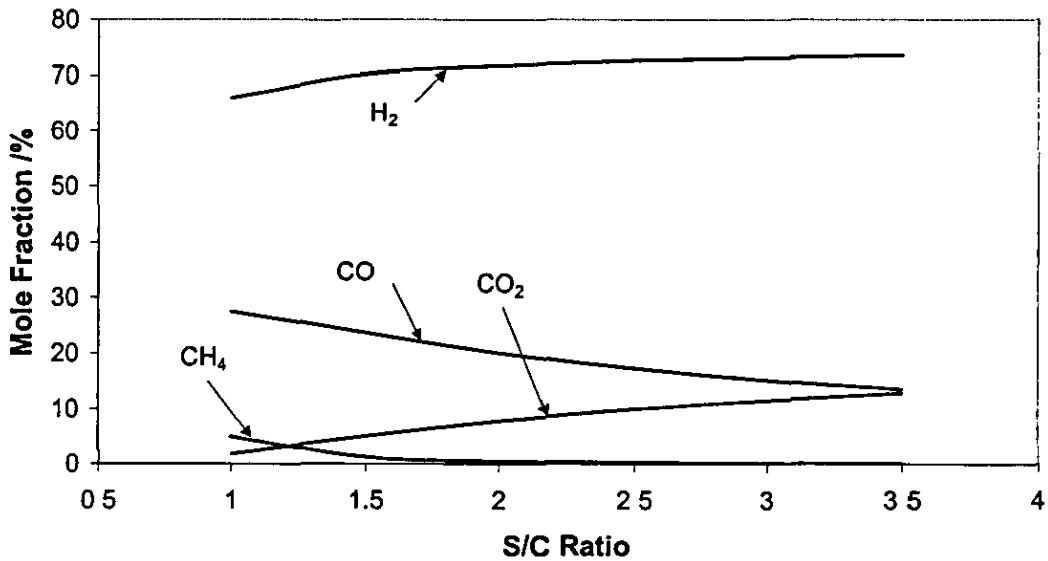


Figure 2.2: The Effect of Steam to Carbon Ratio on the Dry Products of Steam Reforming LPG at 750°C

For LPG it can be seen that the influence of temperature on the composition of the reactants is very strong. It can clearly be seen that as the temperature increases so does the production of H₂. Unfortunately this also accompanies an increase in the production of CO. However, it can be seen that there is a limit to the amount of

hydrogen produced by raising the reaction temperature. Conversely, it can be seen that CO production continues to increase. From this it can be seen that there is a maximum useful operating temperature for the steam reforming process beyond which the reformer efficiency will decrease. It can be seen that by increasing the S/C ratio the amount of CO produced can be reduced. This accompanies an increase of H₂ production and can be accounted for by the influence of the water gas shift reaction. This was mirrored by the results for the steam reforming of CH₄ (Figures 2.3, 2.4)

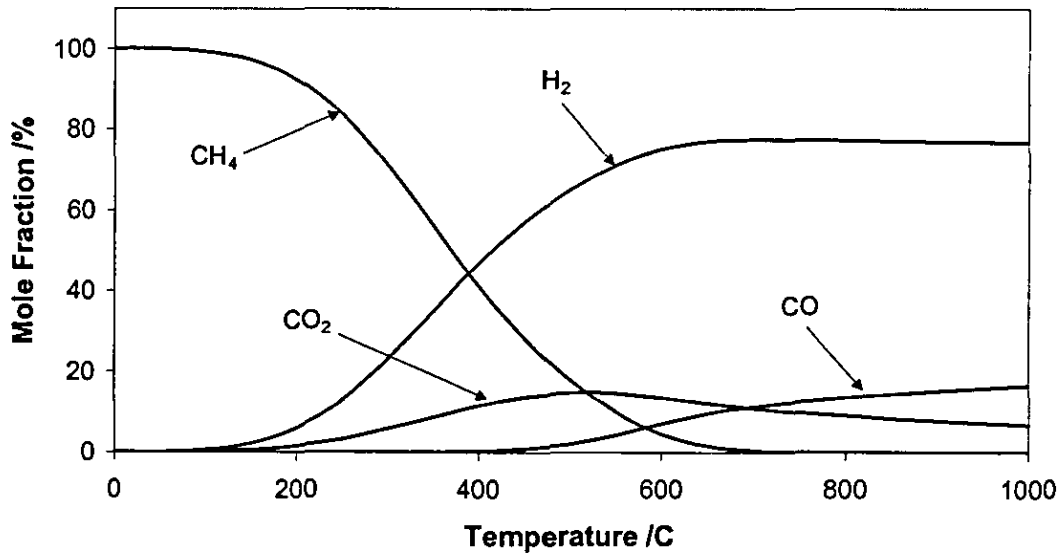


Figure 2.3: The Effect of Temperature on the Dry Products of Steam Reforming of CH₄ at S/C = 3.5

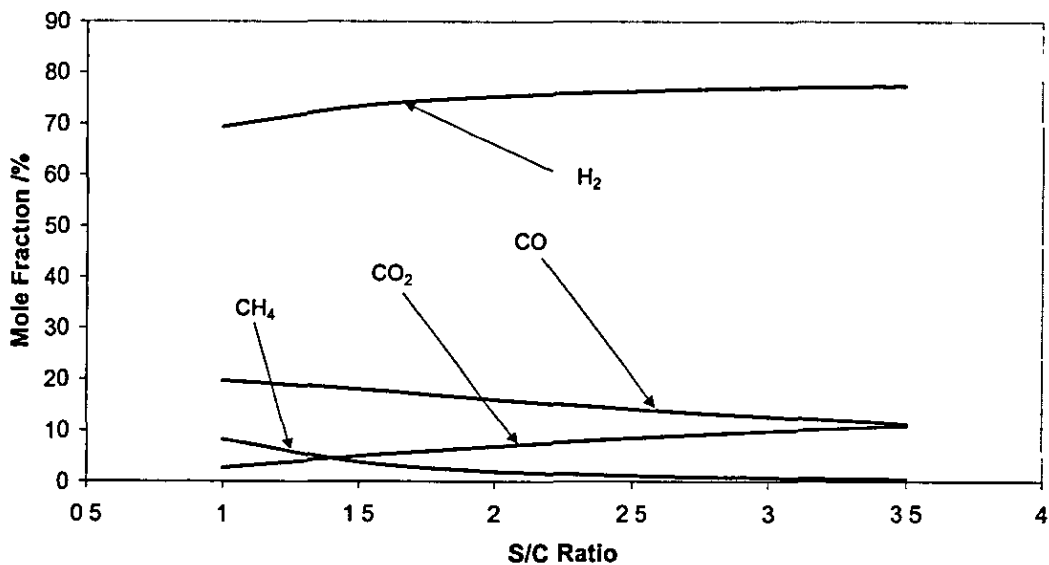


Figure 2.4: The Effect of Steam to Carbon Ratio on the Dry Products of Steam Reforming CH₄ at 700°C

It can be seen from the simulation results that the temperature control of the steam reformer is critical for determining the product composition of the reformer. It also shows that by operating at higher than stoichiometric S/C ratios the production of CO can be reduced.

2.2.2 Autothermal Reforming

It was decided to model the autothermal reforming of LPG and CH₄ to compare the output of an ATR with a steam reformer to determine if ATR held any advantages over steam reforming for the use of LPG reforming.

2.2.2.1 Method

The method for autothermal reforming (ATR) using Aplus is more complex than that required for steam reforming. The effect of steam to carbon and oxygen to carbon ratios were examined as well as the effect of the inlet temperature to the reformer. It is first necessary to determine the autothermal point.

The S/C ratio was varied from 1 to 2 in intervals of 0.5. For each S/C ratio the O₂/C ratio was set to 0.38 and 0.5. For each of these set points the reactants temperature was varied from 300 – 900°C in 50°C increments. At the same time the reformer temperature was varied from 300 –900°C in 50°C steps. When the net duty of the reformer is equal to zero, autothermal conditions are reached. To improve the accuracy of the results net heat duty was plotted against the reformer outlet temperature for all inlet temperatures (Figure 2 5).

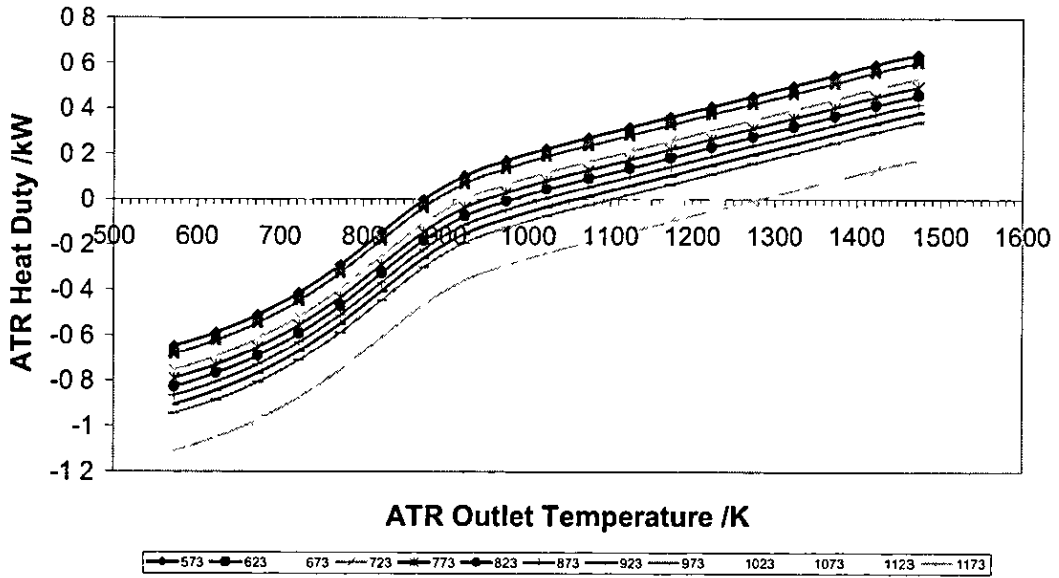


Figure 2.5: The Heat Duty of the ATR of LPG for Varying Inlet and Reformer Temperatures at $S/C = 2$, $O_2/C = 0.38$

Where the net heat duty is equal to 0 the point was recalculated using a finer increment. When the correct reformer temperature was found the results were fed back into Aspen Plus and the percentage reformat composition was plotted against inlet temperature (figure 2.6).

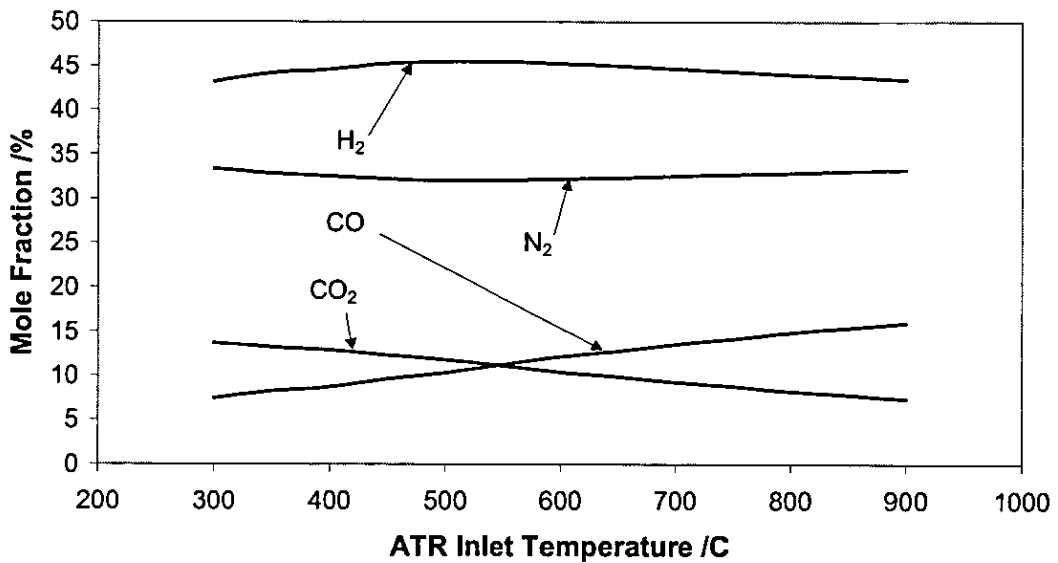


Figure 2.6: The Effect of Inlet Temperature on the ATR of LPG at $S/C = 2$, $O_2/C = 0.38$

2.2.2.2 Results

The behaviour of ATR with regards to the influence of S/C ratio is as expected from the steam reforming results. Increasing the S/C ratio increases the hydrogen production, whilst reducing the production of CO. Increasing the reactor temperature also increases the amount of CO produced. However with increasing temperature the hydrogen production also begins to reduce after it peaks. This is due to combustion of the hydrogen. Increasing the O₂/C ratio has little effect on the CO production as a percentage volume of the products flow. It does however reduce the percentage of hydrogen in the product stream, whilst increasing further the dilution of the products by nitrogen. The best results for LPG were found to occur at 550°C with an O₂/C ratio of 0.38 and S/C ratio of 2. For CH₄ the best results were found to occur at 800°C with an O₂/C ratio of 0.38 and S/C ratio of 2.

2.2.3 Conclusions

It is clear from the above simulations that steam reforming produces a higher purity of H₂ from a given amount of feedstock than does ATR. This is largely because of the dilution of the products with nitrogen from the air provided to the reactor. The percentage of CO produced by either method is comparable.

2.3 Determining the Reactant Feed Requirements

Equilibrium simulations were also used to determine the size of the mass flow controllers (MFC) required to supply the steam reformer with the required amount of LPG.

2.3.1 Method

To calculate the size of MFC required to feed the combustor, sensitivity analysis was carried out using Aspen Plus. The flow rate of LPG to the reformer was varied from 1

to 5 SLPM in increments of 1 SLPM. The steam to carbon ratio was set to 1.5, 2 and then 2.5. The reactor exit temperature was set to 600, 700 and 800°C. Aspen Plus was then used to calculate the heat required to support the steam reforming reaction

A stoichiometric mixture of H₂ and air was reacted in a Gibbs reactor. The flow rate was varied until the heat produced matched the heat required to support the steam reforming reaction.

2.3.2 Results

It was decided to operate the reformer initially at a power rating of 0.5kWe. This equates to a flow rate of 7.5 SLPM of hydrogen in the product stream [Ref. M. Virgi (2000)]. The required amount of LPG and water to produce 7.5 SLPM H₂ was evaluated over several temperatures and steam to carbon ratios using Aspen Plus. The results can be seen in Table 2.2

LPG					
Reformer Temperature	2	2.5	3	3.5	S/C Ratio
700°C	2.17	1.72	1.47	1.31	SLPM
750°C	1.99	1.52	1.29	1.17	
H ₂ O					
Reformer Temperature	2	2.5	3	3.5	S/C Ratio
700°C	3.49	3.44	3.54	3.70	Fluid ml/min
750°C	3.19	3.05	3.12	3.30	

Table 2.2: The Required Flow Rate of LPG and H₂O to Produce 0.5 kWe at Equilibrium

From the data in Table 2.2 and the results shown in Figures 2.7 – 2.8, the required mass flow controllers were sized according to what was already available and that which required buying in.

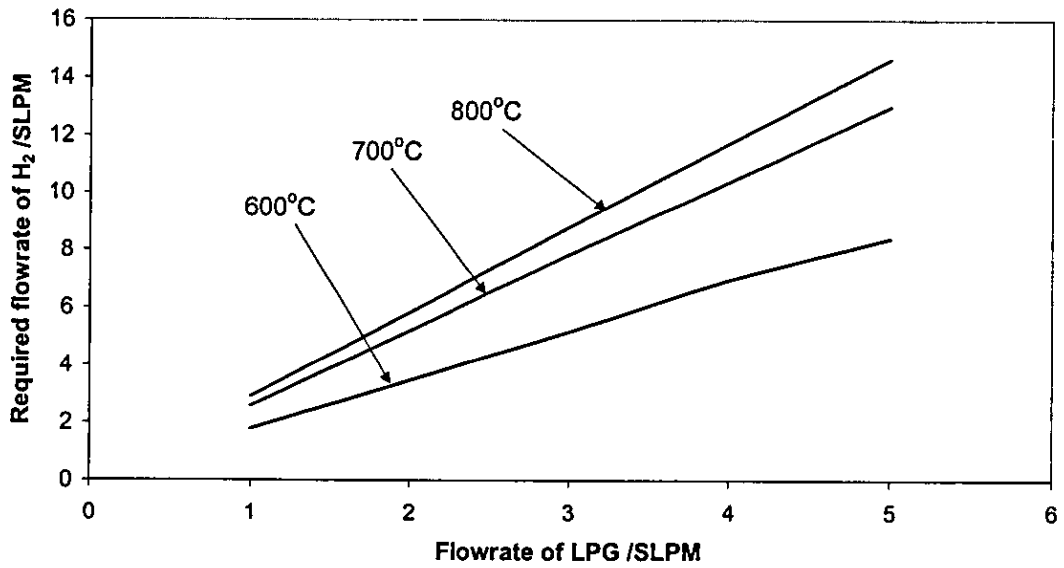


Figure 2.7: The Required H₂ to Support the Steam Reforming Reaction Over Varying LPG Flowrates and Temperatures at S/C = 2.5

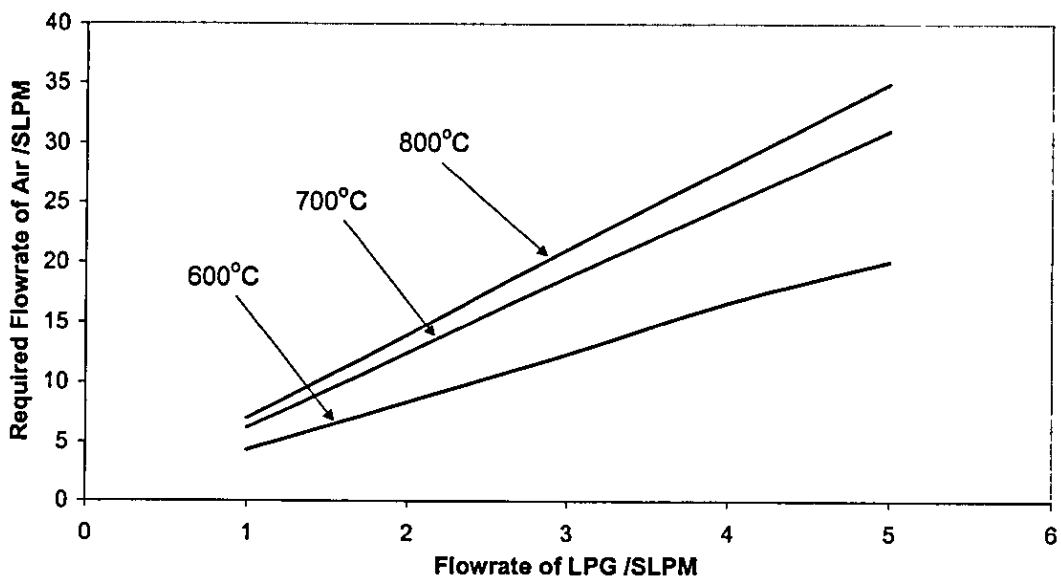


Figure 2.8: The Required Air Feed to the Combustor to Support the Steam Reforming Reaction Over Varying LPG Flowrates and Temperatures at S/C = 2.5

The required hydrogen and air flow rates to support the steam reforming of LPG at the above set-points are summarised in Table 2.3.

H ₂					
Reformer Temperature	2	2.5	3	3.5	S/C Ratio
700°C	3.14	3.06	2.98	2.91	SLPM
750°C	3.32	3.26	3.20	3.12	
Air					
Reformer Temperature	2	2.5	3	3.5	S/C Ratio
700°C	7.52	7.32	7.13	6.95	SLPM
750°C	7.92	7.78	7.65	7.45	

Table 2.3: The Required Flow Rates of H₂ and Air Required to Support the Steam Reforming Reaction.

2.3.3 Conclusion

It was decided to scale the mass flow controllers for a fuel cell with an output of 0.5kWe. It was determined that a supply of 7.5 SLPM H₂ needed to be produced by the reformer to allow the fuel cell to run at those conditions. From the result above it was decided to size the MFCs for reformer temperatures of 700 and 750°C and steam to carbon ratios of 2 to 3.5. The resulting sizes of the MFCs can be seen in Table 2.4. The oversizing of the air and LPG MFCs was due to the availability of existing MFCs in the Laboratory stores.

H ₂	0 – 5 SLPM
Air	0 – 25 SLPM
LPG	0 – 25 SLPM
Water	4 ml/min (LPG)

Table 2.4: The size of the Mass Flow Controllers

2.4 A Fuel Cell System Simulation

It was decided that in order to better understand the place of the combustor/reformer in a complete system as regards the efficiency of operation of the system and the effect of different operating strategies on the efficiency, that some systems modelling would be necessary. Excel was chosen as a starting point for ease of use and simplicity of operation. The significance of this modelling work for the real life operation of the combustor/reformer is that it serves as a tool to set good first approximations of suitable operating parameters. It allows the user to make connections between the experimental work and how it fits in to a complete fuel cell system in terms of the end product of electrical power. It also gives guidance as to the direction that the development of the control strategy by suggesting features that the controller should contain. An example of this may be the calculation of extra fuel needed to sustain the reforming process and how this can then be metered along with the H₂ effectively.

To further improve the usefulness of the model in this respect it is necessary to develop a transient model of the reactor behaviour.

2.4.1 Excel Model Description

The systems model uses a combination of calculated results based on thermodynamic formulas and look-up tables generated by Aspen Plus, as well as model data previously developed [Ref. M. Virgi (2000)].

The systems model is divided into 5 sections.

- Data and constants.
- User settings.
- Reformer.
- Combustor.
- Power Balance

2.4.1.1 Data and Constants

The specific heats are calculated according to Equation 2.2.

$$C_p = a + bT + cT^{-2} \quad [\text{Ref. G F.C. Rogers (1980)}] \quad \text{Equation 2.2}$$

Where a, b and c are gas specific constants.

Because C_p is temperature dependent it becomes necessary to integrate Equation 2.2 for use in calculating the thermal energy in a gas or the enthalpy of combustion for a gas at a specific temperature. Equation 2.3 shows the equation for calculating the change in enthalpy of formation of a gas.

$$\Delta H_{f_i} = \Delta H_{f_o} + \int_{T_o}^{T_i} C_p dT \quad [\text{Ref. G.F C Rogers (1980)}] \quad \text{Equation 2.3}$$

All of the thermal calculations are based around a datum temperature of 25°C (298.15K).

2.4.1.2 User Settings

The user has five choices to make as regards the operation of the model.

- Fuel Cell electrical output
- Fuel to be reformed (LPG/CH₄)
- Reformer temperature
- Reformer inlet temperature
- Steam to Carbon ratio

2.4.1.3 Reformer Model Description

The flow rate of H₂ required at the fuel cell anode depends on the amount of power the fuel cell is required to produce. Setting the fuel cell power output in the user section therefore determines the amount of H₂ that needs to be produced by the reformer. From this, the amount of fuel and steam required for reforming is calculated, using look-up tables that were generated using Aspen Plus and the steam to carbon ratio. The amounts of fuel and steam are then modified to take into account incomplete conversion of the fuel using a fuel conversion factor.

The reformer products are calculated using look-up tables developed using Aspen Plus. These tables use the flow rate of the fuel to be reformed with the reformer temperature and steam to carbon ratio to calculate the composition of the reformat stream. A mass balance check is performed to ensure that the model is working correctly. The thermal power required to support the reforming process is calculated in four parts. Firstly the amount of thermal power contained in the reactants at inlet temperature is calculated. This is done by using the reactants temperature, and mass flow rate [Equation 2.4].

$$P_t = \left(m \times \int_{T_i}^{T_2} C_p dT \right) / \eta_h \quad \text{Equation 2.4}$$

Where P_t is the thermal power, and η_h is the heater efficiency.

In the case of heating the water, the partial pressure of the mixture is calculated. This is then used to find the boiling point of the water using a look up table. From this the appropriate specific heat is used, as well as the latent heat of vaporisation if required. The amount of power supplied to the heater to raise the temperature to the desired temperature is also calculated. Secondly, the power required to raise the reactants to the desired temperature of the reformer is calculated. Next, the power required to support the steam reforming process is gained from a look-up table again generated using Aspen Plus, before the thermal power lost in the exhaust is calculated. The

thermal power required to support the steam reforming reaction at the desired temperature is then calculated as shown in Equation 2.5.

$$P_C = P_R + P_{SR} + P_P - P_I \quad \text{Equation 2.5}$$

Where P_C is the total power required from the combustor, P_R is the power required to raise the reactants to the reactor temperature, P_{SR} is the power required to support the steam reforming reaction, P_P is the power in the reformer product stream, and P_I is the power in the reactants at the inlet to the reformer.

2.4.1.4 Combustor Model Description

Since the fuel cell is practically operated at above H_2 stoichiometry, the excess H_2 can be burnt to heat the reformer. The amount of hydrogen available depends on the fuel cell operating power. As stated CO_2 passes straight through a SPFC and so this is exhausted with the excess H_2 . For the model the amount of CO_2 in the fuel stream is taken from the reformer products look-up table as described above. There is also air available in the cathode exhaust (10% O_2 , 90% N_2) The amount is again dependent on the fuel cell operating power.

The power produced by the combustion of the H_2 is calculated as follows in Equation 2.6

$$P_c = (\dot{m} \times \Delta H_{f_{H_2O}} \times \% H_2 \text{ Conversion}) \quad \text{Equation 2.6}$$

Where P_c is the power released due to combustion of hydrogen.

The power used to heat the reactants to the desired temperature is calculated as before. The combustion products are calculated using Equations 2.7-8 with unburned fuel and excess air also being taken into account.



From Equations 2.7-8 the production of water and CO₂ are calculated. For every mole of H₂ burnt, 1 mole of H₂O is produced and so on. This allows for incomplete combustion of the fuel to be taken into account. Any unburned fuel is also accounted for in the exhaust by multiplying the available fuel by the percentage fuel conversion. The N₂ goes straight through the combustor without reacting and the O₂ is calculated by first calculating how much is used to burn the fuel and then subtracting this amount by the O₂ available. The model can then add extra O₂ in the form of air if so required.

The power available for use from the combustor is then calculated as shown in Equation 2.9.

$$P_C = P_F + P_A - P_E \quad \text{Equation 2.9}$$

Where P_C is the power available from the combustor, P_F is the power generated by combustion of fuel, P_A is the power in the air at the combustor inlet, and P_E is the power in the combustor exhaust.

The air is preheated using a heat exchanger (HEX), which takes heat from the combustor exhaust and transfers it to the incoming air. This is to increase system efficiency. The effectiveness of the HEX can be set by the user. The available power from the combustor is then factored using the thermal efficiency of the HEX between the combustor and reformer and compared with the power required to support the steam reforming reaction. If extra power is required to support the steam reforming process, the model adds in some extra fuel in the form of either CH₄ or LPG depending on the fuel selected by the user. The amount of extra CH₄ or LPG is calculated iteratively so that the amount of fuel takes into account the new exhaust composition caused by burning the fuel and the power required to heat the fuel to the combustor temperature

2.4.1.5 Power Balance

This is in the form of a thermal power balance which takes into account all of the sources and sinks of the system. This is to verify that the model is working properly and not creating or destroying energy.

The model also calculates the overall system efficiency by comparing the total amount of thermal power available to the reformer with the amount of thermal power that is actually used to support the steam reforming

2.5 Results

The Excel model was used to inform the development of a dynamic reactor model developed using the Matlab/Simulink software and detailed in Chapter 7

3 Reactor Design and Novel Technology

3.1 Reactor Design

The design of the reactor used for fuel reforming has a significant effect on reforming efficiency, system start-up time and transient response. As has been seen, this is particularly important in steam reforming since the rate of reformation is limited by the rate of heat transfer to the reactants. There are a number of potential technologies that can be used for the reactor design.

3.1.1 Packed Bed Reactors

Packed bed reactors typically contain a series of tubes filled with a catalyst in the form of pellets or granules. The design is relatively simple and easy to maintain [Ref. C.D. Dudfield (2000)]. They have been widely used in the industrial-scale steam or partial oxidation methods of reforming. At small-scale, the residence time of the reactant is limited and the performance of the reactor suffers as a result. Additionally, the rate of heat transfer through walls and within the catalyst bed limits the rate of reaction of the reactants [Ref. D.G. Loffler (2003)]. Another difficulty with down-scaling tubular reactors is that if the diameter is decreased the length of the reactor needs to be increased. This leads to bundled tubes like that of the IdaTech reformer shown in Figure 1.8. The catalyst needs to be used much more effectively than at industrial-scale to maintain good reaction efficiency. The major advantage of using catalyst pellets in a tubular reactor is that it produces a torturous path. This has the advantage that it offers some resistance to poisoning agents. This is due to the outermost layers being greatly poisoned but the poison not penetrating to the subsequent layers. The major disadvantage of this type of arrangement is that a lower active surface area is available, so the volume of catalyst required for equivalent performance is much higher than that for a washcoated catalyst. A more compact and efficient reactor design is needed.

3.1.2 Ceramic Monolith Reactors

Ceramic monolith reactors coated with catalyst offer several advantages over packed bed reformers. They have a higher surface area to volume, large frontal open area, low thermal mass, low heat capacity, low thermal expansion, high strength, and high temperature of operation. These advantages give the reactor quicker start-up, a higher conversion rate, reduced pressure drop along the reactor and improved thermal and mechanical shock resistance than the packed bed type of reactors. The drawbacks are lower content of active material per reactor volume and poor heat transfer performance due to the heat conductivity of ceramic material [Ref. B. Lindstrom (2002)]. Monolith reactors have been favoured for ATR use (rather than steam reforming) where heat management is not as critical. Catalysts are applied to the monolith using a washcoating technique. Firstly, the monolith is coated with a washcoat solution. This increases the surface area of the monolith by roughening it. In this way the surface area of the monolith can be improved by a magnitude of 5000. The catalyst can be applied to the washcoated surface by dipping or injecting the catalyst. The main advantage of a washcoated monolith is that they allow a more even distribution of the reactants. This helps to eliminate any hot or cold spots as a result of localised areas of reaction. A disadvantage is that because the monolith is basically made up of a bundle of tubes, any poison in the reactant stream will quickly coat the catalyst

3.1.3 Microchannel Heat Exchangers

Microchannel heat exchangers are made of a diffusion bonded laminate. Inside the heat exchanger multiple layers of shims create alternating microchannels and fins (Figure 3 1). The microchannel widths are determined by the thickness of the shim material whilst the heights and lengths of the channels are determined by the machined surface. The machining can be either by photochemical or stamping processes. This allows for a low cost method of making the shims. The shims are diffusion bonded together under high temperature and pressure (1173 K, 27 MPa for 4 h) to yield a monolithic metal block that removes the need for gaskets or other seals. This kind of heat exchanger has significantly higher heat transfer rates than most

conventional designs. Experiments at Imperial Chemical Industries plc. evaluating the heat transfer performance of microchannel type, photochemically etched heat exchangers, found that a heat exchanger containing channels with a depth of 0.3mm, had a volumetric heat transfer performance equivalent to 7 MW/m³K with a water velocity of 0.18m/s. The equivalent shell and tube, and plate heat exchangers had performance listed as 0.21 MW/m³K and 1.25MW/m³K respectively. [Ref. E.A. Foumeny (1991)]. Table 3.1 [J.L. Zilka-Marco (2000)] shows the advantages of microchannel technology when used as a fuel vaporiser (CMFV) for fuel cell applications. It highlights the heat transfer advantages of using microchannels as well as its size and transient response time advantage over other technologies.

Feature	CMFV	Other Emerging technologies*	Conventional Boiler Technology	Competitive Advantage
Volume	0.35 litres	3 litres	>10 litres	One-tenth the size
Weight	4 lb	10 lb	>50 lb	Lightweight, Portable
Transient Response	Response time of seconds	Response time of minutes	Response time of minutes	Responsive to variable automotive load requirements
Heat Flux per Unit Volume (W/cm ³)	11.5	~1.2	0.1 to 1	10 times more heat per unit volume
Fabrication Method	Low-cost laminate fabrication	Conventional extrusion, machining and welding	Conventional extrusion, machining, and welding	Low labour cost, consistent quality
* All work is in the development stage, information is proprietary, estimates are provided where possible				

Table 3.1: A Comparison of Microchannel with other Competing Technologies

If microchannel technology is used as the basis of a steam reformer, high rates of heat transfer will be available between the combustor and reformer. As a limiting factor of steam reformer performance is the rate of heat transfer to the reactants this is advantageous

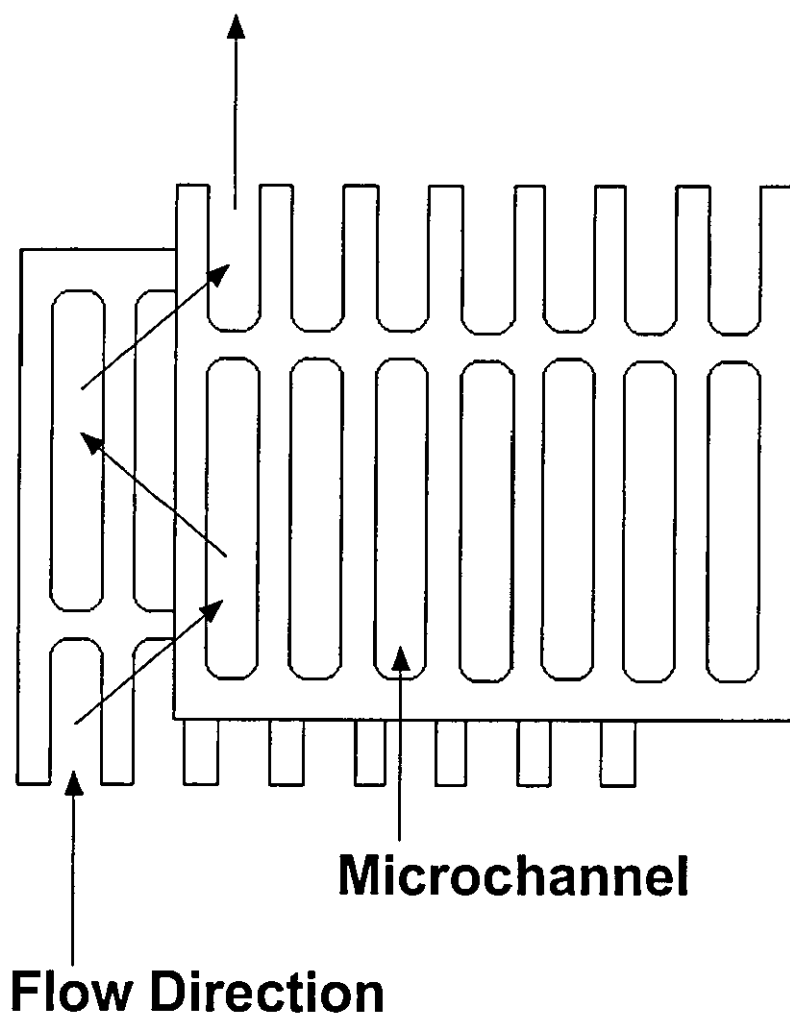


Figure 3.1: Simplified Microchannel Shims

Microchannel reactors can be made more compact than the equivalent tubular reactor. This has advantages from a packaging point of view as well as from a marketing standpoint. The size can be reduced in this way because of the high rates of heat transfer possible using this technology. This type of reactor also has a very high active surface area to volume ratio. The high rates of heat transfer also mean that the efficiency of the reactor is better than that of an equivalent tubular reactor. Microchannel reactors also show significantly lower pressure drops than tubular reactors, whilst still maintaining the ability to provide thorough mixing of the reactants [Ref. C.D. Dudfield (2001)].

The nature of the microchannel design means that the whole fuel processor can in theory be made as one unit. This is because the internal flow path of the reactor can be designed as desired, by simply etching grooves into the shims where required. This removes the need for external piping, which would otherwise be a source of heat loss from the system. It also removes the need for gasketing joints between the components of the fuel processor. Because of the temperature of operation of a steam reformer this offers a considerable advantage when building a system. The technology is scaleable so can be used to make up a modular system. If a 2 kW reformer is required, two 1 kW reformers can be coupled together. This flexibility of design means that an open architecture approach to system design can be undertaken. Each system built of common components, but only the components required for that system.

A drawback of this type of reactor is the possibility that the microchannels will become blocked. The most likely cause of a blockage would be carbon deposition inside the reactor. This can be overcome by operating at a sufficiently high steam to carbon ratio or by using filters at the inlets to the reactor to stop foreign objects in the feeds from causing a blockage. Because of the self-contained nature of the reactor design, maintenance on the internal structure of the reactor is impossible. Additionally if the catalyst becomes damaged it would not be able to be replaced. Coupled with the standalone cost of the reactor this is a big disadvantage over current technologies. However, the cost is high presently due to the small volume production of this novel technology. It is anticipated that the cost will fall as production volumes go up

3.2 Manufacturing Methods

Diffusion bonding makes use of the electrostatic bonds between molecules to produce a seamless join between two substances. In the case of the reactor the bond is made between each stainless steel layer.

Diffusion bonding takes place at elevated temperature and load. The surfaces to be bonded are held together under these conditions, usually in a vacuum or protective atmosphere, for an extended period of time. The process can take place as a liquid

phase or solid phase. In the case of the reactor a solid phase method was employed Heat can be applied to the metal by radiant, induction, direct or indirect resistance heating Pressure can be applied uniaxially or isostatically. Under uniaxial conditions the pressure is limited because of a desire to minimise macrodeformation of the parts This requires that the initial surface finish of the parts to be bonded is critical. Under isostatic conditions the pressure can be elevated much higher. This means that the initial surface finish of the parts does not need to be as high quality, it also allows complex geometries to be bonded.

3.3 Description of the Microchannel Reactor

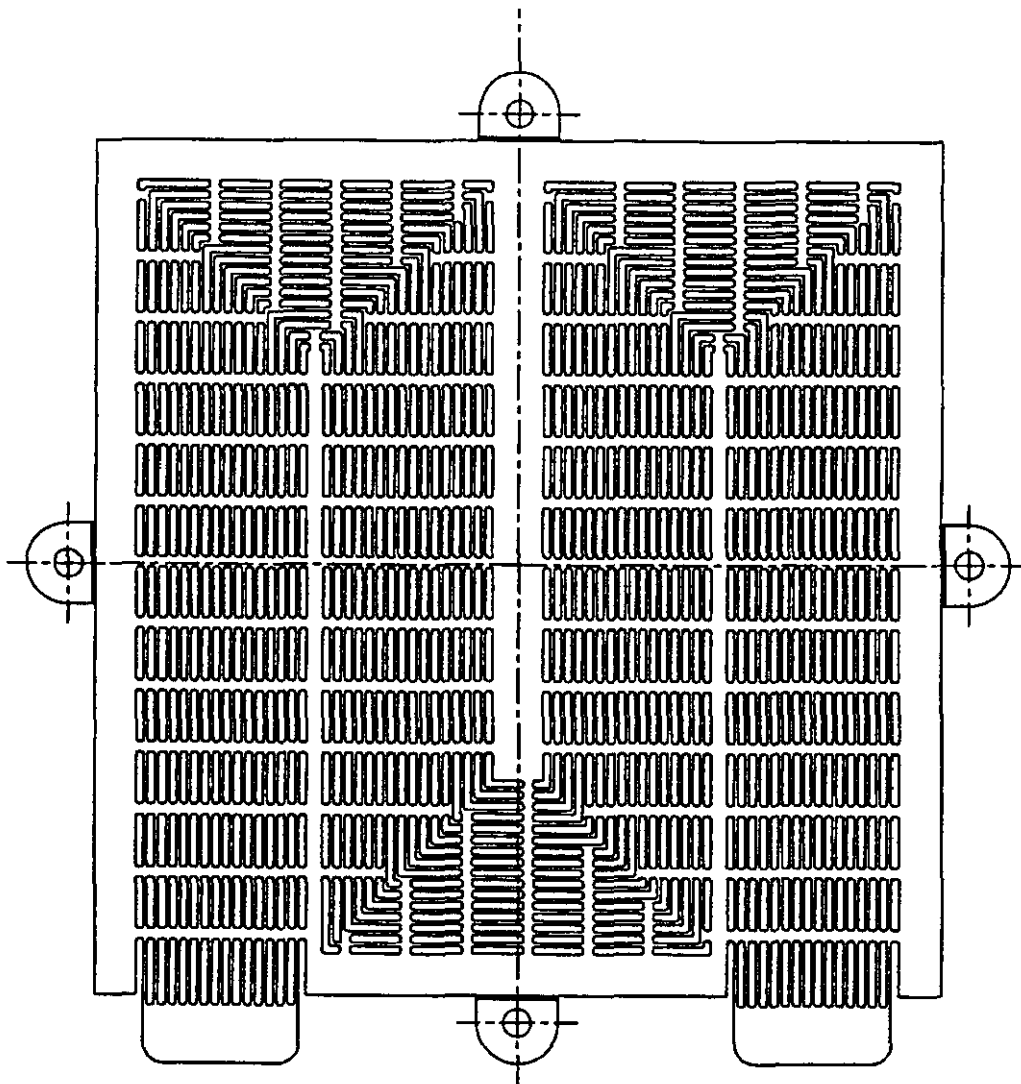
3.3.1 Plate Details

The reactor is built up out of 113 shims. Each shim is made of 316 Stainless Steel with dimensions of 125 x 125 x 0.5 mm. The shims are arranged as shown in Table 3.2.

Number of Shims	Part Number	Description
12	KTS10004	Side Plate
8 of each	KTS10014 KTS10015 KTS10016	Reformer Stream
1	KTS10004	Separating Plate
3	KTS10018	Thermocouple Plate
1	KTS10004	Separating Plate
8 of each	KTS10001 KTS10002 KTS10003	Combustor Air Stream
1	KTS10017	Perforated Plate
2 of each	KTS10011 KTS10012 KTS10013	Combustor Fuel Stream
1	KTS10004	Separating Plate
3	KTS10018	Thermocouple Plate
1	KTS10004	Separating Plate
8 of each	KTS10014 KTS10015 KTS10016	Reformer Stream
12	KTS10004	Side Plate

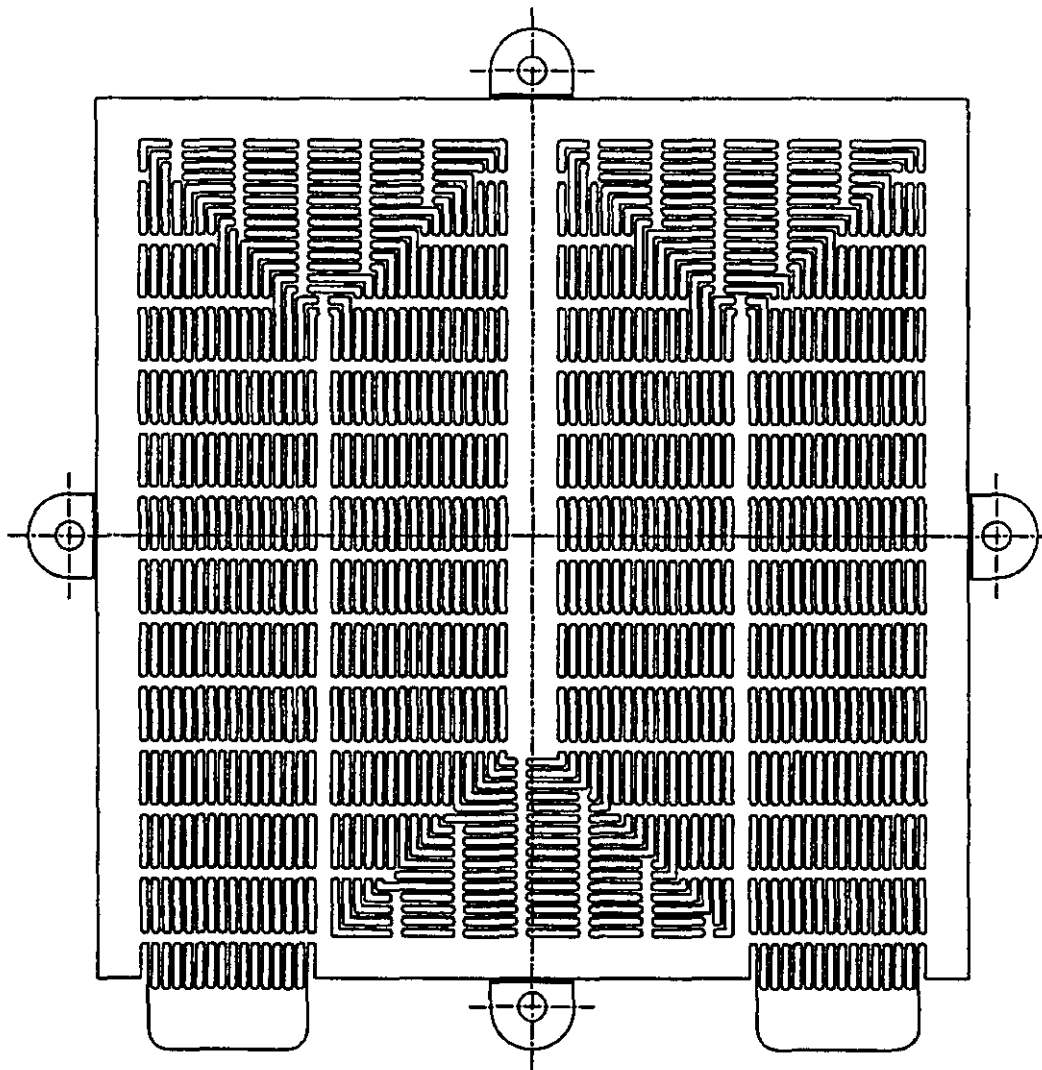
Table 3.2: Shim Designations

The shim patterns can be seen in figures 3.2-3 12.



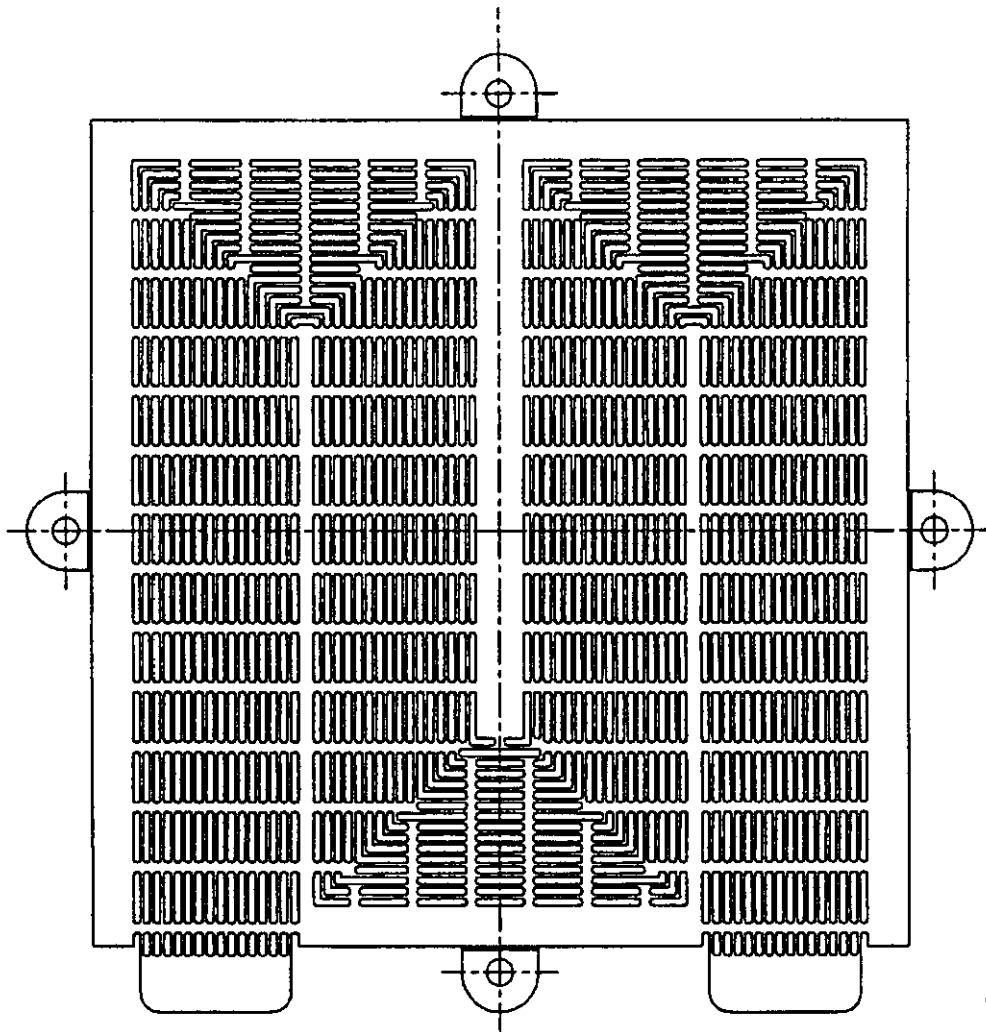
KTS10001

Figure 3.2: Shim Number KTS10001



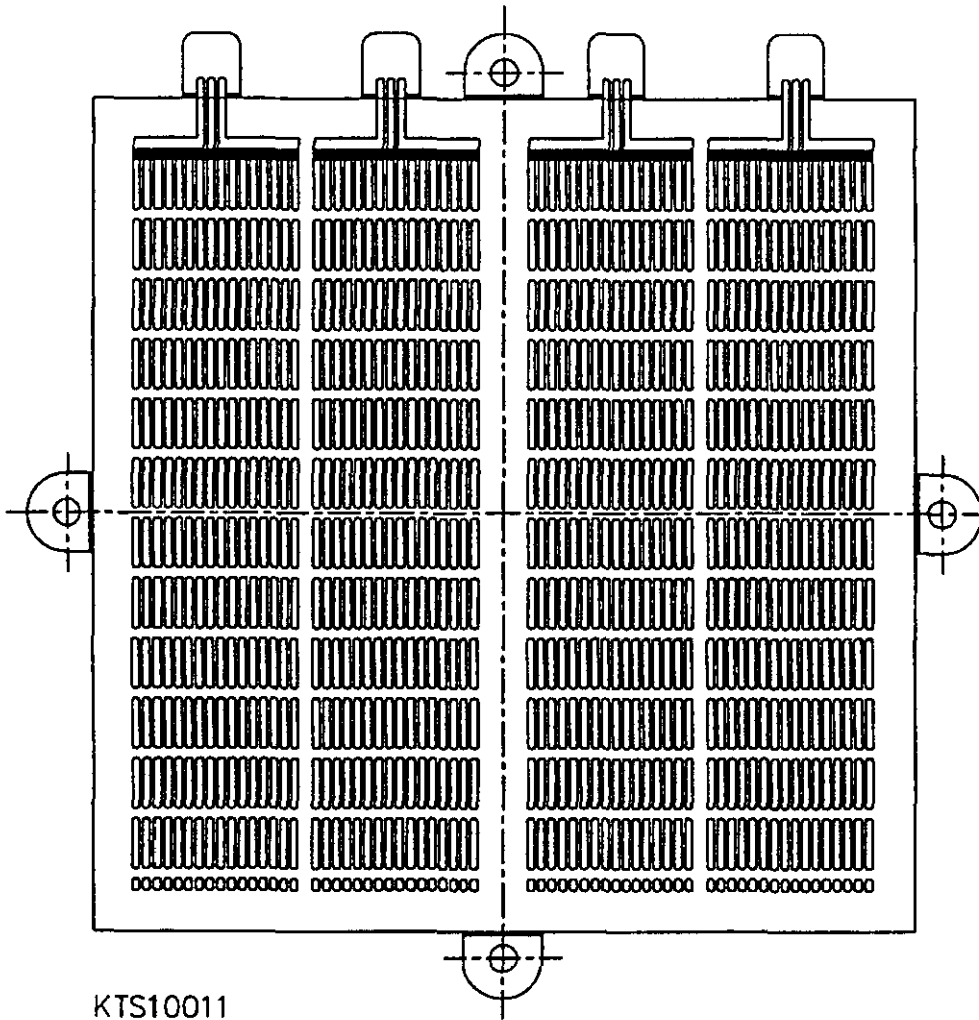
KTS10002

Figure 3.3: Shim Number KTS10002



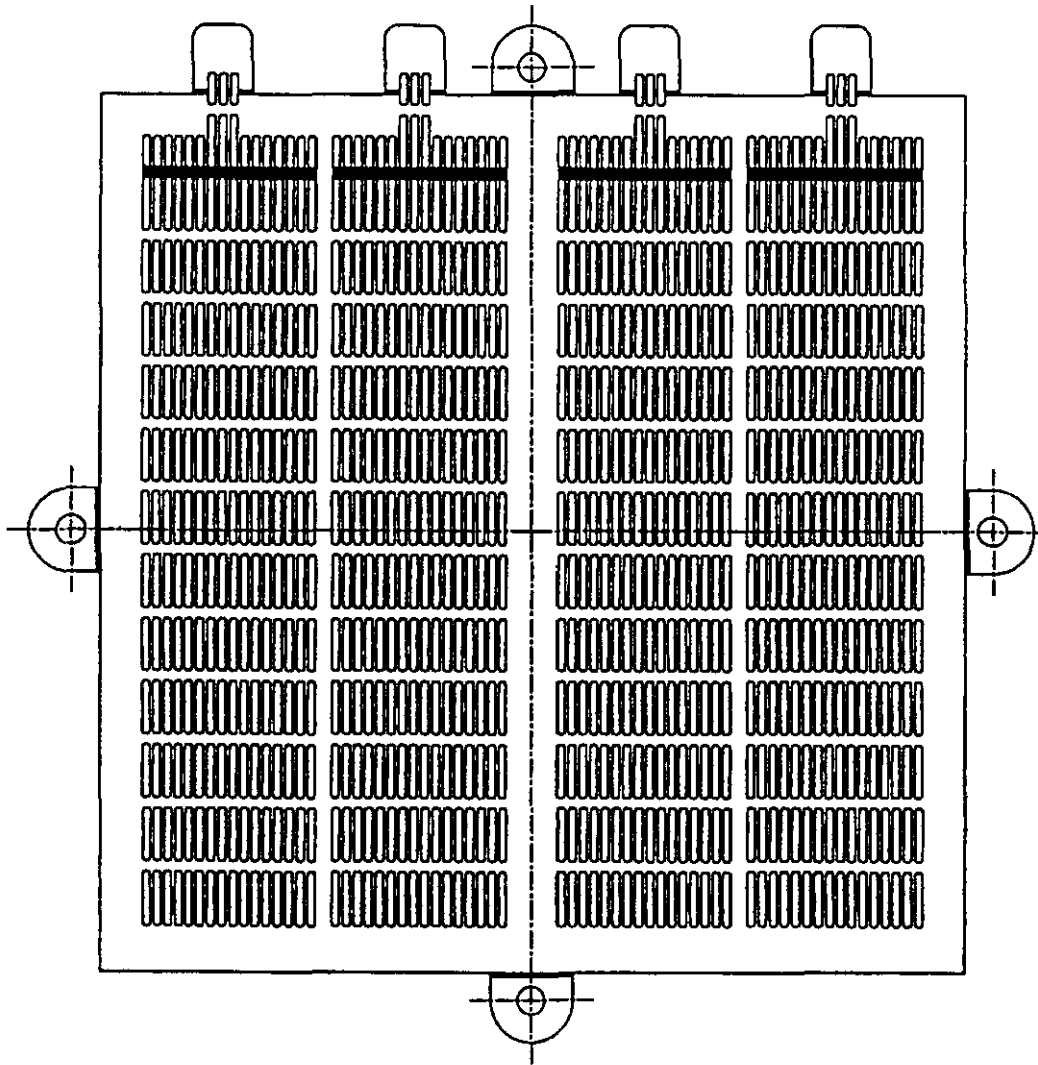
KTS10003

Figure 3.4: Shim Number KTS10003



KTS10011

Figure 3.5: Shim Number KTS10011



KTS10012

Figure 3.6: Shim Number KTS10012

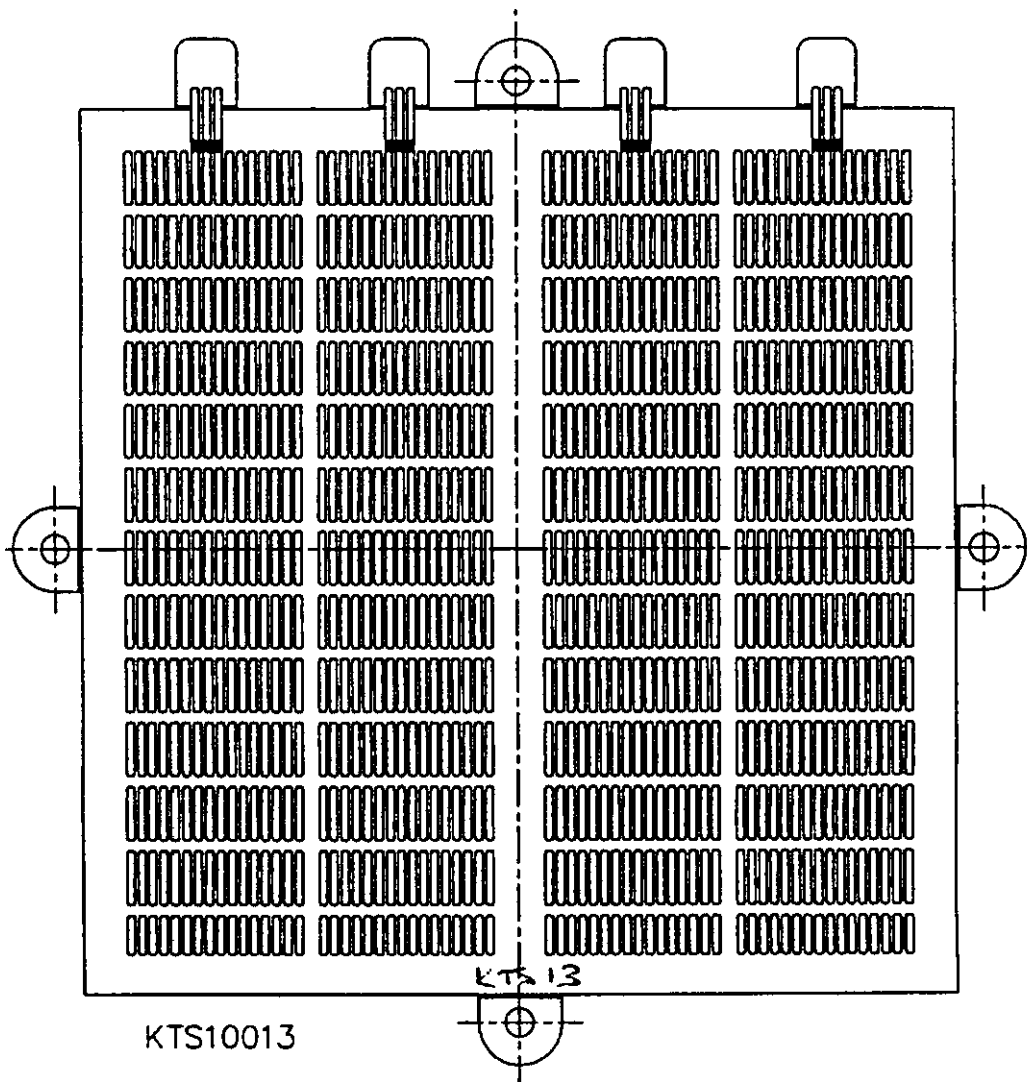


Figure 3.7: Shim Number KTS10013

KTS10014

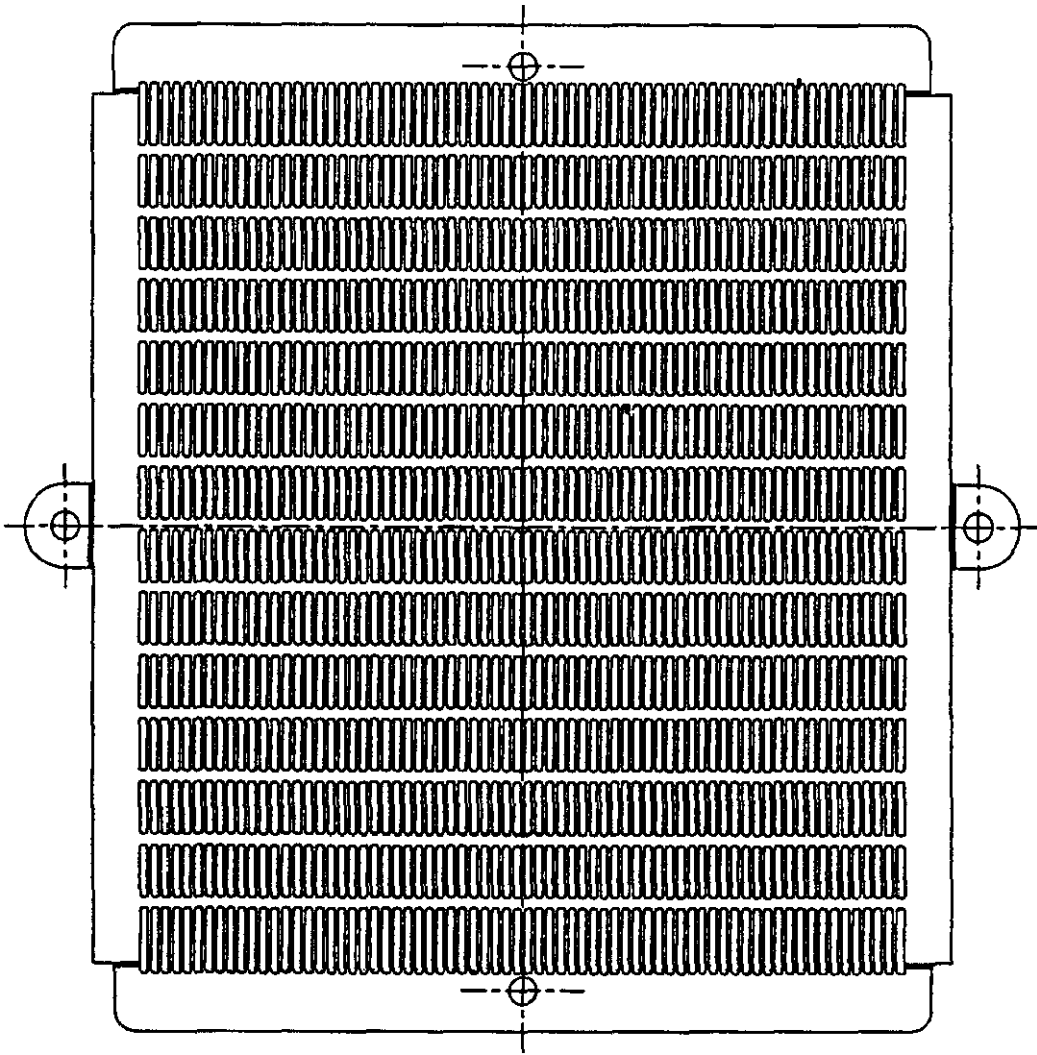


Figure 3.8: Shim Number KTS10014

KTS10015

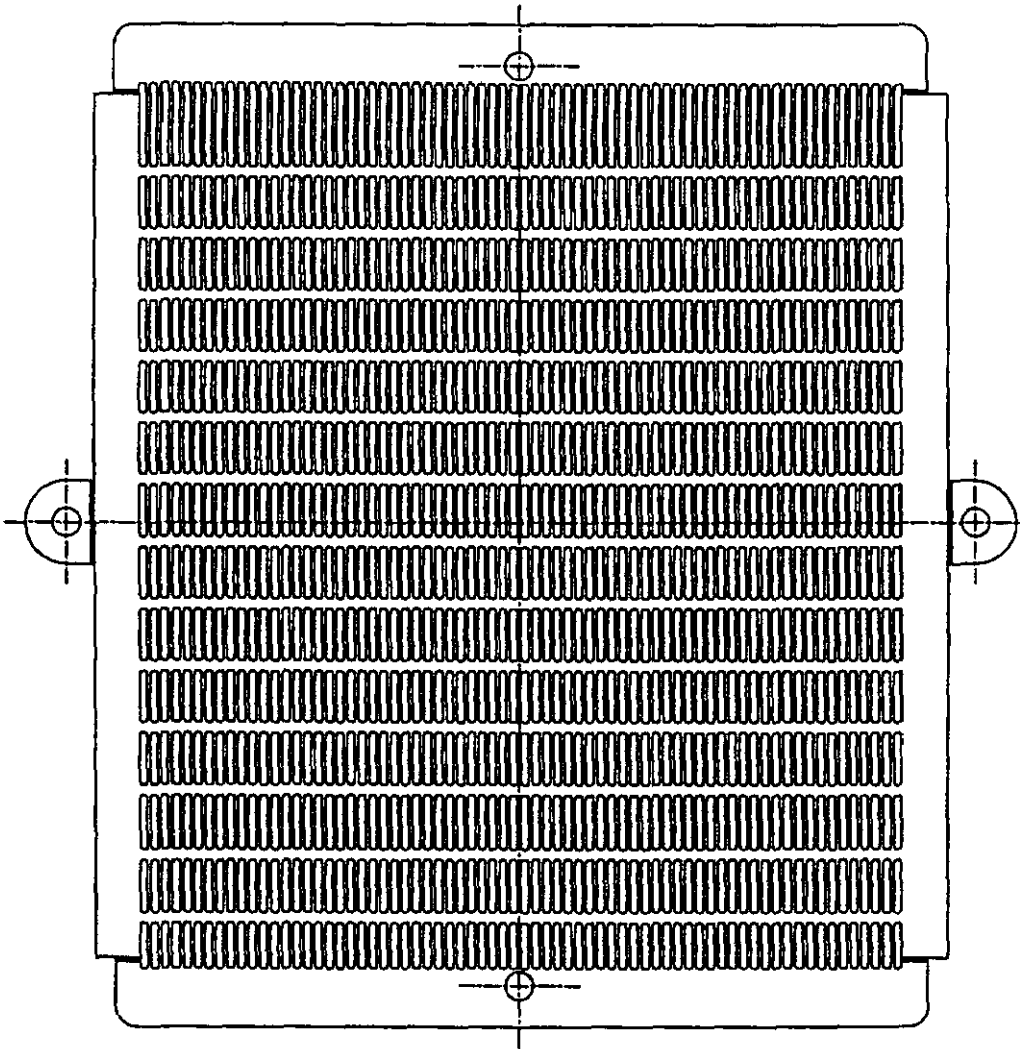


Figure 3.9: Shim Number KTS10015

KTS10016

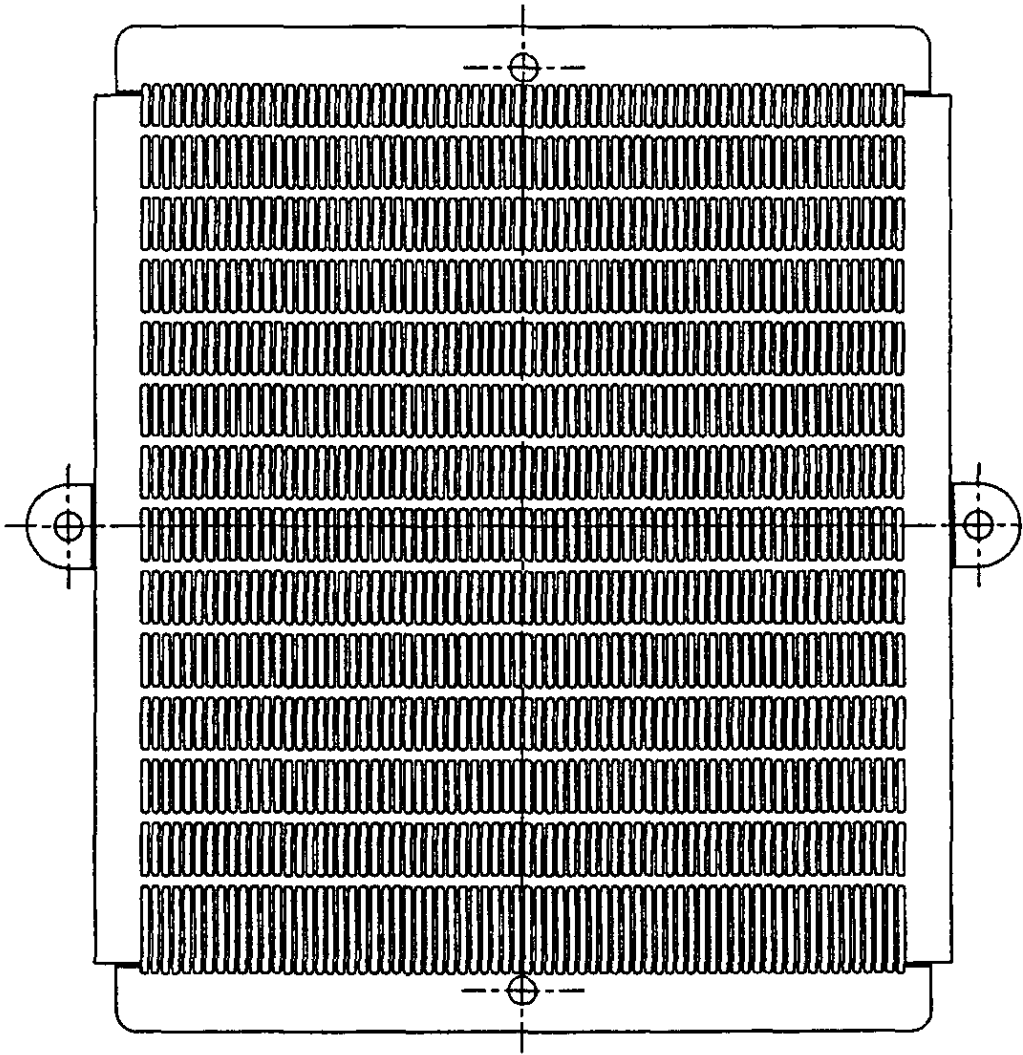


Figure 3.10: Shim Number KTS10016

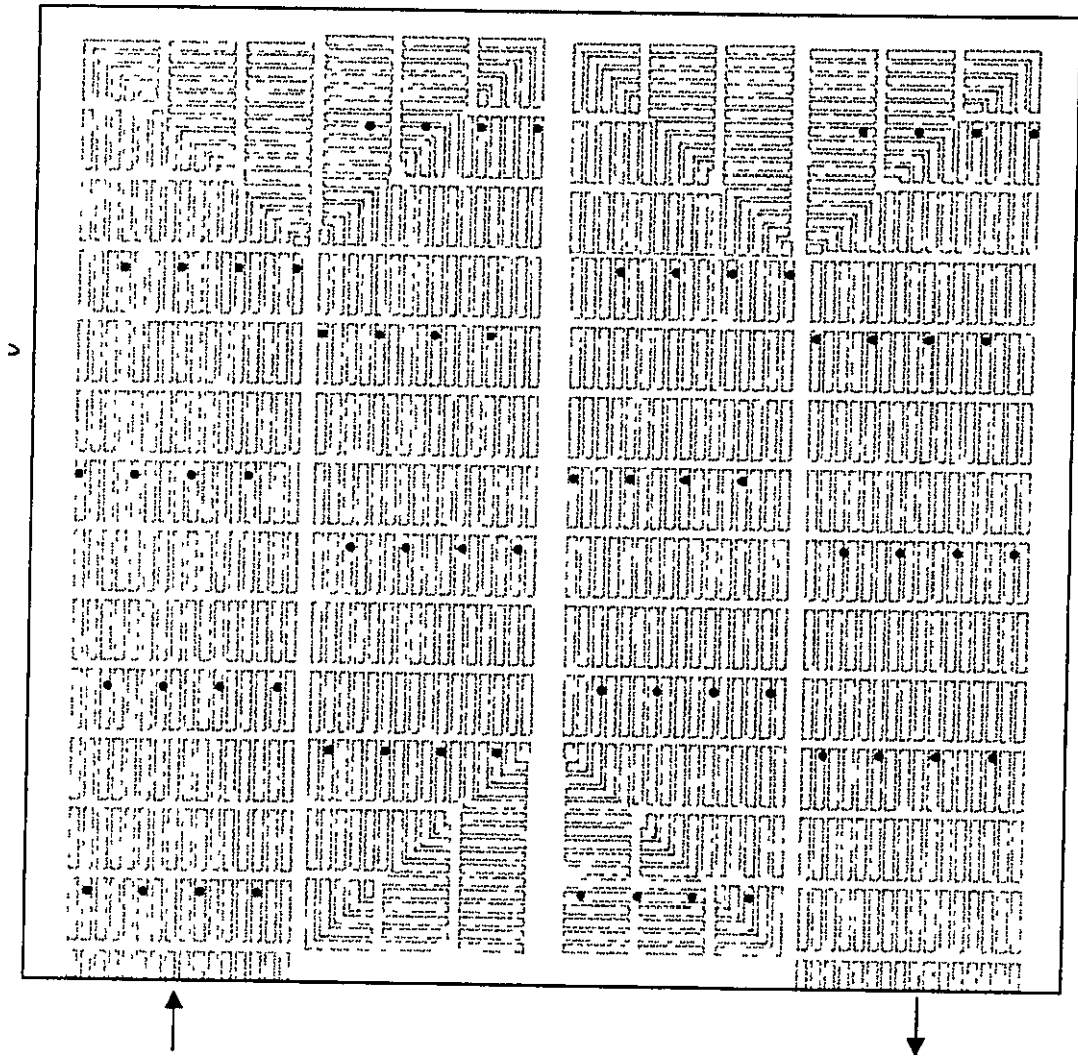
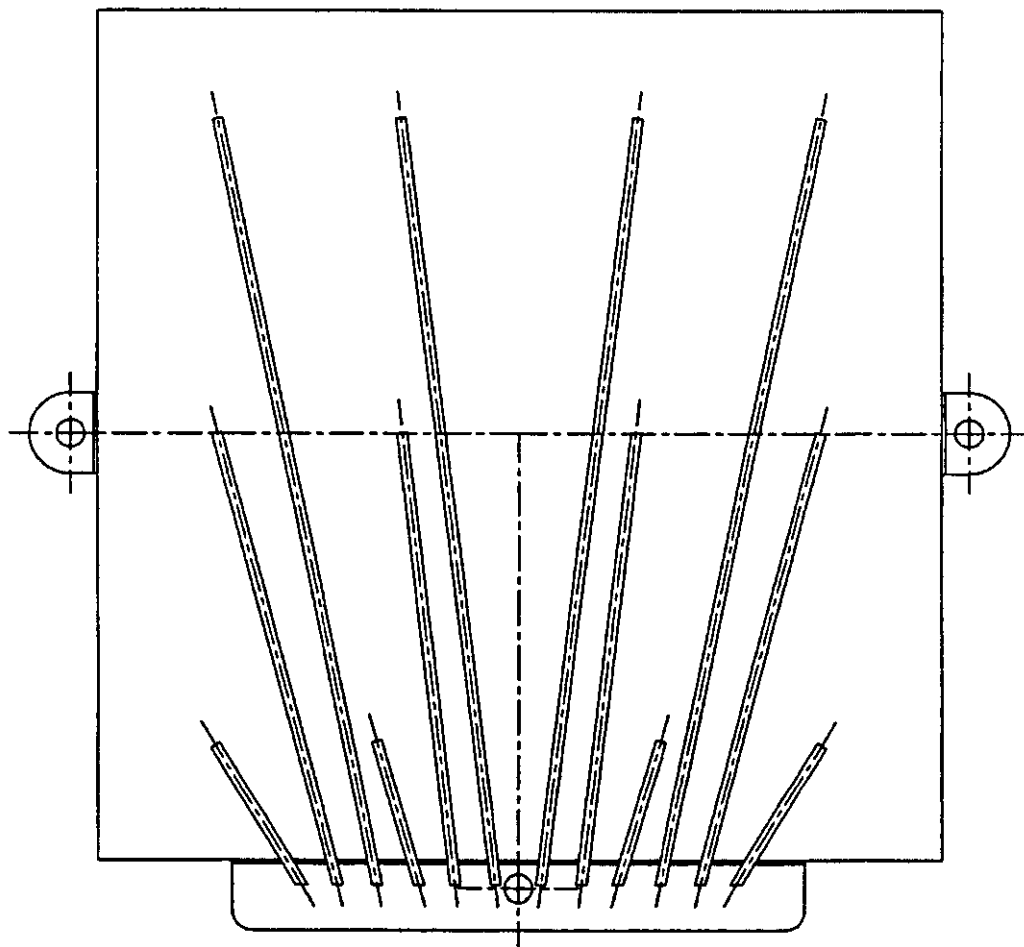


Figure 3.11: Shim Number KTS10017



KTS10018

Figure 3.12: Shim Number KTS10018

This produces a reactor with outside dimensions 125 x 125 x 56.5 mm. In addition the reformer inlet manifold is manufactured as a full semicircular tank with flat ends. The tank wall thickness is 3 mm. The reactor can be seen in Figure 3.13.

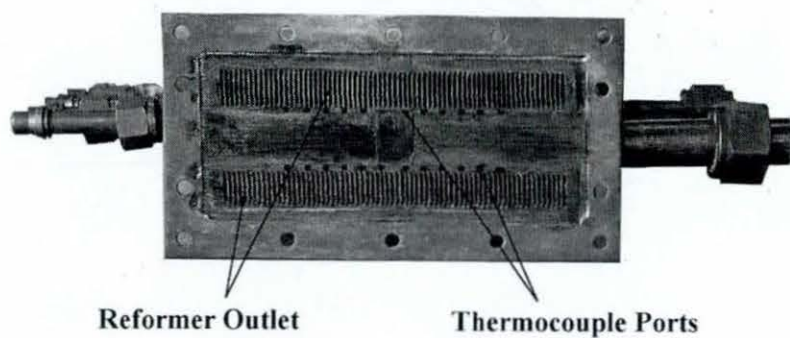
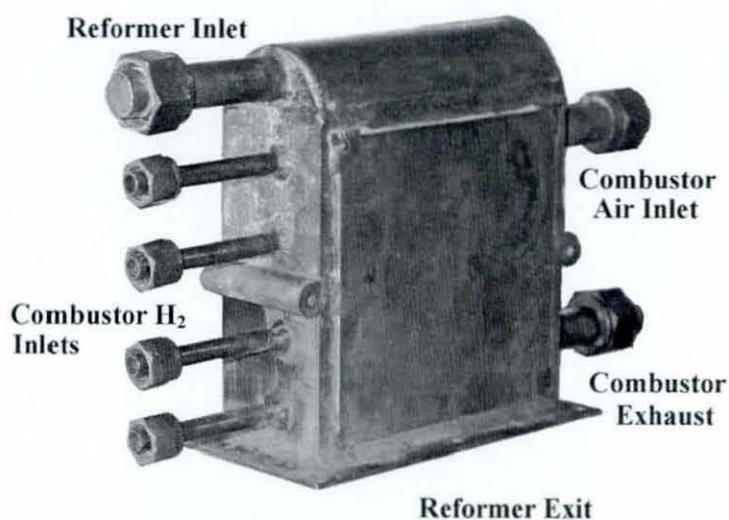


Figure 3.13: The microchannel reactor

3.3.2 Function Layer Description

The reactor is divided into three groups of layers, a combustion layer, a temperature sensing layer and a reforming layer as illustrated in Figure 3.14.

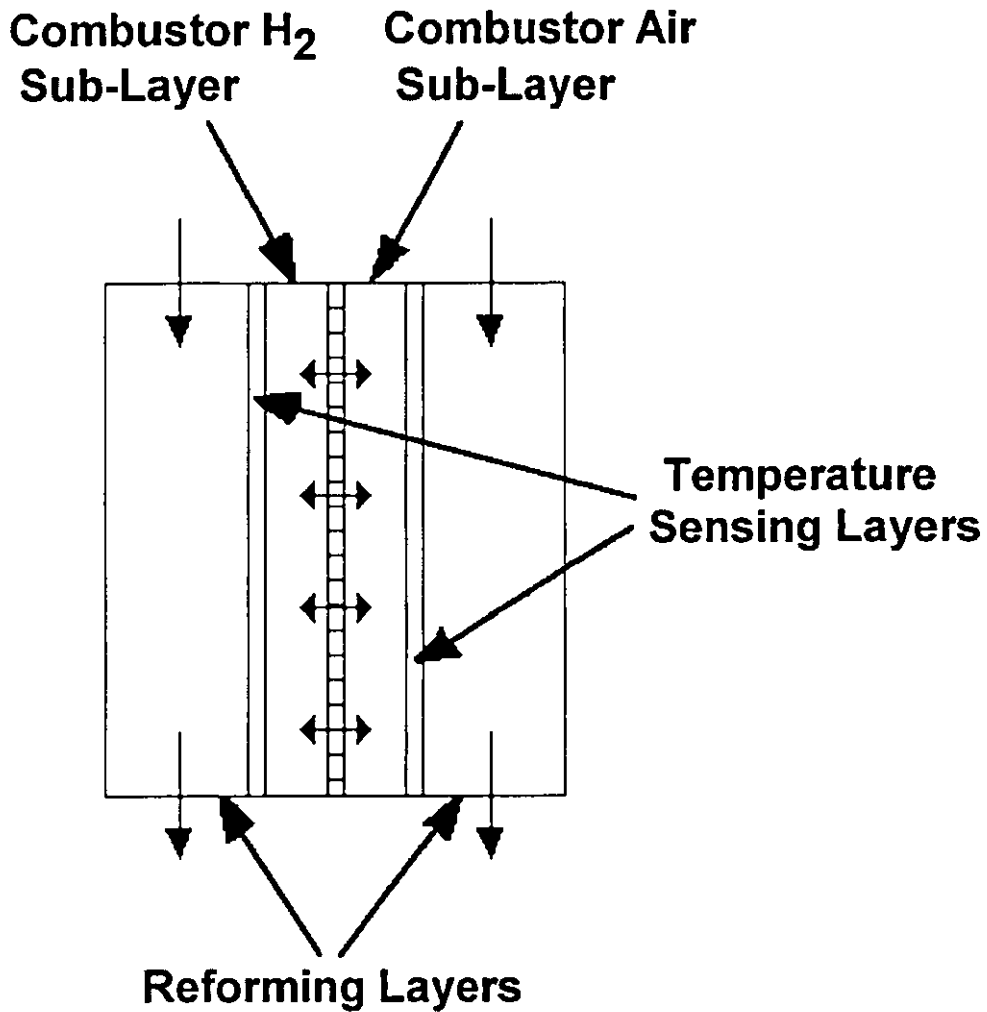


Figure 3.14: A Cross-Section of the Microchannel Reactor

The internal volumes of the layers are as follows. Each individual reforming layer has a reactor volume of 115.5 cm^3 . Each combustor fuel zone has a volume of 6.6 cm^3 . The combustor air layer has a volume of 105.6 cm^3 . Each reforming layer has a reaction surface of 222.5 cm^2 . The reactor weighs 5.112 kg . (This includes the weight of the exhaust manifold and thermocouples.)

The combustion layer, which is located in the centre, consists of fuel and air supply sub-layers in which the two sub-layers are inter-connected through a diffusion shim. The air is diffused into the fuel sub-layer and reacts with it to produce the heat required for the reforming reaction. The fuel sub-layer is split into four zones and wash-coated with a platinum-based catalyst. The four zones each have an individual fuel feed and a common air feed as shown in Figure 3.15. By controlling the quantity of the fuel supplied to each individual zone, the heat released from each can be dynamically controlled. This setup is designed to avoid the formation of hot or cold spots.

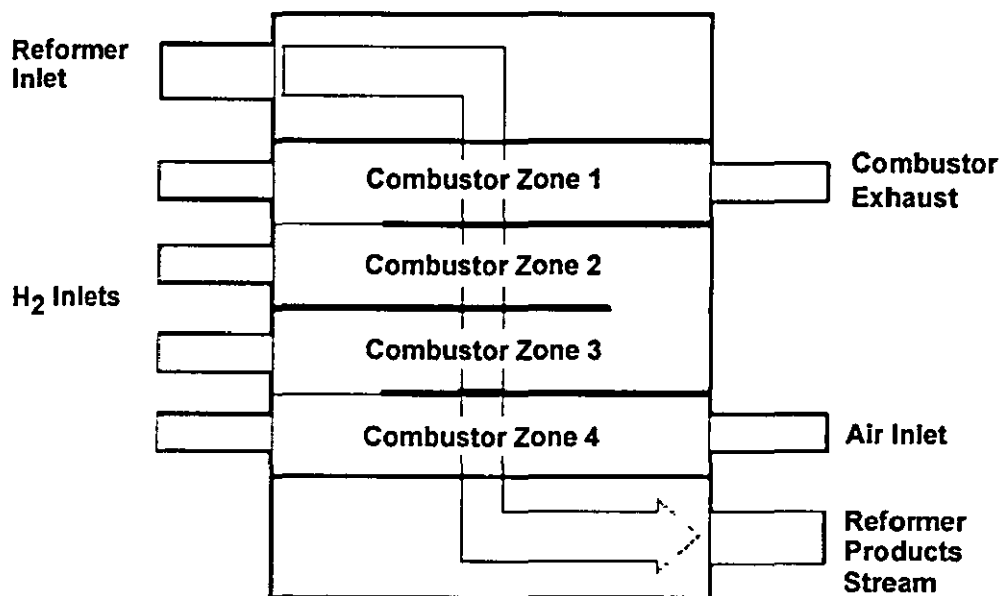


Figure 3.15: The reactor layout

The temperature sensing layer is designed for the allocation of four groups of three temperature sensors. However the reactor was constructed with the thermocouple plate rotated by 90 degrees. (This occurred due to the placement of the inlet and outlet manifolds for the combustion layers. It meant that the desired place for the thermocouple ports was not available.) This meant that the thermocouples were located in three groups of four instead. These are located inside the reactor next to the combustion layer as shown in Figure 3.16.

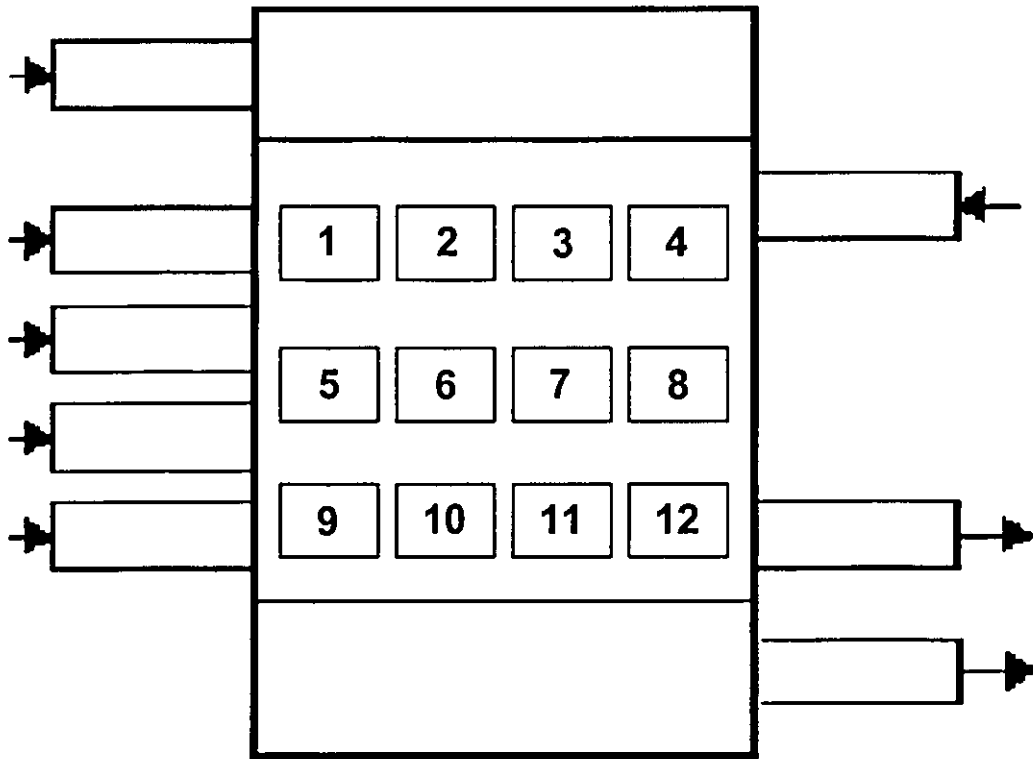


Figure 3.16: The Position of the Internal Thermocouples

In the combustion layer, zone 1 is directly connected to the inlet of the reforming reactants while zone 4 is directly open to the air supply to the combustion layer. In order to overcome the quenching effect of the inlet flows and maintain the desired reforming temperature in these zones, more fuel is needed here than for the middle zones and it was decided that the two middle zones would operate satisfactorily in unison. For this reason it was decided that the thermocouple's new position would be satisfactory.

In order to efficiently use the heat produced from the combustion layer, a reforming layer was placed on each side of the combustion layer. It allows direct control of the reforming temperature with minimum lag time whilst making use of the maximum amount of heat available from the combustor. This results in fast transient responses and start up times, which are essential if the reformer is to be integrated into a complete system.

3.4 Assembly Description

The individual shims contain micro-channels and splitter bars. The micro-channels have widths of 1.10 mm. The splitter bars contain grooves of 0.5 mm depth to help retain the catalyst.

The flow field through the reforming layer is straight through (Shims KTS10014-KTS10016). This keeps the pressure drop across the reforming side to a minimum. The reforming layers are made up of 8 "groups" of three shims. The shims when placed on top of each other produce a series of micro-channels along the length of the reforming stream, which contain changes in the vertical plane in order to promote heat transfer and mixing of the reactants. The channels also contain "notches" to improve the adhesion of the catalyst to the surface of the micro-channel.

The combustor air stream is similarly made up of eight groups of three shims (KTS10001-KTS10003), whilst the combustor fuel stream is made up of 2 groups of 3 different shims (KTS10011-KTS10013).

The combustor fuel shims are arranged so that four distinct zones are formed inside the combustor fuel layer. Each zone has its own fuel inlet. The combustor air stream shims are machined so that the air stream passes along each of the combustor fuel zones in turn (figure 3.15). In order to allow mixing of the combustor fuel and air, a perforated shim is placed between them (KTS10017). The shim contains 48 holes. These are aligned so that they link micro-channel directly to micro-channel. There are 12 holes per combustor fuel zone, and these are arranged in three groups of four. This facilitates the mixing of the combustion reactants whilst preserving the integrity of the combustion fuel zones. The combustion products are exhausted via the combustor air layer. To prevent internal cross over between the reformat and combustion layers separating plates are employed between them (KTS10004).

In order that the temperature of the reactor can be accurately measured, thermocouple plates (KTS10018) are employed between the separating plates. These allow the accurate placement of twelve thermocouples on either side of the combustion layer.

3.5 Reformer Outlet Manifold

Due to the orientation of the thermocouple plates, the reformer exit is inline with the thermocouple ports. This means that a manifold needed to be built that would allow the thermocouples to be installed whilst allowing the reformat to pass out unimpeded. The design can be seen in Figure 3.17. In order to allow the thermocouple fittings to seal they need to be positioned away from the reformer otherwise the heat would make a seal impossible to achieve. For this reason the thermocouple ports were positioned away from the main body of the reactor at right angles to the flow.

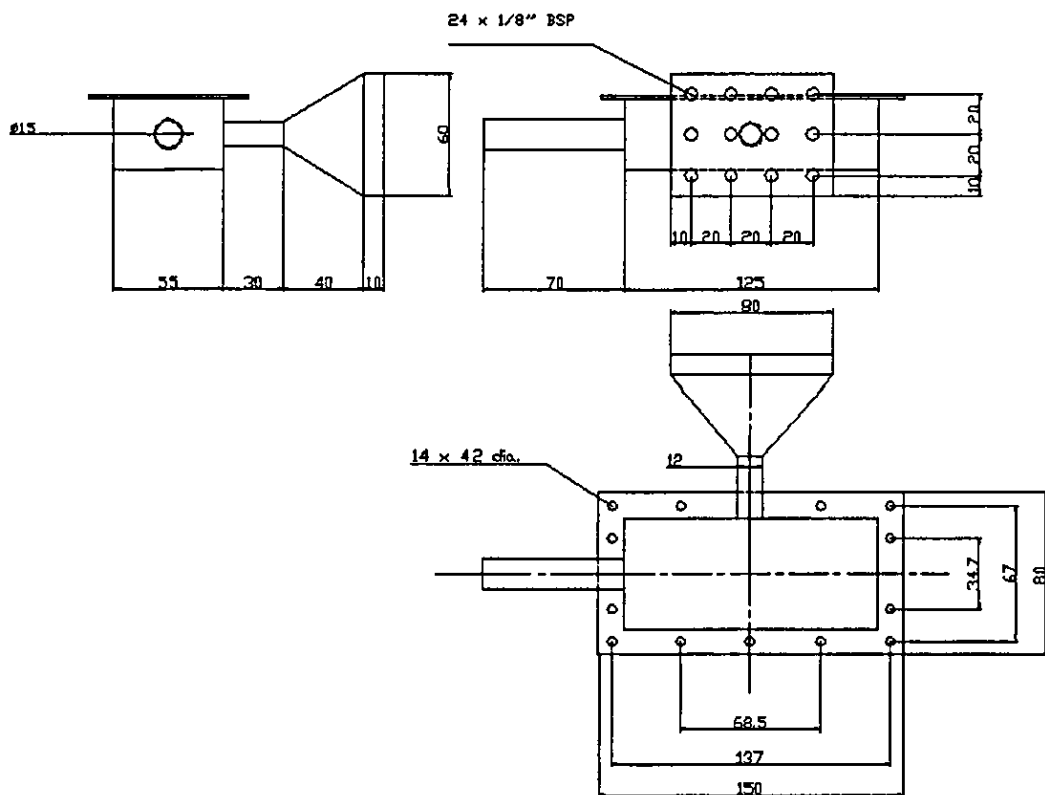


Figure 3.17: Reformer Exit Manifold Drawing

It was decided that 12 thermocouple ports would be sufficient as that would allow the temperature of the combustion zones to be determined. Access to the reactor was via an end plate. This allowed the thermocouples to be fed into the correct ports on the reactor as shown in Figure 3.18.

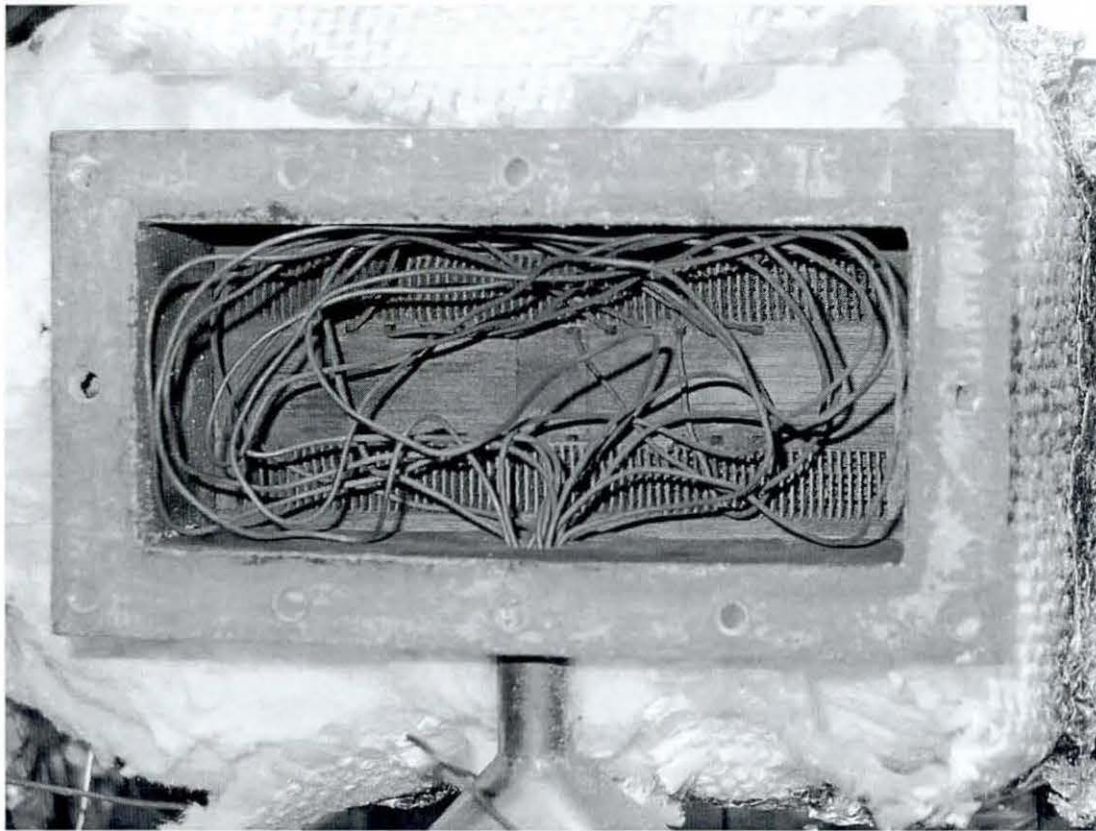


Figure 3.18: A View of the Exit Manifold Showing the Positioning of the Internal Thermocouples

The manifold was attached to the reactor using 4mm dia bolts. The endplate was attached to the manifold using 4mm dia bolts. Each join was initially gasketed until the operating conditions made this unworkable.

3.5.1 Gasketed/ Welded Join

A number of methods were used to join the reformer exit manifold to the reactor. Under initial test conditions it was found that 2mm Grafoil (a flexible graphite manufactured by GrafTech) was sufficient to seal the manifold join. This was successful until the dual-stage catalyst was tested. The tests carried out using the dual-stage catalyst were carried out at a higher localised (zone 4) temperature than those with the single stage. At this higher temperature the Grafoil could not maintain the integrity of the seal between the manifold and the reactor. This was a result of the Grafoil oxidising.

The first modification was to use a double thickness Grafoil gasket. This was to dissipate the heat. This also did not maintain a seal under operating conditions. The Grafoil gasket was combined with exhaust paste (CarPlan FirePutty) in an attempt to reinforce the seal. The extreme heat degraded the gasket too quickly. A further gasket was sourced. Thermiculite manufactured by Flexitallic was employed, this can be seen in Figure 3.19.

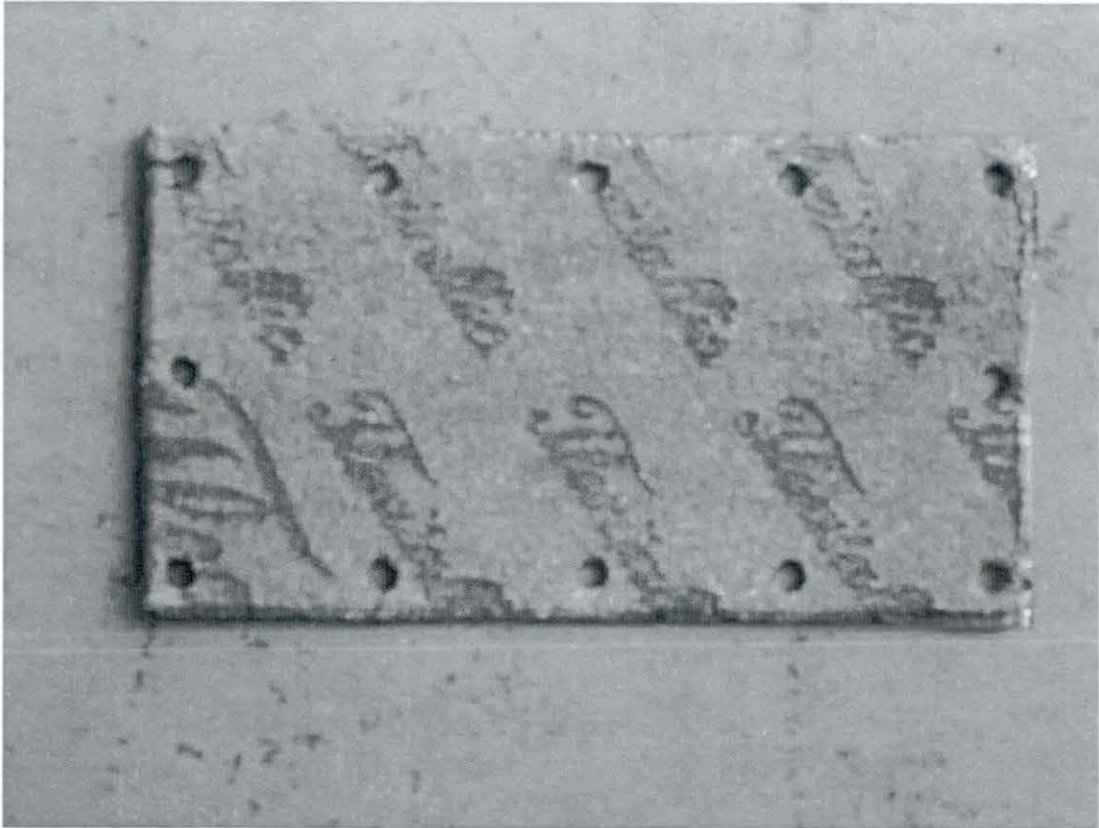


Figure 3.19: The Flexitallic Gasket

This time a ceramic fibre paste was used to help seal the join. Unfortunately by this time the flanges had become deformed by successive heat and repair cycles and a seal was not possible. This necessitated that the manifold be welded directly to the reactor (Figure 3.20).

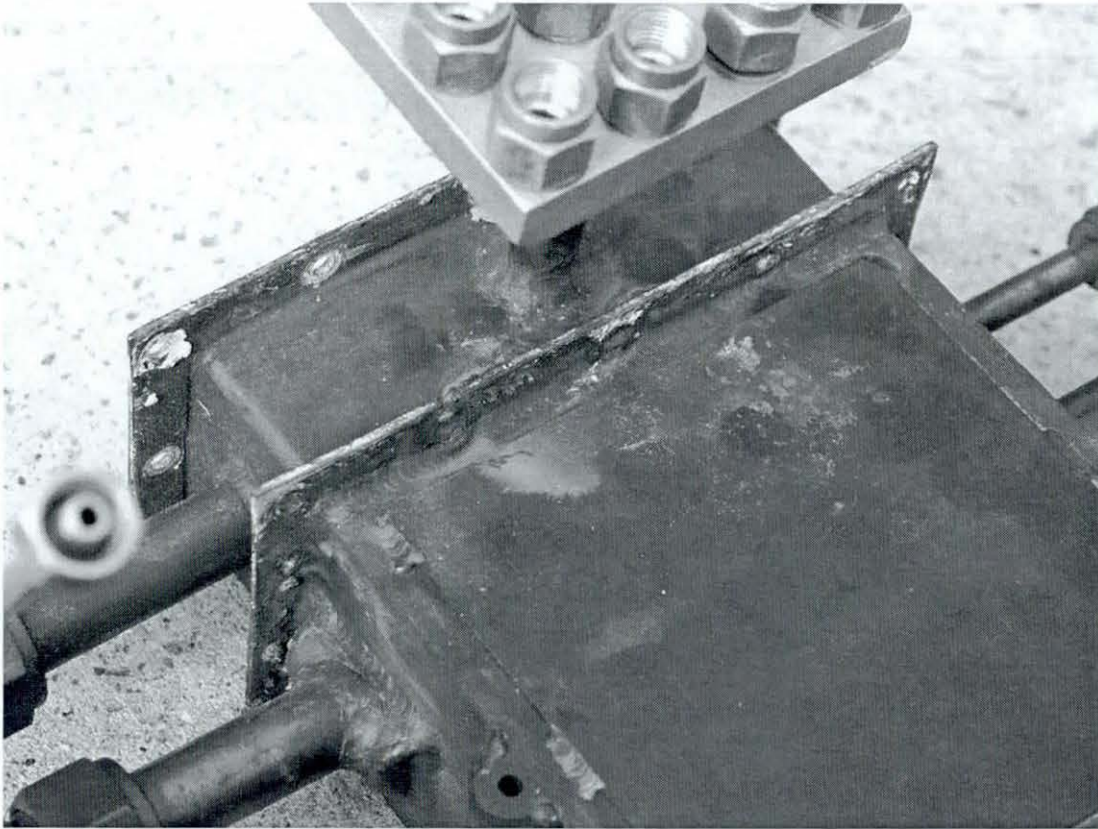


Figure 3.20: The Welded Reformer Exit Manifold

The end plate was successfully gasketed using Thermiculite and ceramic fibre paste. The Reactor can be seen installed in the test-rig with the ceramic fibre paste used as sealant in figure 3.21.

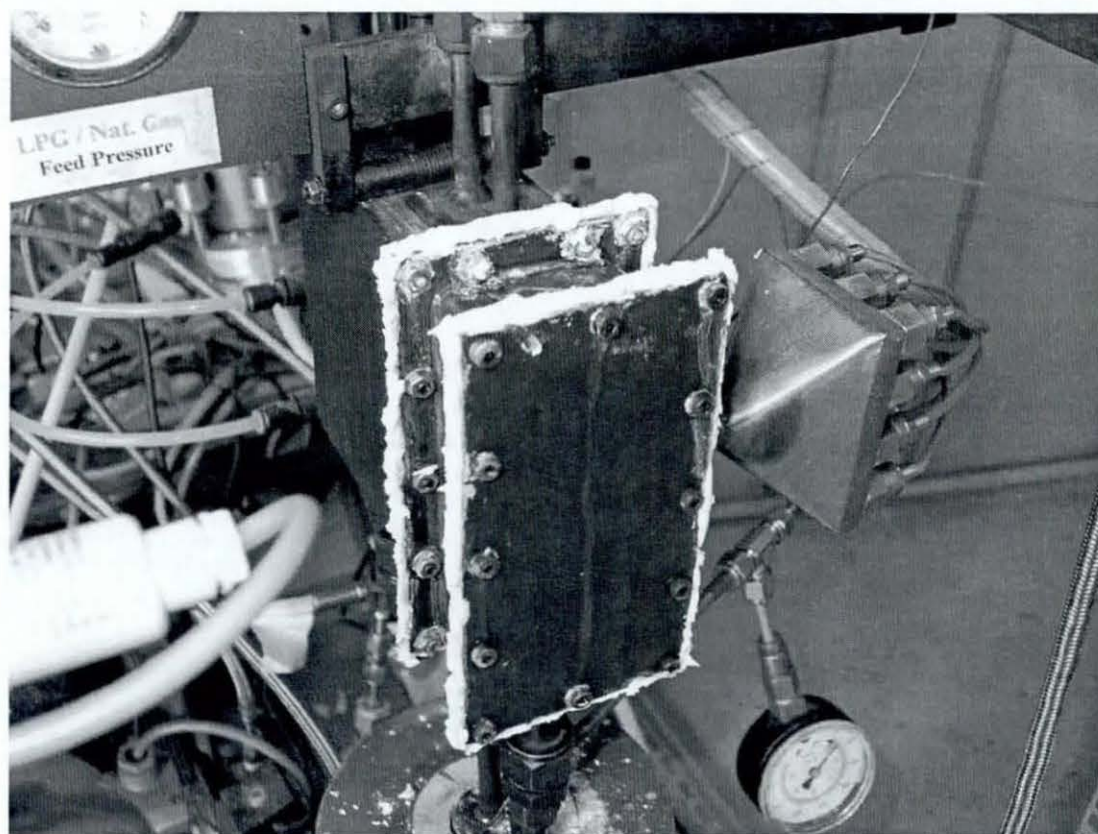


Figure 3.21: The Reactor Installed in the Test Rig

3.6 Catalyst Application

The catalyst was applied to the reactor using a washcoating process. The catalysts were supplied by Catal International Ltd. The combustion catalyst used was 0.3% Pt/0.1 % Pd on alumina, The sulphur tolerant catalyst was 0.15% Ru on 2.5% MgO/Al₂O₃, and the second reforming catalyst used was 8% Ni on 2.5%MgO/Al₂O₃.

4 Description of the Test Assembly

4.1 Test Assembly

The test assembly was designed as a self-contained unit. This was so that it could be easily transported if necessary. The equipment is mounted in a 19-inch rack mount enclosure. This means that the equipment can be positioned as required inside the enclosure, allowing a compact rig to be produced with the minimum of extra mounts required (Figure 4.1). Briefly, the rig contains; two electric heaters, two heat exchangers, two catchpots, the reactor, three mass flow controllers (MFCs) and the thermocouple i/o board.

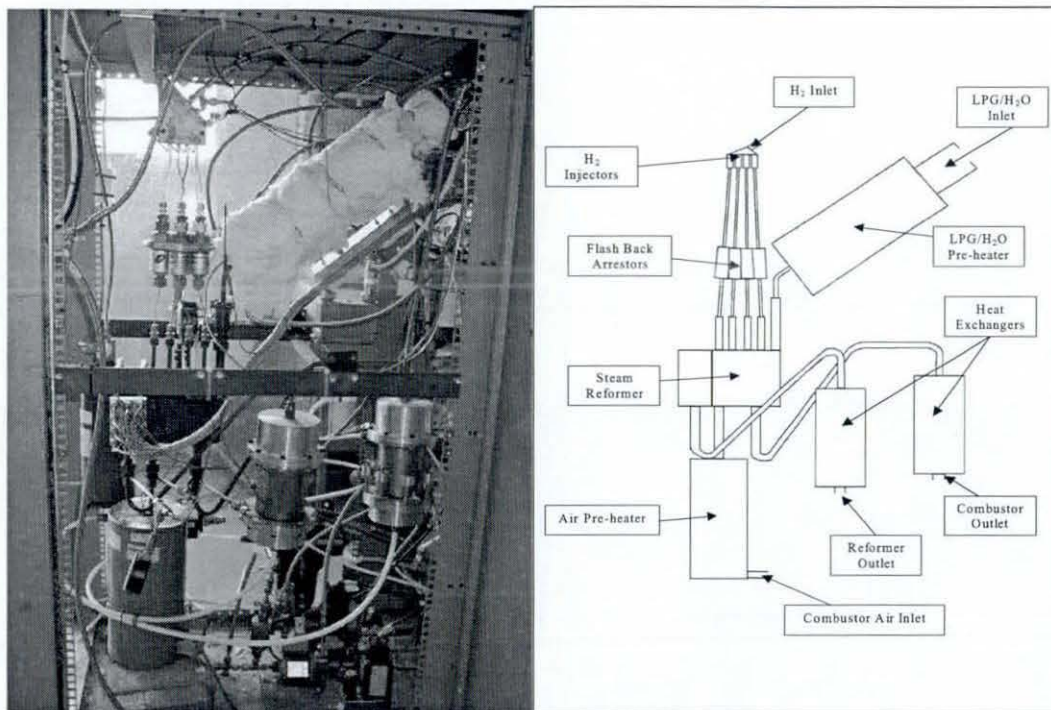


Figure 4.1: The Test Rig

4.1.1 Test Assembly Safety System

The gases pass through solenoid valves after the MFCs (Figure 4.2). The LPG, H₂ and air pass through normally closed solenoids, whilst the N₂ passes through a normally

open solenoid. The electronic system (Figure 4 3) is set up so that in the event of an emergency there are two clearly marked emergency stop buttons (both of which are linked and have the same function). Pressing the emergency stop button cuts off the power from the test rig gas supply system. This has the effect that the solenoids go to their unpowered positions. This stops the combustible gases whilst purging the system with N₂. The power to the H₂ “injector” solenoids remains on to facilitate the purging of the combustion zones. This is because they are normally closed and require powering to allow gas to pass through them.

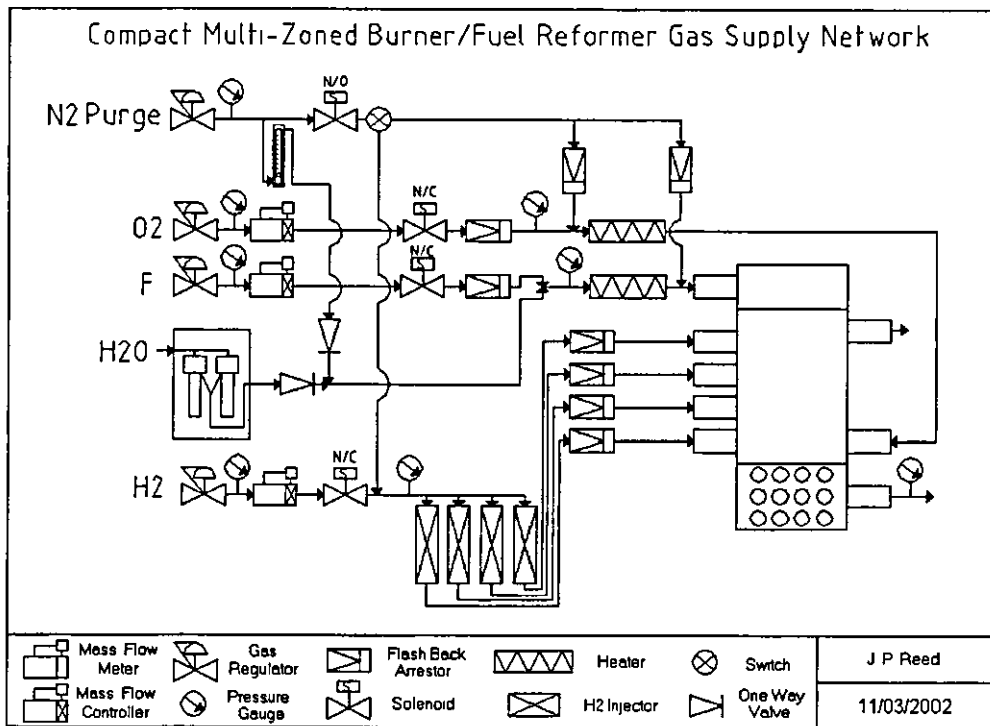


Figure 4.2: The Gas Layout for the Test Rig

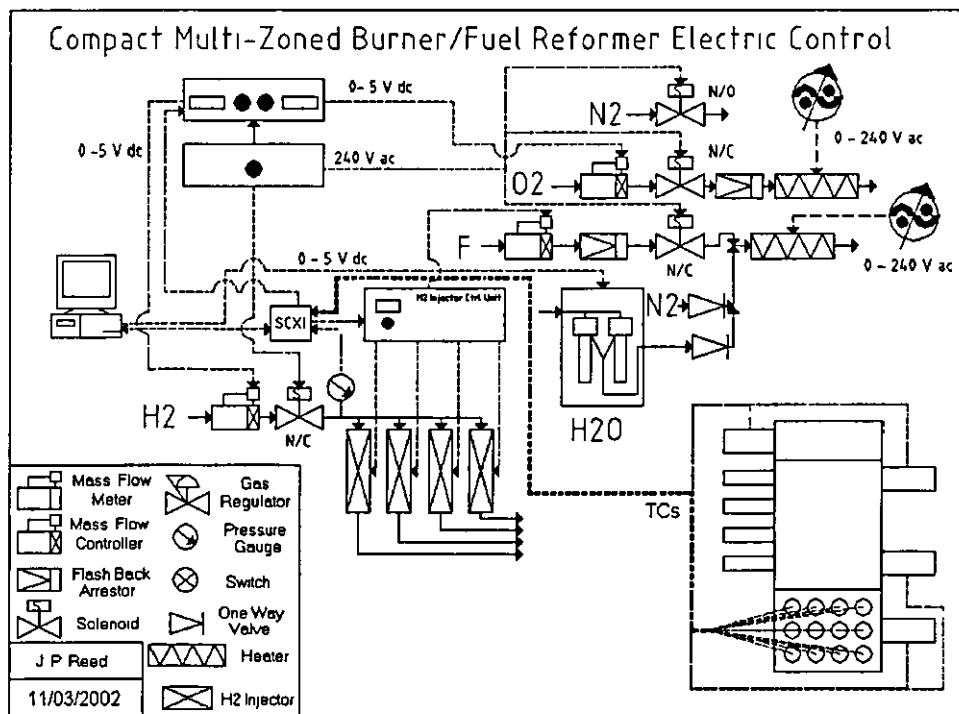


Figure 4.3: The Electrical Layout for the Test Rig

There is an onboard fire extinguisher system plumbed into the test rig enclosure. If the ambient temperature of the cabinet exceeds 80°C the fire extinguisher is set off

4.1.2 Laboratory Safety System

The laboratory is fitted with CO and combustible gas sensors as well as smoke alarms. The activation of the CO or combustible gas sensors causes the laboratory gas supply to be shut off. This stops the flow of H₂ and air to the reactor. LPG/water and N₂ are unaffected by this. For this reason the test rig must always be manned when it is operating as its emergency stop button requires manual activation when the laboratory sensors shut off the external gases.

4.2 Mass Flow Controllers

A Hastings HFC 202 0-5 SLPM mass flow controller was initially used to supply the combustor with hydrogen. For later tests the mass flow controller was recalibrated to allow a maximum flow rate of 10 SLPM of hydrogen. This was to allow higher flow rates of LPG to be reformed at the desired temperature. The air supply to the combustor was metered by a Brooks 5851S 0-25 SLPM mass flow controller. This was replaced by a Brooks 5851C 0-50 SLPM model to accommodate the increased hydrogen flowrate after the hydrogen mass flow controller had been recalibrated. The LPG was metered by a Brooks 5851S 0-25 SLPM mass flow controller. The same mass flow controller was used to meter the CH₄ flow during the steam reforming of CH₄ tests. To accommodate the difference in the masses of the fuels a calibration constant was introduced in the control software.

4.3 Water Supply Pumps

During the course of the work, two different water pumps were utilised. These were a continuous flow syringe pump and a diaphragm pump.

4.3.1 Continuous Flow Syringe Pump

Initial testing of the reformer used a continuous flow syringe pump designed in-house. It made use of Hamilton Gastight Syringes.

The syringe pump consists of two syringes, with two-way non-return valves mounted to each syringe, and drivers for the syringes. The non-return valves are used as inlets and outlets for each syringe. The operation of the pump is as follows. The syringes are both primed together. The first syringe then empties. Once the first syringe is empty the second syringe starts to empty. As it does this, the first syringe is reprimed. This process is repeated for the duration of the pumps operation. This provides a continuous flow of water to the reformer. By changing the size of the syringes flow

rates from 0 – 20ml/min can be set. The flow rate is set by using software written using LabVIEW that communicates with the pump in real time using a serial port.

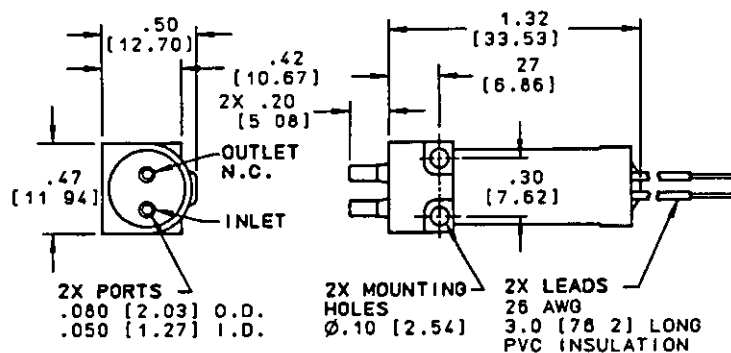
4.3.2 Diaphragm Pump

During operation of the reformer the non-return valves wore out. Due to the failure of the non-return valves on the syringe pump it was not possible to accurately meter the water to the reformer. This obviously has a detrimental effect on the reformer performance. For this reason the syringe pump was replaced with a diaphragm pump. This also allowed higher flow rates of water to be used. The model chosen was a KNF 08 RC. This model allowed the use of serial port communication with a PC for automatic control or the option of manual control via its user interface. It was decided to use manual control of the flow rate, as this was sufficient for the operation of the test rig for the tests undertaken. This is because the nature of the tests did not require the steam to carbon ratio to be constantly varied. This meant that it was sufficient to set the water flow rate manually, as it was required. This did not impair the performance of the reformer.

4.4 Hydrogen Feed Solenoids

The H₂ injectors are small solenoid valves shown in Figure 4.4. They are manufactured by the Lee Company. They have low power consumption and a low internal volume. Their small size makes them ideal for use in a compact fuel processor. However, they have a maximum ambient operating temperature of only 49°C which is a problem in a system with components operating in excess of 700°C. For this reason the valves were mounted away from the reactor and the ambient temperature monitored and logged. Another limitation is the maximum operating pressure of the valves, in this case 1.5 bar. This set a limit on the H₂ feed pressure to the combustor. The H₂ feed pressure was set at the pressure regulator where the H₂ came into the laboratory.

The valves used were LFAA1200210H 2-Way valves. They had an internal volume of 93 μl and operated at 12 Vdc. They were surface mounted on a custom manifold. The manifold split a single H_2 feed into 4 separate streams, one for each valve.



R

Figure 4.4: A Schematic of the LEE Products Solenoid Valve

4.5 Exhaust Heat Exchangers and Recovery System

The exhaust from the combustor and reformer are passed through separate water-cooled heat exchangers in order to condense the water out of the streams (Figure 4.5). The cooled streams are then each passed through a catchpot to remove the condensate from the streams. The reformat stream is then passed through a further condenser/chiller to remove any remaining water before it reaches the online analysers and gas chromatograph.

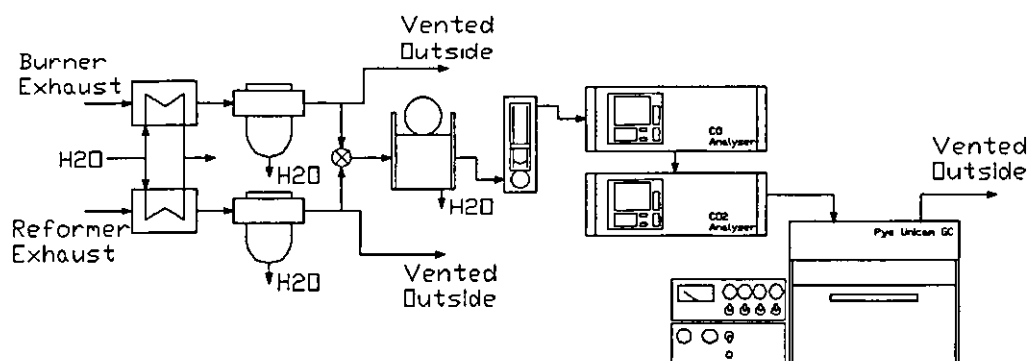


Figure 4.5: The Exhaust Paths for the Test Rig

4.6 Electric Preheaters

There are two electric heaters. These are used to preheat the gases before they enter the reactor. This is done to mimic the effect of heat exchangers in a complete fuel processor.

4.6.1 Combustor Air Preheat

The air flow into the combustor is passed through a 500W ceramic heater before entering the combustor. The tubular ceramic heater has a steel tube running along its centre. This tube is a packed bed containing stainless steel powder/pellets in order to promote heat transfer to the air as it passes through (Figure 4.6). Initial testing of the heater without the pellets showed that convection inside the tube was insufficient on its own to heat the air sufficiently before it entered the combustor.

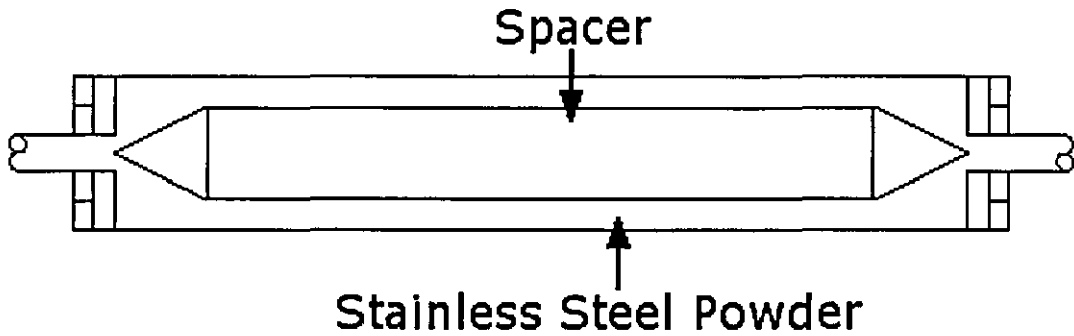


Figure 4.6: Air Preheater Tube Showing Position of S.S. Powder

4.6.2 Liquid Petroleum Gas and Water Preheat

The flow of LPG/water into the reformer first passes through a 750 W ceramic heater. In the centre of the tubular ceramic heater are three coiled tubes through which the LPG and water are passed. To ensure good mixing of the LPG and water the three tubes are passed through a mixer after the heater and before the reformer inlet. The heater is made up of two 375W Watlow ceramic heaters arranged physically in series and wired together in parallel. The heater dimensions are 1 ¾ inches internal diameter and 4 inches external diameter. Due to the necessary maintenance operations on the test rig, the ceramic fibre that covered the heater elements was eroded bringing the element into contact with the coiled tubes, this shorted out the heater. To solve this problem the inside of the heaters were coated with ceramic fibre paste. This reinforced the insulation around the heater elements whilst still allowing adequate heat transfer from the heater to the coiled tubes.

4.7 Control Units

The MFCs and hydrogen injectors were controlled by the computer software, but required control boxes to convert the output from the software into the appropriate signals for the MFCs and solenoids. The electric heaters were controlled using closed loop controllers

4.7.1 Hydrogen Fuel Injection Control Unit

The H₂ solenoids are controlled by the Hydrogen Fuel Injection Control Unit. This takes the 0-5 Vdc control signal from the LabVIEW software and converts it into a square wave. The driver circuit (Figure 4.7) for the solenoid valves takes a linear voltage from the control software and converts it into a square wave. The frequency of the square wave is kept constant, in this case at 50Hz, though this is adjustable by manual means if the need arises. The circuit acts as a comparator. It generates a fixed frequency triangular wave. If the incoming voltage is less than the current wave voltage, the circuit sends out 0 V. If the incoming voltage is greater than or equal to the wave voltage then it sends out 12 V. In this way a simple voltage signal can be used to set the duty cycle on-time of the solenoid valve and so control the flow rate through the valve. This simplifies the control software and optimises processor time for running the control software.

Solenoid Pulse Width control circuit

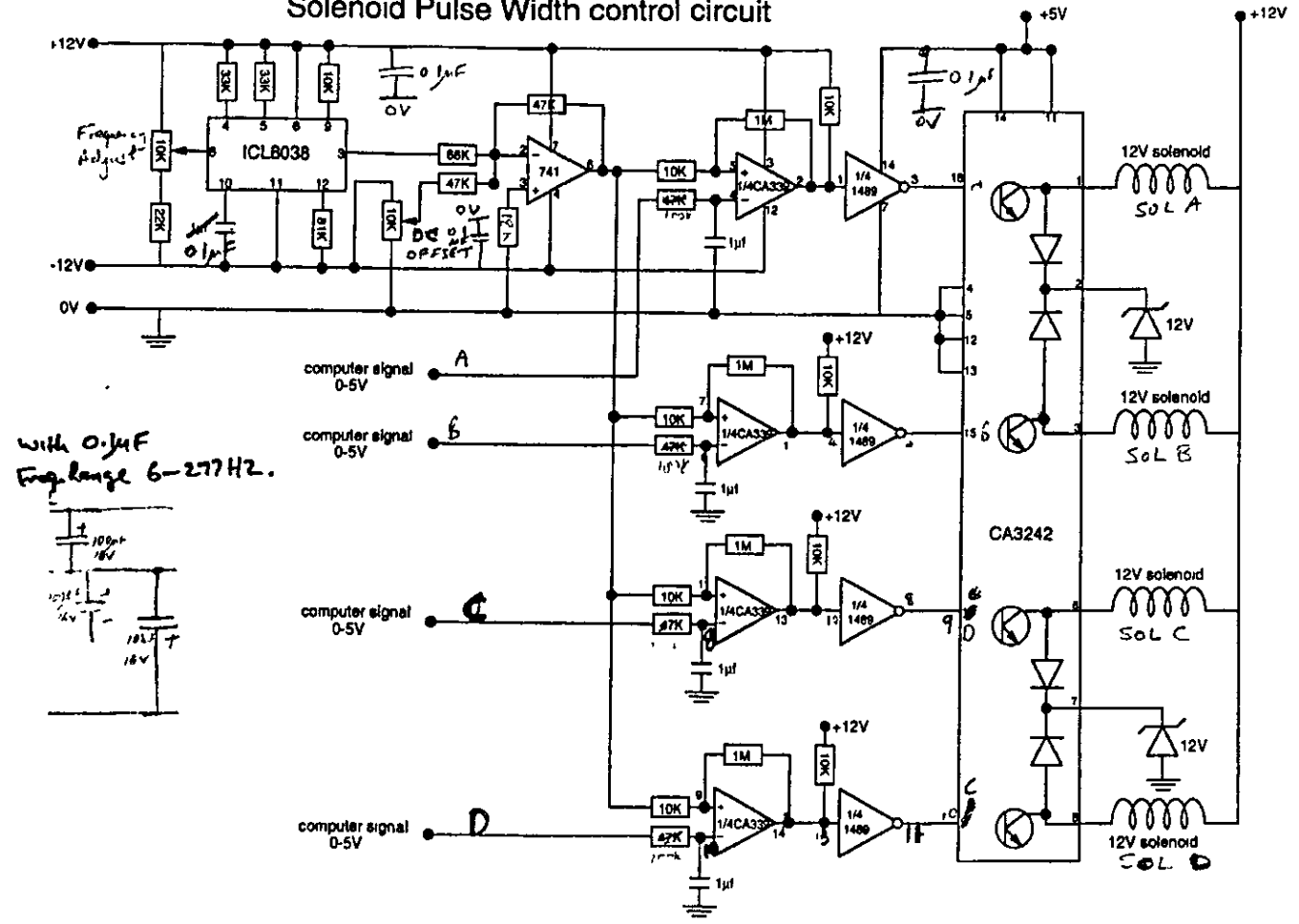


Figure 4.7: Solenoid Driver Circuit

4.7.2 Air and Hydrogen Control Unit

The H₂ and Air MFCs are controlled using a control box. Potentiometers are used to produce a variable control signal of 0-5Vdc, which is sent to the appropriate MFC. The box also includes a bypass switch, which allows the control signal from the LabVIEW software to be used instead of the signal from the potentiometers. This allows automatic control of the flow rates required for closed loop control of the reactor temperature.

4.7.3 Heater Control Units

The electric heaters are controlled using matched temperature controllers operating at 240 Vac. The controllers have built in PID controllers that can be automatically tuned to the system they are used for. Those used in this case were a Watlow 93 controller for the LPG/water heater and a Cal Controls 9400 for the air heater.

4.8 Gas Supply Network

The gas supply to the test rig was from bottled gases. Hydrogen, nitrogen, methane, and a CO₂/H₂ cocktail were sourced from the BOC Group. The LPG used in the steam-reforming tests was sourced from Calor Gas Ltd. and was used straight from the bottle with no treatment taking place before the reformer. De-ionised water for the steam generation was sourced from Fischer Chemicals. De-ionised water was used rather than just distilled water because it was available in the laboratory due to its use in running fuel cell stacks. The air for the combustor was supplied by an on-site compressor.

4.9 Analysis Equipment

A variety of analysis equipment was used to monitor the reformer performance. A major part of the analysis equipment was the control software, which will be discussed in Chapter 5.

Analysis of the reactor performance took place using gas chromatography, online gas analysis, pressure measurements and temperature measurements

4.9.1 Gas Chromatography

A Pye Gas Chromatograph (GC) was used to measure the percentage dry composition of the reformer products. The GC was used to measure the amounts of CH_4 , H_2 and CO present in the gas stream. It could also pick up O_2 and N_2 .

4.9.1.1 Calibration

Before each test run the GC required calibration. The GC was first calibrated for air. This was done to check the operation of the GC and so that the presence of any anomalous air in the reformat stream could be checked for, indicating a fault in the system. As the reading for the concentration of O_2 and N_2 increases linearly with increasing O_2 and N_2 content, only one non zero calibration point was required.

Next the GC was calibrated for use with CH_4 . Again, this produces a linear relationship and two calibration points were used to determine the slope of the calibration curve. The calibration of CO also revealed a linear relationship and so, again only two calibration points were required.

Calibrating the GC for H_2 produced a non-linear calibration curve. For this reason several calibration points were used. To begin with calibration points between 80% – 30% of H_2 in air, with steps of 10% were used. Later when the output of the reformer could be inferred from previous tests, the calibration range for H_2 could be reduced

4.9.2 Online Analysis

Two Siemens Ultramat 6E gas analysers were employed to monitor the CO and CO_2 output from the reformer. It was necessary to separately monitor the CO_2 content of the reformer products because the GC was not able to test for it. CO was monitored

online, as when combined with the CO₂ reading it gives a reliable and quick visual indicator of reformer performance, something that could not be achieved in real time using the GC.

4.9.3 Pressure Tappings

There are four pressure tappings on the test rig. One of the pressure tappings is logged. This is the pressure at the inlet to the H₂ injector solenoid manifold. This is because in an early development of the control software the H₂ pressure was used as a control variable to control the flow rate of the H₂ to the combustor. The pressure transducer used was a 0-1 bar mini pressure transducer sourced from R.S. Ltd. The other three were used as visual indicators to spot potential blockages in the reactor/test rig assembly. These monitor the pressure of the air at the inlet of the combustor, the pressure of the fuel/water mixture at the inlet to the reformer (though this was moved to the inlet of the fuel/water heater on occasion for diagnostics and problem solving), and the pressure at the exit of the reformer.

4.9.4 Thermocouples

The reactor contains 12 K type mineral insulated thermocouples in order that the temperature distribution inside the reactor was known. Details of the thermocouple placements are shown in Chapter 3.

In addition to the 12 internal thermocouples of the reactor, thermocouples were located at the inlet and exit of the reformer, and the inlet of the combustor air. A thermocouple to measure the ambient cabinet temperature was also logged. This was included so that the user would be aware if the temperature got close to the automatic fire extinguisher threshold. The user could then shut down the system without triggering the fire extinguisher unnecessarily. In practise the temperature reading was used to determine the temperature of the air in proximity to the H₂ solenoid valves. This is because the valves cease functioning at or above 45°C [Ref. The Lee

Company (1994)]. The use of the ambient air temperature thermocouple allowed the user to halt a potential operating problem

Additionally, in order to check that the indicated temperature from the internal thermocouples was realistic, an external thermocouple was positioned at the base of the reactor and connected to a stand alone thermocouple display. This provided a back up system and allowed any major discrepancies in actual and recorded temperature to be quickly discovered and rectified.

4.10 Reformer Start Up Procedure

The reformer start up procedure was as follows

1. Switch on electronic controls.
2. Start New Display2dll5.vi
3. Start newpump.vi
4. Switch on GC (see GC operation notes)
5. Check the TC operationality using the Cabinet ambient temperature TC.
6. Check H₂ pressure (1.5 Bar)
7. Check Air Pressure (2Bar)
8. Check LPG Pressure (2 Bar)
9. Check N₂ Pressure (2Bar)
10. Check Water level.
11. Switch on Hex coolant
12. Purge Combustor with N₂ (set Duty cycle 100%)
13. Purge Reformer with N₂
14. Set control to "Warm Up"
15. Set zone temps to 400C
16. Set LPG Preheat to 500C
17. Set Air preheat to 500C
18. Start N₂ flow through LPG preheat.
19. Start Controller.
20. When Combustor is at 400C start H₂O at desired rate (newpump.vi)

- 21 After 10-15 mins introduce LPG at S/C = 8
22. ENSURE THAT THE REFORMER INLET TEMPERATURE DOES NOT EXCEED 300C OR IS LESS THAN 250C
23. Switch control to "Running"
24. Ramp Combustor temperature to operational temperature (600C)
25. Bring down the S/C ratio gradually to the desired S/C ratio.

4.11 Reformer Shut Down Procedure

The shut down procedure for the reformer was as follows.

1. Switch control to off.
2. Set air preheat to 0C
- 3 Allow Combustor to cool to 450C
4. Switch off LPG
5. Allow Combustor to cool to 400C
6. Switch off water
7. Set reformer preheat to 0C
8. Allow to cool to 100C
9. Purge Combustor with N₂
10. Purge Reformer with N₂
- 11 Whilst purging make sure to empty any remaining water from the catchpots.
12. Switch off Hex cooling water.
13. Switch off Control boxes
14. Exit LabView.
- 15 Switch off GC.

5 Design and Development of the Control and Data Acquisition Software

5.1 Software Overview

5.1.1 LabVIEW

The data acquisition and control software was developed using LabVIEW. LabVIEW is a programming environment developed by National Instruments Ltd. It uses a language called G. The programming environment is of a visual “circuit diagram” type. The user builds up the software by adding components to the circuit diagram. In LabVIEW these components are called “virtual instruments” (VI). LabVIEW comes complete with a library of ready made VIs but the user can customise these as desired and create new VIs from scratch. This creates a flexible programming environment. Creating a user interface is done by dragging and dropping customisable components on to the control panel. Again the controls/display components are customisable to suit the exact needs of the application. Due to National Instrument’s range of data acquisition equipment LabVIEW is ideally suited to creating data acquisition programs. The user can utilise existing VIs designed for use with National Instruments hardware and incorporate them into his own software easily, without having to devise the communications protocol between the hardware and software himself. The biggest drawback with the visual programming style employed by LabVIEW is that the circuits become overly complex when iterations are involved or where mathematical routines are required to be used. For this reason the controller, rather than being of PID type was limited to a simple proportional type for simplicity. Additionally the interpolation of the look-up tables, whilst initially implemented using LabVIEW, was carried out using a custom DLL written using Delphi.

5.1.2 Delphi

Delphi is an object orientated programming (OOP) environment. This differs from conventional programming systems in that it deals with objects rather than actions and data rather than logic. This means that it is concerned with the actual interface and it's operation rather than the logic behind it. To begin you decide what objects you require and how they should relate to each other. Once this is done the logic part of the program is dealt with. In this way it is simple to build user-friendly applications. The language that the Delphi interface uses is Pascal. Because Pascal is also a stand-alone language it is possible to use Delphi in the same way as conventional programming environments. Delphi was used to write dynamic link libraries (DLLs) for use with the LabVIEW software. As described above, LabVIEW programs become overly complex when handling iteration and mathematical routines. It is simpler to use conventional code to handle these tasks.

5.2 Control Software Overview

The circuit diagram for the control and data acquisition software can be seen in Figure 5.1. The software developed using LabVIEW contains two main sections. These are data acquisition and logging, and the controller (enclosed by the dotted line).

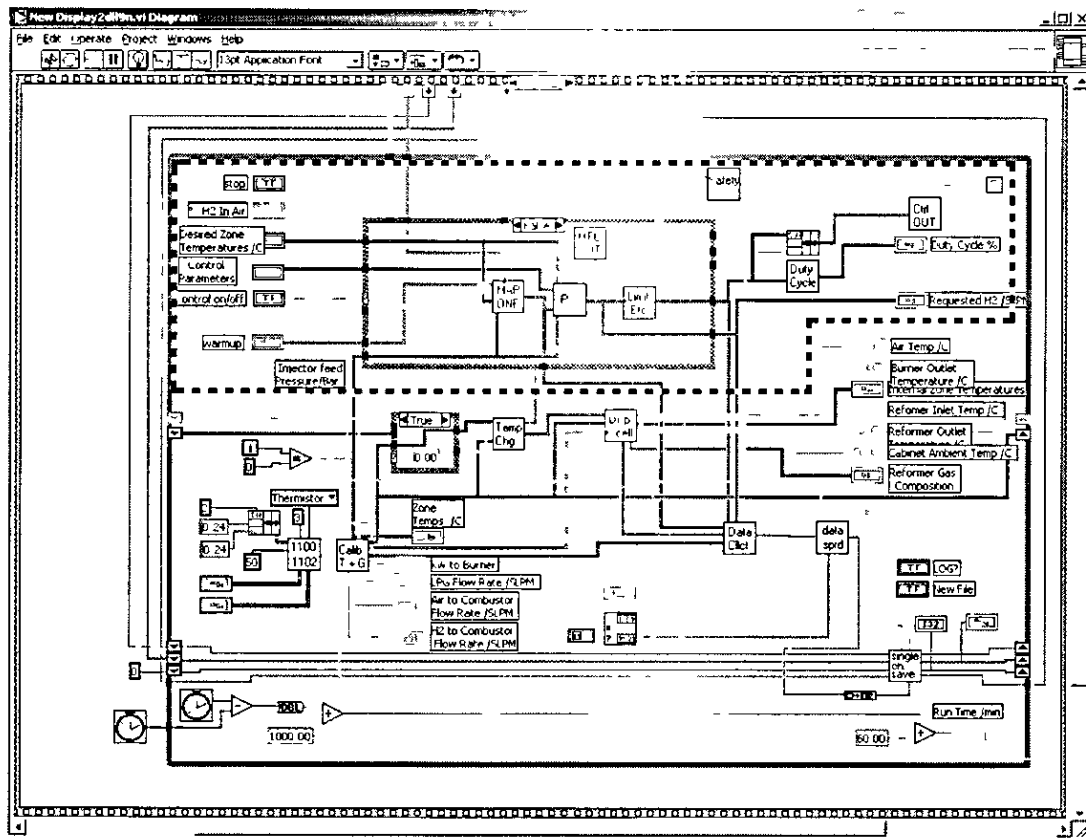


Figure 5.1: LabVIEW Circuit Diagram for the Control and Data Acquisition Software

5.2.1 Controller Design Basics

The primary purpose of the software was to act as a temperature control for the reactor and to gather data from the reactor that could then be used to develop the reactor and control strategy further. The first step in designing such a system is identifying the parameters that need to be controlled. That is to identify the primary influence on the reactor temperature. After that it should be determined whether other factors will also influence the controlled parameter. In this case the controlled variable is the reactor temperature. The primary control parameter is the amount of fuel/air to the combustor. The other main factors that will effect this are the flow rate of fuel to the reformer and the steam to carbon ratio. Once the parameter to be controlled is determined it is necessary to decide what data needs to be acquired in order that the controller can operate effectively. In this case, trivially, the reformer temperature needs to be measured in order to control it at the desired set point.

5.2.2 Data Acquisition and Logging

The control software also handles data acquisition. The data logged is a combination of the raw data from the test rig and the control signals produced by the control software. The logged data is written to an MS Excel file, which is periodically opened and closed so as to prevent the loss of all the data if a power failure occurs.

The raw data acquisition takes place using National Instruments equipment. There are 18 thermocouple readings, 3 MFC signals, a pressure transducer signal and 16 channels for the online gas analysers.

The inputs and outputs are routed through a National Instruments Signal conditioning (SCXI) chassis. The chassis is installed with 3 modules. The modules are connected in turn to front mounted SCXI terminal blocks.

Two of the modules are for data acquisition and one is for sending control outputs to the test rig. The first input module is a SCXI 1100. This is connected to a SCXI 1300 terminal block. The SCXI 1100 has capacity for 32 analogue input channels. The channels are multiplexed into a single channel on the DAQ device being used with the PC. In this case a NI-DAQ AT-MIO-16XE-50. The second input module is a SCXI 1102 designed for high-accuracy thermocouple use. This is connected to a SCXI 1303 terminal block. This allows the use of 25 thermocouples. The thermocouple signals are multiplexed into a single channel on the DAQ device used.

The output module is a SCXI 1124. This has six isolated analogue outputs. It is connected to a SCXI 1325 terminal block designed for connection to the SCXI 1124. The SCXI channel assignments can be seen in Table 5.1.

SCXI 1100 Channel List		SCXI 1124 Channel List		SCXI 1102 Channel List	
0	Brooks MFC Air to Combustor 0-5V	0	H2 Injector 1 0-5V	1	TC Combustor Zone 1-1
1	Hastings MFC H2 to Combustor 0-5V	1	H2 Injector 2 0-5V	2	TC Combustor Zone 1-2
2	Brooks MFC LPG to Reformer 0-5V	2	H2 Injector 3 0-5V	3	TC Combustor Zone 1-3
6	SIEM CO ppm 0-20mA = 0-10V	3	H2 Injector 4 0-5V	4	TC Combustor Zone 1-4
7	SIEM CO % 0-20mA = 0-10V	4	H2 MFC 0-5V	5	TC Combustor Zone 2/3-1
8	SIEM CO2 % 0-20mA = 0-10V	5	O2 MFC 0-5V	6	TC Combustor Zone 2/3-2
9	SIEM O2 % 0-20mA = 0-10V			8	TC Combustor Zone 2/3-4
10	SIEM CO ppm RELAY (1) O = 0V I = 5V			9	TC Combustor Zone 3-1
11	SIEM CO ppm RELAY (2) O = 0V I = 5V			10	TC Combustor Zone 3-2
12	SIEM CO2 % RELAY (1) O = 0V I = 5V			11	TC Combustor Zone 3-3
13	SIEM CO2 % RELAY (2) O = 0V I = 5V			12	TC Combustor Zone 3-4
14	SIEM CO2 % RELAY (1) O = 0V I = 5V			13	TC Reformer inlet
15	SIEM CO2 % RELAY (2) O = 0V I = 5V			14	TC Reformer Outlet
16	SIEM CO2 % RELAY (3) O = 0V I = 5V			15	TC Cabinet
17	SIEM CO2 % RELAY (4) O = 0V I = 5V			16	TC Combustor Air Inlet
18	SIEM O2 % RELAY (1) O = 0V I = 5V			17	TC Combustor Exhaust
19	SIEM O2 % RELAY (2) O = 0V I = 5V			24	TC Combustor Zone 2/3-3
20	SIEM O2 % RELAY (3) O = 0V I = 5V				
21	SIEM O2 % RELAY (4) O = 0V I = 5V				
24	Inj Feed Pressure				
25	(Inj Feed Pressure)				
26	(Inj Feed Pressure)				
27	(Inj Feed Pressure)				
28	(H2 SLPM)				
29	(H2 SLPM)				
30	(H2 SLPM)				
31	(H2 SLPM)				

Table 5.1: SCXI Channel Assignments

The analogue signals are converted to digital by the National Instruments DAQ board. These signals are then sent to the calibration VI in the control software. The calibration VI takes the mean of the reformer zone temperatures and passes them to the controller. The VI also calibrates the incoming signals from the MFCs and sends them to the data logging VI. It also sends the calibrated LPG flow rate to the

controller for use there. The rest of the data including the un-averaged temperature data is calibrated, ordered and sent to the data logger VI.

The data logger collates the calibrated data and passes it to an Excel file. The Excel file is closed and reopened every 10 cycles of the program. This prevents data loss in the event of a computer crash or power failure.

5.2.3 Control Strategy – Basic Principle

The control strategy is a combination of look-up tables and proportional gain closed loop control. Closed loop control is a real-time process. It can be thought of as a controller, actuators, and a feedback loop (Figure 5.2).

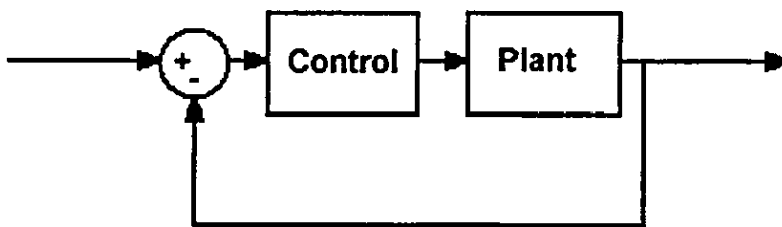


Figure 5.2: A Simple Control Loop

The desired set point is sent to the controller. This converts the value into a control signal, which it sends to the actuators. The actuators then control the plant. The status of the plant is then fed back where it is compared to the set point. The difference between the two values, or the error, is then sent to the controller. This calculates a new signal to send to the actuators, which affect the plant. The cycle is repeated. In this way the error should decrease until the plant is running at the desired set point. The use of look up tables with proportional gain means that low values of gain can be used, whilst still providing responsive control.

5.2.4 Control Strategy – Details of Operation

The controller has two operation modes. In the first the duty cycles sent to the H₂ solenoids can be set to 0% or 100%. This is to allow the purging of the H₂ supply lines to the combustor. In the second mode a closed loop controller determines the duty cycles. There are four such control loops, one for each solenoid valve. This allows each loop to be tuned individually to each valve, allowing for the greatest accuracy of control. The control loops consist of two look-up tables, a proportional controller, MFC calibration, and a limiter. This can be seen in Figure 5.3

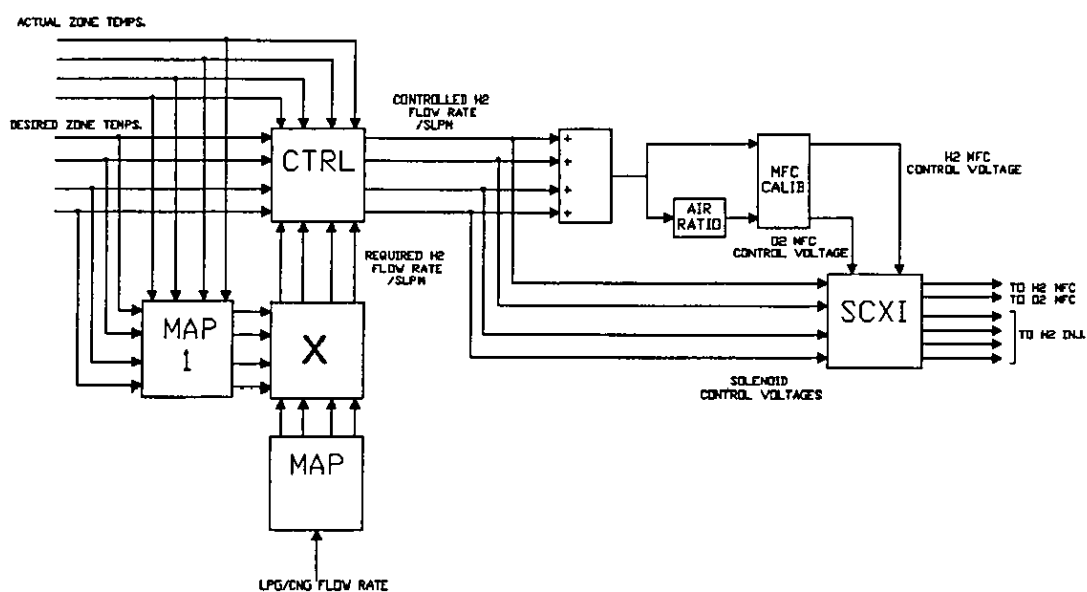


Figure 5.3: The Control Layout for the Multi-Zone Combustor

5.2.5 Development of the Control Strategy

Early versions of the control maps used simply the desired temperature and the flow rate of LPG to determine the amount of H₂ required to heat the reactor. These maps were initially developed using thermodynamic data. Later versions of these maps were modified using experimental data to make them more accurate. It was decided that just using two variables was not sufficient to satisfactorily control the reactor temperature. In order to improve the performance of the reactor under conditions of transient temperature, the first map was changed so that it produced a value for H₂

depending on the temperature difference between the desired and actual temperature of the reactor. This then required the use of a second map to take into account the effects of LPG flow rate

The first control map takes the actual temperature of the reactor and cross references it with the desired temperature. This gives an initial guess at the amount of H_2 required to heat the reactor. The second control map modifies the initial guess by allowing for the flow rate of LPG to the reactor. It does this by producing a modifying factor based on the LPG flow rate. This factor is then applied to the initial guess from the first control map. This helps the controller deal with changes in demand from a fuel cell smoothly. The use of multiple control maps in this way is equivalent to using a 3D look-up table.

The control maps are interpolated using a custom dynamic link library (dll) written using Delphi. The LabVIEW software calls this dll. Dlls were used for this part of the software, as LabVIEW is not well suited to the creation of mathematical routines of that nature

One percent of the H_2 value from the map is used as an initial guess for the proportional controller. The controller modifies the value according to the difference between the actual and desired reactor temperatures. This modified value is then added to the initial guess from the control maps. Provided the map produces a value that is close to that required, the proportional controller acts as a dynamic trim on the map value. This means that the proportional controller acts as a fine tuner on the control map output.

The outputs from the four controllers are summed and sent to the MFC calibration VI. Here the required control signal to the H_2 MFC is calculated. This signal is then modified by a user-defined ratio and converted into the corresponding MFC control signal for the air MFC. The user-defined ratio is used to set the fuel/air ratio for the combustor.

The outputs from the four controllers are also sent individually to the limits VI. This is necessary to stop the controller from asking for control signals that have no effect

on the actuator. The solenoid control unit input is a 0-5 Vdc signal. However, below 1.26V the solenoid is effectively closed. Whilst, above 4.2V the solenoid is effectively wide open. There is no point in the controller trying to progressively reduce the flow rate through the solenoid once the control signal reaches 1.26 V, and likewise no point in trying to increase the flow rate once the control signal reaches 4.2 V. For this reason the signals are passed through a saturation routine, which limits the upper and lower bounds of the control signal to 1.26V and 4.2V respectively.

5.3 Description of the Graphical User Interface

The Graphical User Interface (GUI) for the control software needs to be intuitive. This means that it needs to be easy for a user to gain an appreciation of the operating condition of the reactor at a glance, with the controls clearly defined and clearly laid out. The control software GUI can be seen in Figure 5.4.

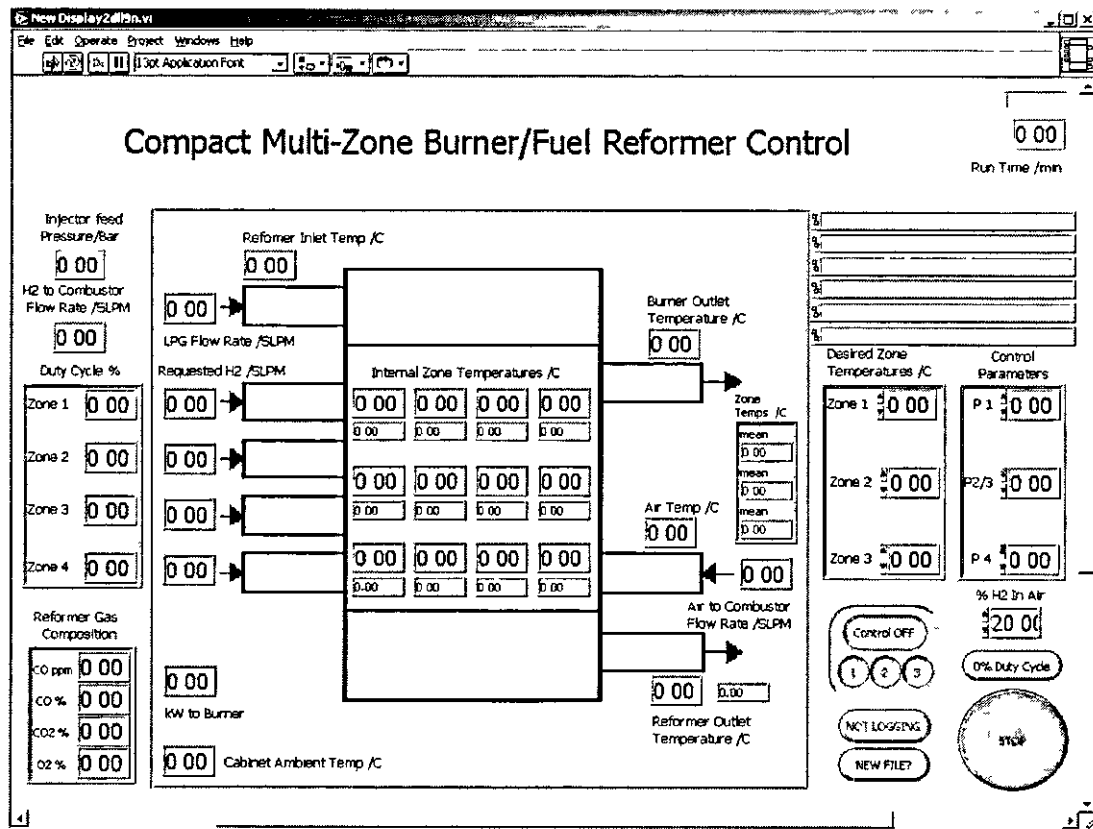


Figure 5.4: The Graphical User Interface

The central part of the GUI was taken up by a simple graphical representation of the reactor. This then had the individual thermocouple temperatures represented numerically, in the positions they take up inside the reactor, on the screen. Additionally, the change in temperature over a program cycle was also represented numerically adjacent to the actual temperatures. This allows the user to quickly assess the status of the reactor. Whether it is cooling down or heating up, as well as the temperature distribution inside the reactor. The zone-averaged temperatures were also displayed. This allows the user to evaluate quickly if the reactor has reached the desired operating set point, and is useful as a guide to setting the proportional gain for the controllers. Each of the inlet and outlet temperatures were displayed in their appropriate locations on the display along with the inlet flows. The temperatures were displayed in degrees centigrade and the flows in standard litres per minute (SLPM). Also included in the central part of the display were the cabinet ambient temperature and an approximation of the kW released by the combustion of H₂ in the reactor.

The left-hand side of the display consisted of (from top to bottom); the pressure at the inlet of the H₂ solenoids in bar, the H₂ flow rate from the MFC, the duty cycles for each of the four H₂ solenoids, and the reformat composition from the online analysers. This consisted of, CO ppm, CO%, CO₂ % and O₂%. Though the O₂% was not used.

The right hand side of the display consisted of user controls. At the top of the right hand side was a display of the control map file names, for reference purposes. Beneath these were the control parameters for the system. Firstly the temperature set-points for the reactor zones, and then adjacent to them the proportional gains for each combustor zones individual control loop. These are real-time controls and as such can be operated as the system is running. This allows the user to alter the temperature set-point to that required during a test run and for the proportional gain to be adjusted as the test proceeds. The right hand side also contains the controls for setting the fuel/air mixture to the combustor, the on/off switch for the closed loop control, including the warm-up switches, and the purge switch. The purge switch sets all the duty cycles to 100% provided that the closed loop control is switched off. The final controls on the right hand side are those that turn the data logger on and off, and a switch to open a

new log file. Next to these is the stop button for the program. Pressing the button shuts down the program. It sets all the flows to zero and shuts the H₂ solenoids.

5.4 Control Software Development

The software was developed over time, as the need for more features was determined during test rig operation. Additionally, the controller was continuously developed as the test matrix for the test rig was carried out. The following discussion documents the software development.

5.4.1 Initial Software Development

The initial development of the software centred on producing software to interface with the solenoid driver control box. This then led to initial testing and calibration of the solenoid valves.

5.4.2 Calibration of the Hydrogen Solenoid Injectors

The first stage in calibrating the valves is to determine the minimum and maximum useable duty cycle. This was done in the following way. To determine the maximum duty cycle the valves were tested individually in turn. The feed pressure was adjusted to 1 bar and the MFC was set at a constant flow rate. The setting was sufficiently high that the solenoid valves would control the flow and that any decrease in the flow through the valve would be shown as an increase in feed pressure. The valves were set fully open (100% duty cycle) and the duty cycle decreased until an increase in feed pressure was observed. The increase in feed pressure signified a decrease in flow through the valve and so the higher operating limit was reached.

To determine the minimum useable duty cycle the valves were set to 0% duty cycle and slowly opened until the feed pressure dropped. This signified an increase in flow through the valve and therefore the lower limit of operation. The minimum and

maximum useable % duty cycles were found to be 24 and 86% respectively. These values equate to control voltages of 1.26 and 4.2 V respectively.

5.4.3 Solenoid Valve Operating Characteristics

It could be seen from the calibration of the solenoids using air that firstly, the flow rate through the valves was dependent on the feed pressure to the valves only. Secondly, allowing for errors in flow rate measurement the valves themselves operate linearly with respect to the control voltage applied for a given pressure. From this information it becomes clear that when more than one valve is used together it becomes difficult to determine the flow rate through any one valve without knowing the feed pressure to the valves. An assumption was made that the feed pressure to the valves was the same for each valve. This was reasonable as the manifold design was such that the valves were all fed from a common source, which was then split and fed to the individual valves.

For a single valve, if the feed pressure is not controlled, then as the valve is opened or closed the feed pressure varies accordingly. If the valve closes, the feed pressure increases and *visa versa*. This has the side effect of altering the flow rate by either too much or too little. For example, if it is desired to half the flow rate through the valve, it is common sense to close the valve halfway. However due to the accompanying increase in feed pressure the flow rate will be greater than half the original flow rate. An obvious solution is to control the feed pressure with a regulator. But the drawback is that in order to control the pressure in this way it will be necessary to vent some of the fuel to atmosphere. As the fuel being used is H_2 this is out of the question due to the low percentage required for combustion in air. Because of this it was decided to create a look up table that would produce a control signal based on the feed pressure to the solenoid valves and the amount of H_2 required by the controller.

5.4.4 Controller Development

The original controller concept was to adopt a system where the controller would decide how much fuel was required for the combustor, and then a look up table would take the control signal and convert it into the appropriate voltage to be sent to the solenoid valves. The initial controller design utilised two look-up tables. The first of which provided an initial guess for the amount of H_2 required to reach the set point temperature, based on coolant flow and the set point temperature. The second of which was used to turn the control signal into the correct voltage for the solenoid valve to produce the desired amount of fuel to the combustor. It did this by comparing the desired H_2 flow rate with the measured feed pressure at the inlet to the H_2 solenoid manifold. Each combustor zone had its own controller. This was so that differences in fuel demands between the zones could be easily accommodated, and the controller could be fine tuned to the needs of each zone.

5.4.5 Look-up Table Generation

The first look-up table was produced as follows. Firstly the integral of the specific heat capacity of N_2 for the appropriate temperatures corresponding to the look-up table axis were calculated. This data was used to create a table of temperature against N_2 flow rate (SLPM). The intersecting points gave values of thermal power in the N_2 stream (kW).

To calculate the amount of H_2 required to heat the N_2 , the enthalpy of formation of H_2O at the appropriate temperatures was calculated. This was done in the same way as for the Excel system model described in Chapter 3.

In order to take into account the amount of H_2 required to heat the combustor air to the required temperature, the amount of thermal power (kW) in the combustor air was calculated. It was assumed that the combustor air would be preheated to $500^\circ C$. This meant that beneath $500^\circ C$ the air would have excess thermal power and above that it would require further thermal power. To calculate the amount of air required for the combustor an iterative loop was used. The loop calculated the amount of H_2 required

to heat the N_2 on its own. It then calculated the amount of air required for the combustor and the appropriate amount of thermal power in the air. It then repeated this calculation until convergence. In this way an initial first look-up table was created for the reactor temperature controller.

5.4.6 Development of the Look-up Table

The look-up table was modified for use during the steam reforming tests, in the following way.

Aspen Plus was used to calculate the thermal power required to support the steam reforming reaction, for temperatures from 300 – 1000°C, LPG flow rates of 0 - 2 SLPM, and steam to carbon ratios of 1 – 3. The thermal power required to heat the combustion components to the reactor temperature was also calculated. This was added to the energy required to support the steam reforming reaction. This was then converted into the required flow rate of H_2 assuming 100% conversion of the fuel. This new map was again used as a first iteration. The look-up table was modified using empirical data gained from running the steam reformer. This allowed each combustor zone to have a look-up table produced especially for it.

5.4.7 Initial Controller Testing

Using the first iteration of the controller, under start up, the solenoid valves kept decreasing the flow until they closed. The feed pressure then built up and the H_2 flow stopped. To counter this a routine was coded that increased the duty cycle by 25% to all of the valves equally, when two or more of the valves had closed. This was meant to keep the flow rate split across the valves the same, but change the operating pressure of the H_2 inlet. This was to allow the controller to accommodate the large changes in flow rate required for quick start up times. Unfortunately the system didn't work as planned. The solenoid valves duty cycle oscillated between two states. This provided adequate control but was not an elegant solution to the problem.

5.4.8 Simplification of the Controller

From a review of the solenoid valve calibration tests, it was also found that by controlling the MFC that feeds the solenoid valves it is possible to keep the feed pressure constant. When one of the solenoid valves is closed halfway, and the MFC flow rate is also reduced by half, the feed pressure remains constant and the flow through the solenoid is halved. This seems obvious when applied to a single valve, but when this method is extended to more than one valve at once, it still holds true regardless of the position of the other valves. The flow through the other valves is unchanged and the flow rate through the valve that is required to be changed, is altered by the desired amount.

This means that it is possible to control the flow through the individual valves without the need to know or directly control the feed pressure. As a result of this it was decided to remove the valve calibration look-up table from the controller. This improved the controller performance by removing the oscillation of the valves described above.

5.4.9 Final Controller Development

In order to allow the controller to respond to transients in fuel demand from a fuel cell, a second look up table was added to the controller. This created the equivalent of a 3D look-up table. The input variables for the look-up table were the set point temperature, the actual temperature and the flow rate of LPG to the reformer.

The first look-up table was a 2D Array. This compared the set point temperature with the actual temperature and produced a value for H₂ flow rate. The first map was designed to augment the proportional control. It set a maximum flow rate to the zones of 2.5 SLPM H₂, this was so that each zone had an equal split of the maximum 10 SLPM delivered by the MFC. This was later raised to 5 SLPM H₂ to take into account the increase in size of the MFC (required when higher reactor temperatures and LPG flow rates were used). The maximum flow rate was in place until the reactor reached the desired set point. Then a flow rate determined from the experimental running data

was set. The experimental data used to determine the values of the look up table results was taken from a test where the flow rate of LPG to the reformer was 1 SLPM. Above the set point temperature a desired flow rate of 0 SLPM was set. This was to minimise overshoot. It was important to minimise controller overshoot as excessive temperatures could damage the catalyst inside the reformer. Because the first look-up table compares the desired temperature with the actual temperature it can be used to help control the start up time of the reactor. By making the map mimic the effect of a proportional gain (K_p) the actual proportional controller has to do less work. This allows the use of lower values of K_p and promotes control stability.

The second look up table was one-dimensional. This modified the value produced by the first look up table according to the flow rate of LPG through the reformer. As lookup one was produced using an LPG flow rate of 1 SLPM as a reference. This meant that for flow rates of LPG less than 1 SLPM, the 1D look up table reduced the amount of requested H_2 , and for flow rates of LPG greater than 1 SLPM, the requested H_2 was increased. In this way the temperature change in the reactor due to changes in the flow rate of LPG could be easily accommodated. It was not necessary to include steam to carbon ratio as a control factor because under ordinary operating conditions the steam to carbon ratio would be kept constant.

The interpolation and extrapolation of the look up tables was originally done using a custom VI in LabVIEW. This was later altered so that a dynamic link library (dll) using Delphi was used instead. This was a more computationally efficient way of doing the same job.

5.5 Syringe Pump Software

The syringe pump was also controlled using software built using LabVIEW. The software allowed the flow rate of H_2O to be varied from 0 – 20ml/min. It allowed the pump to take two different syringe sizes, which were manually set by the user. This allowed the range of flow rates available to be increased.

6 Multi-Zone Combustor Evaluation

6.1 Initial Operation

The initial tests carried out on the reactor were concerned with the performance of the combustor. Tests were carried out to determine whether the combustor could light-off at room temperature using hydrogen and methane. Tests were also carried out to determine the optimum amount of insulation for the reactor. The effect of coolant flow through the reformer was investigated as well as the effect of the direction of flow through the combustor. The effect of the combustor flow path on the controllability of the reactor temperature was investigated as were the heat transfer properties of the reactor.

6.1.1 Determination of the Pressure Drop

The pressure drop across the reforming layers and the combustor was recorded. For the combustor this was done by first recording the pressure drop across the solenoid valves, flash back arrestors and rotometer and fittings, and then recording the pressure drop across the combustor and the flashback arrestors and valves together. The results were subtracted from each other to produce the value for the pressure drop. This was repeated for the following flow rates; 5, 10, 15, 20 and 24 SLPM N₂. The results can be seen in Table 6.1.

N ₂ SLPM	Pressure drop across all fittings /mbar	Pressure Drop across fittings and Combustor /mbar	Pressure Drop Across Combustor /mbar
5	76	75	-1
10	173	178	5
15	318	326	8
20	498	510	12
24	674	681	7

Table 6.1: Pressure Drop Across the Combustor

To test the pressure drop across the reformer it was necessary to use high flow rates in order to take a reading. As before, the pressure drop across the rotometer and fittings was taken followed by the pressure drop across the fittings and reformer, and the results subtracted from each other. This was repeated for the following flow rates 60, 120, 180 SLPM N₂. The results can be seen in Table 6.2.

N ₂ SLPM	Pressure drop across all fittings /mbar	Pressure Drop across fittings and Reformer /mbar	Pressure Drop across Reformer /mbar
60	0.128	2	1.872
120	0.522	5	4.478
180	1.424	14	12.576

Table 6.2: Pressure Drop Across the Reformer

It can be seen that the pressure drop is much higher across the combustor than the reformer. This is due to the more complex flow field inside the combustor. The use of a diffusion plate between the air and H₂ streams is likely the major contributing factor to the losses. In contrast, the reformer flow field is straight through with no blockages. The pressure drop across the reactor has implications for the system design. It is desirable to have as low a pressure drop as possible. This reduces the need for additional compressors, which bring parasitic losses to the system, reducing its efficiency.

6.2 Initial Lighting Off Experiments

The initial combustor test was to see if the combustor would light off at room temperature or if some form of external heat would be required to start the reaction.

2.5 SLPM of H₂ was introduced to the combustor with air in a ratio of 1/5. The H₂ was split equally between the four combustor zones. The reactor was successfully heated from room temperature to a maximum temperature of 300°C. This showed that no heating of the reactor was required prior to introduction of the H₂/air mixture. This is good because it cuts down on parasitic losses from the system.

For clarity when interpreting the following results the thermocouples are numbered as seen in figure 6.1.

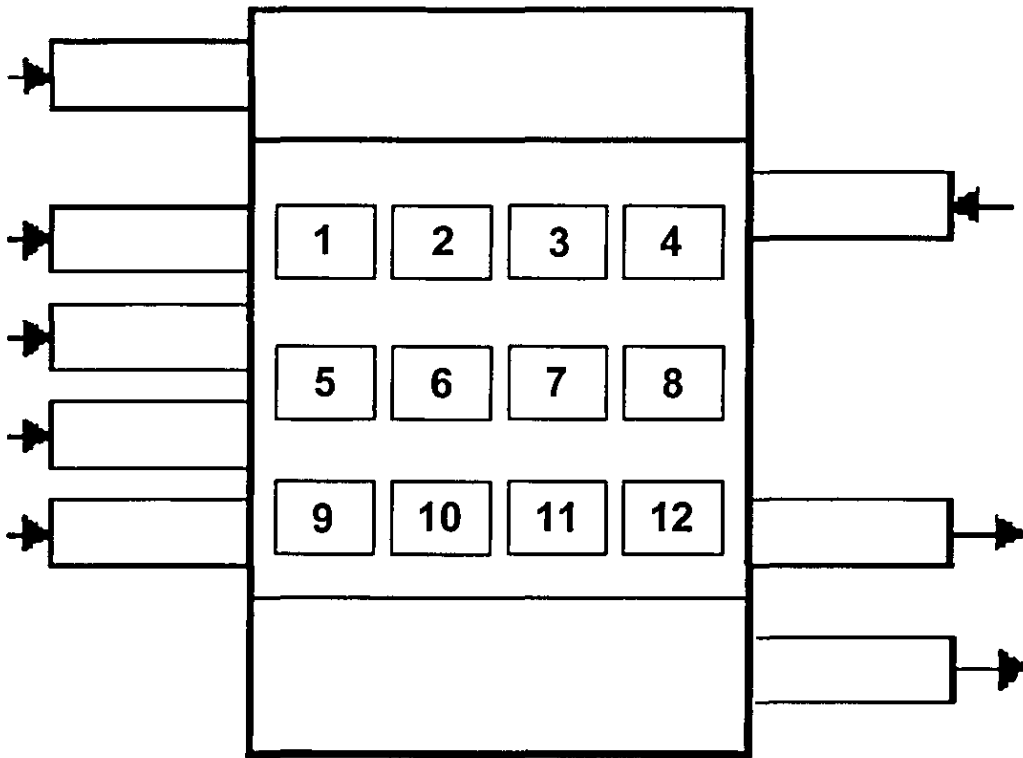


Figure 6.1: The Position of the Internal Thermocouples

6 2 1 Tests Without Coolant and the Addition of Insulation

The first set of tests carried out using the reactor doubled as a way of becoming familiar with the operation of the test rig and as a means of determining the optimal amount of insulation to be applied to the reactor. Determining the optimum amount of lagging for the reactor is not as trivial a problem as it seems at first glance. There is a trade off between the cost of the insulation material and the cost of the fuel required to heat the reactor. There are also space considerations. In this case space limitations were the deciding factor in determining the amount of insulation added to the outside of the reactor. It was not possible to add more than 3 layers of fibre wool to the reactor due to the tubing attached to the reactor. It was also necessary to allow the

thermocouple manifold sufficient access to the air so that its temperature would be low enough to allow the thermocouple ports to seal effectively. The initial tests also allowed any unforeseen problems with the test rig to be acknowledged.

6.2.2 Operational Failure of the Hydrogen Solenoids

During initial running the H₂ solenoids became overheated. They have a maximum recommended ambient temperature of 45°C [Ref. The Lee Company (2000)]. This was exceeded and three of the solenoid valves lost control response. Once they had been allowed to cool down controllability returned. The effect of this can be seen in Figure 6.2. One of the valves failed in the closed position. The results of this can be seen by the decrease in temperature in one area of the reactor whilst other areas experience a temperature increase. This is because the flow rate of H₂ to the reactor as a whole stayed the same but the split to the zones was altered. The cause of the failure was the positioning of the valves in the test rig. The valves were positioned away from the reactor but directly above it. This meant that heat from the reactor was transferred to the valve by convection. To stop this from happening again an insulating shield was placed between the valves and the reactor.

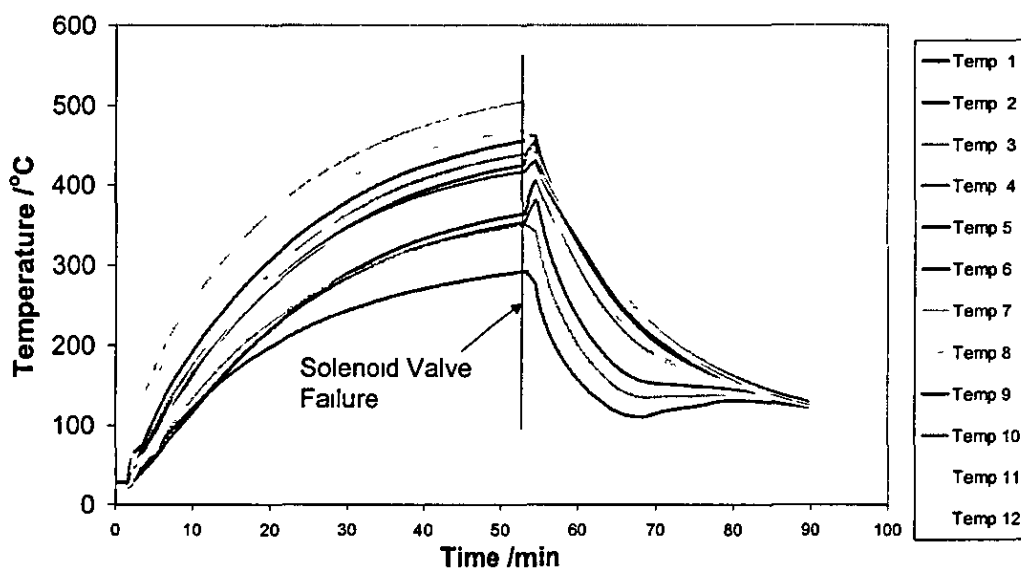


Figure 6.2: Start Up of the Combustor Showing Solenoid Valve Failure

6.2.3 Start Up Times of the Microchannel Reactor

It can be seen in Figure 6.3 that as further layers of insulation are added to the reactor, the start up time decreases. This is a consequence of reduced heat loss due to the insulation. It can also be seen that the internal temperature spread decreases with the addition of insulation but that adding further insulation has little effect.

6.2.4 Internal Reactor Temperature Distribution

It can be seen in Figure 6.2 that the temperature distribution in the reactor varies not only longitudinally, but transversely as well. This has implications on the effectiveness of the multi-zoned design's ability to control the temperature of the reformer accurately. This is because there is no facility to control the temperature transversely in the design of the reformer. This can lead to the formation of hot and cold areas in the reformer. This will be discussed further in Section 6.3.

6.2.5 Effect of Preheating the Air on the Temperature Distribution

The combustor was fed 1 SLPM H_2 into each zone with 20 SLPM air across all of the combustor zones. The Air was preheated in stages. Firstly using the heater temperature as a guide. The heater was raised to 250°C and 500°C. The addition of a thermocouple on the air inlet to the combustor showed that the air temperature was much lower than the heater temperature (An actual air temperature of 270°C with an indicated heater temperature of 600°C). This led to the heater being modified by the addition of stainless steel granules inside the heater tube as discussed in Chapter 4. The air temperature was then raised to 480°C.

Start up time to 700C (Temp7) and burner temperature spread.

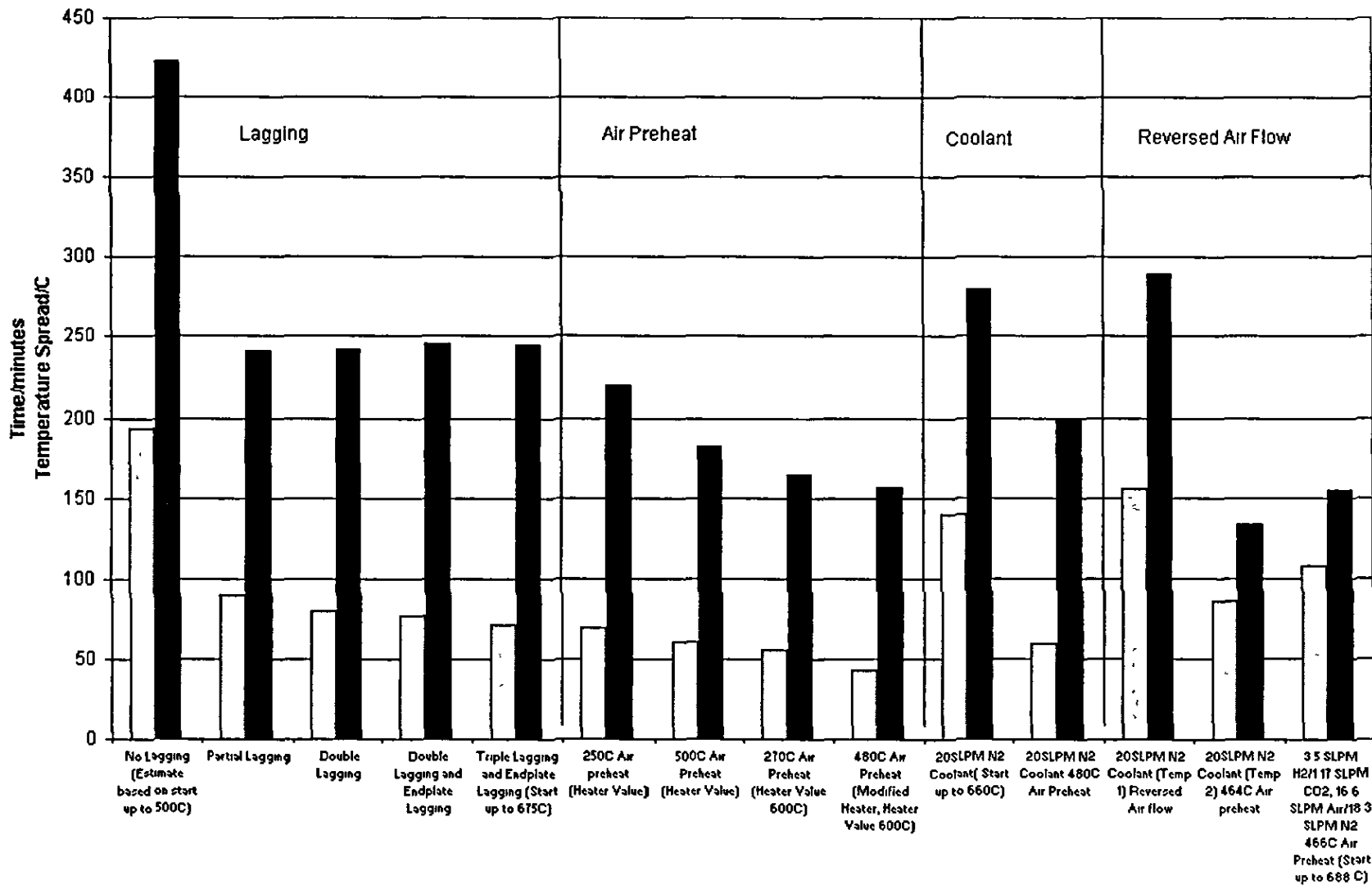


Figure 6.3: Start up times and temperature spread of the combustor

The introduction of pre-heated combustor air has a positive effect on both the start-up time and the temperature spread across the reformer. This can be seen in Figure 6.3. The effect on the start up time is due to the extra energy transmitted to the reactor via the air stream. The decrease in temperature spread is also due to the increased energy in the combustor stream. It manifests this by raising the temperature of zone one. An effect of the increase in energy in the combustor stream is that it has a greater effect on the temperature profile further downstream. It increases the temperature spread across each combustor zone, which is undesirable due to the controller set-up.

6.2.6 Effect of Coolant on the Temperature Distribution

The reactor was next tested with 20 SLPM of N_2 running through the reforming side of the reactor. This was done firstly to make sure that the reactor would still light off when there was coolant being used, and to determine the effect of the coolant flow on the temperature distribution inside the reactor. It can be seen in Figure 6.3 that the effect of the coolant was to increase the temperature spread inside the reactor, and to increase the start up time of the reactor. The increase in the temperature spread is a result of the coolant moving heat from the reactor inlet towards the outlet. This combined with the action of the combustor exhaust retards the performance of the inlet zone of the reactor.

6.2.7 Effect of Combustor Air Direction on the Temperature Distribution

The initial testing took place with parallel flow of the coolant and macro-combustor flow. Testing then progressed to running the reactor in a counter flow configuration. This was to determine the optimal configuration for the control of the system.

The coolant flow rate was set to 20 SLPM, the flow rate settings for the combustor were as before. The test was run both without any air preheat, and with an air preheat of 480°C.

The direction of flow of the combustor air was found to have an effect on the temperature distribution inside the reactor. As seen in Figure 6.3, in the parallel configuration the reactor exhibited a faster start-up time than in the counter flow configuration, but the counter flow configuration produced a smaller temperature spread. The decision was made to run the reactor in the counter-current configuration for subsequent tests of the reactor. This was due to the constraints placed on the controller due to the lack of transverse temperature control. It was decided that the configuration with the smallest temperature spread should be the one to use, as it would improve the temperature distribution inside the reformer. It was decided that that was a bigger consideration than the start up time as that could be affected more easily by the control strategy.

6.2.8 Lighting Off the Combustor Using Methane

A series of tests was carried out to determine if the combustor could be started using CH_4 only, rather than H_2 . This is because, depending on the overall fuel processor design, it may be advantageous or necessary to start the combustor using the fuel to be used for the reformer. The flow rate of CH_4 in this case was determined by comparison of the enthalpy of combustion of CH_4 and H_2 , the equivalent amount of CH_4 to 4 SLPM H_2 was found to be approximately 1 SLPM.

The first test took place at room temperature 0.25 SLPM CH_4 was fed into each combustor zone and 20 SLPM Air was fed across the combustor. The test was run for 30 minutes and no temperature change was observed.

In the second test the same flow rates of CH_4 and Air were used as before. But this time the air was heated from 150 – 500°C in steps of 50°C. This was done to supply activation energy to the reaction in order to try and start the combustion of CH_4 inside the reactor. Again no evidence of combustion was seen.

In the third test, the fuel feed to the combustor was modified so that H_2 and CH_4 could be sent to the combustor independently of each other or together. The reactor was heated by combusting H_2 until the minimum temperature reached 450°C. The reactor

was then purged with N_2 until the temperature reached $400^\circ C$. This served the purpose of setting the reactor temperature whilst removing any H_2 from the combustor. CH_4 was then fed into the combustor for 10 min in order that any slight temperature change to be observed clearly. The process was repeated, each time raising the reactor temperature by $50^\circ C$ until combustion of CH_4 was achieved.

At each temperature the CH_4 flow rate was varied from 1, 2, 3 SLPM. This was to determine the effect, if any, of altering the fuel/air ratio inside the combustor on the light off point.

As can be seen in Figure 6.4 light off was achieved at approx. $500^\circ C$. This is too high a temperature to be useful in a fuel processor as this would require the reactor to be preheated by combusting H_2 or using electric heaters to directly heat the reactor. However as the catalyst was designed for use with H_2 this is not an unexpected result. To facilitate the use of other fuels in the combustor a new catalyst formulation would have to be produced.

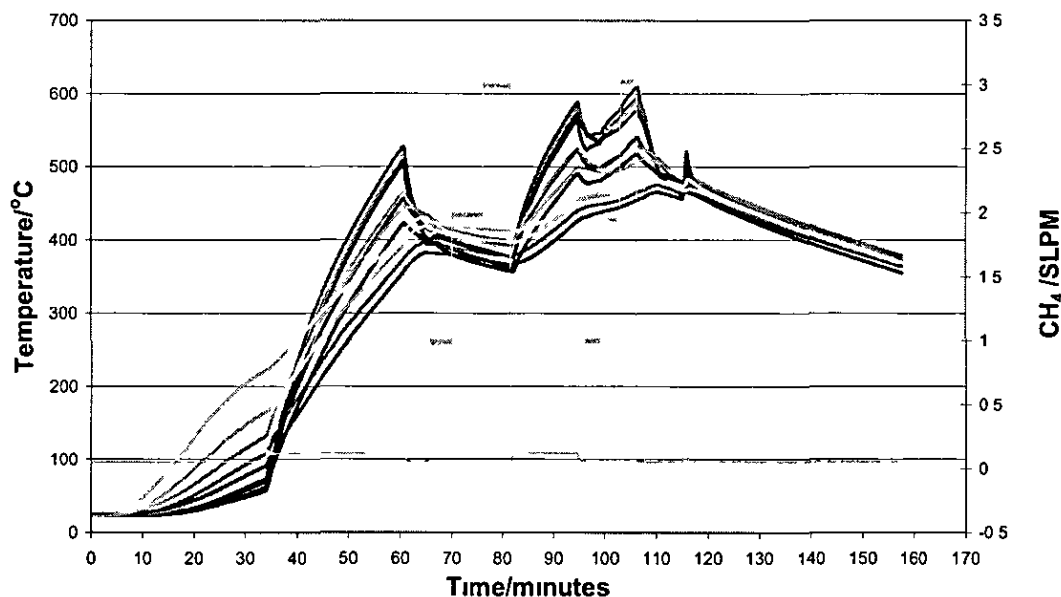


Figure 6.4: Start Up of the Combustor Using CH_4

6.3 Individual Combustion Zone Tests

Before the combustor was run under closed loop control, it was necessary to determine whether the zones could be controlled individually and if the thermocouples were located correctly in the reactor. Therefore, the reactor was further tested by giving a H_2 supply, at a flow rate of 4 SLPM, to each of the four inlets sequentially, in a procedure of 5 minutes operation to zone 1, followed by 5 minutes stop, then shift to zone 2 and so on in turn. The air was supplied to the reactor, synchronised to the H_2 supply, at a H_2 to air volume ratio of 1:5. Figures 6.5-6.8 show the measured rate of change of temperature as recorded by each individual thermocouple.

It can be seen in Figure 6.5 that when the H_2 supply is switched on to zone 1, the temperatures at the four positions inside zone 1 perform differently. Position 4 has the highest temperature gradient while the temperature at position 1 has hardly increased. From Figure 6.1, it can be seen that position 1 is geometrically next to the H_2 inlet. Incidentally, the air flows in the same direction after passing the rest of the zones. The coincident flows, therefore, move the heat from position 1 to the downstream positions, and reduce its temperature. Position 4 is situated just before the outlet. It therefore accumulates the heat delivered through the flows and the heat generated due to the combustion reaction at that position. As a result it ends up with the largest temperature gradient among the four positions inside zone 1.

When the H_2 is switched to zone 2 as shown in Figure 6.6 after the 5 minutes cooling period, the temperature gradient at positions 1 and 2 inside zone 1 are large and well above the gradients in zone 2. Again, this is because the airflow brings some of the heat generated in zone 2 and some of the unburnt H_2 downstream. However, inside zone 2, where the H_2 is supplied, it appears that little combustion occurs at position 3. Clearly, this is due to the heading impact between the H_2 supply and the airflow. The H_2 is pushed away from the position by the airflow. The highest temperature gradient in zone 2 is at position 2, which potentially contains the highest H_2 concentration.

When the H_2 is further switched to zone 3, as seen in Figure 6 7, the temperatures are monitored by the same group of temperature sensors as zone 2. Clearly, the temperature gradient at position 3 becomes the highest followed by position 4. Again, this is mainly due to coincident flows of H_2 and air.

Finally, when the H_2 is switched to zone 4 in Figure 6 8, the gradients at positions 1 and 2 are the highest. Again, this is because of the heading impact between the H_2 and airflows.

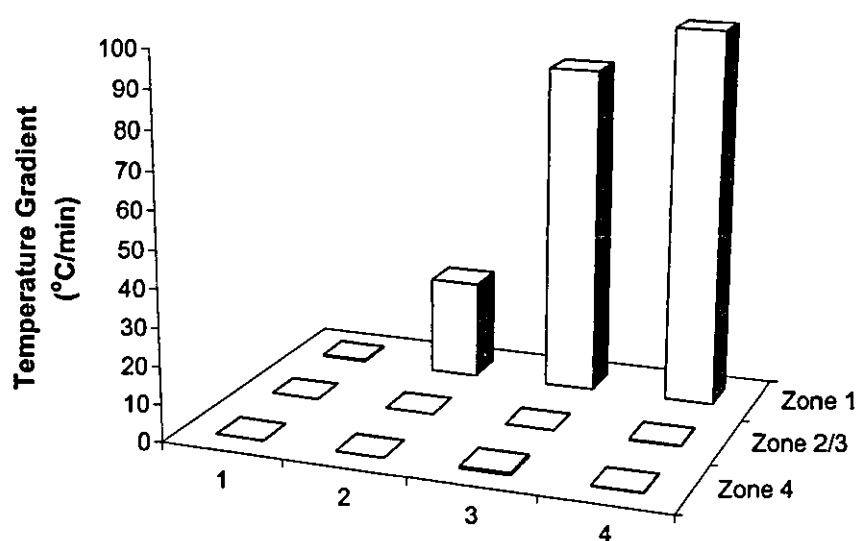


Figure 6.5: The Rate of Change of Temperature Due to H_2 fed to Zone One

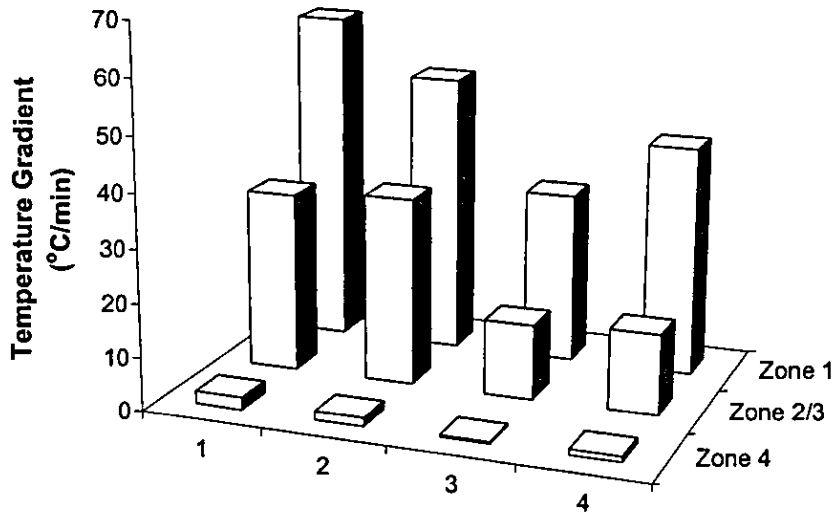


Figure 6.6: The Rate of Change of Temperature due to H₂ Fed to Zone Two

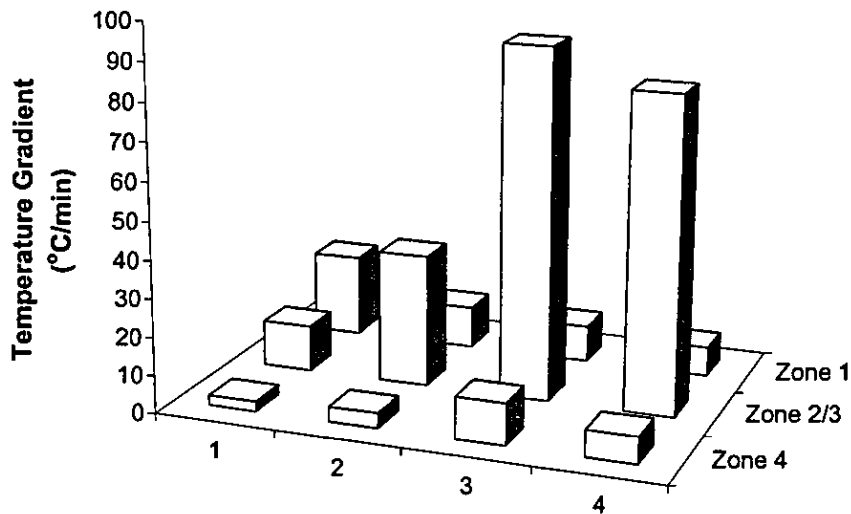


Figure 6.7: The Rate of Change of Temperature due to H₂ Fed to Zone Three

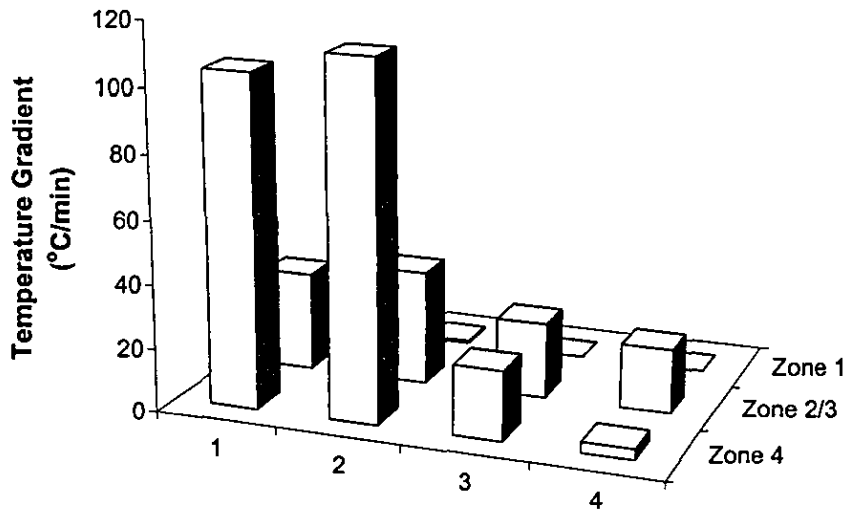


Figure 6.8: The Rate of Change of Temperature due to H₂ fed to Zone Four

It can be seen that each zone can for the most part be controlled individually. However, due to the internal flow interaction between the H₂ and air, there is some spill over from each zone to the next downstream one.

6.4 Closed Loop Control of the Combustor

A series of tests were run using the closed loop controller developed in LabVIEW and described in Chapter 5. These were to test the effectiveness of the controller before the heat transfer tests and subsequently steam reforming was carried out. The development of the control strategy continued throughout the running of the reformer under steam reforming conditions. These results represent the first iteration of the control system. Figure 6.9 shows the test results obtained by using the closed loop controller. The temperatures shown in the figure were the averaged zone temperatures. These averaged temperatures are also used as the feedback to the control system for adjusting the H₂ flows. The results showed that the zone average temperatures agree well at all three set points, 400 °C, 550 °C and 600 °C.

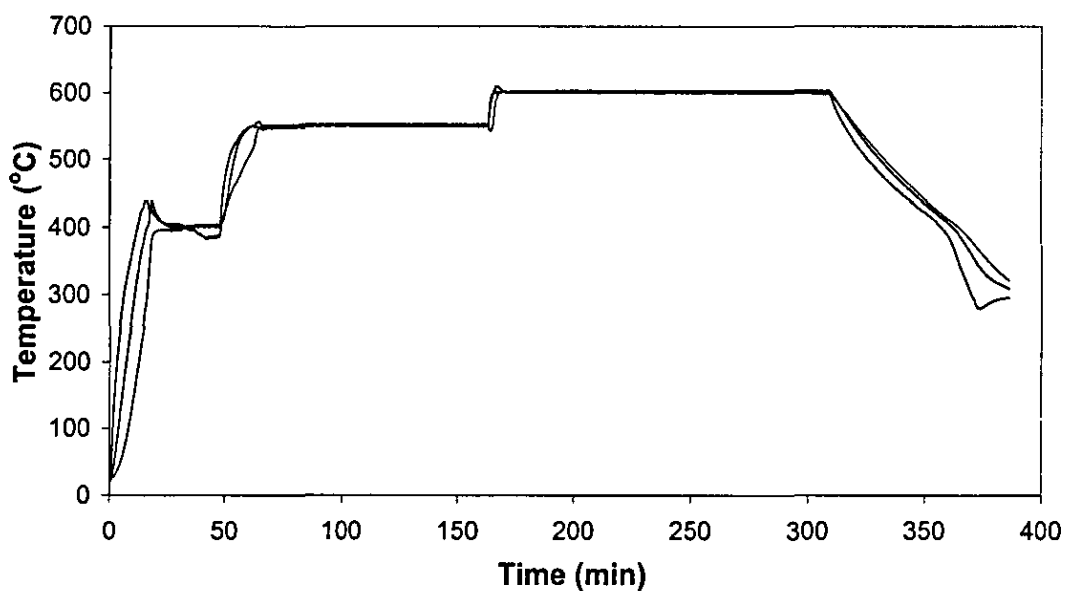


Figure 6.9: Closed Loop Control of the Combustor Temperature

It can be seen that the system provides sufficient controllability to set the reactor temperature longitudinally along the reforming stream.

Figure 6.10 compares the longitudinal temperature distribution of the multi-zone reformer with that of a more traditional packed bed reformer design [Ref A. Henzel (2002)] The improvement in temperature control can clearly be seen. The multi-zone approach allows the temperature to be accurately controlled and so by extension the reformate composition.

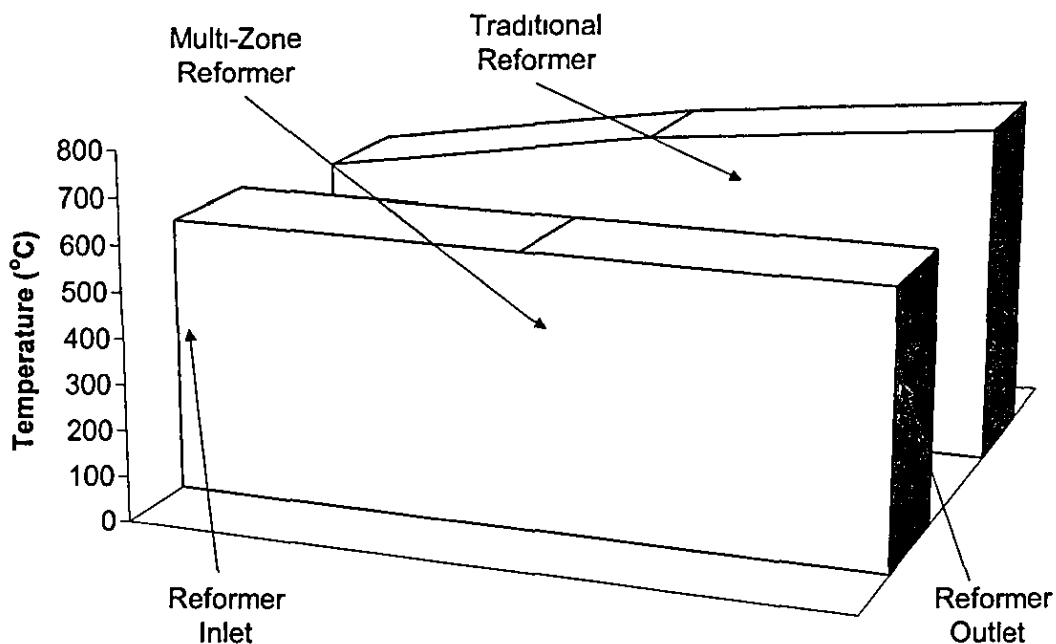


Figure 6.10: A Comparison of Traditional Reformer Temperature Control and the Multi-Zoned Approach

6.5 Heat Transfer Performance

The motivation for the following tests was to determine the effectiveness of the microchannel heat exchanger at distributing heat from the catalytic combustion of the H_2 air mixture, to the reforming reactors on either side of the combustor. During the test, H_2 and air in a ratio of 20% H_2 : 80% air, was fed to the combustor. The combustor temperature was controlled by varying the amount of H_2 fed to each zone, with the airflow being adjusted accordingly. N_2 was used as a coolant and was passed through the reforming reactors to take up the heat from the combustor. Measurements of the values required to perform a power balance on the reactor were taken once the temperatures of the various flows and the reactor had settled. The measured parameters were as follows.

- 1) Coolant inlet temperature (°C)
- 2) Coolant exit temperature (°C)
- 3) Air inlet temperature (°C)
- 4) Combustor exhaust temperature (°C)

- 5) Coolant flow rate (SLPM)
- 6) Air flow rate (SLPM))
- 7) H₂ flow rate (SLPM)
- 8) Combustor temperature (°C)
- 9) Ambient temperature (°C)
- 10) H₂O (liquid) produced from H₂ combustion (cm³)

With the exception of the H₂O produced from the combustion of the H₂ the above parameters were averaged over a time of 10 min. The amount of H₂O recorded was the total H₂O produced over the 10 min period. By comparing the amount of H₂O produced with that which, would have been produced by complete combustion of the H₂, the percentage of H₂ combusted was calculated and hence the H₂ conversion efficiency. The Figures 6.11 and 6.12 show the effects of combustor temperature and coolant flow rate on the H₂ conversion efficiency respectively.

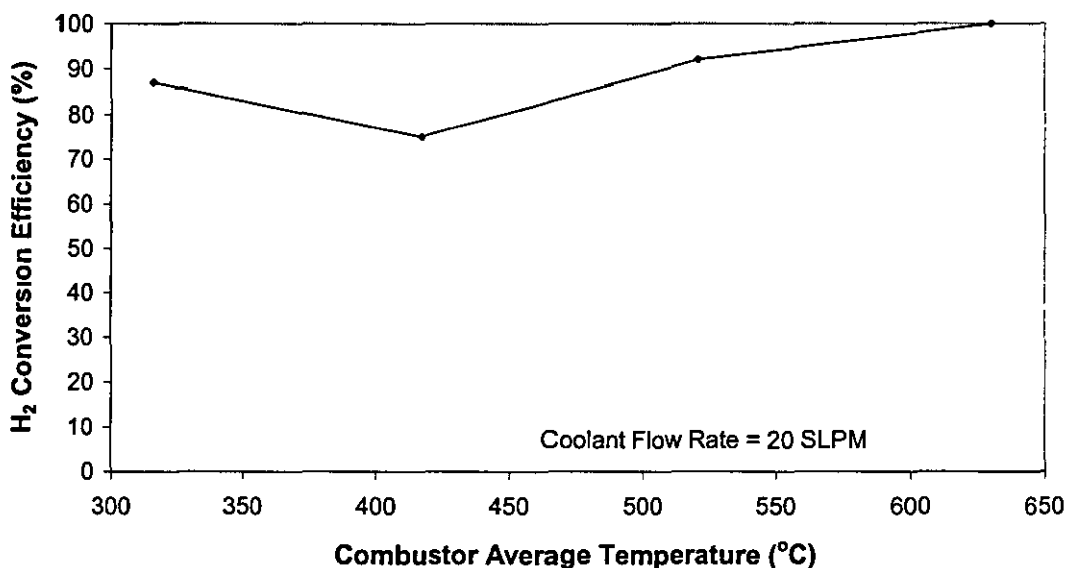


Figure 6.11: The H₂ Conversion Efficiency w.r.t. Combustor Temperature

It can be seen there is a trend, which suggests that the greater the combustor temperature the higher the H₂ conversion efficiency becomes. It can be seen that H₂ conversion at 400°C does not follow the observed trend. This is due to experimental error regarding the calculation of H₂ conversion based on the collected H₂O from the combustor exhaust, which can never be exact. On the other hand, the influence of the

coolant flow rate on the H₂ conversion is relatively small. There does appear to be a trend of increasing H₂ conversion with N₂ flow rate but this is by no means clear and can be accounted for in the same way that as the anomaly in Figure 6.8. It can be seen that the averaged H₂ conversion efficiency is in the region of 90%.

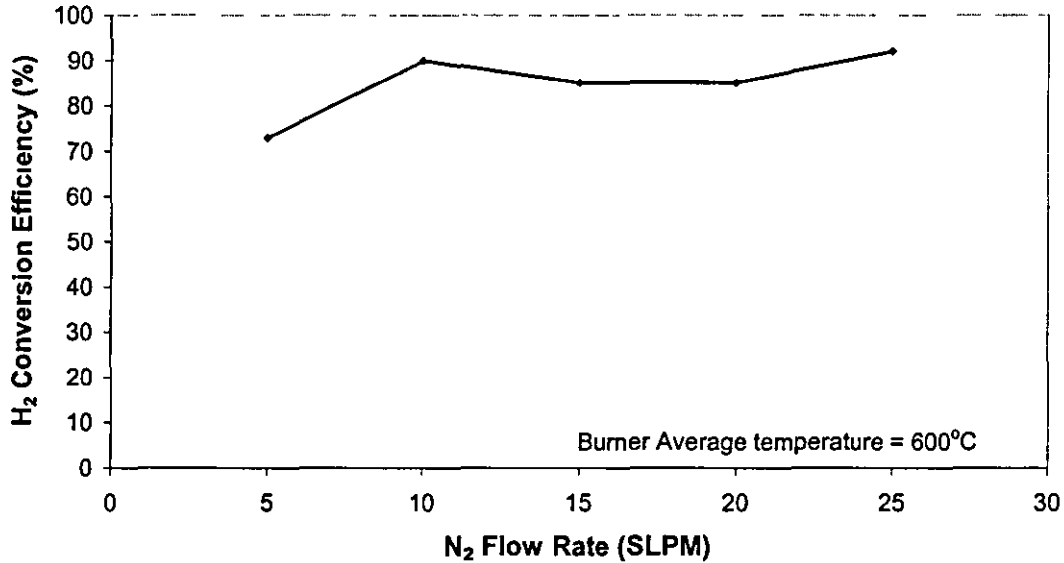


Figure 6.12: The H₂ Conversion Efficiency w.r.t. Coolant Flow Rate

To calculate the heat transfer efficiency a thermal power balance of the reactor was performed. The thermal power transferred to the reforming reactor, which is the thermal power obtained by the reforming streams was calculated by

$$P_{reactor} = m_R \times \int_{T_1}^{T_2} C_{p,R} dT \quad \text{Equation 6.1}$$

where m_R is the flow rate of the reforming stream, $C_{p,R}$ is the specific heat capacity at constant pressure, T_1 is the reformer inlet temperature, and T_2 is the observed outlet temperature of the reforming stream. The pressure drop across the reactor at the operating flow rates was negligible.

The thermal power produced from the combustion of the H₂ in the combustion layer of the reactor was obtained as

$$P_{burner} = (\dot{m}_{H_2} \eta_b \Delta H_{f_{H_2O}}) + P_{air} - P_{exhaust} \quad \text{Equation 6.2}$$

where m_{H_2} is the flow rate of H_2 in moles per second, η_b is the H_2 conversion efficiency of the combustor, and $\Delta H_{f_{H_2O}}$ is the enthalpy of formation of H_2O at the combustor temperature. P_{air} and $P_{exhaust}$ are the thermal power in the combustor air supply and combustor exhaust respectively. They were calculated using the same method as $P_{reactor}$ with the appropriate temperatures and specific heats for each stream used.

The heat transfer efficiency was then defined as

$$\eta_{HEX} = \frac{P_{reactor}}{P_{burner}} \quad \text{Equation 6.3}$$

The heat flux from combustor to reforming streams was calculated as

$$q = \frac{P_{reactor}}{A} \quad \text{Equation 6.4}$$

where A is the area available for heat transfer.

Figure 6 13 shows the effect of the temperature of the combustion layer of the reactor on the heat transfer efficiency and heat flux. The reforming stream flow rate was set to 20 SLPM. It can be seen that the heat transfer efficiency decreases as the average temperature of the combustor increases. At an average combustor temperature of 420°C, the heat transfer efficiency peaks at 85%. As temperature increases, it decreases to a level of 65% at an average temperature of 630°C.

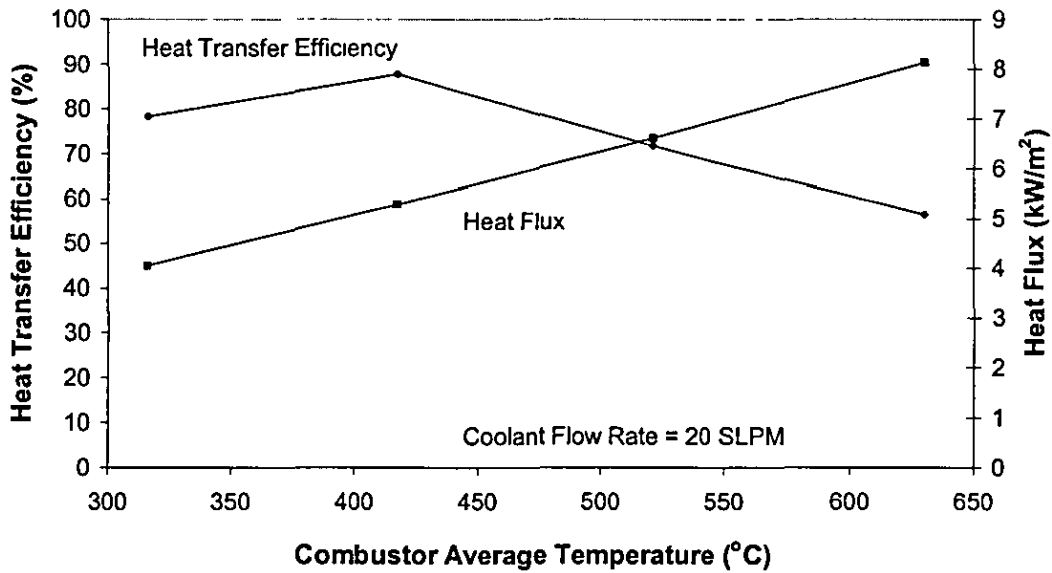


Figure 6.13: Heat Transfer Efficiency and Heat Flux w.r.t. Combustor Temperature

Figure 6.14 shows the temperature difference between the reforming stream and the average combustor temperatures, against the average combustor temperature. It can be seen that the temperature difference increases as combustor temperature increases, which means that the temperature increase of the reforming stream is not as high as that of the combustor. This indicates that the increase in temperature of the reforming stream is not sufficient to overcome the effect of the increased H_2 conversion rate. Therefore, the heat transfer efficiency of the reactor decreases.

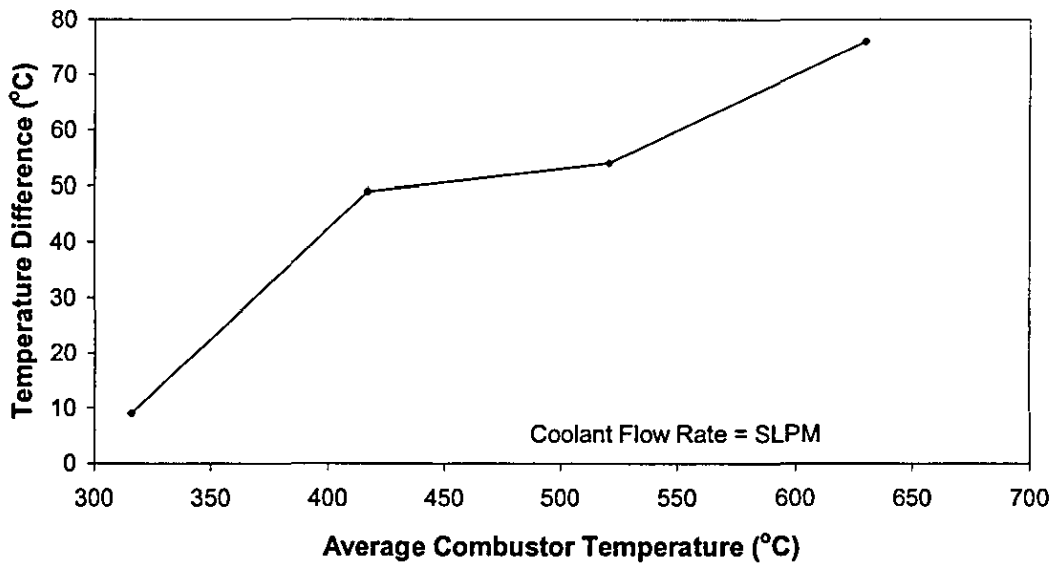


Figure 6.14: Temperature Difference Between the Combustor and Coolant Exhaust w.r.t. Combustor Temperature

The heat flux increase is mainly due to the fact that the H_2 conversion efficiency is generally proportional to the temperature of the combustor as shown in Figure 6.11. As temperature increases, more heat is generated from the combustor. As a result, both heat flux and the thermal power of the combustor increase.

Figure 6.15 shows the effect of the reforming stream flow rate on the heat transfer efficiency and the heat flux. The reforming stream was tested using N_2 . The combustor temperature remained constant at $600^\circ C$ throughout the test by controlling the amount of H_2 supplied to the combustor. It can be seen that as the flow rate of the reforming stream increases so does the heat transfer efficiency and the heat flux. This is due to the fact that the increased reforming flow is able to absorb more heat from the combustor, and the controller responds by increasing the amount of H_2 to the combustor. Since the H_2 conversion efficiency of the combustor is approximately independent of reforming stream flow rate, the thermal power of the combustor increases, and the heat flux rises.

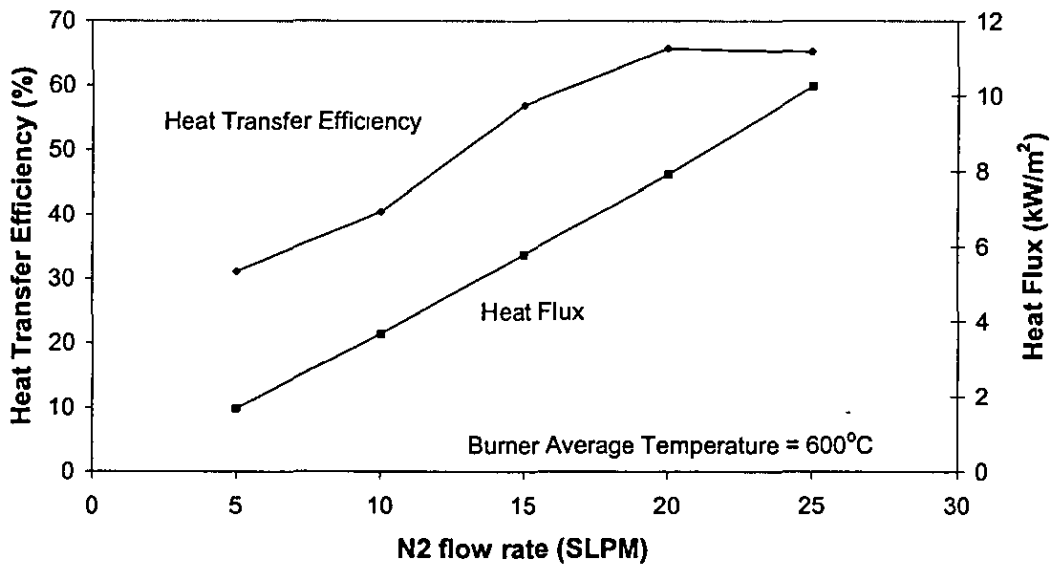


Figure 6.15: Heat Transfer Efficiency and Heat Flux w.r.t. Coolant Flow Rate

Figure 6.16 shows temperature difference between the reforming stream and the average combustor temperatures, against the N₂ flow-rate. As the N₂ flow-rate increases, the temperature difference decreases. This is because the higher flow-rates of N₂ enable more energy to be absorbed from the combustor and therefore improves the heat transfer efficiency.

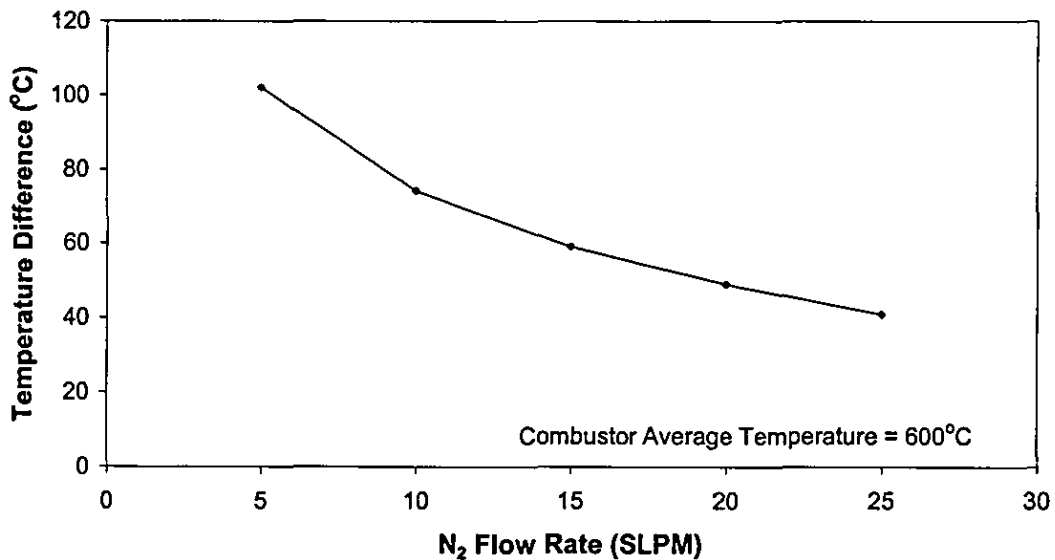


Figure 6.16: Temperature Difference Between the Combustor and Coolant Exhaust w.r.t. Coolant Flow Rate

The thermal power transferred to the reforming stream at a combustor average temperature of 600°C and a N₂ flow rate of 25 SLPM was approximately 320 W. This is enough thermal power to support the steam reforming of 0.7 SLPM propane at a molar steam to carbon ratio of 2 and a temperature of 600°C. Therefore, the reactor is capable of a sufficiently high rate of heat transfer for use as a steam reformer. In addition, as the flow rate of the reforming stream increases the heat flux also increases. This suggests that the reactor is capable of supporting higher flow rates of propane.

6.6 Conclusion

It was found that zones 1 and 4, which are positioned at inlet and exit of the reforming stream, respectively, required the most control input. Zones 2 and 3, which are located in the middle of the combustor, could be controlled together without a detrimental effect on the controllers' performance. Additionally, it was found that the flow of the gases in the combustion layer adversely affects the temperature distribution in the combustor. However, it was shown that the multi-zone combustor layout provides accurate temperature control along the length of the reformer. This improves the traditional reformer designs. The catalytic combustor works effectively with between 90 and 100% of the H₂ seen to be converted. The heat transfer efficiency of the reactor between the combustor and reforming layer was found to be in the region of 65% to 85% at a temperature of 600°C to 400°C, respectively.

The reactor is capable of a sufficient rate of heat transfer for use as a steam reformer. In addition, as the flow rate of reforming stream increases the heat flux also increases. This suggests that the reactor is capable of supporting higher flow rates of reforming fuel than demonstrated here

7 Simulation of the Reactor

7.1 Aims

Experimental work evaluating the performance of a micro-channel steam reformer has led to the development of a model of the reactor to evaluate possible development paths for the fuel processing system. In order to keep the model manageable, it was decided that a complete CFD model of the reactor was not desirable. Rather a modular simplified representation of the reactor was developed, so that it could be modified for different flow patterns.

7.2 Software

The software used to build the model was the Matlab/Simulink suite of programs from MathsWorks. This was chosen because of its flexibility and ease of use. Simulink allows the user to build models out of subsystems in a similar manner to that used by the LabVIEW software utilised for the DAQ and control software used for the test assembly. Simulink has the advantage of being able to call upon user designed functions programmed in Matlab. This allows the user to call upon Matlabs powerful set of mathematical functions where necessary, and allows the user to write original functions as required using the Matlab programming language.

7.3 Assumptions

Several assumptions were made in order to simplify the model

- The reactor would be split into 16 modules. This would be sufficient to model new reactor layouts.

- The combustion chamber temperature in each module is equal to the overall reactor temperature in each module.

- Conduction between zones is steady-state. Each module is modelled as a solid block of steel for the purpose of conduction. It is assumed that the temperature profile in each block is linear and that at the instant the conduction function is evaluated the temperature profile is constant. The wall thickness is taken to be the distance between the centres of each module

- There is negligible pressure drop in the reactor.

- 100% H₂ conversion takes place in the combustor provided enough oxygen is present.

- The flow field inside each module can be simplified to the direction of flow only. This removes the need to model the flow through the microchannels.

- No modelling of the microchannels is necessary to predict overall reactor behaviour.

7.4 Brief Description of the Model

The model was built up out of separate modules. This would mean that the layout of the model could be rearranged to try out new reactor flow path designs. A simplified schematic of a module can be seen in Figure 7.1.

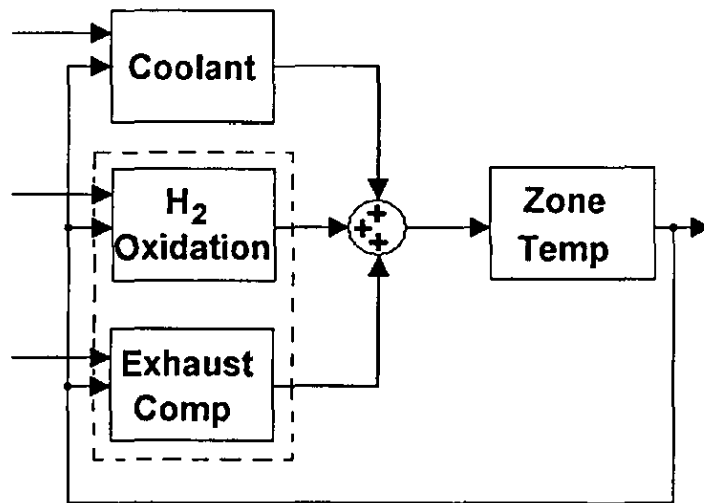


Figure 7.1: A Simplified Schematic of a Module

Each module calculates the products of combustion and hence thermal power released by the H_2 and the thermal power in the combustor exhaust. It also calculates the thermal power required to heat the coolant to its current temperature. The thermal powers are integrated w.r.t. time to give the thermal energy from each part of the model. These values are then summed. Radiation losses are subtracted and the model then uses the resulting energy to calculate the reactor temperature based on its thermal mass.

The specifics of the flow paths inside the zones along the microchannels were not included for simplicity, more important were the interactions between the modules themselves on the macro scale. This would allow the overall behaviour of the reactor to be modelled. The inputs and outputs of each module were as follows

Inputs:

- Ambient Temperature /K
- H_2 flowrate (combustor) /SLPM
- Air/Exhaust flowrate (combustor) /SLPM

- Air/Exhaust Composition (combustor)
- Air/Exhaust temperature (combustor) /K
- Coolant Composition
- Coolant flowrate /SLPM
- Coolant temperature /K
- Mass of the module /g

Outputs.

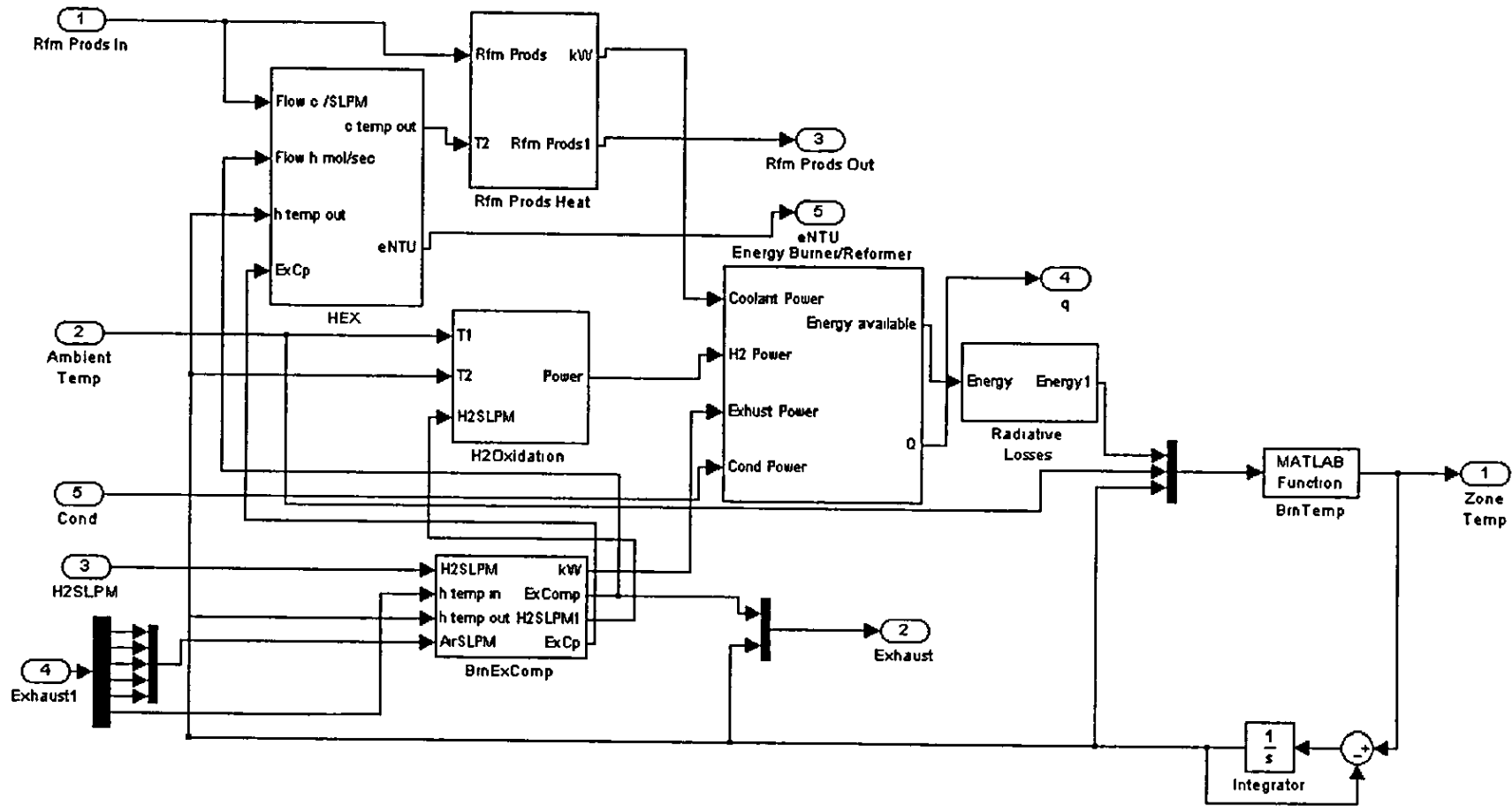
- Module Temperature /K
- Air/Exhaust flowrate (combustor) /SLPM
- Air/Exhaust temperature (combustor) /K
- Air/Exhaust Composition (combustor)
- Coolant Composition
- Coolant flowrate /SLPM
- Coolant temperature /K

In order to make the model 'gas flexible' it was designed so that the functions would adjust themselves to different species, H₂O, H₂ etc. automatically. This meant that a lot of the components could be reused throughout each module simplifying things further. This was achieved by giving each species a unique identifier, which was bundled with the flow-rate and temperature of the stream. The model would then calculate the integral of the specific heat for each gas species as required, based on the initial and current temperatures of the reactor.

7.5 Single Module Description.

The reactor model is based around a power balance. It is a development of the steady state Excel model described in Chapter 2. Each module is constructed using the following Simulink subsystems; "Rfm Prods Heat", "H₂Oxidation", "BrnExComp", "Energy Burner/Reformer", "Radiative Losses", and "Brn Temp" as shown in Figure 7.2. The following is a description of the subsystems and functions contained within each module.

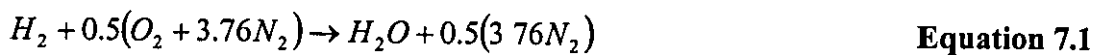
Figure 7.2: A Schematic of a Single Module



7.5.1 The BrnExComp Subsystem

This subsystem calculates the combustor exhaust composition, the amount of H₂ burnt and the thermal power contained in the combustor exhaust. The subsystem calls two functions, ExComp and BrnExPower.

The subsystem uses a custom function called ExComp to calculate the exhaust composition of the combustor. It uses a modification of the simple combustion formula of hydrogen in air (Equation 7.1.) to do this.



The ExComp function compares the amount of inputted O₂ with the amount of inputted H₂ and determines if the mixture is stoichiometric, air rich or fuel rich. It then chooses which variation of the formula to use. The ExComp function then calculates the percentage composition of the exhaust, the total flow rate in SLPM and the amount of H₂ combusted, also in SLPM.

The BrnExPower function calculates the thermal power in the combustor exhaust. It does this by first calculating the specific heat capacity of the exhaust, based on its composition and temperature. It then uses that value and the flow rate of the combustor exhaust to calculate the thermal power stored in the combustor exhaust as shown in Equation 7.2

$$P = \frac{(tot * Cp)}{1000} \quad \text{Equation 7.2}$$

. Where Cp = the integral of the specific heat at constant pressure of the combustor exhaust, tot = the flow rate of the exhaust mol/sec, P = thermal power in the combustor exhaust kW.

7.5.2 The H₂Oxidation Subsystem

This subsystem calls the functions IntCp, dHfH₂O, and H₂Power. The subsystem calculates the integral of the specific heat capacity at constant pressure of the species and uses them to calculate the enthalpy of formation of water. It then uses this along with the flowrate of H₂ generated by the ExComp function in the BrnExComp subsystem to calculate the thermal power generated by burning the H₂

$$\int_{T_1}^{T_2} Cp = \left(aT_2 + \frac{b^{-3}T_2^2}{2} - c^5T_2^{-1} \right) - \left(aT_1 + \frac{b^{-3}T_1^2}{2} - c^5T_1^{-1} \right) \quad \text{Equation 7.3}$$

$$\int_{T_1}^{T_2} Cp = \left(aT_2 + \frac{b^{-3}T_2^2}{2} - \frac{c^{-6}T_2^3}{3} \right) - \left(aT_1 + \frac{b^{-3}T_1^2}{2} - \frac{c^{-6}T_1^3}{3} \right) \quad \text{Equation 7.4}$$

The function IntCp is used to calculate the integral of specific heat capacity (Cp) at constant pressure (Equation 7.3-7.4). This is necessary because the value for Cp is temperature dependent. If instead of using the sum of the Cps at temperature 1 (T₁) and 2 (T₂), the integral of Cp between those temperatures is used, a greater accuracy is achieved. The two equations are used depending on which gas is passed to the function, and used in conjunction with the appropriate gas dependant values for a, b and c.

The function dHfH₂O calculates the enthalpy of formation of water at the reactor temperature. It does this by using the integral of specific heats of the reactants and products at the reactant temperature (Equation 7.5)

$$H = \frac{(H_f - (H_{2O} - (H_2 + 0.5O_2)))}{1000} \quad \text{Equation 7.5}$$

H = enthalpy of formation of H₂O at T₂. kJ/mol, *H_f* = LHV H₂O kJ/mol, *H₂O* = IntCp H₂O, *H₂* = IntCp H₂, *O₂* = IntCp O₂

The Function H2Power calculates the thermal power released by the combustion of H₂. It uses the enthalpy of formation of H₂O and the amount of H₂ burnt to do this

$$P = (H2SLPM/22.41/60)dHf \quad \text{Equation 7.6}$$

P = thermal power in kW, H2SLPM = flow rate of H₂ burnt, dHf = enthalpy of formation of H₂O at T2.

7.5.3 The RfmProdsHeat Subsystem

This subsystem contains three subsystems of its own, "Heat," LPG Heat," and "water heat."

7.5.3.1 The Water Heat Subsystem

This subsystem calls the functions IntCp, Pressure, and WaterHeat. The subsystem calculates the amount of thermal power in water. It calculates the integral of Cp for water as a liquid and a gas and also calculates the boiling point of the water based on its partial pressure. It then uses this data to calculate the thermal energy in the water.

The function Pressure calculates the partial pressure of the water in the LPG stream. It then sends its result to a look-up table which outputs the water's boiling point (Equation 7.7).

$$P = \frac{W/22.41}{T/22.41} \quad \text{Equation 7.7}$$

P is the partial pressure of the water, T is the total flow rate of the water mixture, W is the flow rate of the water.

The function WaterHeat uses the boiling point of water generated by a look-up table and uses it to decide which value of Cp to use when calculating the thermal power in the water. It then calculates the thermal power stored in the water appropriately

7.5.3.2 The LPG Heat Subsystem

This subsystem calls the functions IntCp, IntCpLPG and Heat. The subsystem calculates the integral Cp for the constituents of LPG and then combines them to give the Integral Cp for LPG. This is then used to find the thermal energy in the LPG.

The function IntCpLPG calculates the integral of the specific heat capacity at constant pressure of LPG (Equation 7.8). It does this by taking the individual integrals of the specific heats of the constituents of LPG and multiplying them by their proportions in the LPG then summing the results.

$$\int_{T_1}^{T_2} Cp = 0.914a + 0.061b + 0.02c + 0.004d + 0.001e \quad \text{Equation 7.8}$$

Where a = IntCp of propane, b = IntCp of propylene, c = IntCp of ethane, d = IntCp of butane, e = IntCp of methane. The multiplication factors are the percentages of each species in the LPG mixture.

The WaterHeat and LPGHeat subsystems are only enabled when reformat/LPG is passed to the RfmProdsHeat subsystem. This lowers the processing load for the model whilst maintaining its flexibility.

7.5.3.3 The Heat Subsystem

This subsystem calls the functions IntCp and Heat. The subsystem calculates the integral Cp of the gas passed to it and uses that to calculate the thermal energy in the stream.

The function Heat calculates the thermal power in the gas stream. It uses the integral of the specific heat capacity of the gas in question and its flow rate to do this as shown in Equation 7.9.

$$P = \frac{(F/22.41/60) \int_{T_1}^{T_2} C_p}{1000} \quad \text{Equation 7.9}$$

F = gas flow rate in SLPM, P = Thermal power in kW

7.5.4 The Energy/Burner Reformer Subsystem

This subsystem takes the thermal powers calculated above and integrates them to give the thermal energy in each stream. This means that the values change with time and produces a transient model of the reactor. It then sums the values to produce the amount of energy available for heating the reactor (Equation 7.10)

$$E = \int P_C + \int P_{H_2} + \int P_{EX} + \int P_{CO} \quad \text{Equation 7.10}$$

E is the thermal energy available up to that time, P_C is the thermal power of the coolant, P_{H₂} is the thermal power from the combustion of H₂, P_{EX} is the thermal power of the combustor exhaust stream, P_{CO} is the thermal power due to conduction

7.5.5 The Radiative Losses Subsystem

This subsystem calls the radiation function. The subsystem subtracts a user-defined percentage of the available energy from the available energy before sending it to the BrnTemp function.

The Radiation function reduces the energy total by a user-determined percentage (Equation 7.10) This is to simulate the effect of losses via radiation.

$$E = E_1 - (l * E_1) \quad \text{Equation 7.11}$$

Where E_1 = The thermal energy from the streams and combustion, l = percentage energy loss due to radiation, E = new value of available thermal energy.

7.5.6 The Brn Temp Subsystem

This subsystem calls the BrnTemp function. The Subsystem uses the available thermal energy calculated by the previous subsystems to calculate the reactor temperature at that time, based on the heat capacity of stainless steel and the mass of the reactor zone.

The BrnTemp function calculates the new reactor temperature (Equation 7.11). It does this by first calculating the specific heat capacity of steel at the initial temperature. It then uses this data with the mass of the reactor in grams and the energy transferred to the metal to calculate the new temperature.

$$T_2 = T_1 - \frac{E}{m * Cp} \quad \text{Equation 7.12}$$

Where T_1 = the initial reactor temperature K, E = thermal energy from the reformer stream and combustion of H_2 , m = mass of reactor zone g, C_p = Specific heat of Stainless Steel, T_2 = new reactor temperature K

7.5.7 Module Subsystem Integration.

The various subsystems of each module are integrated by using the output of the BrnTemp function as the new temperature (T_2) for each subsystem of the module.

7.5.7.1 Internal Heat Transfer

In the 4-module model described in Section 7.6 the issue of heat transfer from the combustor to the coolant is dealt with by assigning each module a fixed value for heat exchanger effectiveness. This is then used to calculate the coolant temperature using Equation 7.13. In the 16-module model described in Section 7.7 a more complex method was used. This is described below. The reason for the change in approach was that by using data gained from test running the real reactor it was hoped that a greater level of accuracy could be achieved than by using a "ballpark" figure.

A heat exchanger subsystem, called HEX, modifies the temperature of the coolant/reformer stream to take into account the heat exchanger effectiveness between the combustor and reforming layers. The subsystem incorporates heat transfer data gathered in Chapter 6, to generate a value for the overall heat transfer coefficient. This value is fed to the eNTU function. The eNTU function uses the ϵ -NTU method. The function uses variables calculated by the model to firstly calculate a value for NTU and then uses that value to calculate the heat exchanger effectiveness for that module. The effectiveness value is then used to calculate the temperature of the coolant stream according to Equation 7.12

$$T = \text{eff}(T_{hi} - T_{ci}) + T_{ci} \quad \text{Equation 7.13}$$

Where eff = the heat exchanger effectiveness, T_{hi} is the temperature of the reactor T_{ci} is the ambient temperature

The function allows for parallel flow, counter flow and cross flow heat exchanger configurations. To define which flow configuration is used, the user enters a trigger value into the HEX subsystem to tell the function which variation of the equation used to calculate the effectiveness is used.

7.5.8 Inter-Module Connectivity

The exit streams of one module are connected to the appropriate inlet streams of the adjacent modules. Details of stream composition, temperature and flow-rate are passed from one module to the next. The stream data is then used as the initial condition for the next module. In this way the model variables of each module are affected by the flow of the reactant streams through the reactor. This allows different flow configurations to be evaluated using the model.

7.5.8.1 Conduction

The 2dCond function calculates the amount of thermal power transferred from one module to the surrounding modules via conduction. It assumes that at each simulation time step the conduction is steady state. It also assumes a linear temperature profile for each module. It first calculates the thermal conductivity (k) of steel for each initial module temperature. These values are then used to calculate the thermal conductivity between each module

The resulting values are then placed into a standard conduction equation as seen in Equation 7.14.

$$Q = \frac{kA\Delta T}{x}$$

Equation 7.14

where Q is the heat transfer in kW, k is the thermal conductivity in W/cmK, A is the area available for heat transfer in cm^2 , x is the wall thickness in cm, and ΔT is the temperature difference between adjacent modules in K.

The equation is evaluated for each module to module boundary. Within the Cond2d function, facility to set boundary conditions for the model is incorporated in order to tailor the model to a specific circumstance. Firstly the boundary conditions are set. In this case the temperatures of the model boundaries are specified. Equation 7.14 is then used to determine the heat transfer at the model boundaries. Finally the heat transfer into and out of each module is summed and the resultant value sent to the appropriate modules Energy/Burner Reformer subsystem to be incorporated into the model.

In initial testing of the module the boundary conditions were set as mirrors. This was to simulate complete lagging of the reactor.

7.6 A 4-module Reactor Model.

It was decided to produce a simple model of the reactor using Matlab/Simulink. Initially a four-module model was developed in order to evaluate the model concept. Each module represented a combustor zone in the reactor. A simplified representation of the model can be seen in Figure 7.1.

The four-module model was used to make sure that the model was working as expected. That is that the behaviour of the model was that which could be reasonably expected. To do this the following tests were carried out.

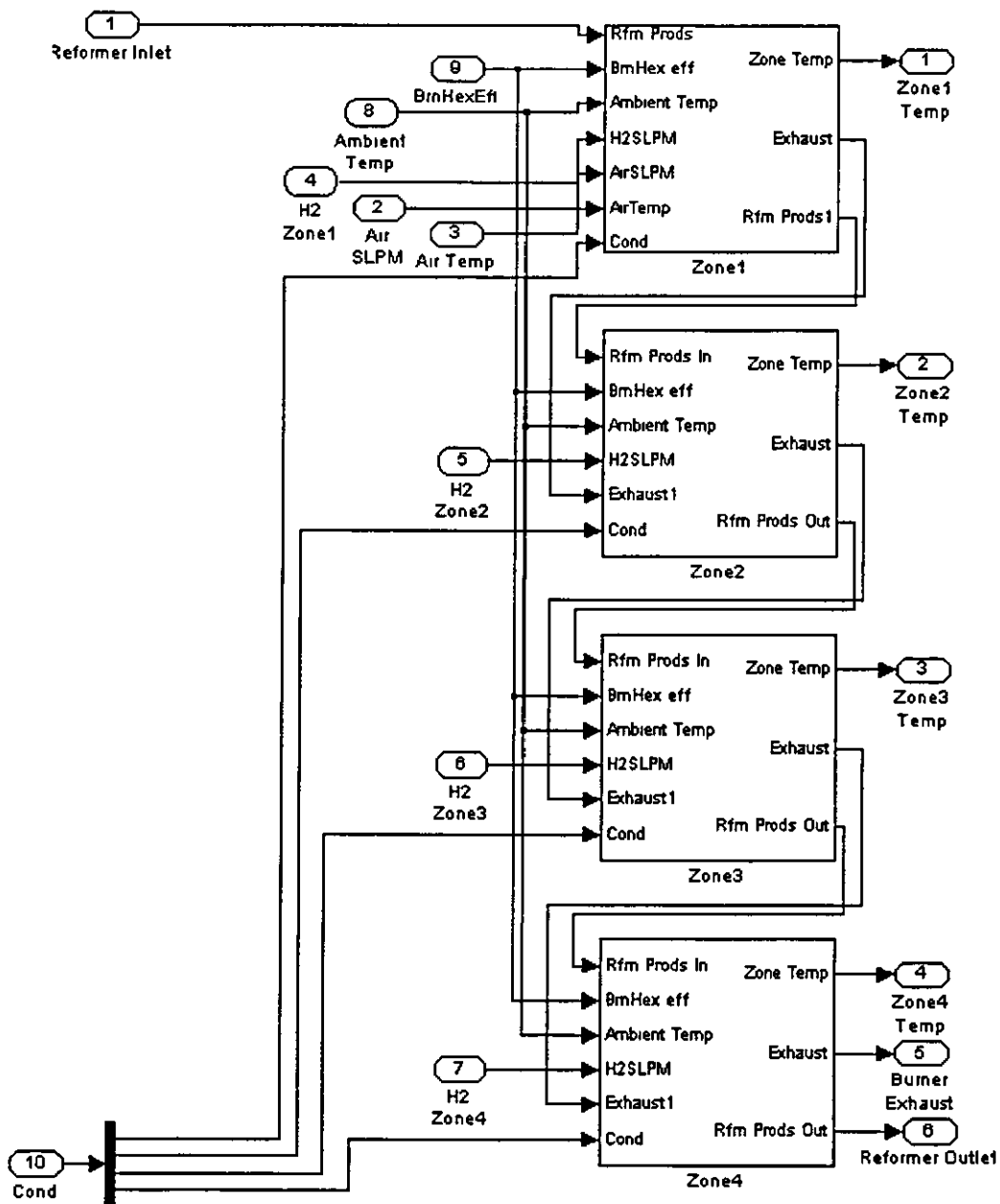


Figure 7.3 The four-module reactor model.

The first test carried out consisted of running the model without coolant. The modules were connected so as to mimic the layout of the combustor zones in the reactor. This means that there was a single air feed to all of the modules and that the exhaust path was from module 1 to module 4. The model inputs were set up as shown in Table 7.1. Each test was run for 70 simulated minutes

Module Mass	1 25 kg
Ambient Temperature	298.15 K
Air flow Rate	20 SLPM
H2 Flow rate per module	1 SLPM
Air temperature	298 15 K
Coolant	N/A
Coolant Flow rate	0 SLPM
Coolant Temperature	N/A
HEX type	Parallel flow

Table 7.1: Input Settings for the 4-Module Model Test 1

Figure 7.4 shows the temperature outputs from the four modules that make up the model. It can be seen in Figure 7.4 that the temperature distribution throughout the model is as expected. The increase in temperature between modules 1 and 4 is a result of the heat transferred due to the combustor exhaust. The shape of the curves is similar to that produced by the actual reactor. This shows that the model is simulating the heating process correctly.

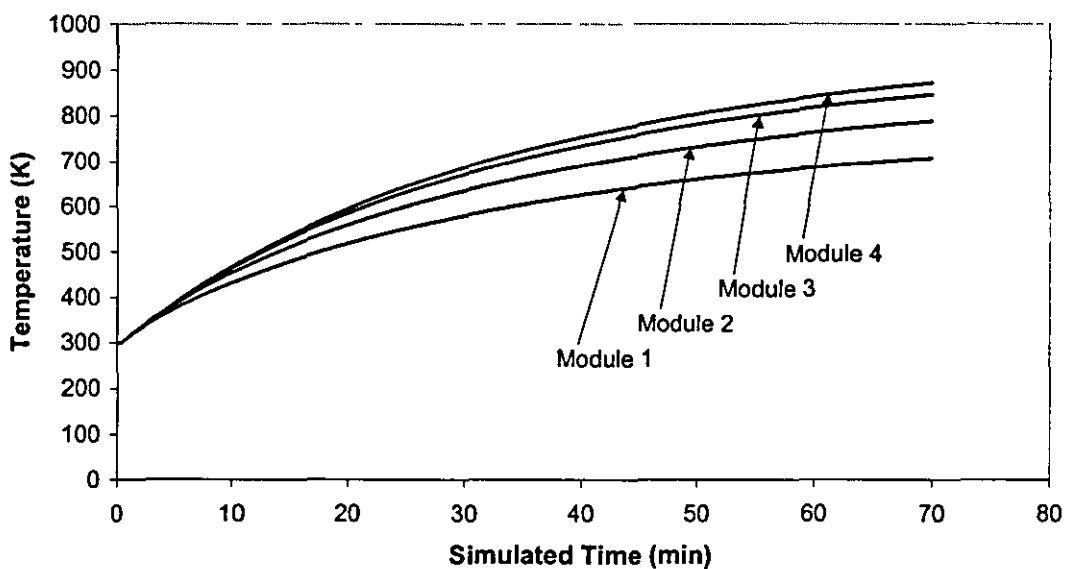


Figure 7.4: Temperature Output from the Four-Module Reactor Model Without Coolant

Table 7.2 shows the input settings for the second test. In this case a supply of 20 SLPM N₂ was fed to the model to act as a coolant. The direction of coolant flow was from module 1 to module 4

Module Mass	1.25 kg
Ambient Temperature	298.15 K
Air flow Rate	20 SLPM
H2 Flow rate per module	1 SLPM
Air temperature	298.15 K
Coolant	N ₂
Coolant Flow rate	20 SLPM
Coolant Temperature	298.15 K
HEX type	Parallel flow

Table 7.2: Input settings for the 4-module model Test 2.

Figure 7.5 shows the temperature output from the modules whilst coolant is running through the reforming side of the model. This time as shown in Table 7.2, 20 SLPM of N₂ was used to simulate the coolant flow through the reformer side of the reactor. The results are as expected with the temperature of the modules decreasing due to the heat transferred to the coolant. The overall temperature spread is also increased. This is due to the coolant transferring heat along the reactor from module 1. This also has the effect of slightly reducing the temperature spread between the other modules

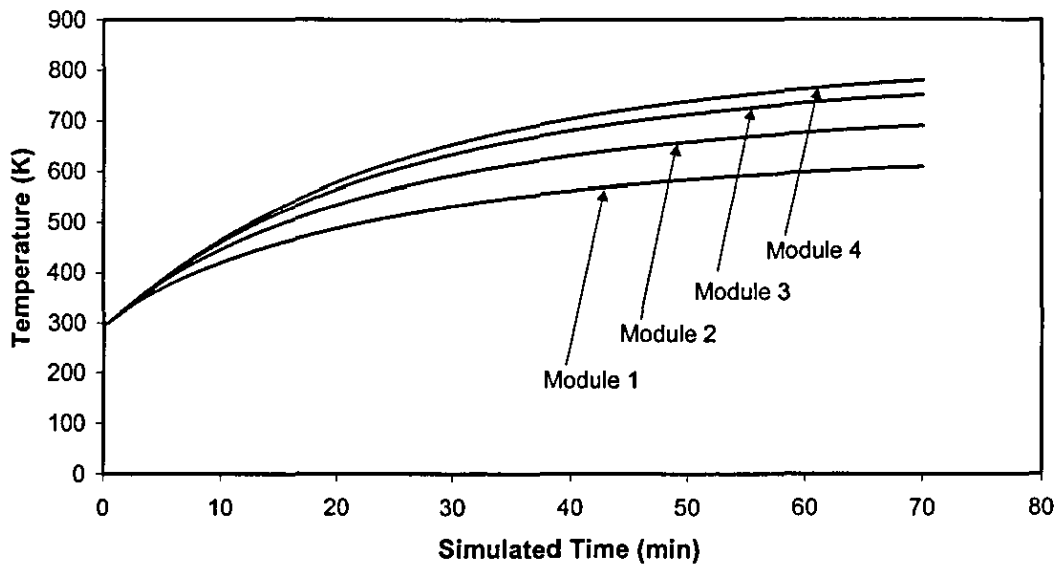


Figure 7.5: Temperature Output from the Four-Module Reactor Model with Coolant

Table 7.3 shows the model input settings for test 3. In this instance the direction of the combustor exhaust was reversed so that it flowed from module 4 to module 1.

Module Mass	1.25 kg
Ambient Temperature	298.15 K
Air flow Rate	20 SLPM
H2 Flow rate per module	1 SLPM
Air temperature	298.15 K
Coolant	N/A
Coolant Flow rate	0 SLPM
Coolant Temperature	N/A
HEX type	Counter flow

Table 7.3: Input Settings for the 4-Module Model Test 3

Figure 7.6 shows the temperature output from the modules, this time with the air flow to the combustor reversed. It can be seen that the temperature distribution is the opposite of that shown in Figure 7.4 and shows the flexibility of the model as regards the interconnection of the modules. This is important for the development of the 16-module model as any directional bias in the model would render the model useless.

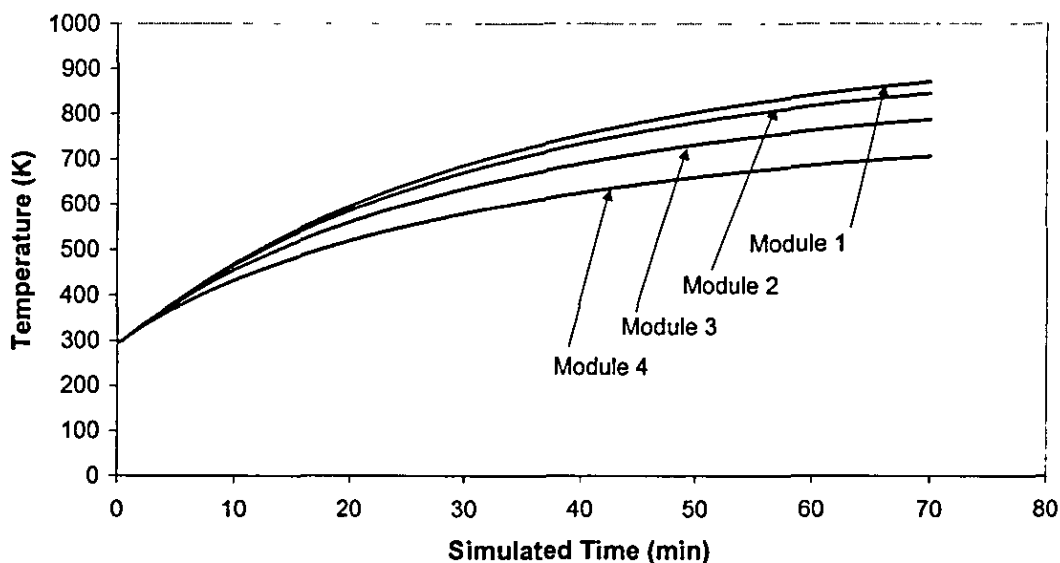


Figure 7.6: Temperature output from the four-module reactor model without coolant.

Table 7.4 shows the input settings for test 4 with the 4-module model. As was the case for the second test, a supply of 20 SLPM N_2 was fed to the model so that it flowed from module 1 to module 4.

Module Mass	1.25 kg
Ambient Temperature	298.15 K
Air flow Rate	20 SLPM
H2 Flow rate per module	1 SLPM
Air temperature	298.15 K
Coolant	N_2
Coolant Flow rate	20 SLPM
Coolant Temperature	298.15 K
HEX type	Counter flow

Table 7.4: Input Settings for the 4-Module Model Test 4.

Figure 7.6 shows the temperature output from the modules, with the air flow to the combustor reversed and 20 SLPM N_2 to simulate coolant flow through the reforming side of the reactor in the same direction as shown in Figure 7.5. As can be seen the presence of the coolant is shown by the reduction in temperature of the modules due

to heat transfer to the coolant. Module 1 is noticeably quenched and the temperature of module 4 is raised noticeably again, due to the heat transfer properties of the coolant.

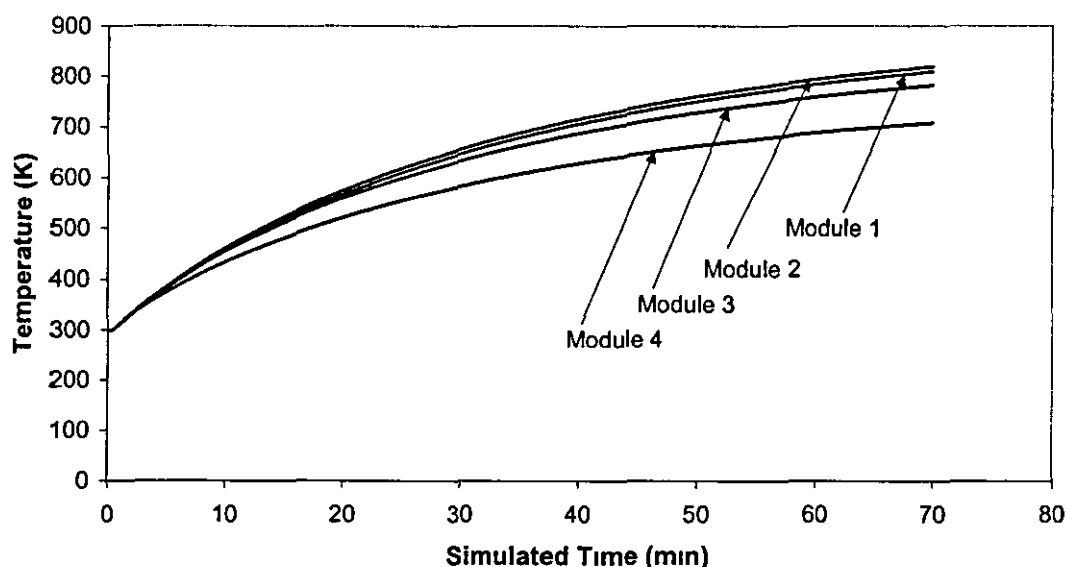


Figure 7.7: Temperature Output from the Four-Module Reactor Model with Coolant

The results show that the modular approach to building the reactor model is sound. They show that it is possible to link the modules together as desired to create different flow paths, which can then be evaluated against each other. In this instance the influence of the coolant on the temperature distribution of the model demonstrates this. This is important in the case of the 16-module model, as that is the primary reason for developing such a model.

7.7 A 16-module Reactor Model.

In order to provide a good base for further reactor development paths the 4-module test model was expanded to produce a 16-module model. A 16-module layout was chosen because it corresponds well with the layout of the real reactor. In Figure 7.8 the layout of the model can be seen. In this instance it has been set-up to mimic the real reactor in counter flow configuration. The 16-module layout allows the easy subdivision of the model into the four combustor zones whilst allowing the temperature along each zone to be evaluated. It also allows for simplicity of model

design as each module has the same dimensions and mass. This means that the construction of the conduction function is simplified.

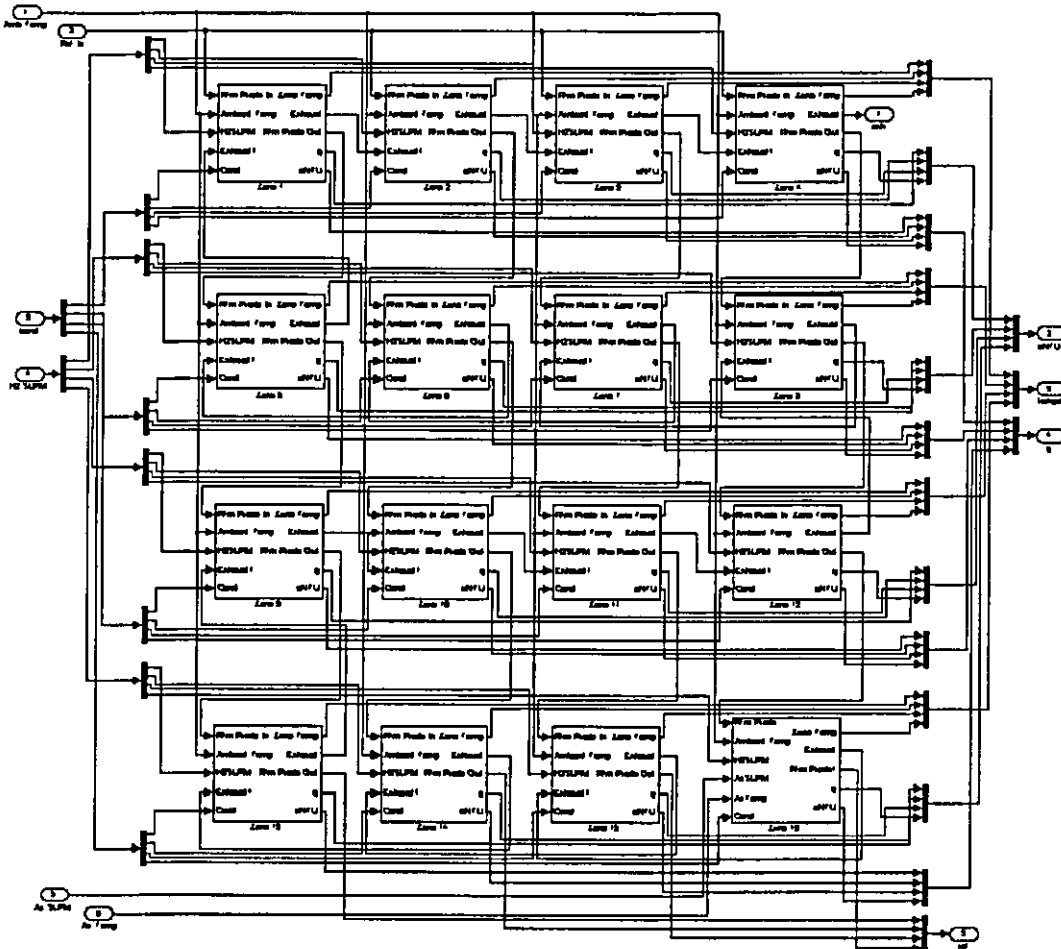


Figure 7.8 The 16-Module Reactor Model

Each module has an individual H_2 input for the combustor. This is so that the model can be used to mimic the flow field inside the reactor and model the uneven distribution of H_2 along each combustion zone. For the purposes of the following tests modules were connected together to mimic the flow configuration of the real reactor. This created a single serpentine path for the combustor exhaust and 4 parallel flow paths for the reforming side of the reactor.

Initial tests using the 16-module model used as closely as possible the same or equivalent input settings as those for the 4-module model. This was to check that the model behaved as expected. The input settings for each module can be seen in Table 7 5, where macro-HEX type refers to the input and output positions of the serpentine

combustor exhaust path not the individual modules. Each test was run for 70 simulated minutes to allow comparison with the 4-module reactor model tests.

Module Mass	0.3125 kg
Ambient Temperature	298 15 K
Air flow Rate	20 SLPM
H2 Flow rate per module	0.25 SLPM
Air temperature	298 15 K
Coolant	N2
Coolant Flow rate	0 SLPM
Coolant Temperature	N/A
Macro-HEX type	Parallel flow

Table 7.5: Input Settings for the 16-Module Model Test 1

Figure 7.9 shows the temperature generated by each of the modules over time. It can be seen that the shape of the curves, again, follows that demonstrated by the actual reactor. This is as expected as the subsystems used are the same as that used for the four module model.

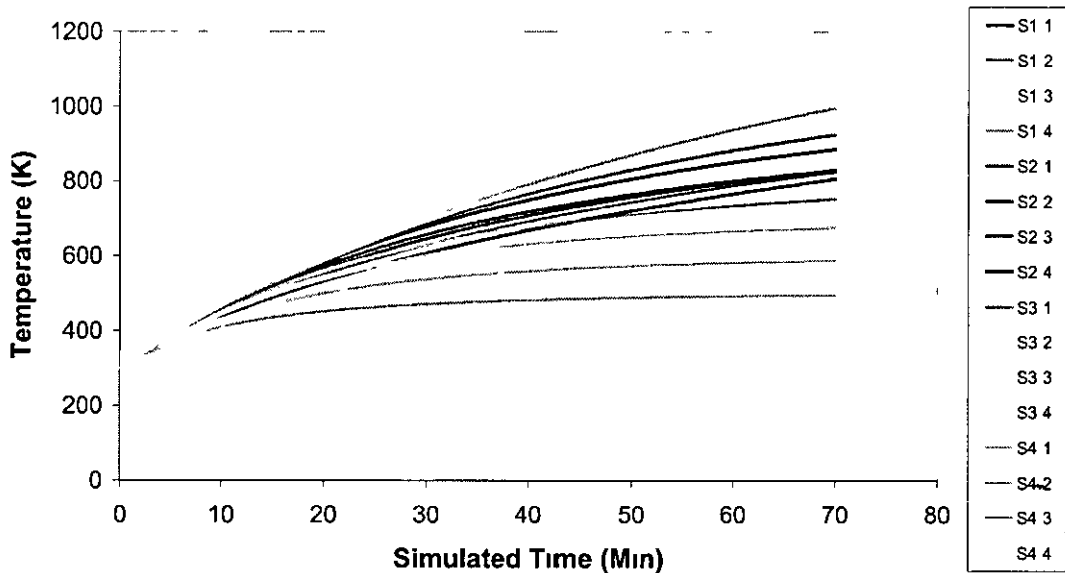


Figure 7.9: The Temperature Output of the 16-Module Model

Figure 7.10 shows the temperature profile generated by the model at the end of the simulation run. The air supply to the combustor is at S1:4 and the exit of the combustor exhaust is at S4:4. It can be seen in Figure 7.10 that quenching occurs at the combustor inlet. The effect of this quenching is transferred to S2 due to the conduction function. Without the conduction function there would be a steady temperature rise from S2:1 to S2:4 due to the increase in temperature of the combustion gases.

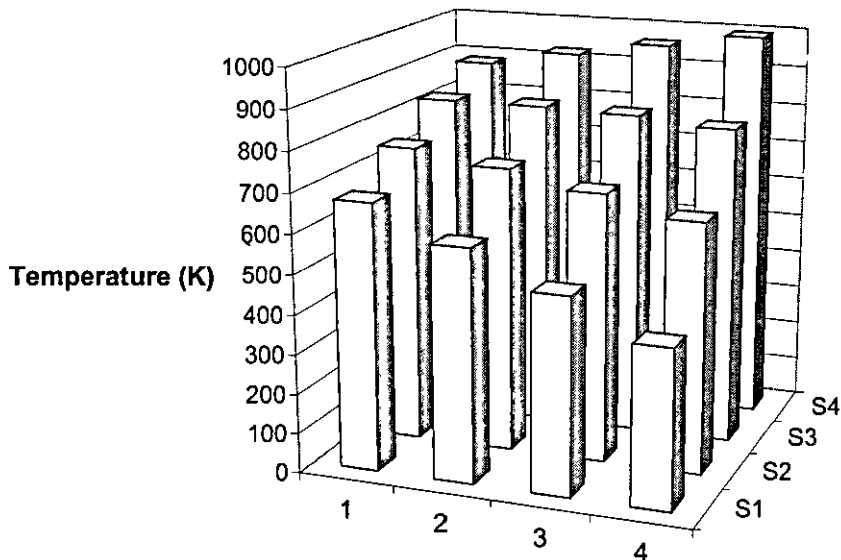


Figure 7.10: The Temperature Distribution of the 16-Module Model

Table 7.6 shows the input settings for the model for the second test. This time a coolant flow of 20 SLPM N₂ was specified. This was in the direction of S1 to S4.

Module Mass	0.3125 kg
Ambient Temperature	298.15 K
Air flow Rate	20 SLPM
H2 Flow rate per module	0.25 SLPM
Air temperature	298.15 K
Coolant	N2
Coolant Flow rate	20 SLPM
Coolant Temperature	298 K
Macro-HEX type	Parallel Flow

Table 7.6 Input Settings for the 16-Module Model Test 2

It can be seen that the effect of the coolant on the model is to reduce the overall temperature of the model. This is due to the heat transfer taking place between the combustor and coolant sides of the model. The coolant reduces the temperature spread along the model from S1 to S4. This is a slightly different result to that seen in the 4-module model and could be due to the manner of determining the heat transfer from the combustor to the coolant in the two models. The 4-module model uses a static value for the effectiveness of the heat exchanger, whilst the 16-module model uses a dynamic value for the heat exchanger effectiveness which is in part temperature dependent. The low temperature of S1 means that the value for effectiveness will be lower than that used by the 4-module model and so the quenching effect of the coolant on S1 will not be as great.

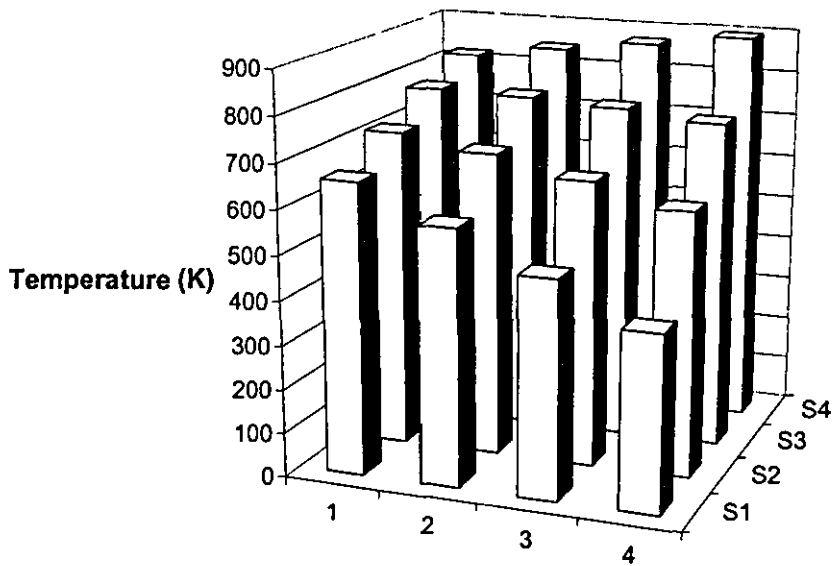


Figure 7.11: The Temperature Distribution of the 16-Module Model with 20 SLPM N₂ as Coolant

Table 7.7 shows the input settings for the third test of the 16-module model. For this test the direction of the combustor stream was reversed. The air for the combustor entered at S4:4 and exited at S1:4. This has the effect of replicating the set-up of the real reactor when in it's reversed flow configuration.

Module Mass	0.3125 kg
Ambient Temperature	298.15 K
Air flow Rate	20 SLPM
H2 Flow rate per module	0.25 SLPM
Air temperature	298.15 K
Coolant	N2
Coolant Flow rate	0 SLPM
Coolant Temperature	N/A
Macro-HEX type	Parallel flow

Table 7.7: Input Settings for the 16-Module Model Test 3

As expected, without the addition of coolant, the temperature distribution of the model is simply the reverse of that produced by the first test. This shows that the model can be linked together as the user desires, without any unwanted effects. In particular this shows that the 2D conduction model is operating satisfactorily and that it is directionally independent

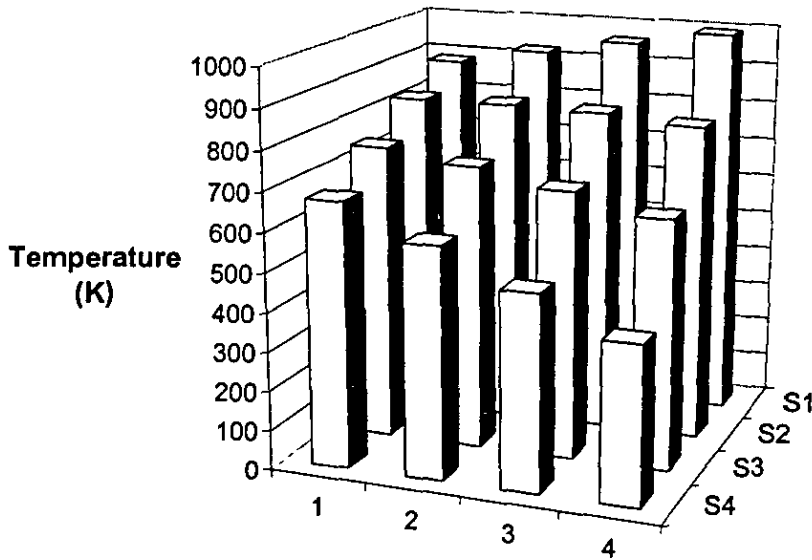


Figure 7.12: The Temperature Distribution of the 16-Module Model

Table 7.8 shows the input settings for the fourth test. For this test 20 SLPM N₂ was supplied to the model travelling from S1 to S4.

Module Mass	0.3125 kg
Ambient Temperature	298.15 K
Air flow Rate	20 SLPM
H2 Flow rate per module	0.25 SLPM
Air temperature	298.15 K
Coolant	N2
Coolant Flow rate	20 SLPM
Coolant Temperature	298 K
Macro-HEX type	Counter flow

Table 7.8: Input Settings for the 16-Module Model Test 4

Again the effect of the heat transfer from the combustor to the coolant can be seen in the lowering of the overall temperature. Again it can be seen that the results do not match those of the 4-module model. And again this is probably due to the effect of the differing heat exchanger models. The temperature spread along the length of the model from S1 to S4 is again reduced. But the quenching of S1 is again less pronounced than that of the 4-module model. It can be seen that the direction of flow of the combustion gases affects the heat distribution inside the model when coolant is present. This can be seen by a comparison of Figure 7.11 and 7.13. This shows that the model will provide results specific to the configuration of the flow field. This is important as it shows that the model can be developed further to become a useful design/development tool.

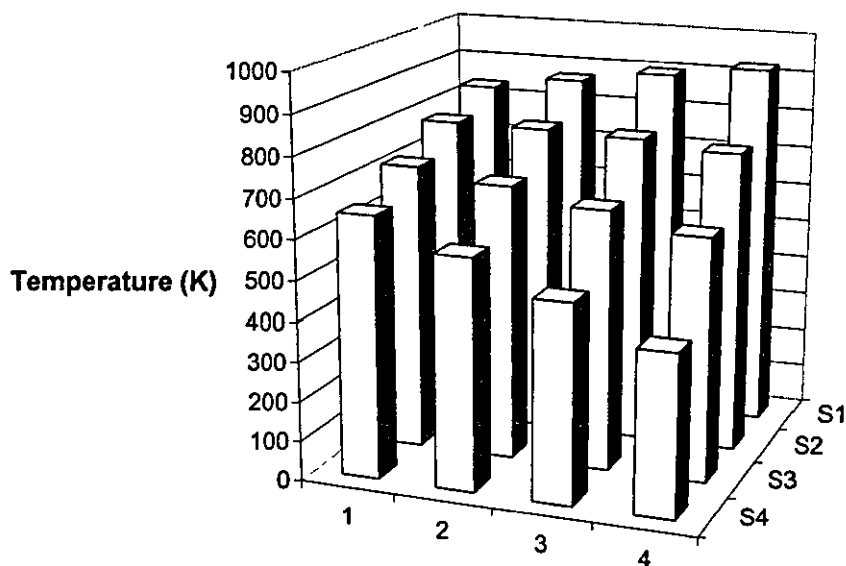


Figure 7.13: The Temperature Output of the 16-Module Model with 20 SLPM N_2 as Coolant

7.8 A Comparison of the Model Performance to that of the Reactor

To determine areas of the model that needs improvement and development the results gained in the previous tests will be compared to results from the real reactor testing. The results of the comparison will be used to develop the model further in the future so that its accuracy and usefulness is improved.

Figure 7.14, 7.15 and 7.16 shows the temperature distribution of the real reactor under similar operating conditions to tests 1, 2, and 4 of the 16-module reactor model respectively. Each combustor zone was supplied with 1 SLPM H_2 and the combustor was supplied with 20 SLPM air. The temperature distribution is taken after 70 minutes of operation. No coolant was passed through the reforming side of the reactor for Figure 7.14, whilst 20 SLPM of N_2 was used as a coolant for Figures 7.15 and 7.16.

Firstly by comparing the results of the first and second tests to Figures 7.14, and 7.15 the following comments can be made.

The first thing to note is that in the 16-module model S2 and S3 both correspond to S2 in the real reactor results. This is due to the placement of the thermocouples inside the reactor, so that there are four thermocouples responsible for acquiring the temperature data for combustor zones 2 and 3 together in the reactor. This results in the distribution seen in S2 in Figures 7.14 to 7.16 being the average of S2 and S3 in the 16-module results. There are three major differences between the model results and the reactor results.

The first is that the overall temperature range is much smaller in the real reactor. The effect of the quenching of the incoming air is much greater in the model and this has a follow on effect through out the rest of the reactor. The second is a greater level of temperature uniformity in the reactor. Although the peak temperatures are similar between the reactor and the model the reactor has a more uniform temperature distribution. This suggests a higher rate of heat transfer from one part of the reactor to another than currently modelled by the conduction function in the model. The third difference also concerns the conduction model, but more specifically the boundary conditions. The model is set up so as to mimic a completely insulated block. In reality heat loss occurs from auxiliary piping and in particular the reformer exit manifold. This explains the excess heat in S4 in the model results in comparison to the real reactor S3.

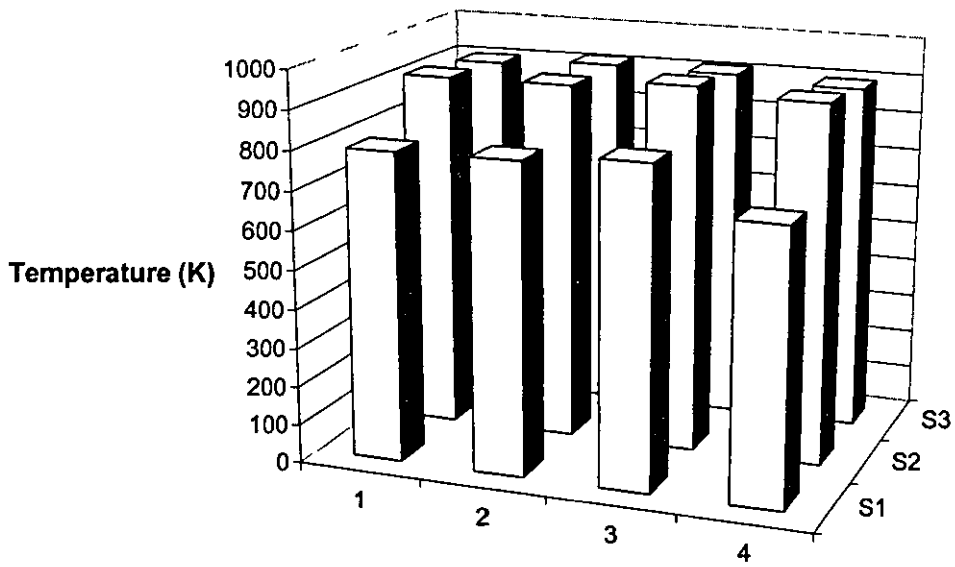


Figure 7.14: The Temperature Distribution of the Reactor

With the addition of coolant, in this case 20 SLPM N_2 , as shown in Figure 7.15, the effect on the reactor is much closer to the model results. The reactor is uniformly quenched. This effect can also be seen in the model results. The reactor is quenched more along S1 than the 16-module model and the greater initial temperature of the reactor at S1 explains this. The temperature dependant HEX model used means that at low temperatures the heat exchanger effectiveness is decreased and so less heat is transferred to the coolant.

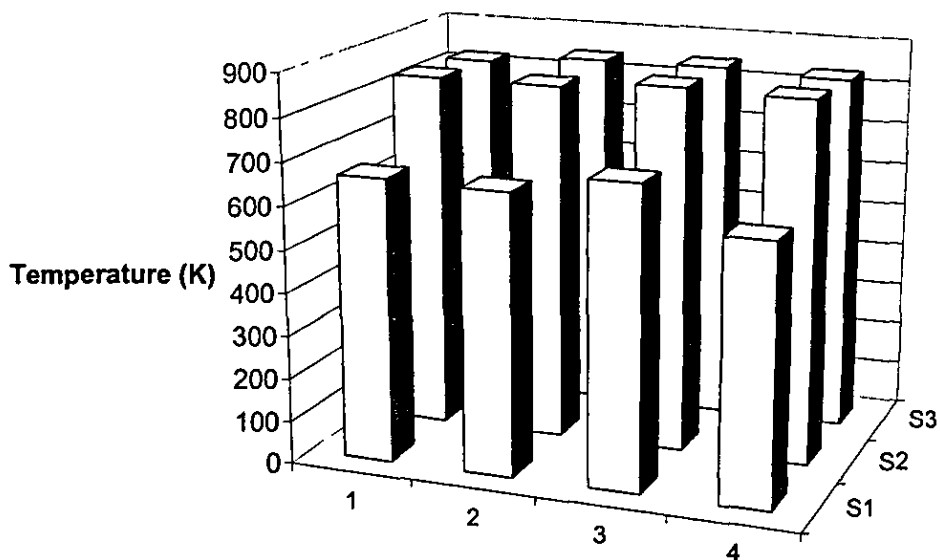


Figure 7.15: The Temperature Distribution of the Reactor with 20 SLPM N_2 as Coolant.

Figure 7.16 shows the temperature distribution in the reactor with the combustor air entering at S3:4. 20 SLPM N_2 was used as coolant. Again it is clear that the actual temperature S3 at the air inlet is greater than that predicted by the model. It can also be seen that as the model predicts, the temperature of S3 is raised above that of S1 in test 1 due to the transfer of heat via the coolant. The temperature distribution in S1 shows the opposite trend to that predicted by the model and this may be due to the distribution of N_2 across the width of the reactor, or possibly the distribution of H_2 in the combustor.

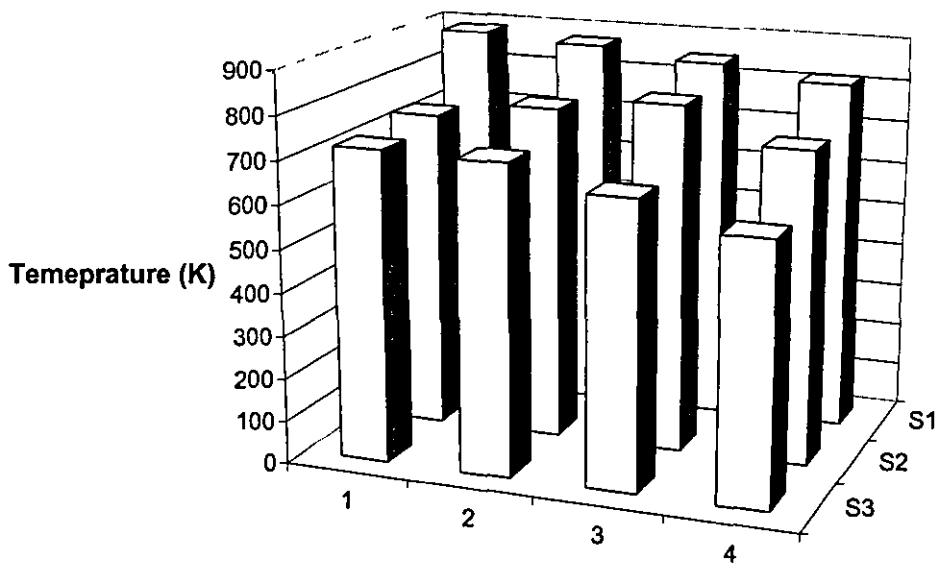


Figure 7.16: The Temperature Distribution of the Reactor with 20 SLPM N_2 as Coolant

7.9 Conclusion

It can be seen from the results that the reactor model in this form does not yet accurately enough model the performance of the existing reactor design. In order for the model to be truly useful in modelling new reactor designs it must first be validated against the existing design so that confidence can be had in the results of any subsequent simulation of new designs.

An initial view of the model results shows that the curves produced by the model and that of the reactor have the same basic shape. This is a good indicator that the model is performing as designed, however a closer look shows discrepancies between the model and the reactor.

The most serious discrepancy is between the real combustor air inlet on the reactor and the modelled combustor air inlet. The modelled air inlet consistently under performs, predicting a much higher level of quenching than actually occurs. The level of quenching also differs between the 4-module and 16-module models, with the 4-

module model experiencing less quenching than that shown by the 16-module model. This leads to the conclusion that it is the modelling of the flow inside the combustor, and consequently the distribution of H_2 that is at fault. One way of more accurately modelling the combustor flow distribution would be to use kinetic data to create a kinetic model of the combustion. This would allow the H_2 flow to be modelled in the same way as for the combustor exhaust by specifying a flow rate and route and allowing the model to calculate the amount of H_2 burned in each module. Any unburned H_2 from one module could then be used in the next module, in this way it may be possible to model the H_2 distribution effect seen in Section 6.3. This would also allow the model to take into effect the thermal content of the H_2 in each separate module.

The apparent discrepancy between the conduction model and the actual heat transfer inside the model can be adjusted by modifying the internal parameters of the conduction model. In addition the boundary conditions can also be adjusted from inside the conduction model. In any case as the boundary conditions are application sensitive, any boundary settings used for a new design will always be a judgement call.

The performance of the 16-module model whilst running on a 800 MHz Pentium III PC with 128 Mb of RAM is not desirable. It manages to operate in "real-time" that is to say that each simulated second of run time takes a real second of time to execute. However, as modern PCs are commonly being sold with 3.5 GHz processors at this time, this is not an insurmountable problem with the model.

It must be remembered that the model as developed is meant to provide a "first guess" for future reactor designs and as such necessarily simplifies some of the processes that take place inside the reactor, in order that it can be used to quickly evaluate possible design paths. As such, some accuracy is always going to be missing from the model results when it is compared to the actual reactor. The model as described is a good first step to reaching the goal of producing a "first guess" for reactor design.

7.9.1 Further Development of the Model

In order to model the heat transferred from combustor to the reformer during steam reforming a kinetic steam reforming model needs to be developed. It will be integrated into the existing model inside the RfmPrdsHeat subsystem. A kinetic combustion model will also be integrated into the model. It will take the place of the existing combustion model and allow more accurate modelling of the H₂ flow inside the reactor. Before the kinetic modelling takes place the kinetic data needs to be collected. This will be outsourced to a specialist company, but before that can happen the catalyst to be used for the reformer needs to be finalised.

8 Single Stage Sulphur Tolerant Steam Reformer

A novel precious metal based catalyst was applied to the reforming side of the reactor using a wash-coating process. The catalyst was designed to be sulphur tolerant and to convert the sulphur into H_2S to be removed at a later stage. The catalyst operating range is limited to $600^{\circ}C$ in order to avoid sintering of the catalyst and the accompanying loss of activity. The purpose of the following tests is to determine if the sulphur tolerant catalyst is effective when subjected to a fuel containing sulphur. In this case a commercial grade LPG was used. It was fed straight from the bottle to the pre-heater where it was mixed with de-ionised water. In order to try and prevent thermal cracking of the LPG inside the pre-heater, the water and LPG were mixed before the heater. The test matrix was chosen based on the results of the Aspen modelling discussed in Chapter 2 the test points chosen provide a good understanding of the reformer performance.

The reforming side of the reactor was washcoated with a sulphur tolerant steam reforming catalyst as described in Chapter 3.

8.1 Evaluation of the Sulphur Tolerant Catalyst using Liquid Petroleum Gas as a Feedstock

The test procedures were as follows:

- The temperature was set to the set-points of 450, 500, 550 and $600^{\circ}C$ whilst for each temperature the steam to carbon ratio was set to 2.5, 3, 3.5 and 4
- The flow rate of LPG was set at 0.75 SLPM as this corresponds to approximately 0.5kWe (based on equilibrium data) from a fuel cell, given total conversion of the LPG.
- The set-point with the best performance was then chosen and the LPG flow rate was varied from 0.25 to 1.75 SLPM whilst the temperature and S/C ratio were kept constant.

8.1.1 Results

The effect of reformer temperature on dry reformat composition can be seen in Figure 8.1. The LPG supply rate to the reformer was 0.75 SLPM and the steam to carbon ratio was 4 during the test. It can be seen that as the reformer temperature increases so does the conversion of LPG. The increased conversion rate can be explained by the increase in energy provided to the reaction at higher temperatures. The increased conversion rate results in increased production of H_2 , CO_2 and CO . The production of CH_4 is via methanation. It is interesting to note that the amount of methane decreases when the reactor temperature is above $500^\circ C$. This is due to the reformation of the methane. If the results are compared to those found under equilibrium conditions (Figure 3.1), with the exceptions of LPG conversion and CH_4 production, it can be seen that the same trends occur. The differences here are due to the steam reforming reaction in the real reactor not having sufficient time to reach equilibrium. It is noted that a potential further 10% H_2 can be produced from the LPG

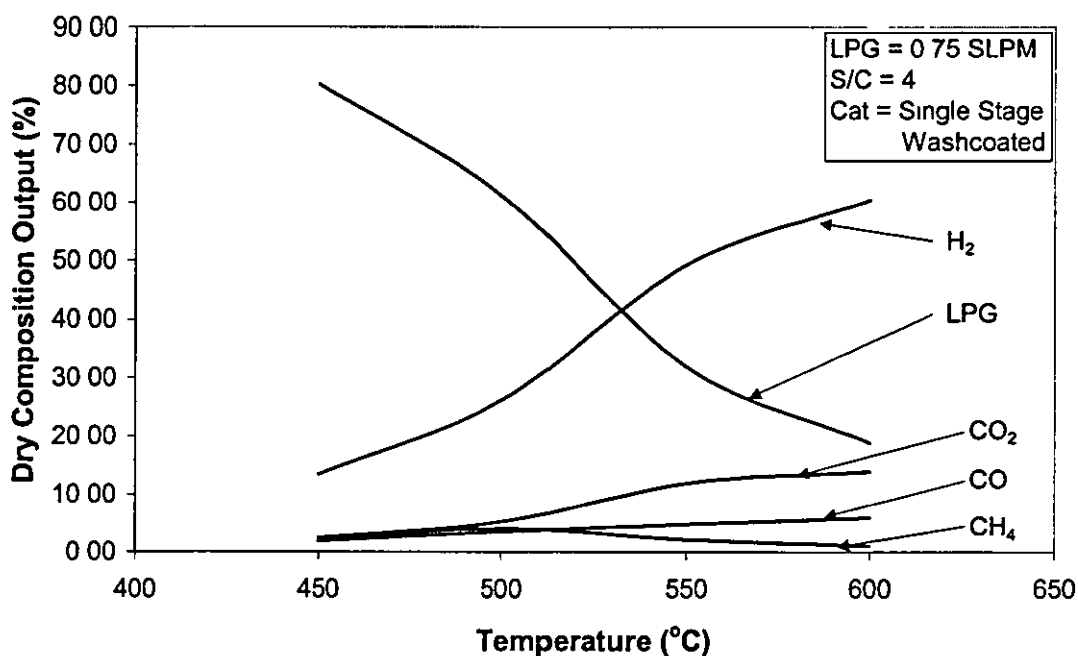


Figure 8.1: Dry Reformate Composition at Varying Temperature

The effect of the steam to carbon ratio on the dry reformate composition is shown in Figure 8.2. During the test, the LPG supply rate to the reformer was 0.75 SLPM, and

the reactor temperature was set to 600°C. It can be seen that as the steam to carbon ratio is increased so does the conversion of LPG. It increases the production of H₂. In addition, the concentration of CO decreases whilst the amount of CO₂ increases. The change in proportion of CO/CO₂ is due to the water shift reaction. Hydrogen from the water is liberated when the water reacts with the CO to produce H₂ and CO₂. Again, if the results from the experiment are compared to the predicted equilibrium results (Figure 3 2) it can be seen that with the exception of the percentage conversion of the LPG and the production of CH₄ in the equilibrium results, the spread of values is similar. The maximum steam to carbon ratio investigated was four This is twice the stoichiometric value From simulated results it is clear that as long as the steam to carbon ratio increases, the amount of hydrogen produced will increase. However, it is more efficient to liberate this hydrogen, whilst removing carbon monoxide from the reformat, in a separate lower temperature reactor. In this way the carbon monoxide content can be reduced to approximately 1% without the need for extra heat to be applied to the reformer. Therefore, a steam to carbon ratio maximum limit of 4 was utilised

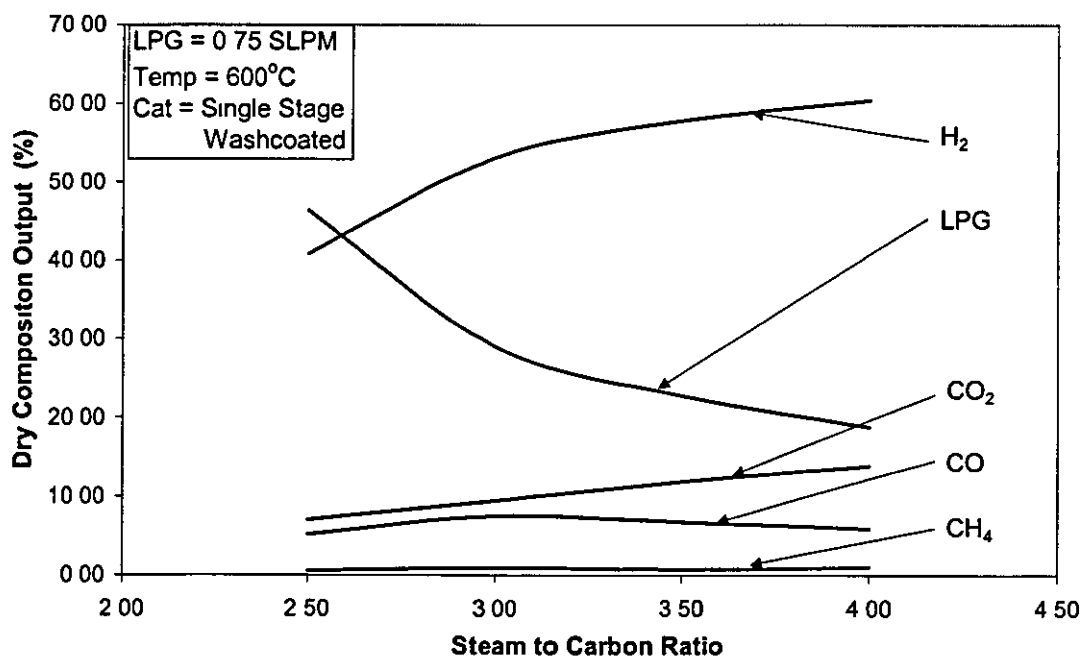


Figure 8.2: Dry Reformat Composition with Varying Steam to Carbon Ratio

The effect of the flow-rate of the reformer reactants on the dry reformat composition is shown in Figure 8.3. The steam to carbon ratio during the test was 4, and again the

reactor temperature was set at 600°C. It can be seen that as the flow rate of reactants to the reformer was increased the conversion of the LPG decreased. This is due to the reduction of residence time in the reformer itself. It suggests that the activity of the catalyst needs increasing for a reformer of this volume. This will be taken into account during the next stage of work.

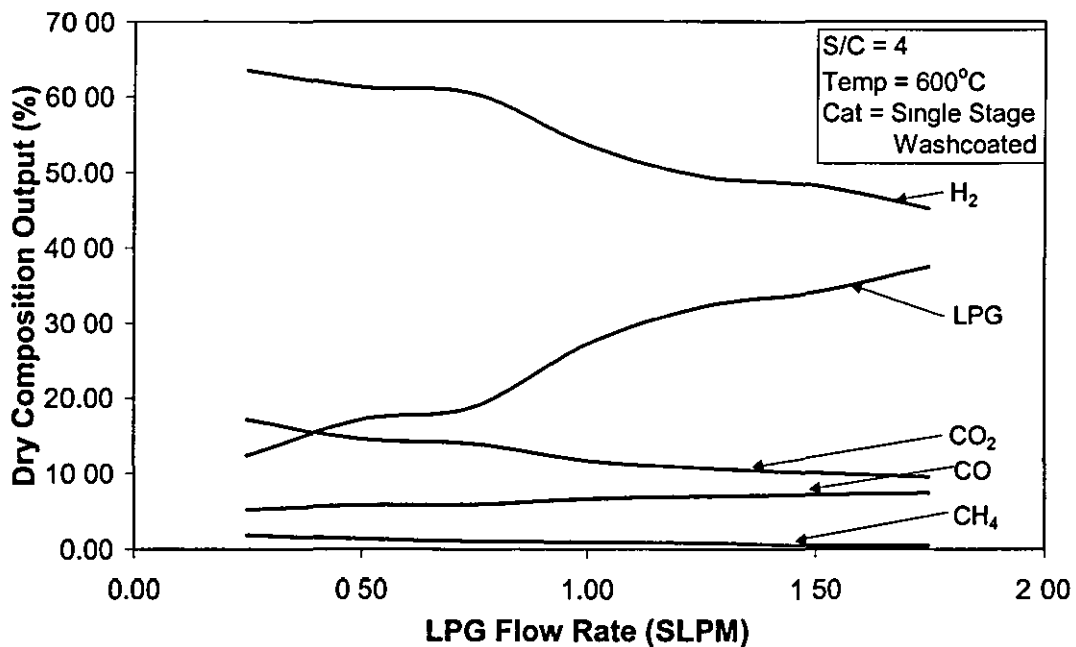


Figure 8.3: Dry Reformate Composition with Varying Reactant Flow-rate

Space velocity is defined as the volume of gaseous reformat per hour per volume of catalyst which is widely regarded as GHSV. In this study the maximum space velocity was found to be 9420 GHSV. This figure is based on the reformer performance at a LPG flow rate of 1.75 SLPM and steam to carbon ratio of 4. The reformer was at a temperature of 600°C. However, this figure is not based on the volume of the catalyst but on the volume of the reformer itself. This is because the catalyst is wash-coated on to the reforming surface, the volume of the catalyst will be much lower than that of the reformer. This would increase the GHSV figure in real term.

The energy conversion efficiency of the reformer can be defined as the ratio between the energy contained by the reformate products and the energy contained by the reactants,

$$\eta = \frac{P_{LHV}}{R_{LHV}}$$

Equation 8.1

where P_{LHV} is the lower heating value of the products and R_{LHV} is the lower heating value of the reactants.

$$P_{LHV} = H_{2LHV} + CO_{LHV}$$

Equation 8.2

$$R_{LHV} = LPG_{LHV} + H_2^C_{LHV} - LPG^R_{LHV} - H_2^R_{LHV}$$

Equation 8.3

Where H_{2LHV} is the thermal power released by burning the H_2 , CO_{LHV} is the thermal power released by burning the CO , LPG_{LHV} is the thermal power released by burning the LPG feed to the reformer, $H_2^C_{LHV}$ is the thermal power released by burning the H_2 in the combustor, LPG^R_{LHV} is the thermal power released by burning the unconverted LPG in the combustor, and $H_2^R_{LHV}$ is the thermal power released by burning the unused H_2 from the fuel cell.

The thermal power is calculated as follows.

$$P = \left(\dot{m} / 22.41 / 60 \right) \Delta H_{fT}$$

Equation 8.4

Where P is the thermal power, \dot{m} is the flow rate of the gas, and ΔH_{fT} is the enthalpy of formation of the gas at a given temperature T .

The carbon monoxide is included because after water gas shift reaction, most of the CO has been converted into hydrogen during the water gas shift reaction. It has been assumed that any unconverted LPG and any hydrogen in the fuel cell off gas, which is approximately 1/3 of the H_2 to the stack, are burnt in the combustor. The energy used by the electric preheaters is not included in the calculation, as in an ideal fuel processor this energy would be provided by the heat from the reformer and combustor flue gases.

To calculate the flow rate of hydrogen produced by the reformer the following procedure was followed. Using equilibrium modelling the amount of H_2 produced by steam reforming 1 mol/min of LPG for a given steam to carbon ratio and temperature was calculated. This value was then modified by the percentage conversion of LPG reforming tests. This gave an approximate figure for the H_2 flow rate. A similar procedure using equilibrium modelling was used to calculate the CO flow rate.

This method was used due to the unavailability of a reliable flow meter. It makes the assumption that the equilibrium data is correct. It assumes that the production of H_2 varies linearly with the conversion of LPG everything else being equal.

Figure 8.4 shows the conversion efficiency of the reformer at different reactant flow rates. A steam to carbon ratio of 4 and a reactor temperature of $600^\circ C$ were used during the test. It can be seen that the average conversion efficiency of the reformer is between 0.5 and 1.5 SLPM is 74%. This value is higher than would be expected by a reformer operating at a LPG conversion rate of around 81%. This is due to the manner in which the reformer efficiency was calculated, which took into account unconverted LPG from the reformer flue and recycled it by burning it in the combustor.

For a reformer of this size 0.25 SLPM of LPG is too low. At such low rates, the reformer is too big to operate efficiently. At a LPG flow rate of 1.75 SLPM, the flow of H_2 to the combustor needs to be increased dramatically. This is due to the LPG/ H_2O preheat not being powerful enough to heat the reactants sufficiently to vaporise the H_2O before entering the reformer. As a result the reformer's temperature controller has to increase the H_2 flow rate to compensate and vaporise the H_2O at the entry to the reformer. This lowers the efficiency of the reformer.

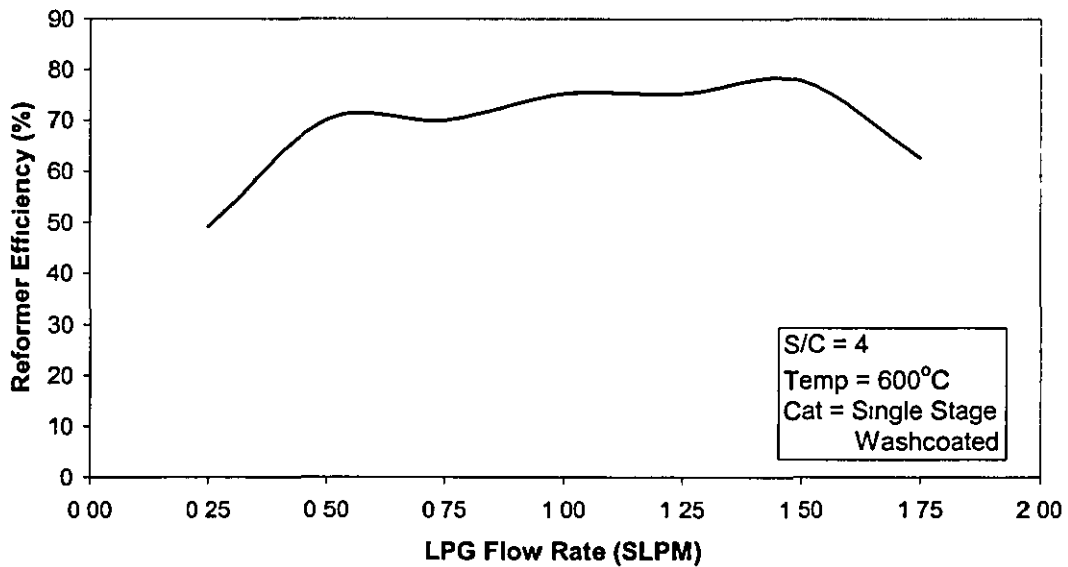


Figure 8.4: Reformer Efficiency at Varying Reactants Flow Rate

The energy conversion efficiency of the reactor at the higher range of flowrates can be further improved by improving the integration of the reformer with the rest of the test rig/system by providing sufficient heat to the feedstock to vaporise the water content before it entered the reformer.

The power output of the reformer is based on calculated equilibrium data, which was then modified according to the percentage conversion of the LPG feedstock as follows.

$$P_a = \frac{C_a \times H \times 22.41}{F} \quad \text{Equation 8.5}$$

Where P_a is the predicted power output from the fuel cell in kWe, C_a is the percentage conversion of the LPG, H is the flow rate of hydrogen (mol/min) produced at equilibrium by 1 mol/min of LPG for a given steam to carbon ratio and F is the flow rate of hydrogen (SLPM) required to produce 1 kWe output from a fuel cell.

Figure 8.5 shows the effect of the reactants flow rate on the predicted power output of a fuel cell. It can be seen that as the LPG flow rate increases the projected power output from the fuel cell increases. The maximum output achieved was 0.86 kWe at

an LPG flow rate of 1.75 SLPM and S/C ratio of 4. However, the conversion of LPG decreases with increasing LPG flow rate as shown in Figure 8.5. When the power output reached 0.86 kWe the conversion of LPG was only 62.5% which, would not be realistic for use in a complete system because of the additional processing required. Using the sulphur tolerant catalyst in this form, complete conversion can not be achieved under any of the operating conditions tested.

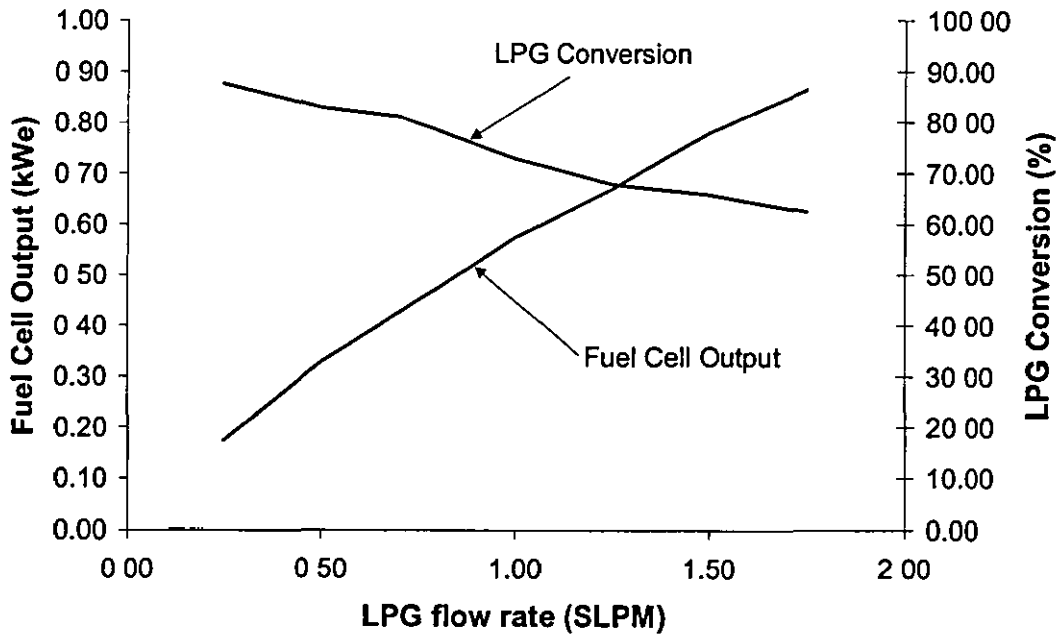


Figure 8.5: Predicted Fuel Cell Power Output at Varying Reactants Flow Rate

8.1.2 Summary

	Experimental	Equilibrium
Reformer Temperature	600°C	600°C
LPG Flow Rate	0.75 SLPM	0.75 SLPM
Steam to Carbon Ratio	4	4
Power Output	0.45 kWe	0.59 kWe
H ₂	60.4%	72.7%
CH ₄	1 %	2.7%
CO ₂	13.9 %	17.6%
CO	5.9%	7.1%
Balance (LPG + other HCs)	18.8 %	Trace
LPG Conversion %	81.2 %	100 %
Space Velocity (LPG = 1.75 SLPM)	9450 GHSV	N/A
Reformer Efficiency	74%	N/A

Table 8.1: Results Summary of the Single-Stage Reforming

8.2 Conclusion

The microchannel technology is capable of transferring enough heat to support the steam reforming reaction and offers advantages in size compared to traditional steam reformer reactor designs.

The results obtained using the sulphur tolerant catalyst suggest that a sulphur tolerant fuel reformer is feasible. However, this work is only the first stage in the development of such a reformer. The sulphur tolerant catalyst allowed for 81% conversion of the LPG and produced results near to that expected by equilibrium modelling, with the overall behaviour of the reformer with respect to temperature and steam to carbon ratio as expected. There is not complete conversion of the LPG even at the lowest flow rate tested. Because of the loss in efficiency of the reformer at this flow rate, it can be inferred that, the sulphur-tolerant catalyst is not sufficient in this form for use

as the basis of a steam reformer for LPG. The maximum usable temperature of the catalyst is 600°C so it would not be possible to improve the performance of the reformer by increasing the operating temperature without extending the thermal range of the catalyst. The next stage of work would be to increase the activity of the catalyst. Possible development routes would be to design a new sulphur tolerant catalyst, or to use a more conventional steam reforming catalyst in combination with the existing sulphur tolerant catalyst to increase the activity in that manner. Because of the temperature control available using this reformer design, the addition of a second catalyst running at a higher temperature than the existing catalyst is feasible. This would create the effect of a dual-stage steam reformer.

9 Dual-Stage Steam Reformer

It can be seen from the results in Chapter 8 that the activity of the sulphur tolerant catalyst is not high enough for use in a reformer of this size. To improve the reformer performance a second reforming catalyst was washcoated over the top of the original catalyst, over the second half of the reactor. This can be seen in Figure 9.1. The second catalyst is a standard nickel based reforming catalyst. The multi-zoned combustor allows each catalyst zone to be operated at the temperature best suited to that catalyst. The sulphur tolerant catalyst is limited to 600°C before degradation takes place. The nickel-based catalyst can withstand temperatures of up to 800°C before the same happens.

Some advantages of choosing this method to improve the reformer performance are that it allows the possibility of investigating whether any sulphur tolerant effect from the original catalyst is enough to allow LPG to be reformed over a standard catalyst. It is also a cost-effective method of increasing the performance of the reformer that could be implemented quickly with a minimum of further catalyst or reactor development, which would have been time consuming and entailed expenses beyond the scope of this work. It also allows the multi-zoned combustor to be operated so that each catalyst is operated at a different temperature, which helps to explore the feasibility of using the technology to develop an all in one fuel processor, with close temperature control as required for the various stages of the fuel processor.

One such stage in such a fuel processor might be that of a two-stage reformer. By using a two-stage reformer the formation of coke can be suppressed. If the reactants are first fed to a low temperature reactor the heavy hydrocarbons will react to give methane and carbon oxides. These are then passed to the second stage of the reactor, which is at a higher temperature where the methane is reformed to produce hydrogen with little risk of forming coke [Ref. D. G. Loffler (2003)]

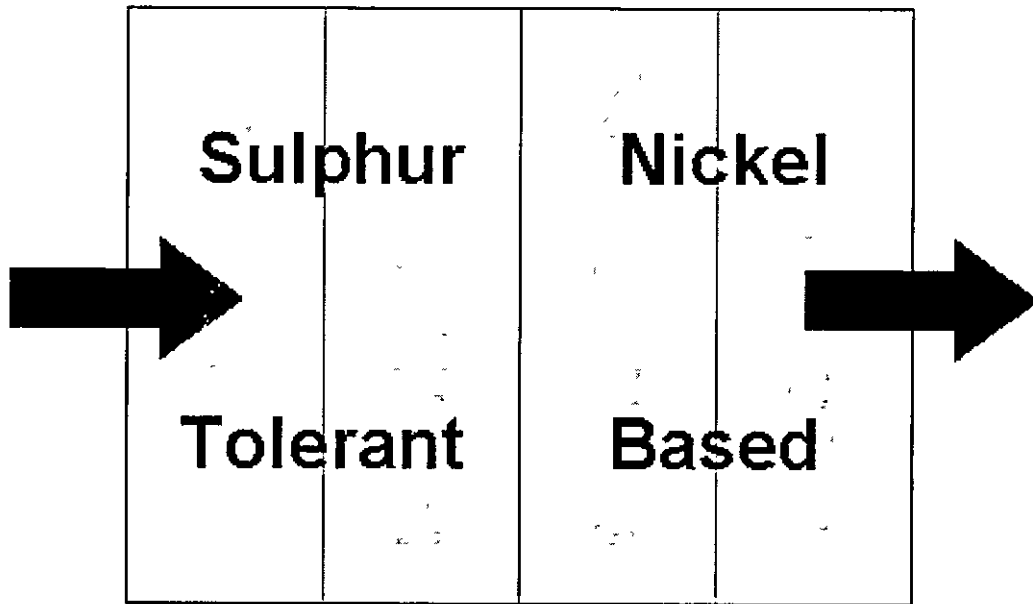


Figure 9.1: Steam Reformer Catalyst Distribution

The multi-zoned combustor design allows the temperature of the two catalysts to be operated at different temperatures to each other. This means that the sulphur tolerant catalyst can be operated safely at 600°C whilst the nickel based catalyst can be operated at a different temperature as required. In this way the temperature profile of the reformer can be tailored to suit the optimal operating conditions of the two catalysts.

9.1 Evaluation of the Dual-stage Reformer using Propane, Liquid Petroleum Gas, and Methane

The tests performed using C_3H_8 were as follows

- The temperature in zone 1 was set to 600°C whilst zone 4 was set to the set-points of 600°C, 650°C, 700°C and 750°C. For each temperature set-point the steam to carbon ratio was set to 2.5, 3, 3.5 and 4

- The flow rate of C_3H_8 was set at 0.75 SLPM as this corresponds to approximately 0.5kWe (based on equilibrium data) from a fuel cell which given total conversion of the C_3H_8
- The set-point with the best performance was then chosen and the C_3H_8 flow rate was varied from 0.25 to 2.5 SLPM whilst the temperature and S/C ratio were kept constant

The tests performed with CH_4 were as follows

- The temperature in zone 1 was set to 600°C whilst zone 4 was set to the set-points of 600°C, 650°C and 700°C. For each temperature set-point the steam to carbon ratio was set to 2.5, 3, 3.5 and 4.
- The flow rate of CH_4 was set at 1.88 SLPM as this corresponds to approximately 0.5kWe (based on equilibrium data) from a fuel cell, given total conversion of the CH_4 .
- The set-point with the best performance was then chosen and the CH_4 flow rate was varied from 0.6 to 2.5 SLPM whilst the temperature and S/C ratio were kept constant.

For the tests using LPG a commercial grade LPG supplied by Calor Gas was used as the reactant. This was the same composition as the LPG used in the single stage reforming tests. This fuel contains sulphur as an odourant and was chosen to compare the performance with that when using C_3H_8

The test procedures were as follows

- The temperature in zone 1 was set to 600°C whilst zone 4 was set to the set-points of 600°C, 650°C, and 700°C. For each temperature set-point the steam to carbon ratio was set to 2.5, 3, 3.5 and 4.
- The flow rate of LPG was set at 0.75 SLPM as this corresponds to approximately 0.5kWe (based on equilibrium data) from a fuel cell when total conversion of the LPG is assumed.

- The set-point with the best performance was then chosen and the LPG flow rate was varied from 0.25 to 1.25 SLPM whilst the temperature and S/C ratio were kept constant.

9.1.1 Evaluation of the Reformer using Propane as a Feedstock

As expected running zone 4 of the reformer at higher temperatures increased the H₂ yield (Figure 9.2). It also decreased the CO₂ % and CH₄ % whilst the CO % increased. As the conversion of the propane remains almost constant through out, the additional H₂ produced is derived from the methane content in the reformat. The CH₄ content decreases as the H₂ content of the reformat increases.

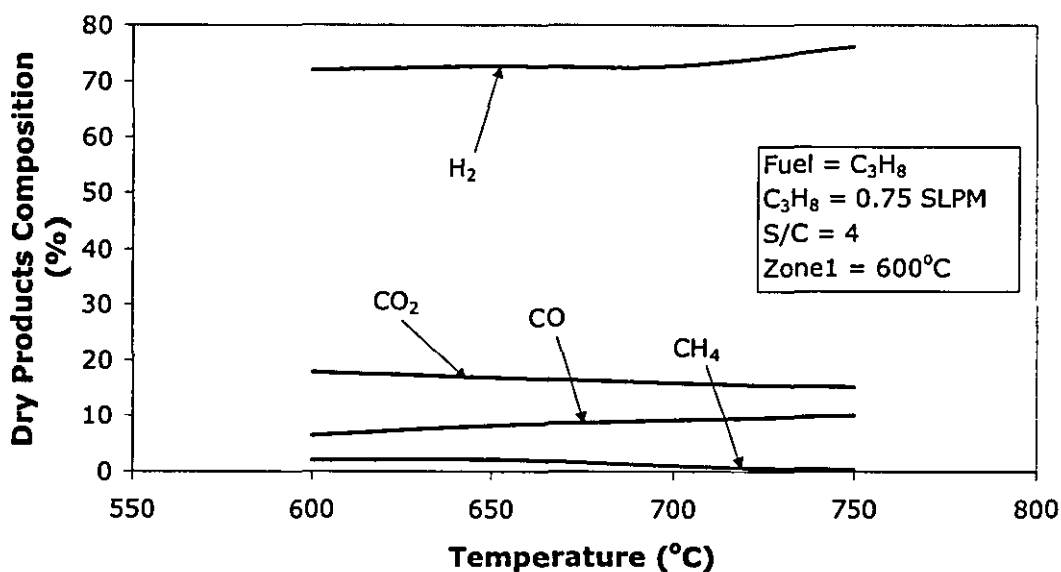


Figure 9.2: The Effect of Zone 4 Temperature on Reformer Performance

As expected, increasing the steam to carbon ratio increased the H₂ and CO₂ yield whilst decreasing the CO and CH₄ yield (Figure 9.3). The increase of CO₂ against CO is indicative of some shift reaction activity due to the properties of the addition of the nickel-based catalyst. Some of the CO is combined with H₂O to form CO₂ and H₂. The maximum S/C ratio tested was 4. This is because it is more efficient to use a specialised water gas shift reactor to liberate H₂ from the excess water and reduce CO levels in the reformat than simply keep increasing the steam to carbon ratio for the

reformer. This is due to the fact that the water shift reaction is exothermic and as such is promoted at lower temperatures than those which promote the endothermic steam reforming reaction.

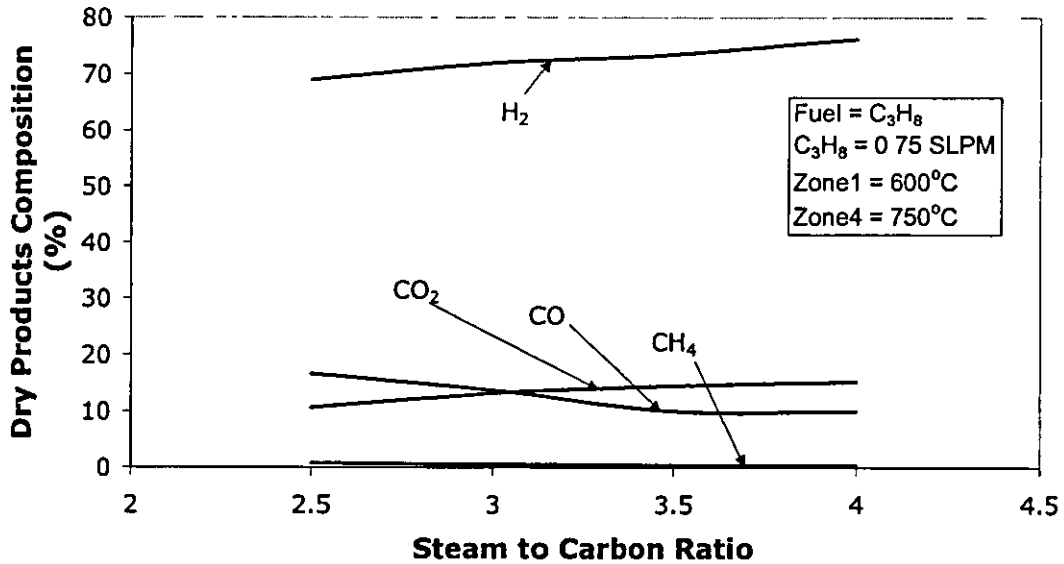


Figure 9.3: The Effect of Steam to Carbon Ratio on the Reformer Performance

Under the test conditions observed, the H₂ % output did not decrease even at the higher flow rates tested (Figure 9 4). This shows that the addition of the nickel-based catalyst has had a positive effect on the reformers performance. This was expected due to the higher activity of the new catalyst compared to the sulphur tolerant one. The maximum flow rate used for the tests was determined by the peripheral equipment such as, the power rating of the reformer inlet electric preheater rather than the reformer itself. If the flow rate of reactants into the electric preheater was too high, the preheater was unable to vaporise the H₂O before it entered the reformer This lowered the efficiency of the reformer and lowered the temperature of zone 1 below that which the temperature controller could compensate for.

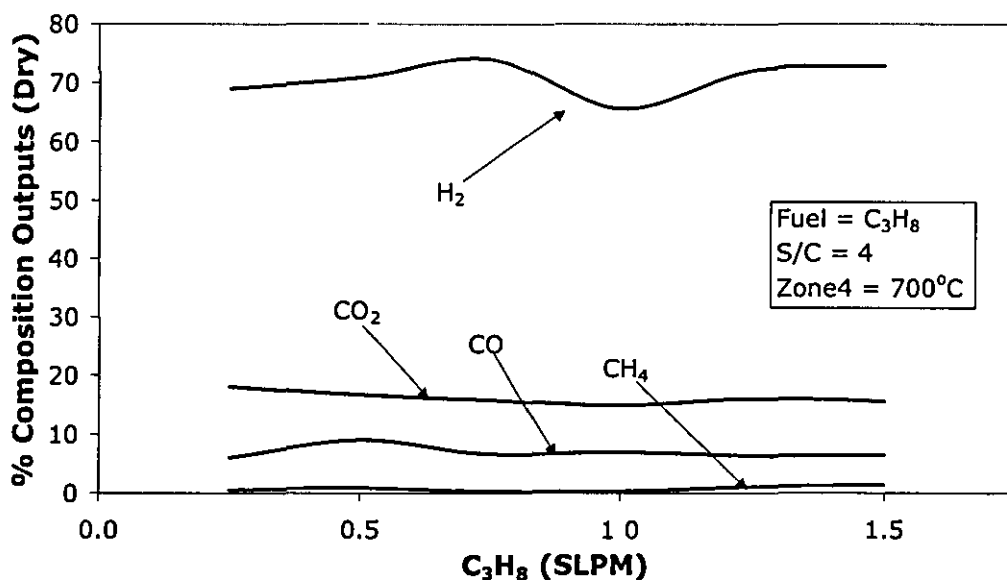


Figure 9.4: The Effect of C₃H₈ Flow Rate on the Reformer Performance

The average efficiency (as calculated in Chapter 8) of the reformer over varied feed flow rates (disregarding the two end points on the chart, Figure 9.5) is approximately 70%. 0.25 SLPM is a very low C₃H₈ flow rate in comparison with the reformer design. At such low rates, the reformer is too big to operate efficiently. At high flow rates the preheater for the fuel/water mixture was not powerful enough to vaporise the water before it entered the reformer. This meant that the temperature controller would inject extra H₂ into the zone 1 combustion chamber to compensate. This increase in H₂ consumption lowered the reformer efficiency. Because of this it would be possible to improve the reformer efficiency at the higher flow rates by better system integration.

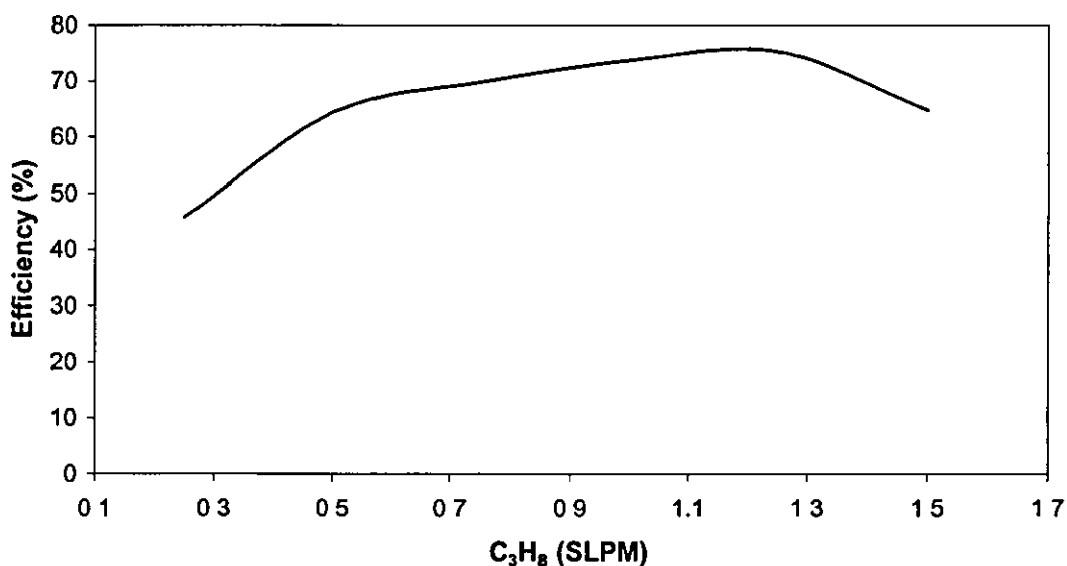


Figure 9.5: The Effect of C₃H₈ Flow Rate on Reformer Efficiency

The maximum power output achieved was 1.98 kWe at LPG = 2.5 SLPM and S/C = 4, Zone 4 temperature 600°C. This figure was calculated using the same method described in Chapter 8. This value could be improved by increasing the zone 4 temperature and by integrating the system more effectively. It can be seen in Figure 9.6 that there is no drop off in H₂ % volume even at the highest flow rate. Provided that the system integration was improved, i.e. a higher level of preheating of the reactants before the reformer inlet, the power output of the reformer could be above 2 kWe. The gas hourly space velocity at a feed rate of 2.5 SLPM and steam to carbon ratio of 4 was calculated to be 13800 GHSV based on the exit flow

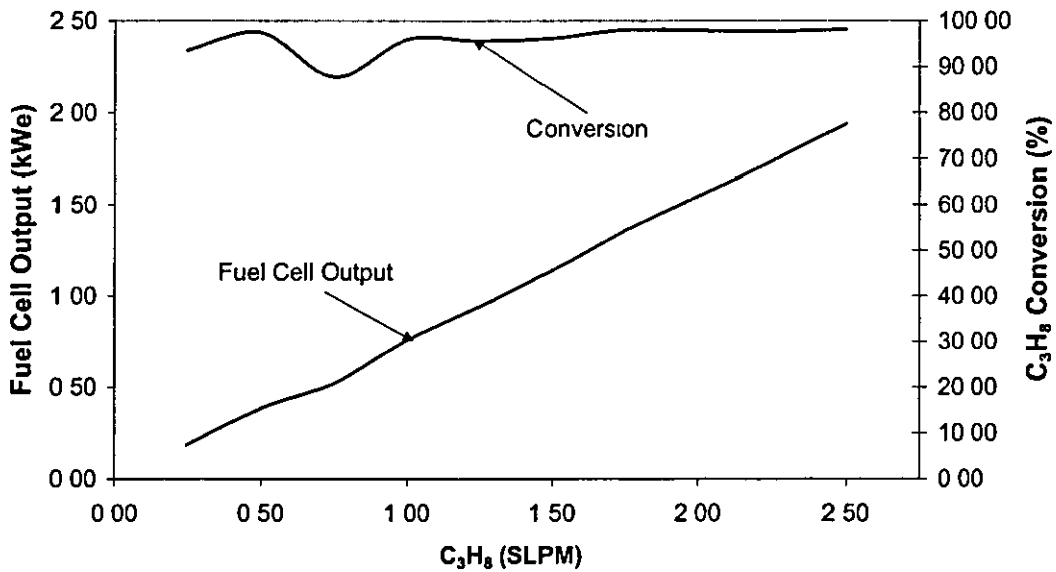


Figure 9.6: The Effect of C₃H₈ Flow Rate on Fuel Cell Power Output

The maximum flow-rates in the tests were imposed by the preheater for the reformer reactants. The tests using C₃H₈ where the flow-rate was increased to 2.5 SLPM were not repeated using LPG or CH₄ to protect the reformer from damage. It was observed that the temperature controller was unable to supply enough heat to the first zone in order to vaporise the incoming water. This was because the flow rate of H₂ requested was so high that the majority of the H₂ passed through the combustor before combusting and in fact burnt in the combustor exhaust. This raised the temperature of the exhaust beyond that which was thought safe. Therefore during the subsequent tests the maximum feedstock flow rate was limited.

9.1.2 Evaluation of the Reformer using Methane as a Feedstock

It can immediately be seen in Figure 9.7 that the performance of the reformer is not as good when CH₄ is used as a feed stock rather than C₃H₈. This is because methane is more endothermic per carbon atom than C₃H₈ [Ref. F. Joensen (2002)].

It can be seen in Figure 9.7 that the flow rate of the reformer feed stock greatly affects the performance of the reformer. This is due to the shorter residence time of the CH_4 due to the increased flow-rate. This performance drop is also noticeable when the S/C ratio is increased from 2.5 to 4 (Figure: 9.9).

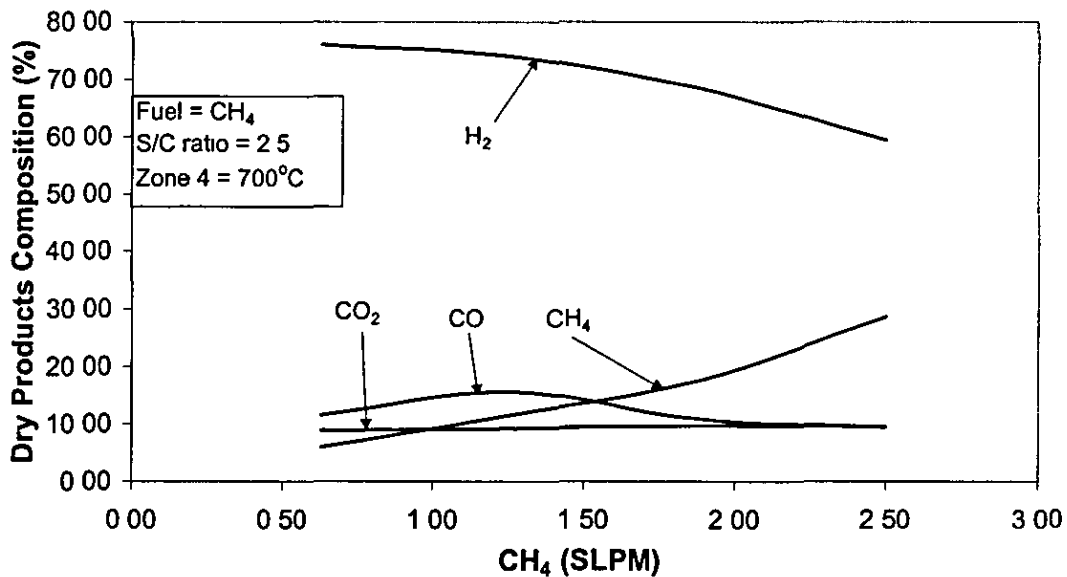


Figure 9.7: The Effect of CH_4 Flow Rate on the Reformer Performance

As expected increasing the temperature of the back end of the reformer increased the H_2 % yield whilst also increasing the CO % and CO_2 % (Figure 9.8). The CH_4 % decreased. This is due to the increase in energy supplied to the reformer at the higher temperatures

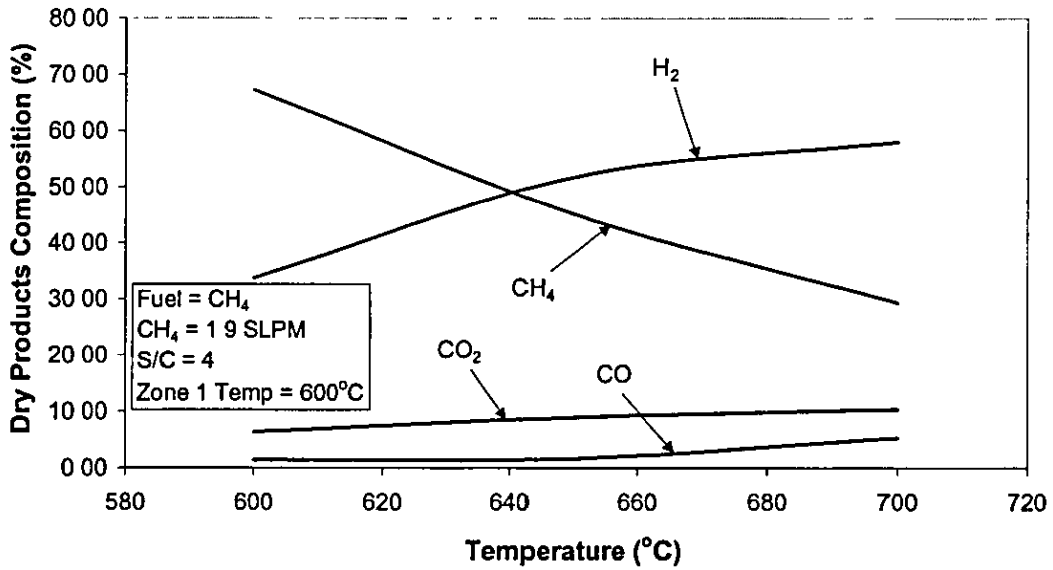


Figure 9.8: The Effect of Zone 4 Temperature on Reformer Performance

Increasing the S/C ratio caused a drop in CH₄ conversion. This was due to the increase in flow rate through the reformer. As can be seen from Figure 9.9 the reformer performance is particularly sensitive to changes in CH₄ flow rate but not to changes in the C₃H₈ flow rate. This is due to the reaction kinetics of CH₄ when compared to C₃H₈.

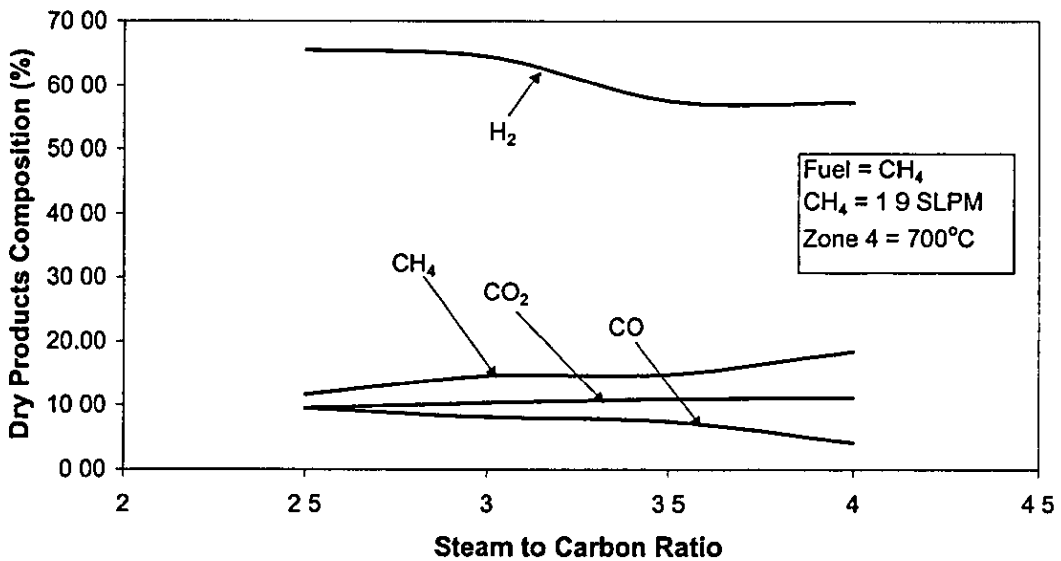


Figure 9.9: The Effect of Steam to Carbon Ratio on Reformer Performance

The average efficiency of the reformer over varied feed rates was approximately 60%. It can be seen in Figure 9.10, that unlike the efficiency curves for C_3H_8 and LPG the curve for CH_4 does not drop off at higher flow rates. This is because of the reduced water content (compared to that when using C_3H_8 or LPG) of the flow entering, firstly the pre heater and secondly the reformer. The majority of the energy used to heat the feedstock is for the vaporisation of water. This means that despite the decreasing performance of the reformer the efficiency increased. As the conversion drops off so too does the amount of heat required to support the reaction. This combined with the increase in H_2 production due to the higher flow-rates means that the reformer efficiency increases.

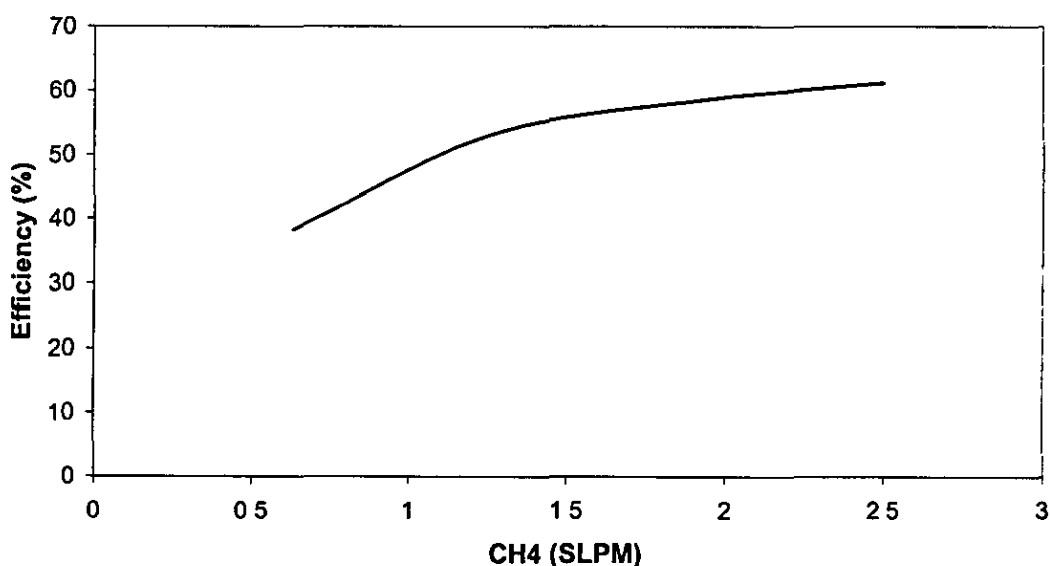


Figure 9.10: The Effect of CH_4 Flow Rate on Reformer Efficiency

It can be seen in Figure 9.11 that despite a loss of conversion at higher flow-rates the H_2 output increases and the predicted power output of a fuel cell improves accordingly. It can be seen that for the same flow rate the power output is lower than that when using C_3H_8 . When an equivalent flow rate is used the performance is still lower than that for C_3H_8 and LPG but the gap is not as large. The gas hourly space velocity at a CH_4 flow rate of 2.5 SLPM and S/C ratio of 4 is 4151 GSHV based on the exit flow.

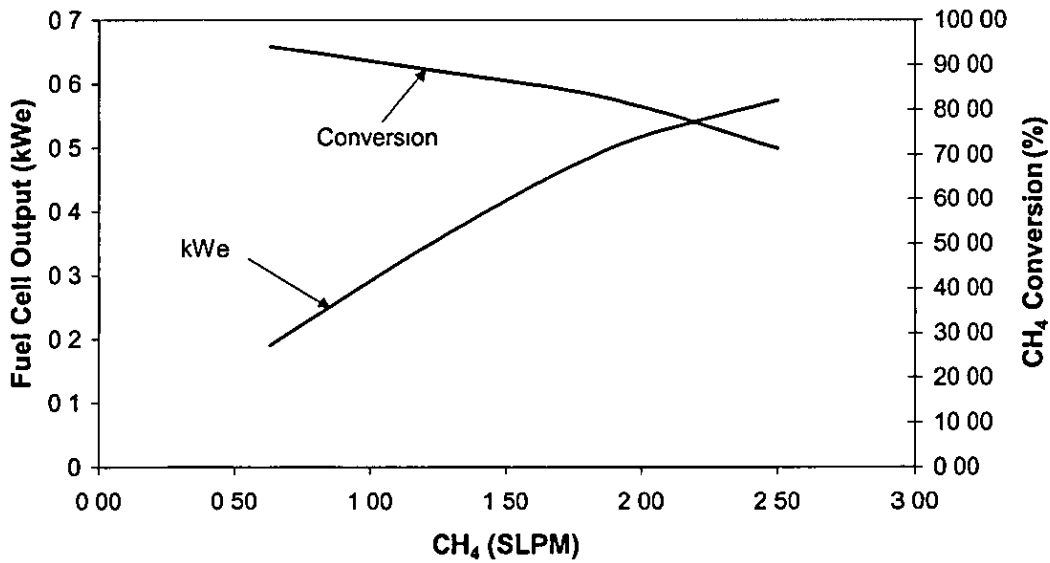


Figure 9.11: The Effect of CH₄ on Fuel Cell Power Output

9.1.3 Evaluation of the Reformer using Liquid Petroleum Gas as a Feedstock

It can be seen in Figure 9.12, that the flow rate of the feedstock does have some effect on the reformer performance. It is possible that the difference between the performance here and when using C₃H₈ is the sulphur in the LPG or just the age of the catalyst. It can be seen that at higher flow rates the conversion of LPG is still above 95% so the effect on the reformer performance is not large.

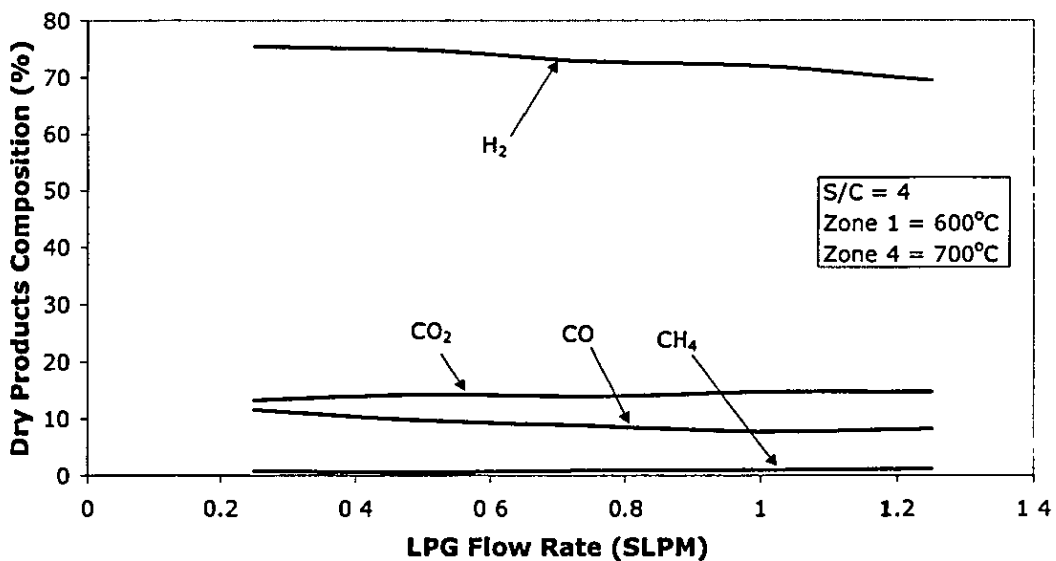


Figure 9.12: The Effect of LPG Flow Rate on Reformer Performance

Increasing the zone 4 temperature increased the H₂ yield (Figure 9.13). It also increased the CO₂ yield whilst the CO yield decreased. This is the opposite behaviour than predicted by equilibrium modelling and suggests that the extra H₂ is produced via the water shift reaction. This is at odds with the results gained from equilibrium modelling and those when C₃H₈ was used as a feedstock.

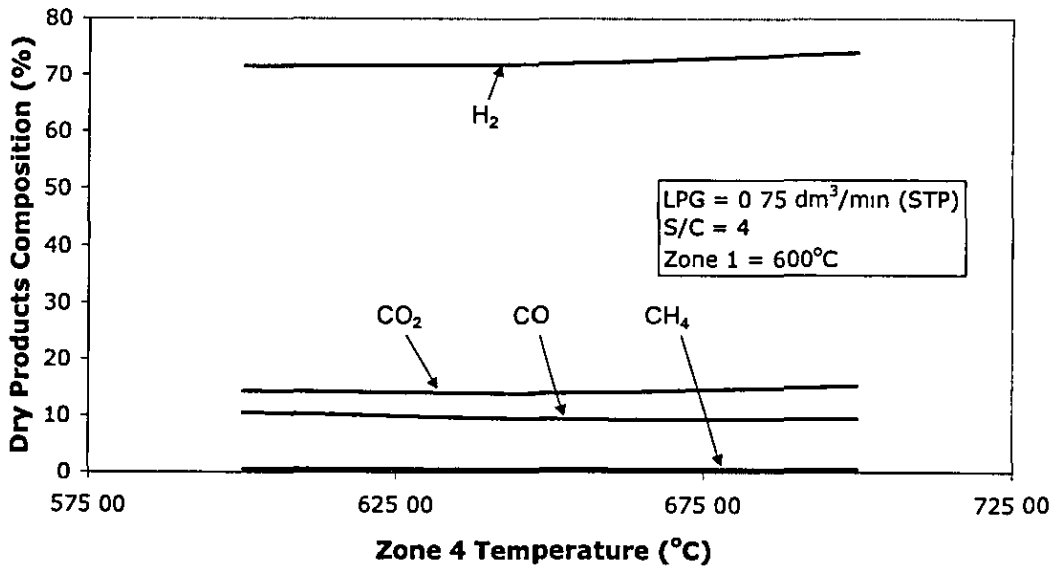


Figure 9.13: The Effect of Zone 4 Temperature on Reformer performance

Increasing the S/C ratio increased the H₂ yield. It also increased the CO₂ yield whilst the CO yield decreased (Figure 9.14). This is due to increased water shift activity caused by the excess water.

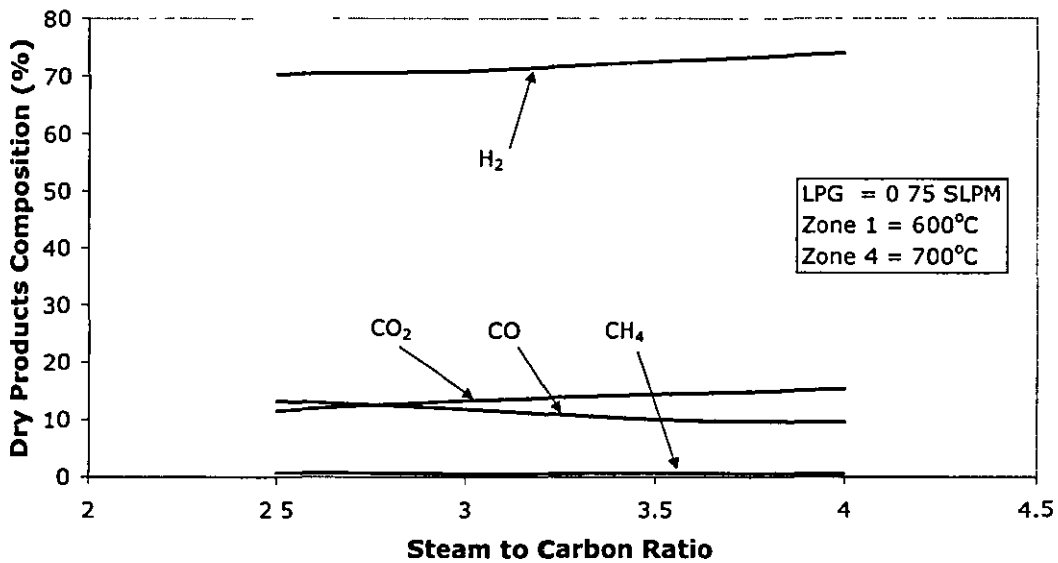


Figure 9.14: The Effect of Steam to Carbon Ratio on Reformer Performance

The average reformer efficiency over varied flow rates was 70%. This is the same as that for C₃H₈ and again shows that due to the sulphur tolerant catalyst in zones 1 and 2, there is no performance loss when using a fuel containing sulphur. Again it can be seen that at low flow rates the reformer is oversized (Figure 9.15)

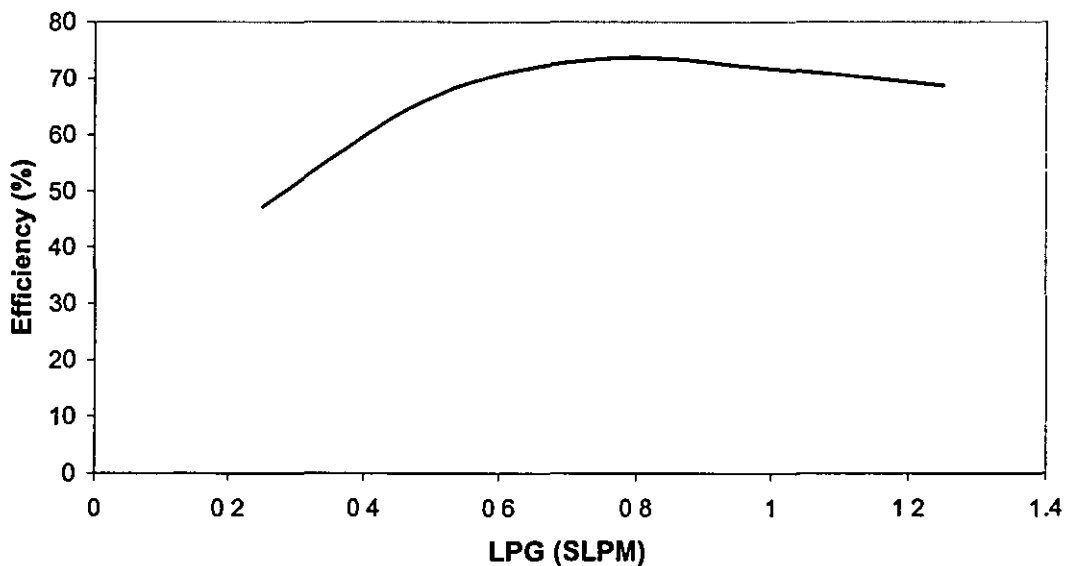


Figure 9.15: The Effect of LPG Flow Rate on the Reformer Efficiency

It can be seen in Figure 9.16, that for the flow-rates tested the power output of the reformer whilst using LPG are very similar to those when the reformer was run using C_3H_8 . This suggests that there may be a synergetic effect when the nickel based catalyst is used on top of the sulphur tolerant catalyst. To confirm or disprove this, further durability tests would need to be carried out using the dual catalyst arrangement to rule out poisoning of the nickel based catalyst due to extended sulphur exposure. Because there is only a slight drop off in reformer performance at the higher flow-rates when using LPG, it can be assumed that the power output of the reformer using LPG will be close to that when using C_3H_8 . Further tests will be needed to confirm that that is the case. To do that the test rig will have to be adapted so that the higher flow rates can be used safely. The gas hourly space velocity at an LPG flow rate of 1.25 SLPM and S/C ratio of 4 is 8670 GSHV based on the exit flow.

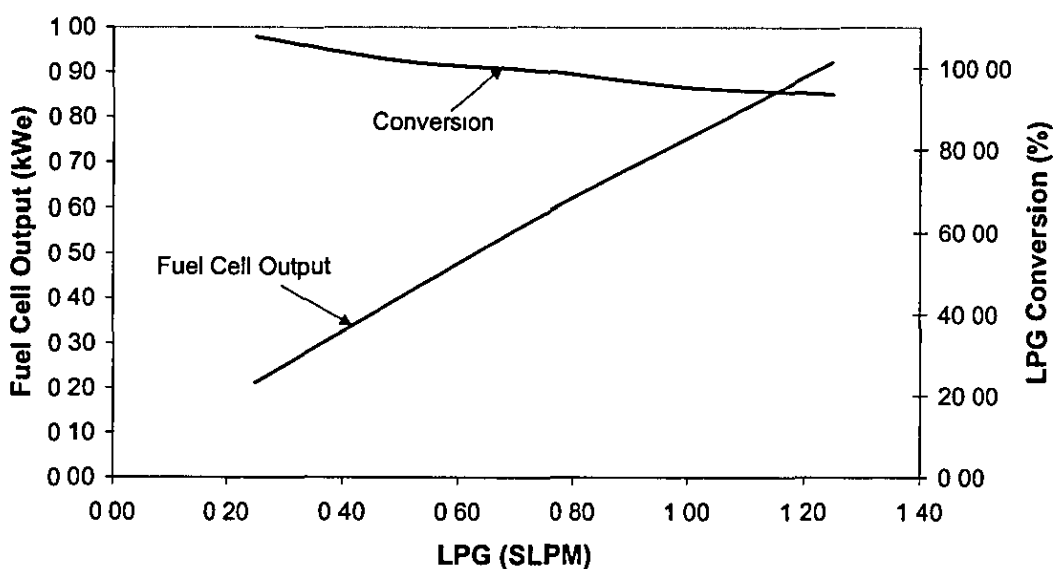


Figure 9.16: The Effect of the LPG Flow Rate on the Fuel Cell power Output

9.2 Summary

	C ₃ H ₈	LPG	CH ₄
Operating conditions	Zone 4 700°C, s/c = 4, 0.75 SLPM	Zone 4 700°C, s/c = 4, 0.75 SLPM	Zone 4 700°C, s/c = 4, 1.88 SLPM
H ₂ %	72.67	74.01	57.96
CO %	9.11	9.49	4.17
CO ₂ %	15.81	15.24	11.09
CH ₄ %	0.91	0.55	18.44
Conversion %	98.49	99.29	81.56
kWe	0.58	0.59	0.49
GHSV	6868	6864	4275
Efficiency %	69.81	73.50	58.27

Table 9.1: A Comparison of Reformer Performance Using Different Fuels

It can be seen from the results summarised in Table 9.1 that there is very little difference between the performance of the reformer when using C₃H₈ and that when using LPG. This suggests that the sulphur tolerant catalyst is effective at preventing the sulphur from the LPG from degrading or at least slowing the degradation of the nickel catalyst. As has been noted the performance of the reformer when using CH₄ is lower than that when using the other fuels. This can be explained by the difference in kinetics of steam reforming CH₄ and steam reforming C₃H₈/LPG.

9.3 Conclusion

A dual stage steam reformer was tested. The reformer utilised a multi-zone combustor. This enabled the two reforming catalysts to be operated at differing temperatures. The composition of the reformat is dependent on the reformer

temperature. The multi-zoned combustor allows accurate control of the reformer temperature and therefore the reformat composition.

The microchannel technology used as the basis of the steam reformer proves itself a viable method of making a compact reformer. The performance of the reformer when using CH_4 is not as good as when using C_3H_8 /LPG. This is due to the reaction kinetics of the respective fuels. Using C_3H_8 as a fuel, at a flow rate of 2.5 SLPM and a steam to carbon ratio of 4, the maximum space velocity attained during the tests was found to be 13800 GHSV. The predicted fuel cell output under these conditions was 1.98 kWe. This is a large improvement over more traditional packed bed steam reformers. The performance is very close to that expected at equilibrium, with conversion rates between 95 and 100%. The performance of the reformer when using LPG as a fuel is similar to that of the non-sulphur fuel (C_3H_8). Because of safety concerns the reformer wasn't tested at the high flow rates that were used with C_3H_8 . But the results gained show that the presence of sulphur in the fuel has had little effect on the performance of the reformer so far. It is anticipated that extended running of the reformer will show some degradation of the nickel catalyst due to the sulphur content of LPG. To further investigate the performance of the reformer using LPG it is necessary to improve the integration of the test rig with the reformer. This would enable higher flow rates of LPG to be tested safely to determine further effects of the sulphur content on the nickel-based catalyst.

10 Conclusion

Due to the twin factors of fossil fuel depletion and environmental concerns, particularly with respect to greenhouse gases like CO₂, the switch to a hydrogen economy looks inevitable. Fuel cells are the ideal technology for use with hydrogen as a fuel. They offer higher practical operating efficiency than internal combustion engines and are well suited to many applications, from transportation, to CHP in the home, to space travel. The question remains however, how to supply the fuel cell with hydrogen?

There is no hydrogen infrastructure available for use today. This leads to the reformation of hydrocarbon fuels in-situ, in order to supply the SPFC with the required high purity hydrogen they require. For stationary home CHP applications natural gas is an obvious choice of hydrocarbon feedstock. In remote areas where there is no formal natural gas infrastructure, a fuel like LPG is a good candidate for reformation. With this in mind a novel steam reformer was constructed. It had an integral multi-zoned catalytic combustor for improved heat management, and the reformer was washcoated with a novel sulphur tolerant catalyst, with the aim of simplifying the fuel processor and improving its thermal efficiency. Alongside this software for data acquisition and thermal control of the reformer was developed.

Initial testing of the reactor concerned itself with characterising the heat exchanger and debugging the control software.

It was shown that the multi-zone combustor layout provides accurate temperature control along the length of the reformer. This improves on the traditional reformer designs. However, although accurate control of the longitudinal temperature was achieved, significant transverse temperature gradient was seen in each combustor zone. This was seen to be a product of the direction of flow of the air supply to the combustor. The catalytic combustor works effectively with approximately 90 to 100% of the H₂ converted. The heat transfer efficiency of the reactor between the combustor and reforming layer was found to be in the region of 65% to 85% at a temperature of 600°C to 400°C, respectively.

The next stage of testing centred on utilising a novel sulphur tolerant reforming catalyst to enable the steam reforming of LPG

The sulphur tolerant catalyst allowed for 81% conversion of the LPG and produced results near to that expected by equilibrium modelling, with the overall behaviour of the reformer with respect to temperature and steam to carbon ratio as expected. There is not complete conversion of the LPG even at the lowest flow rate tested. Because of the loss in efficiency of the reformer at this flow rate, it can be inferred that, further development of the sulphur tolerant catalyst is required to improve its activity.

The final group of tests took place using a dual-catalyst arrangement, which utilised a conventional nickel based reforming catalyst in order to increase the power output of the reformer. With this configuration the reformer was tested using three fuels CH_4 , C_3H_8 , and LPG. The performance of the reformer when using CH_4 was not as good as when using C_3H_8 or LPG. This was due to the reaction kinetics of the respective fuels. Using C_3H_8 as a fuel, at a flow rate of 2.5 SLPM and a steam to carbon ratio of 4, the maximum space velocity attained during the tests was found to be 13800 GHSV. The predicted fuel cell output under these conditions was 1.98 kWe. This represents an improvement over more traditional packed bed steam reformers. The fuel conversion when using C_3H_8 or LPG is very close to that expected at equilibrium, with conversion rates between 95 and 100%. The performance of the reformer when using LPG as a fuel is similar to that of the non-sulphur fuel (C_3H_8). The results gained during the work show that the presence of sulphur in the fuel had little effect on the performance of the reformer. It is anticipated that extended running of the reformer would show some degradation of the nickel catalyst due to the sulphur content of LPG.

The microchannel technology is well suited to steam reforming due to its high rates of heat transfer. The results obtained using the sulphur tolerant catalyst suggested that a sulphur tolerant fuel reformer is feasible, although the sulphur tolerant catalyst would need developing to improve its activity. When using the dual stage reformer it could be seen that the higher activity of the standard catalyst improved the conversion rate of the LPG considerably. In fact the power output of the reformer was limited by the peripheral components of the test rig and not the reactor itself. In its current

configuration the reformer is not suitable for methane reforming, this is due to the catalyst formulation used

Operation of the reformer has led to some clear paths for improvements in the reactor design. To make best advantage of the multi-zone combustor it will be necessary to redesign the internal combustor flow path. This would be to decrease and try to eliminate the transverse temperature gradients produced whilst operating the reactor. This is an important consideration as the reformer products are strongly temperature dependent, and the multi-zone combustor design is intended to provide accurate control of the reactor temperature. A modular model of the reactor was developed in order to facilitate the design of next generation reactors.

An issue with durability of the reactor itself arose during testing. An internal leak developed which linked the combustor and reformer parts of the reactor directly. This was diagnosed by the appearance of nitrogen in the reformer products. The position of the leak was narrowed down to a region near the first thermocouple position at the reformer inlet. A visual inspection of the reactor did not show any obvious damage to the reactor and it is hypothesised that de-lamination of the reactor may have occurred due to sudden quenching of the front face of the reactor during transient operation of the reformer. This has serious implications for the use of the technology as a steam reformer due to the undoubted transient demands placed upon a fuel processor system during normal operation, and the issue needs further investigation. The problem could be overcome by careful system design and control development to ensure that all parts of the system react as required to any transients to avoid quenching of the reformer from occurring

The work undertaken has shown that the microchannel technology used shows real promise for use as a steam reformer. It represents a step forwards in reformer design. Instead of down-scaling industrial scale technology the multi-zone combustor steam reformer is designed specifically for the needs of small scale steam reforming. Its high rate of heat transfer makes the technology particularly attractive. The multi-zone combustor layout used here shows promise for use as a concept for complete fuel processor system, as it would allow effective thermal management of such a system

11 References

- A Heinzl, B. Vogel, P. Hubner, Reforming of natural gas - hydrogen generation for small scale stationary systems, *J. of Power Sources*, 105 (2002) 202-207
- A Ersoz, H Olgun, S. Ozdogan, C. Gungor, F. Akgun, M. Tiris, Autothermal reforming as a hydrocarbon fuel processing option for PEM fuel cell, *J. of Power Sources*, 118 (2003) 384-392
- A. Folkesson, C. Andersson, P. Alvfors, M Alakula, L. Overgaard, Real life testing of a hybrid PEM fuel cell bus, *J. of Power Sources*, 118 (2003) 349-357
- A. Psoma, G. Sattler, Fuel cell systems for sumarines: from the first idea to serial production, *J. of Power Sources*, 106 (2002) 381-383
- A.E. Lutz, R.S. Larson, J. O. Keller, Thermodynamic comparison of fuel cells to the carnot cycle, *Int J of Hydrogen Energy*, 27 (2002) 1103-1111
- A.G. Dutton, J.A.M. Bleijs, H. Dienhart, M. Falchetta, W. Hug, D. Prischich, A.J. Ruddell, Experience in the design, sizing, economics, and implementation of autonomous wind-powered hydrogen production systems, *Int J. of Hydrogen Energy*, 25 (2000) 705-722
- A N. Kuzyukov, Yu. Ya, Nikhayenko, V.A. Levchenko, V.A. Borisenko, V.G Moisa, How hydrogen affects operability of chemical and petrochemical equipment made of carbon and low alloy steel, *Int. J. of Hydrogen Energy*, 27 (2002) 813-817
- B. Arnason, T.I. Sigfusson, Iceland - a future hydrogen economy, *Int J. of Hydrogen Energy*, 25 (2000) 389-394
- B. Lindstrom, L.J. Pettersson, Stema reforming of methanol over copper based monoliths: the effects of zirconia doping, *J. of Power Sources*, 106 (2002) 264-273
- C. Gu, G.-H. Gao, Y.-X. Yu, Density functional study of the adsorption and seperation of hydrogen in single-walled carbon nanotube, *Int J. of Hydrogen Energy*, 29 (2004) 465-473
- C. Qi, D Pollica, M. Hagan, T. Cole, V. Rizzo, Transient CO preferential oxidation (PrOx) for PEM fuel cell, *Society of Automotive Engineers Inc* , 2000-01-0378

- C D. Dudfield, R Chen, P.L. Adcock, A carbon monoxide PROX reactor for PEM fuel cell automotive application, *Int J of Hydrogen Energy*, 26 (2001) 763-775
- C.D. Dudfield, R Chen, P.L Adcock, A compact CO selective oxidation reactor for solid polymer fuel cell powered vehicle application, *J. of Power Sources*, 86 (2000) 214-222
- C K.Dyer Fuel cells for portable applications, *J. of Power Sources*, 106 (2002) 31-34
- C N. Hamelnck, A P C. Faaif, Future prospects for production of methanol and hydrogen from biomass, *J. of Power Sources*, 111 (2002) 1-22
- D. Dellepiane, B. Bosio, E. Arato, Clean energy from sugarcane waste: feasibility study of an innovative application of bagasse and barbojo, *J. of Power Sources*, 122 (2003) 47-56
- D.G. Loffler, K. Taylor, D. Mason, A light hydrocarbon fuel processor producing high-purity hydrogen, *J of Power Sources*, 117 (2003) 84-91
- D K. Liguras, K. Goundani, X. E. Verykios, Production of hydrogen for fuel cells by catalytic partial oxidation of ethanol over structured Ru catalysts, *Int. J. of Hydrogen Energy*, 29 (2004) 419-427
- D L. King, C. Faz, T. Flynn, Desulfurization of gasoline feedstocks for application in fuel reforming, *Society of Automotive Engineers Inc* , 2000-01-0002
- D.R. Palo, J.D. Holladay, R.T. Rozmiarek, C.E. Guzman-Leong, Y. Wang, J. Hu, Y.-H. Chin, R.A. Dagle, E.G. Baker, Development of a soldier portable fuel cell power system Part 1: A bread-board methanol fuel processor, *J of Power Sources*, 108 (2002) 28-34
- D.S. Scott, Hydrogen - the case for inevitability, *Int. J. of Hydrogen Energy*, 29 (2004) 225-227
- D.V. Schur, B.P. Tarasov, S. Yu Zaginaichenko, V.K. Pishuk, T N. Veziroglu, Yu.M. Shul'ga, A G Dubovoi, N.S. Anikina, A.P. Pomytkin, A D. Zolotarenko, The prospects for using of carbon nanomaterials as hydrogen storage systems, *Int J of Hydrogen Energy*, 27 (2002) 1063-1069
- E. Entchev, Residential fuel cell energy systems performance optimization using "soft computing" techniques, *J. of Power Sources*, 118 (2003) 212-217
- E A. Foumeny, P.J. Heggs, *Heat exchange engineering volume 1, design of heat exchangers*, Ellis Horwood Ltd, 1991

- F. Galluci, L. Paturzo, A. Basile, A simulation study of the steam reforming of methane in a dense tubular reactor, *Int. J. of Hydrogen Energy*, 29 (2004) 611-617
- F. Joensen, J. R. Rostrup-Nielsen, Conversion of hydrocarbons and alcohols for fuel cells, *J. of Power Sources*, 105 (2002) 195-201
- G. Pede, A. Iacobazzi, S. Passerini, A. Bobbio, G. Botto, FC vehicle hybridisation: an affordable solution for an energy-efficiency FC powered drive train, *J. of Power Sources*, 125 (2004) 280-291
- G.F.C. Rogers, Y.R. Mayhew, *Engineering thermodynamics, work and heat transfer*, Longman Group Ltd, 1980
- H.S. Lee, S. Jeong, B.S. Oh, An experimental study of controlling strategies and drive forces for hydrogen fuel cell hybrid vehicles, *Int. J. of Hydrogen Energy*, 28 (2003) 215-222
- I. Bar-On, R. Kirchan, R. Roth, Technical cost analysis for PEM fuel cells, *J. of Power Sources*, 109 (2002) 71-75
- I. Schulte, D. hart, R. van der Vorst, Issues affecting the acceptance of hydrogen fuel, *Int. J. of Hydrogen Energy*, 29 (2004) 677-685
- J. Agrell, H. Birgersson, M. Boutonnet, Steam reforming of methanol over a Cu/ZnO/Al₂O₃ catalyst: a kinetic analysis and strategies for suppression of CO formation, *J. of Power Sources*, 106 (2002) 249-257
- J. Larminie, A. Dicks, *Fuel cell systems explained*, John Wiley and Sons Ltd., ISBN 0 471 49026 1, Copyright 2000
- J. Pasel, P. Cremer, B. Wegner, R. Peters, D. Stolen, Combination of autothermal reforming with water gas shift reaction. small scale testing of different water gas shift catalysts, *J. of Power Sources*, 126 (2004) 112-118
- J.-D. Kim, Y.I. Park, K. Kobayashi, M. Nagai, Effect of CO gas and anode-metal loading on H₂ oxidation in proton exchange membrane fuel cell, *J. of Power Sources*, 103 (2001) 127-133
- J.H. Wang, W.-L. Chiang, J.P.H. Shu, The prospects - fuel cell motorcycle in Taiwan, *J. of Power Sources*, 86 (2000) 151-157
- J.M. King, M. J. O'Day, Applying fuel cell experience to sustainable power products, *J. of Power Sources*, 86 (2000) 16-22
- J.M. Moore, J.B. Lakeman, G.O. Mepsted, Development of a PEM fuel cell powered portable field generator for the dismounted soldier, *J. of Power Sources*, 106 (2002) 16-20

- J.M. Vidueira, A. Contreras, T.N. Veziroglu, PV autonomous installation to produce hydrogen via electrolysis, and its use in FC buses, *Int J. of Hydrogen Energy*, 28 (2003) 927-937
- J.M. Zalca, D.G Lofflerb, Fuel processing for PEM fuel cells: transport and kinetic issues of system design, *J of Power Sources*, 111 (2002) 58-64
- J.R. Lattner, M.P. Harold Comparison of conventional and membrane reactor fuel processors for hydrocarbon-based PEM fuel cell systems *Int J. of Hydrogen Energy* 29 (2004) 393-417
- J.R.Rostrop-Nielson, Conversion of hydrocarbons and alcohols for fuel cells, Invited Lecture, *Phys. Chem. Chem. Phys* , Oct 2000
- J.W. Raadschelders, T. Jansen, Energy sources for the future dismounted soldier, the total integration of the energy consumption within the soldier system, *J. of Power Sources*, 96 (2001) 160-166
- K. Agbossou, R. Chahine, J. Hamelin, F. Laurencelle, A. Anouar, J.-M. St-Arnaud, T.K. Bose, Renewable energy systems based on hydrogen for remote applications, *J of Power Sources*, 96 (2001) 168-172
- K. Ledjeff-Hey, J. Roes, R. Wolters, CO₂-scrubbing and methanation as purification system for PEFC, *J. of Power Sources*, 86 (2000) 556-561
- K Otsuka, C. Yamada, T. Kaburagi, S Takenaka, Hydrogen storage and production by redox of iron oxide for polymer electrolyte fuel cell vehicles, *Int. J. of Hydrogen Energy*, 28 (2003) 335-342
- K. Pehr, P. Sauermann, O. Traeger, M Bracha, Liquid hydrogen for motor vehicles - the worlds first LH₂ filling station, *Int J. of Hydrogen Energy*, 26 (2001) 777-782
- K. Tuber, M. Zobel, H. Schmidt, C. Hebling, A polymer slectrolytic membrane fuel cell system for powering portable computers, *J. of Power Sources*, 118 (2003) 1-8
- L. Cardinali, S. Santomassio, M. Stefanoni, Design and Realisation of a 300W fuel cell generator on an electric bicycle, *J. of power Sources*, 106 (2002) 384-387
- L Wang, A Husar, T. Zhou, H. Liu, A paremetric study of PEM fuel cell performances, *Int. J. of Hydrogen Energy*, 28 (2003) 1263-1272
- L. Zhou, Y. Zhou, Y. Sun, A comparative study of hydrogen adsorption on super scvivated carbon versus carbon nanotubes, *Int J of Hydrogen Energy*, 29 (2004) 475-479

- L.F. Brown, A comparative study of fuels for on-board hydrogen production for fuel-cell-powered vehicles, *Int. J. of Hydrogen Energy*, 26 (2001) 381-397
- M Conte, A. Iacobazzi, M. Ronchetti, R. Vellone, Hydrogen economy for a sustainable development state of the art and technological perspectives, *J. of Power Sources*, 100 (2001) 171-187
- M Morimoto, M. Atsuko, A.A.Y. Atif, M.N Ngan, A. Fakhru'l-Razi, S.E Iyuke, A.M. Bakir, Biological production of hydrogen from glucose by natural anaerobic microflora, *Int. J. of Hydrogen energy*, 29 (2004) 709-713
- M. Sundaresan, S. Ramaswamy, R M. Moore, M.A. Hoffman, Catalytic burner for an indirect methanol fuel cell vehicle fuel processor, *J of Power Sources*, 113 (2003) 19-36
- M. Virgi, Private Communication, 2000
- M. Wang, Fuel cell choices for fuel cell vehicles: well-to-wheels energy and emission impacts, *J. of Power Sources*, 112 (2002) 307-321
- M.E E. Abashar, Coupling of steam and dry reforming of methane in catalytic fluidized bed membrane reactors., *Int J. of Hydrogen Energy*, 29 (2004) 799-808
- M G. Sobacchi, A.V. Saveliev, A.A. Fridman, L.A. Kennedy, S. Ahmed, T Krause, Experimental assessment of a combined plasma/catalytic system for hydrogen production via partial oxidation of hydrocarbon fuels, *Int J. of Hydrogen Energy*, 27 (2002) 635-642
- N Edwards, S.R. Ellis, J.C. Frost, S.E. Golunski, A.N.J van Keulen, N.G. Lindewald, J.G. Reinkingh, On-board hydrogen generation for transport applications: the HotSpot(TM) methanol processor, *J. of Power Sources*, 71(1998)123-128
- P. Dondi, D Bayoumi, C Haederli, D. Julian, M. Suter, Network integration of distributed power generation, *J. of Power Sources*, 106 (2002) 1-9
- P. Marty, D Grouset, High temperature hybrid steam reforming for hydrogen generation without catalyst, *J. of Power Sources*, 118 (2003) 66-70
- P.Hollmuller, J.-M. Joubert, B. Lachal, K. Yvon, Evaluation of a 5kW photovoltaic hydrogen production and storage installation for a residential home in Switzerland, *Int. J. of Hydrogen Energy*, 25 (2000) 97-109
- Q. Zheng, A. Gu, X. Lu, W. Lin, Temperature-dependent state of hydrogen molecules within the nanopore of multi-walled carbon nanotubes, *Int J. of Hydrogen Energy*, 29 (2004) 481-489

- R. Buxbaum, H. Lei, Power output and load following in a fuel cell fuelled by membrane reactor hydrogen, *J. of Power Sources*, 123 (2003) 43-47
- R. Sime, J. Kuehni, L. D'Souza, E. Elizondo, S. Biollaz, The redox process for producing hydrogen from woody biomass, *Int J. of Hydrogen Energy*, 28 (2003) 491-498
- R.A.J. Dams, P.R. Hayter, S.C. Moore, The processing of alcohols, hydrocarbons and ethers to produce hydrogen for a PEMFC for transport applications, *IEEE Electrochemical and Solid-State Letters*, 97109
- S. Levesque, M. Ciureanu, R. Roberge, T. Motyka, Hydrogen storage for fuel cell systems with stationary applications-I. transient measurement technique for packed bed evaluation, *Int J. of Hydrogen Energy*, 25 (2000) 1095-1105
- S. Springmann, M. Bohnet, A. Docter, A. Lamm, G. Eigenberger, Cold start simulations of a gasoline based fuel processor for mobile fuel cell applications, *J. of Power Sources*, 128 (2004) 13-24
- S. Tosti, Supported and laminated Pd-based metallic membranes, *Int J of Hydrogen Energy*, 28 (2003) 1445-1454
- S.G. Chalk, J.F. Miller, F.W. Wagner, Challenges for fuel cells in transport applications, *J. of Power Sources*, 86 (2000) 40-51
- S.H. Chan, H.M. Wang, Carbon monoxide yield in natural gas autothermal reforming process, *J of Power Sources*, 101 (2001) 188-195
- T. Kosugi, A. Hayashi, K. Tokimatsu, Forecasting development of elemental technologies and effect of R&D investments for polymer electrolyte fuel cells in Japan, *Int. J. of Hydrogen Energy*, 29 (2004) 337-346
- T. Rampe, A. Heinzl, B. Vogel, Hydrogen generation from biogenic and fossil fuels by autothermal reforming, *J. of Power Sources*, 86 (2000) 536-541
- T. Suzuki, H. Iwanami, T. Yoshinari, Steam reforming of kerosene on Ru/Al₂O₃ catalyst to yield hydrogen, *Int J of Hydrogen Energy*, 25 (2000) 119-126
- T. van der Does, Fuel cell co-generation: the future of co-generation, *J. of Power Sources*, 61 (1996) 49-51
- T.N. Veziroglu, Quarter century of hydrogen movement 1974-2000, *Int J. of Hydrogen Energy*, 25 (2000) 1143-1150
- The Lee Company Electro Fluidic Systems, Component Catalogue with Engineering Reference Material, 6th Edition (1994)

- V. Hacker, A novel process for stationary hydrogen production: the reformer sponge iron cycle (RESC), *J. of Power Sources*, 118 (2003) 311-314
- V Klouz, V. Fierro, P. Denton, H Katz, J.P. Lisse, S. Bouvot-Mauduit, C. Mirodatos, Ethanol reforming for hydrogen production in a hybrid electric vehicle: process optimisation, *J. of Power Sources*, 105 (2002) 26-34
- V.I. Shvachko, Cold cracking of structural steel weldments as reversible hydrogen embrittlement effect, *Int J of Hydrogen Energy*, 25 (2000) 473-480
- V.V. Panasyuk, O.Y. Andreykiv, O.V. Gembara, Hydrogen degradation of materials under long-term operation of technical equipment, *Int. J. of Hydrogen Energy*, 25 (2000) 67-74
- W. Colella, Design options for achieving a rapidly variable heat-to-power ratio in a combined heat and power (CHP) fuel cell system (FCS), *J. of Power Sources*, 106 (2002) 388-396
- W. Merida, P.-C. Maness, R.C. Brown, D.B. Levin, Enhanced hydrogen production from indirectly heated, gasified biomass, and removal of carbon emissions using a novel biological gas reformer, *Int. J. of Hydrogen Energy*, 29 (2004) 283-290
- W. Ruettinger, O. Ilinich, R.J. Farrauto, A new generation of water gas shift catalysts for fuel cell applications, *J. of Power Sources*, 118 (2003) 61-65
- W.G. Colella, Design considerations for effective control of an afterburner subsystem in a combined heat and power (CHP) fuel cell system (FCS), *J. of Power Sources*, 118 (2003) 118-128
- X. Chen, Y. Zhang, X.P. Gao, G.L. Pan, X.Y. Jiang, J.Q. Qu, F. Wu, J. Yan, D Y. Song, Electrochemical hydrogen storage of carbon nanotubes and carbon nanofibres, *Int J. of Hydrogen Energy*, 29 (2004) 743-748
- Y. Choi, H.G Stenger, Water gas shift reaction kinetics and reactor modelling for fuel cell grade hydrogen, *J. of Power Sources*, 124 (2003) 432-439
- Y. Lwin, W.R W Daud, A. B. Mohamad, Z. Yaakob, Hydrogen production from steam-methanol reforming. thermodynamic analysis, *Int. J. of Hydrogen Energy*, 25 (2000) 47-53
- Y. Matsumura, T. Minowa, Fundamental design of a continuous biomass gasification process using a super critical water fluidized bed, *Int. J of Hydrogen Energy*, 29 (2004) 701-707

- Y.M. Ferng, Y C Tzang, B.S. Pei, C C. Sun, A. Su, Analytical and experimental investigations of a proton exchange fuel cell, *Int. J. of Hydrogen Energy*, 29 (2004) 381-391
- Yu S. Nechaev, O.K. Alexeeva, On the nature, capability and reverseability of hydrogen storage in novel carbon nanomaterials for mobile power units, *Int J. of Hydrogen Energy*, 28 (2003) 1433-1443
- Z.Yumurtacı, E. Bilgen, Hydrogen production from excess power in small hydroelectric installations, *Int. J of Hydrogen Energy*, 29 (2004) 687-693
- J.L. Zilka-Marco, A.L.Y. Tonkovich, M.J. LaMont, S.P Fitzgerald, D.P. VanderWiel, Y.Wang, R.S. Wegang, Compact Microchannel Fuel Vaporizer for Automotive Applications, IMRET 4 4th International Conference on Microreaction Technology, Topical Conference Proceedings. AIChE Spring National Meeting March 5-9, 2000 Atlanta, GA, pp. 301-307.

Appendix 1: Results Tables for the Microchannel Steam Reformer

Temperatures						Fuel Feed Rates				Reformer Products Dry Composition				
Temp Setpoint °C	Inlet Temp °C	Zone 1 Temp °C	Zone 2/3 Temp °C	Zone 3 Temp °C	Outlet Temp °C	S/C ratio	kWe	LPG /SLPM	H ₂ O /mil/min	H ₂ %	CH ₄ %	CO %	CO ₂ %	LPG % Conversion
450.00	237.43	449.71	449.86	450.86	223.14	2.50	0.05	0.70	4.00	7.79	0.41	0.89	1.36	10.45
500.00	235.29	501.00	499.57	503.00	253.43	2.50	0.09	0.70	4.00	16.28	0.10	1.52	2.48	20.38
550.00	262.00	549.57	549.86	551.14	285.14	2.50	0.22	0.70	4.00	37.43	0.43	4.54	7.22	49.62
600.00	256.00	600.63	600.25	601.00	317.00	2.50	0.23	0.70	4.00	40.89	0.53	5.14	7.06	53.62
450.00	262.29	449.29	449.86	450.57	215.29	3.00	0.09	0.70	5.00	14.09	0.13	1.39	3.05	18.67
500.00	281.71	500.43	499.86	499.29	236.00	3.00	0.13	0.70	5.00	20.93	0.00	2.19	4.64	27.77
600.00	277.57	600.71	600.14	601.43	310.57	3.00	0.34	0.70	5.00	53.16	0.93	7.50	9.42	71.01
550.00	273.43	550.00	550.00	551.29	280.57	3.00	0.21	0.70	5.00	34.05	0.33	3.86	6.14	44.38
450.00	289.14	448.29	449.86	450.43	223.00	3.50	0.10	0.70	6.00	14.14	0.15	1.49	2.71	18.49
500.00	289.43	500.00	500.00	500.71	240.71	3.50	0.18	0.70	6.00	27.83	0.03	2.47	4.94	35.26
550.00	280.14	549.14	549.71	551.71	293.00	3.50	0.29	0.70	6.00	42.38	0.45	4.82	8.32	55.97
600.00	281.63	599.25	600.13	600.13	317.63	3.50	0.40	0.70	6.00	57.86	0.74	6.77	11.87	77.24
450.00	224.14	448.29	450.00	450.43	212.14	4.00	0.11	0.70	7.00	13.41	2.08	1.82	2.40	19.71
500.00	223.43	499.00	504.43	499.57	240.71	4.00	0.21	0.70	7.00	26.17	4.02	3.47	5.19	38.85
550.00	186.14	546.86	549.71	552.14	272.29	4.00	0.38	0.70	7.00	49.36	2.10	4.80	11.89	68.16
600.00	196.00	598.44	600.00	600.44	294.67	4.00	0.42	0.70	7.00	56.42	1.43	5.04	13.20	76.09
600.00	240.00	600.50	616.00	594.50	263.50	4.00	0.17	0.25	2.40	63.46	1.83	5.20	17.13	87.63
600.00	265.00	601.00	621.00	597.00	277.00	4.00	0.33	0.50	4.80	61.28	1.32	5.76	14.51	82.88
600.00	148.95	599.71	600.00	596.57	279.29	4.00	0.45	0.70	7.00	60.42	1.00	5.87	13.90	81.18
600.00	170.50	601.00	633.00	598.00	292.00	4.00	0.58	1.00	9.60	53.63	0.92	6.62	11.65	72.81
600.00	247.00	603.00	634.50	601.00	295.50	4.00	0.67	1.25	12.10	49.43	0.82	6.89	10.72	67.86
600.00	209.00	603.00	645.50	601.00	294.50	4.00	0.78	1.50	14.50	48.20	0.47	7.15	10.05	65.86
600.00	117.50	596.50	649.50	601.00	298.50	4.00	0.86	1.75	16.90	45.18	0.48	7.37	9.48	62.51

Table A.1: Summary of Results for the Single-Stage Steam Reformer using LPG as a Feedstock

Temperatures						Fuel Feed Rates				Reformer Products Dry Composition				
Temp Setpoint Front °C	Temp Setpoint Back °C	Inlet Temp °C	Zone 1 Temp °C	Zone 2/3 Temp °C	Zone 4 Temp °C	S/C ratio	kWe	C ₃ H ₈ /SLPM	H ₂ O /ml/min	H ₂ %	CH ₄ %	CO %	CO ₂ %	C ₃ H ₈ % Conversion
600 00	600 00	225 00	600 00	599 50	598 00	2 50		0 75	4 51	70 00	7 07	8 66	16 50	102 23
600 00	750 00	97.50	685 25	769 25	746 00	2 50		0 75	4 51	69 00	0 76	16 56	10 59	96 91
600 00	600 00	243 50	600 50	599 50	598 00	3 00		0 75	5 42	70 00	4 21	7.15	18 37	99 73
600 00	750 00	102 00	674 75	765 50	746 25	3 00		0 75	5 42	72 00	0 53	13 65	13 20	99 38
600 00	600 00	264.50	599 50	599 00	599 00	3 50		0 75	6 33	70 00	3 61	7 59	18 14	99 33
600.00	750 00	274 80	655 80	742.60	745 60	3 50		0 75	6 33	73 50	0 40	10 00	14 47	98 37
600 00	600 00	98 80	602 00	593 00	593 00	4 00	0.59	0 75	7 23	72 00	1 97	6 4	17 78	98.15
600 00	650 00	233.75	603 50	654.00	646 00	4 00	0 59	0 75	7 23	72 67	2 09	8.13	16 80	99 68
600 00	700 00	255 25	604 75	680 50	696 25	4 00	0 58	0 75	7 23	72 67	0 91	9 11	15 81	98 49
600 00	750 00	243 83	643 17	733 67	744 83	4 00	0 59	0 75	7 23	76 16	0 32	9 93	15 12	101 53
600 00	600 00	230 50	602 00	605 00	597 00	4 00	0 20	0.25	2 40	69 02	0 54	6 03	18 07	93 65
600 00	600 00	238 00	603 00	612 00	599 00	4 00	0 40	0 50	4 80	70 85	0 90	8 98	16 67	97 40
600 00	600 00	108 00	602 50	616 00	599 00	4 00	0 59	0 75	7 23	74 00	0 30	6 60	15 80	96 70
600 00	600 00	137.50	603 00	614 00	601 50	4 00	0 79	1 00	9 68	65 54	0 30	7 00	14 88	87 73
600 00	600 00	158 50	602 00	606 00	599 50	4 00	0 59	0.75	7 23	72 08	1.53	7 12	16 84	97.57
600 00	600 00	101 00	597 00	620 50	600 00	4 00	0 99	1 25	12 01	72.08	1 08	6 39	16 03	95.59
600 00	600 00	101 50	591 50	632 00	605 00	4 00	1.19	1 50	14 45	72 80	1 38	6 44	15 59	96 20
600 00	600 00	100 00	554 50	620 00	610 00	4 00	1 38	1.75	16 87	70 00	2 16	7 05	18 85	98 05
600 00	600 00	100 00	504 50	606 50	608 00	4 00	1 58	2 00	19 28	70 00	2 18	7 08	18 61	97 86
600.00	600.00	99 00	429 50	600 00	609 00	4 00	1.78	2 25	21 69	70 00	2 08	7 42	18 17	97 67
600 00	600 00	99 00	408 00	599 00	606 00	4 00	1 98	2 50	24 10	70 00	2.62	7 68	17 86	98 16

Table A.2: Summary of Results for the Dual-Stage Steam Reformer using Propane as a Feedstock

Temperatures						Fuel Feed Rates			Reformer Products Dry Composition			
Temp Setpoint Front °C	Temp Setpoint Back °C	Inlet Temp °C	Zone 1 Temp °C	Zone 2/3 Temp °C	Zone 4 Temp °C	S/C ratio	CH ₄ /SLPM	H ₂ O /ml/min	H ₂ %	CH ₄ %	CO %	CO ₂ %
600 00	700 00	248 50	651 75	718 25	709 75	2.50	1 88	3.77	65 46	11 64	9 50	9 49
600 00	700 00	242 50	645 00	713 50	711 75	3 00	1 88	4 52	64 47	14 54	8 14	10 34
600 00	700 00	231 75	635.50	708 25	711 00	3 50	1 88	5 27	57 49	14 81	7 41	10 95
600 00	700 00	206 00	628 00	705 00	711 00	4 00	1 88	6 02	57 22	18 44	4 17	11 09
600 00	600 00	253 25	607 50	620 25	610 25	4 00	1 88	6 02	33 67	67.26	1.35	6 34
600 00	650 00	250 25	609 50	653 00	659 50	4 00	1.88	6 02	51 78	45 13	1.67	8 93
600 00	700 00	251 75	638 50	707 50	708 50	4 00	1.88	6 02	70 05	23 50	5 40	11.17
600 00	700 00	202.67	647.67	701 67	704 67	4 00	0 63	2 01	69 50	9 38	5 73	10 58
600 00	700 00	153 00	641 67	709 00	710 00	4 00	1 25	4 02	63 78	20 23	4 41	11.10
600 00	700 00	100 50	629 00	711.50	713 50	4 00	1 88	6 02	57 96	29 33	5 27	10 32
600 00	700 00	192 00	618 00	707 00	716 33	4 00	2 50	8 03	53 69	37.17	3 46	9 53
600 00	700 00	174 67	648 67	701.33	704 33	2 50	0 63	1.26	76 06	5 90	11 49	8 85
600 00	700 00	192 67	652 67	713 00	711 67	2 50	1 25	2 51	74 13	11 42	15 61	9 24
600 00	700.00	166.33	649 67	719 33	714 33	2 50	1 88	3 77	68 44	17 54	10 84	9 72
600 00	700 00	179 33	647 00	715 67	716 33	2 50	2 50	5 02	59 38	28 65	9 44	9 52

Table A.3: Summary of Results for the Dual-Stage Steam Reformer using Methane as a Feedstock

Temperatures						Fuel Feed Rates				Reformer Products Dry Composition				
Temp Setpoint Front °C	Temp Setpoint Back °C	Inlet Temp °C	Zone 1 Temp °C	Zone 2/3 Temp °C	Zone 4 Temp °C	S/C ratio	kWe	C ₃ H ₈ /SLPM	H ₂ O /ml/min	H ₂ %	CH ₄ %	CO %	CO ₂ %	C ₃ H ₈ % Conversion
600 00	700 00	118 00	652 00	720 00	699 00	2 50		0 75	4 52	70 31	0 79	13 16	11 56	95 82
600 00	700 00	166 80	647 00	717 20	699 20	3 00		0.75	5 42	70 79	0.55	11 80	13 24	96.38
600 00	700 00	120 00	633 00	710.75	699 00	3 50		0 75	6 33	72 48	0 65	10 00	14 37	97 49
600 00	700 00	98 80	613 20	704.20	699 00	4 00		0 75	7 23	74 01	0 55	9 49	15 24	99 29
600 00	600 00	100 40	603 00	623 40	594 20	4 00		0 75	7 23	71 56	0 57	10 51	14 35	96 98
600 00	650 00	98 40	605 00	659 20	647 00	4 00		0.75	7 23	72 00	0 57	9 40	14 00	95 97
600 00	700.00	206 00	663 67	718 67	704 33	4 00	0 21	0 25	2 41	82 32	0 72	11.46	13 16	107 67
600 00	700 00	101.00	648 33	717 33	702 00	4 00	0.40	0 50	4 82	77 26	0 60	9 68	14 23	101 77
600 00	700.00	99 00	623 87	710 47	700 40	4 00	0 59	0 75	7 23	72.78	0 84	8 71	13 82	96 15
600 00	700 00	98 80	605 80	705 20	695 60	4 00	0 75	1 00	9 64	72 00	0 95	7.71	14 61	95 28
600 00	700 00	97.75	604 75	716 00	691 00	4.00	0 92	1 25	12 05	69 48	1 16	8.16	14 63	93 43
600 00	600 00	100 75	584 00	622 00	606 00	4 00		1 50	14 46	65 72	0 39	11.71	14 27	92 08

Table A.4: Summary of Results for the Dual-Stage Steam Reformer using LPG as a Feedstock

Appendix 2.1 A Multi-function Compact Fuel Reforming Reactor for Fuel Cell Applications

Submitted to the International Journal of Hydrogen Energy and Accepted November 2003.

Withdrawn from publication by the author due to the intellectual property concerns of Intelligent Energy Ltd.

A Multi-function Compact Fuel Reforming Reactor for Fuel Cell Applications

James Reed^{a,*}, Rui Chen^a, Christopher Dudfield^b, Paul Adcock^b

^a*Department of Aeronautical and Automotive Engineering, Loughborough University,
UK*

^b*Intelligent Energy Ltd, The Innovation Centre, Loughborough, UK*

Corresponding author TEL (+44) 1509 225860, FAX (+44) 1509 223911, E-mail address: J P Reed@Lboro.ac.uk

Abstract

A multi-function compact chemical reactor designed for hydrocarbon steam reforming was evaluated. The reactor design is based on diffusion bonded laminate micro-channel heat exchanger technology. The reactor consists of a combustor layer, which is sandwiched between two steam reforming layers. Between the two function layers, a temperature monitor and control layer is placed, which is designed to locate the temperature sensors. The combustor layer has four individually controlled combustion zones each connected to a separate fuel supply. The reactor design offers the potential to accurately control the temperature distribution along the length of the reactor using closed loop temperature control. The experimental results show that the variance of temperature along the reactor is negligible. The conversion efficiency of the combustor layer is approximately 90%. The heat transfer efficiency from combustion layer to reforming layers is 65% to 85% at 873 K and 673 K, respectively. The heat transfer rate to the reforming layers is sufficient to support a steam reformation of propane at a rate of 0.7 dm³/min (STP) with a steam to carbon ratio of 2 at 873 K.

Keywords: Steam Reforming; LPG; Propane; Multi-Zone Combustor; Microchannel Heat Exchanger

1. Introduction

The Solid Polymer Fuel Cell (SPFC) is seen as a potential clean power plant for a number of applications. The application that the fuel cell is used for is an example aside from the initial obvious cost issues. Although the automotive sector has invested significantly in the development of SPFC systems over the past decade, technology costs are still at present uncompetitive compared to that for the Internal Combustion Engine (ICE). Near term costs for SPFC systems have been reported to be approximately two orders of magnitude greater than the ICE on a \$/kW basis.

Whilst a consideration of technology improvements and volume production will assist in reducing SPFC costs in the mid-long term, a more cost competitive market for SPFC technology is now seen as the stationary power market and distributed generation in particular. Stationary systems use the same SPFC stack technology that is used in automotive fuel cell systems. As such they need a hydrogen stream with a high level of purity (low sulphur and CO levels) to operate effectively. The source of the H₂ fuel is still an area open to debate for automotive applications with some parties preferring the direct storage of H₂ and others choosing the onboard fuel processor route.

However, for stationary power solutions the fuel processor is seen as the more obvious choice. The infrastructure to supply hydrocarbon fuels, be it natural gas or propane is already in place. The size and weight limitations placed on the fuel cell system are also less critical than if the system were to be used as an onboard H₂ generation system. Figure 1 shows a typical SPFC system in combination with a hydrocarbon/alcohol fuel processor, in which the H₂ fuel is liberated through chemical processing processes.

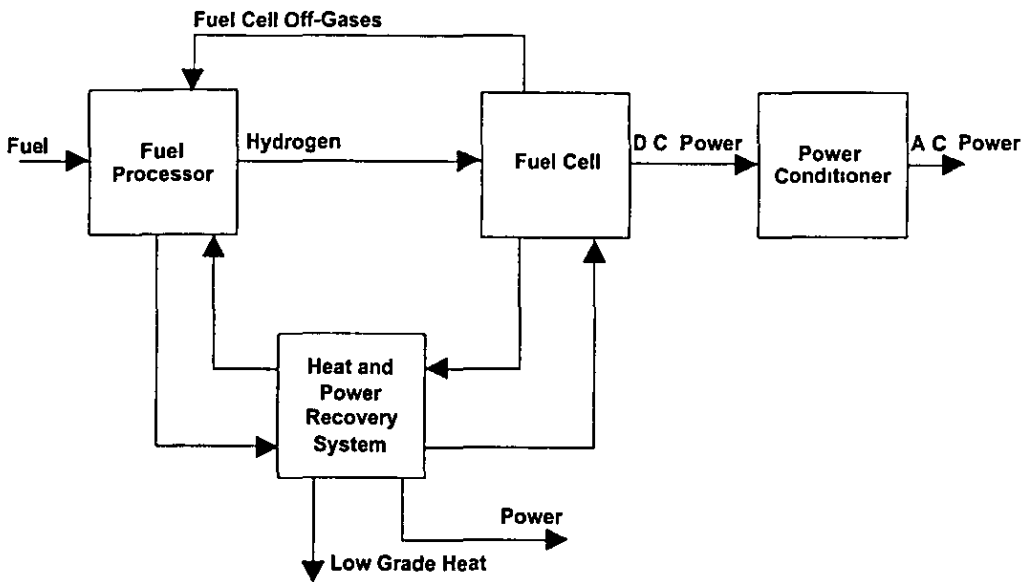


Figure 1: A typical SPFC system in combination with a hydrocarbon/alcohol fuel processor

A 5-stage fuel processor reactor arrangement is shown in Figure 2. These stages include, desulphurisation, fuel reformer, a high and low temperature water gas shift reactor and CO removal (Additional stages of heat transfer between the stages are not shown). During the research reported in this paper, a multi-function compact fuel reforming reactor designed for fuel cell applications has been investigated.

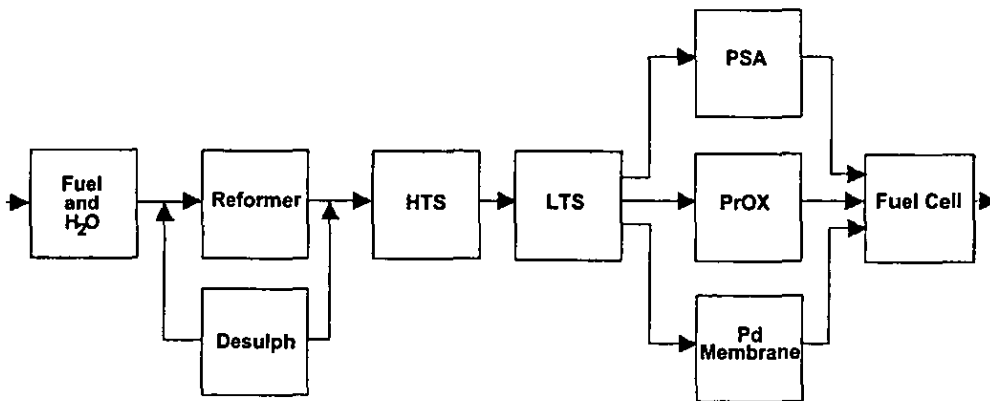


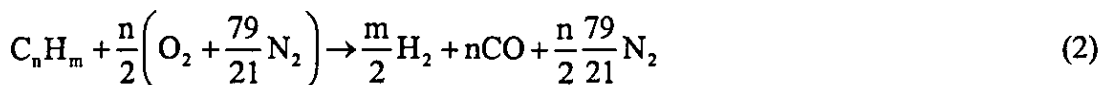
Figure 2: Overview for fuel processors

There are a number of potential chemical methods to reform the hydrocarbon fuels and alcohols into a hydrogen rich gaseous fuel. These are: steam reforming, partial oxidation reforming, auto-thermal reforming, and other novel methods.

Steam Reforming uses water to react with a hydrocarbon fuel to produce a hydrogen rich gaseous product. Carbon in the fuel is converted into CO by oxidation with the O₂ contained in the steam. Hydrogen from both fuel and steam is released as a gas [Equation 1]. A catalyst is used to improve the reaction kinetics, which in turn lowers the reforming temperature and reduces the reactor size. The reaction temperature is critical since it determines the composition of the product gas i.e. the reformat. The reaction is endothermic so a continuous supply of heat to the reformer is required. This is performed by the integration of a combustor with the catalytic reformer.



Partial Oxidation (POX) reforming systems rely on the reaction of the fuel with a limited amount of oxygen to prevent complete oxidation [Equation 2]. POX reforming allows for simpler design by removing the need for external heat and water supplies as required with steam reforming. Also since no additional heat is required, potentially better transient performance is achievable. A wide range of hydrocarbon fuels can be reformed. The drawback is a relatively low H₂ generation rate, since all the hydrogen gas has to be generated from the hydrocarbon fuel rather than partially from water steam. Additionally the H₂ is further diluted by the remaining air in the reformat stream, which lowers fuel cell efficiency [1].



Auto-thermal reforming (ATR) is fundamentally a combination of steam reforming and POX reforming. It utilises the heat generated from the POX reaction to keep the steam reforming reaction at the desired temperature. It is thermally neutral as a result. In practise a near auto-thermal operating point is reached [2]

In comparison, the steam reformer produces the highest volume of H₂ of the methods described above from a given amount of hydrocarbon fuel. In addition, it can use the unused H₂ from the fuel cell exhaust to partially fuel its combustor. This improves the overall system efficiency. Furthermore, since the reaction is endothermic, the reaction will not run away if any error with the control system occurs. Instead, it will naturally quench itself. This makes the steam reformer more efficient and safer than other methods.

2. Reactor Design

2.1 Potential Technologies

The reactor design used for fuel reforming has a significant effect on reforming efficiency, system start-up time and transient response. This is particularly important in steam reforming since the rate of reformation is limited by the rate of heat transfer to the reactants [3]. There are a number of potential technologies that can be used for the reactor design.

Packed bed reactors typically contain a series of tubes filled with a catalyst in the form of pellets or granules. The design is relatively simple and easy to maintain. They have been widely used in the industrial-scale steam or partial oxidation methods of reforming [4]. At portable-scale, the residence time of the reactant is limited and the performance of the reactor suffers as a result. The catalyst needs to be used much more effectively than at industrial-scale to maintain good reaction efficiency. A much more compact and efficient reactor design is needed [5].

Monolith reactors coated with catalyst offer several advantages over packed bed reformers. They have a higher surface area to volume, large frontal open area, low thermal mass, low heat capacity, low thermal expansion, high strength, and high temperature of operation. These advantages give the reactor quicker start-up, a higher conversion rate, reduced pressure drop along the reactor and improved thermal and mechanical shock resistance than the packed bed type of reactors. The drawbacks are lower content of active material per reactor volume and poor heat transfer performance due to the heat conductivity of ceramic material [1]. Monolith reactors have been favoured for ATR use (rather than steam reforming) where heat management is not as critical.

2.2 New Compact Reactor

Micro-channel heat exchangers are made of a diffusion bonded laminate. Inside the heat exchanger, the multi-layer shims create the alternating micro-channels and fins (Figure 3). The micro-channel widths are determined by the thickness of the shim material whilst the heights and lengths of the channels are determined by the machined surface. The machining can be either by photochemical or stamping processes. This allows for a low cost method of making the shims. The shims are

diffusion bonded together under high temperature and pressure (1173 K, 27 MPa for 4 h) to yield a monolithic metal block that removes the need for gaskets and or other seals. This kind of heat exchanger has significantly higher heat transfer rates than most conventional designs. As the basis of the reactor for the fuel steam reforming, the heat energy required for the support of the reforming reaction, supplied from a combustor, can be efficiently transferred to the reaction side. The overall reforming system efficiency can then be improved.

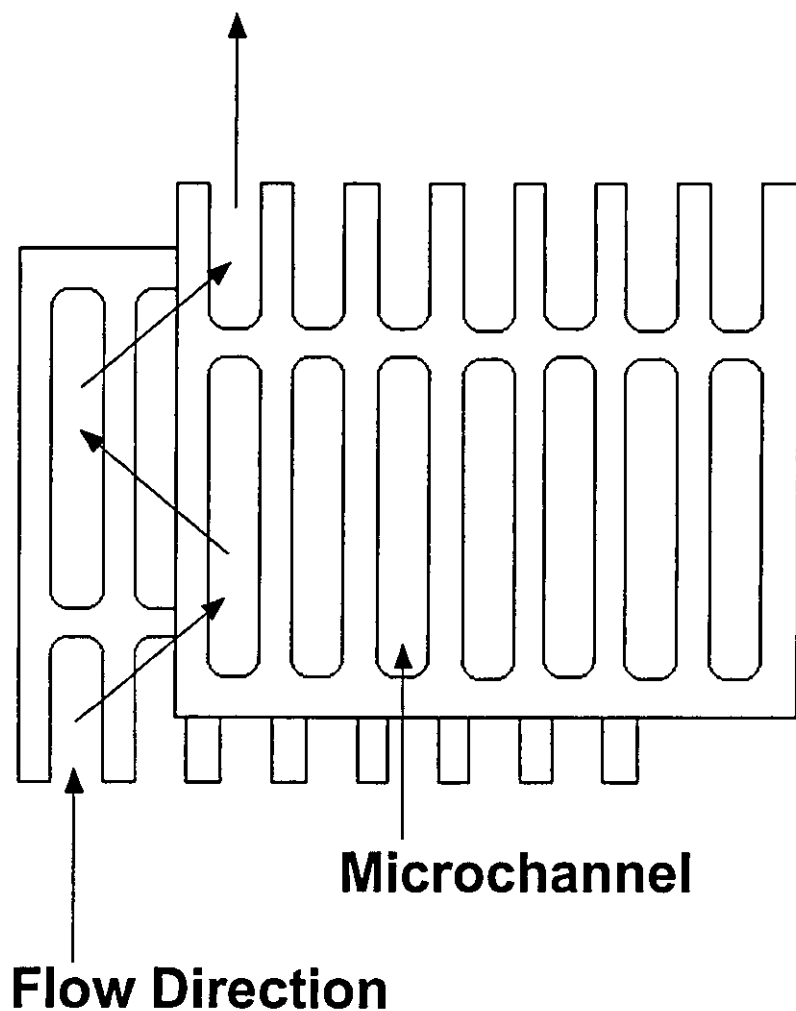


Figure 3: Micro-channel shims

Based on this micro-channel heat exchanger technology, we have developed a new type of catalytic chemical reactor as shown in Figure 4.

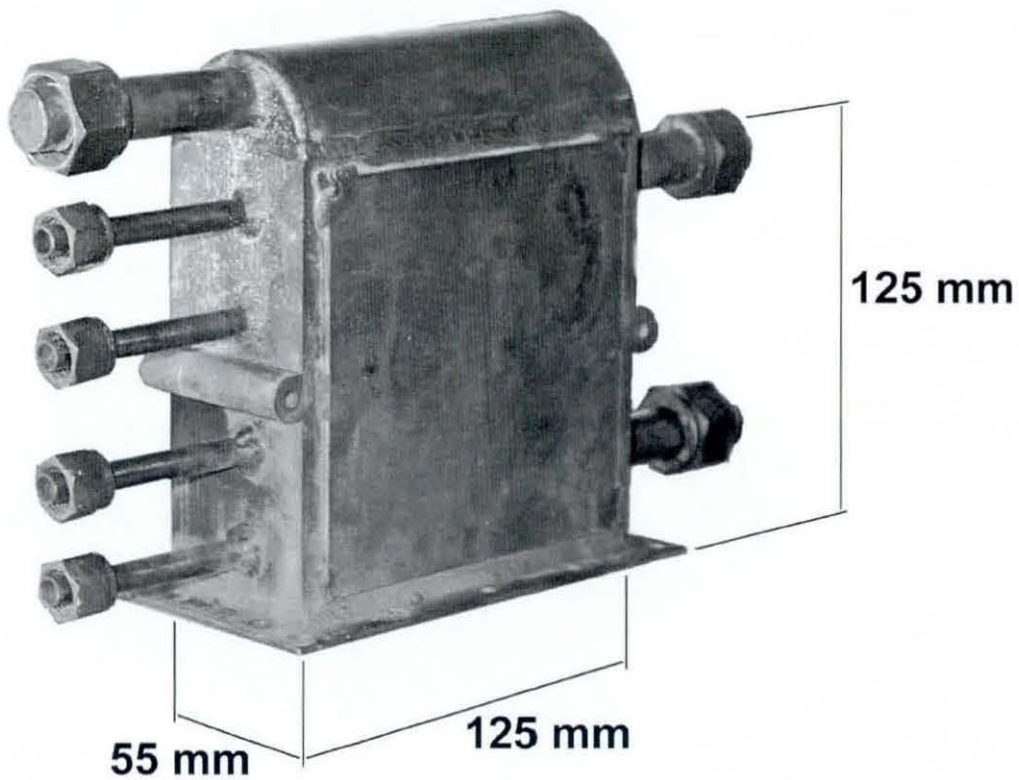


Figure 4: Micro-channel catalytic chemical reactor

Steam reforming is an endothermic reaction and as such needs to be supplied with thermal energy to maintain. Most commercial reformers control the temperature at the exit of the reformer by measuring the temperature of the exit gases. This is an inefficient method of temperature control, since the temperature away from the exit is likely to be different than that required. In the newly developed micro-channel catalytic chemical reactor, the entire heat exchanger is divided into three groups of layers, a combustion layer, a temperature sensing layer and a reforming layer as illustrated in Figure 5.

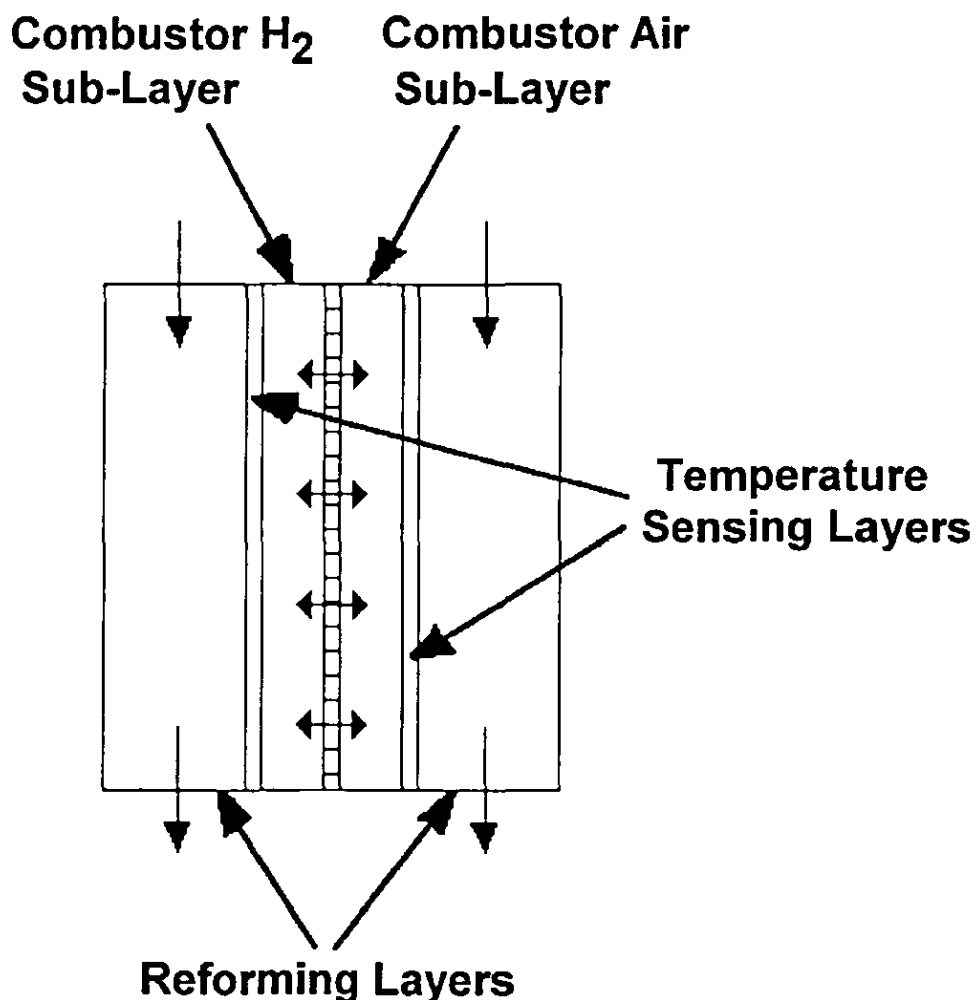


Figure 5: Internal structure of the micro-channel catalytic chemical reactor

The combustion layer, which is located in the centre, consists of fuel and air supply sub-layers in which the two sub-layers are inter-connected through a diffusion shim. The air is diffused into the fuel sub-layer and reacts with it to produce the heat required for the reforming reaction. The fuel sub-layer is split into four zones and wash-coated with a platinum-based catalyst. The four zones each have an individual fuel feed and a common air feed as shown in Figure 6. By controlling the quantity of the fuel supplied to each individual zone, the heat released from each can then be continuously monitored and dynamically controlled. It avoids the formation of hot or cold spots and improves the reformer performance.

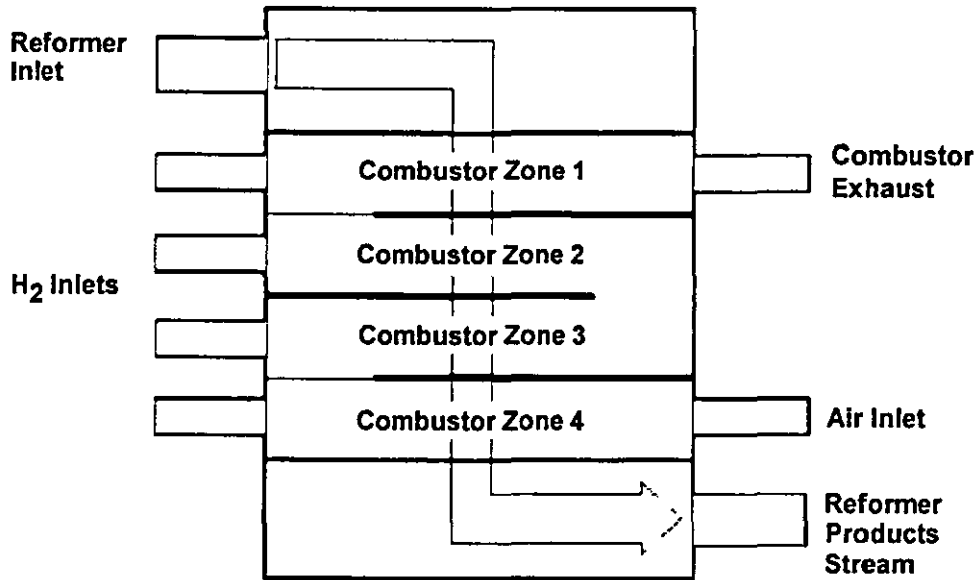


Figure 6: The combustion layer of the micro-channel catalytic chemical reactor

The temperature sensing layer is designed for the allocation of three groups of temperature sensors. These are located inside the reactor next to the combustion layer as shown in Figure 7.

In the combustion layer, zone 1 is directly connected to the inlet of the reforming reactants while zone 4 is directly open to the air supply to the combustion layer. In order to overcome the quenching effect of the inlet flows and maintain the desired reforming temperature in these zones, more fuel is needed here than for the middle zones and it was decided that the two middle zones would operate satisfactorily in unison.

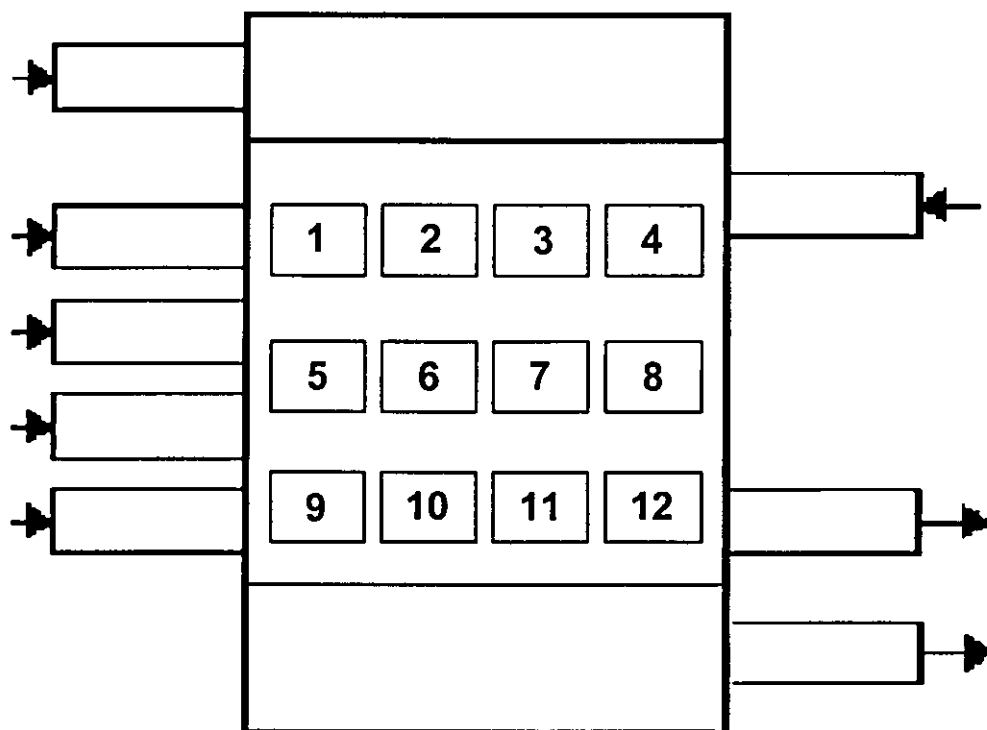


Figure 7: The temperature sensing layer of the micro-channel catalytic chemical reactor

In order to efficiently use the heat produced from the combustion layer, two reforming layers have been allocated, one on each side of the combustion layer. It allows direct control of the reforming temperature with minimum lag time whilst making use of the maximum amount of heat available from the combustor. This results in fast transient responses and start up times, which are essential if the reformer is to be integrated into a complete system. The catalytic combustor will light off at room temperature (293 K) using simulated fuel cell exhaust gases.

3. Experimental Study

3.1 Test Rig

The reactor is of a stainless steel diffusion bonded laminate construction, which is ideally suited to the high temperatures necessary for the steam reforming of fuels such as LPG. Figure 8 shows the gas feed layout for the test rig. The fuel flow to the combustor is controlled by four solenoid valves acting as injectors. These split a common feed into four controllable streams.

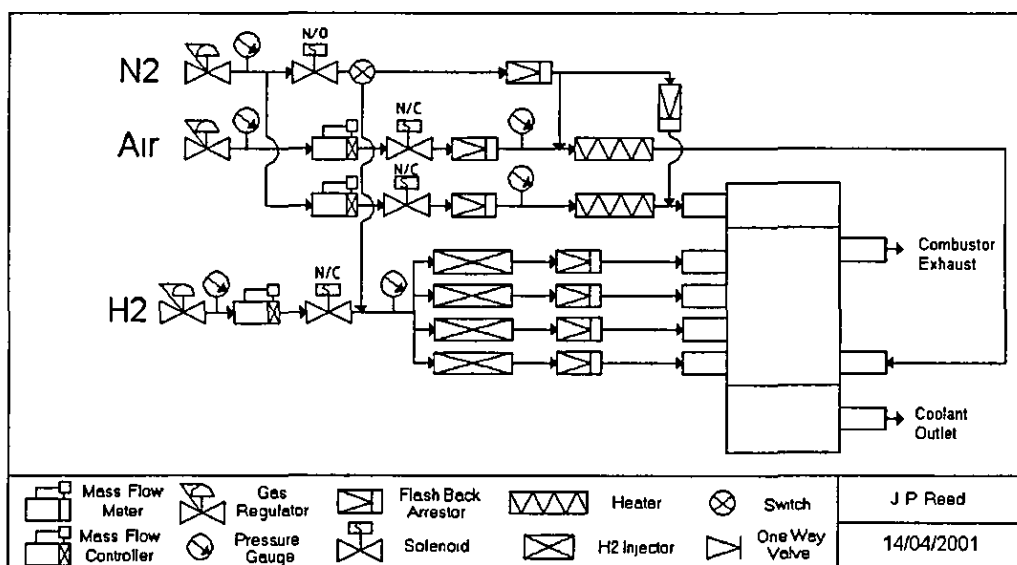


Figure 8: The gas feed layout for the test rig

LabVIEW™ [6] was used to develop data acquisition combined control software for the multi-zone combustor. The control system uses a combination of closed loop control and user defined look up tables to provide individual control of each fuel injector allowing the longitudinal temperature gradient of the reactor to be controlled

The overall fuel flow-rate is set using a mass flow controller and the injectors are used to assign the correct amount of fuel to each combustor zone. The combustor mixture was controlled so as to mimic the proportion of fuel and O₂ from typical fuel cell off gases. The H₂O produced by the combustor is condensed out by passing it through a heat exchanger and catch-pot. The combustor exhaust is then exhausted to atmosphere. The flow of N₂ (used as a coolant to represent the reforming stream) was manually controlled via a mass flow controller. The reforming stream is also passed through a heat exchanger before being exhausted to atmosphere. The system is purged using N₂ controlled by solenoids so that in the case of an emergency shut down, the entire system is purged.

3.2 Temperature Control

The micro-channel steam reforming reactor was first tested without temperature feedback control to ensure that light off could be achieved and the gas supply system was operational. During the test, equal amounts of H₂ were fed to each combustor

zone. On the reforming layer, nitrogen at a constant flow rate of $20 \text{ dm}^3/\text{min}$ (STP) was passed through the reactor in a direction opposite to the combustor air supply. Figure 9 shows the average temperature measured by the three groups of temperature sensors as shown in Figure 7.

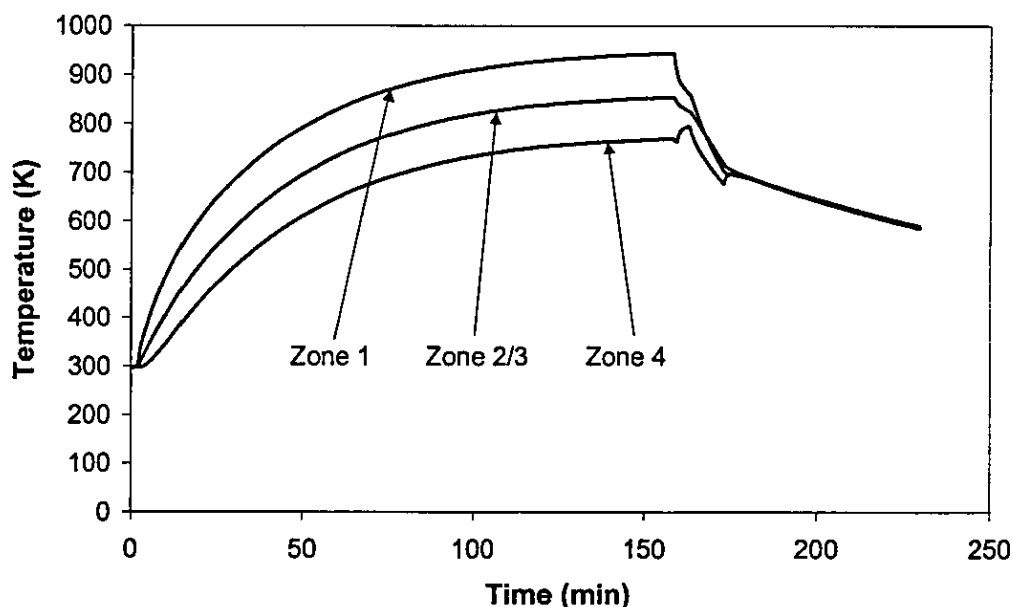
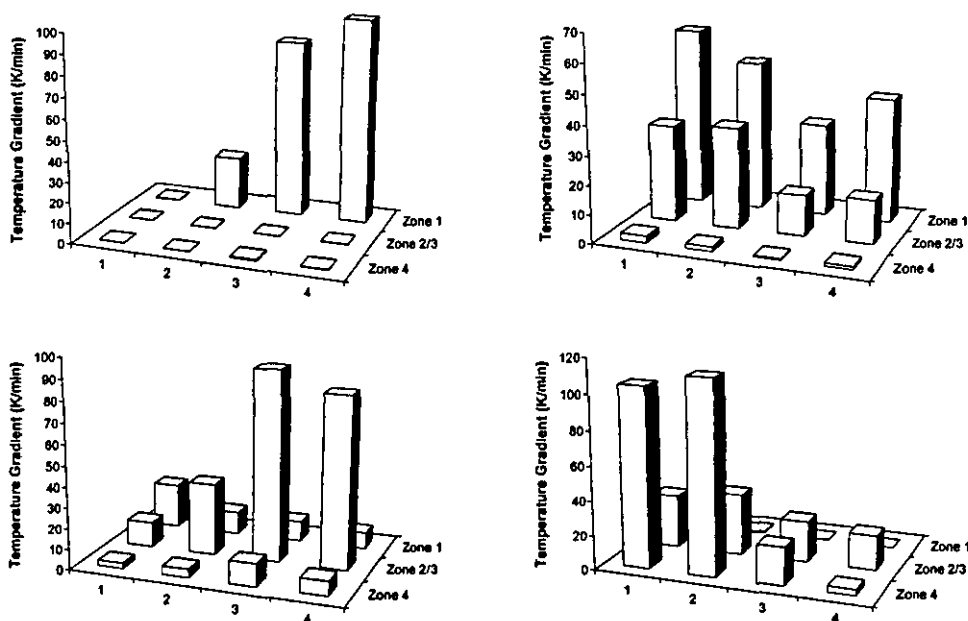


Figure 9: Average zone temperature measured by the three groups of temperature sensors

Zone 1 is directly connected to the nitrogen gas inlet but linked to the outlet of the combustion layer. From the test results, it can be seen that zone 1 has the highest temperature. Zone 4 is open to the air inlet. Although it is directly connected to the outlet of the reforming layer (where the nitrogen has been heated by the previous three zones), it has the lowest temperature. These test results showed that the gas movement and the heat release in the combustion layer have the dominant effect on the temperature distribution throughout the reactor.

Before the combustor was run under closed loop control, it was necessary to determine whether the zones could be controlled individually and if the thermocouples were located correctly in the reactor. Therefore, the reactor was further tested by giving a H_2 supply at a flow rate of $4 \text{ dm}^3/\text{min}$ (STP) to each of the four inlets sequentially, in a procedure of 5 minutes operation to zone 1, followed by 5 minutes stop, then shift to zone 2 and so on in turn. The air was supplied to the

reactor, synchronised to the H₂ supply, at a H₂ to air volume ratio of 1:5. Figures 10a-d show the measured rate of change of temperature as recorded by each individual thermocouple.



Figures 10a–d: The measured rate of change of temperature as recorded by each individual thermocouple

It can be seen in Figure 10a that when the H₂ supply is switched on to zone 1, the temperatures at the four positions inside zone 1 perform differently. Position 4 has the highest temperature gradient while the temperature at position 1 has hardly increased. From Figure 6, it can be seen that position 1 is geometrically next to the H₂ inlet. Incidentally, the air flows in the same direction after passing the rest of the zones. The coincident flows, therefore, move the heat from position 1 to the downstream positions, and reduce its temperature. Position 4 is situated just before the outlet. It therefore accumulates the heat delivered through the flows and the heat generated due to the combustion reaction at that position. As a result it ends up with the largest temperature gradient among the four positions inside zone 1.

When the H₂ is switched to zone 2 as shown in Figure 10b after the 5 minutes cooling period, the temperature gradient at positions 1 and 2 inside zone 1 are large and well above the gradients in zone 2. Again, this is because the airflow brings some of the heat generated in zone 2 and some of the unburnt H₂ downstream. However, inside

zone 2, where the H_2 is supplied, it appears that little combustion occurs at position 3. Clearly, this is due to the heading impact between the H_2 supply and the airflow. The H_2 is pushed away from the position by the airflow. The highest temperature gradient in zone 2 is at position 2, which potentially contains the highest H_2 concentration.

When the H_2 is further switched to zone 3, as seen in Figure 10c, the temperatures are monitored by the same group of temperature sensors as zone 2. Clearly, the temperature gradient at position 3 becomes the highest followed by position 4. Again, this is mainly due to coincident flows of H_2 and air.

Finally, when the H_2 is switched to zone 4 in Figure 10d, the gradients at positions 1 and 2 are the highest. Again, this is because of the heading impact between the H_2 and airflows.

It can be seen that each zone, can for the most part be controlled individually. However, due to the internal flow interaction between the H_2 and air, there is some spill over from each zone to the next downstream one. Figure 11 shows the test results obtained by dynamically adjusting the H_2 supply to each individual zone. The temperatures shown in the figure were the averaged zone temperatures. These averaged temperatures are also used as the feedback to the control system for adjusting the H_2 flows. The results showed that the zone average temperatures agree well at all three set points, 673 K, 823 K and 873 K.

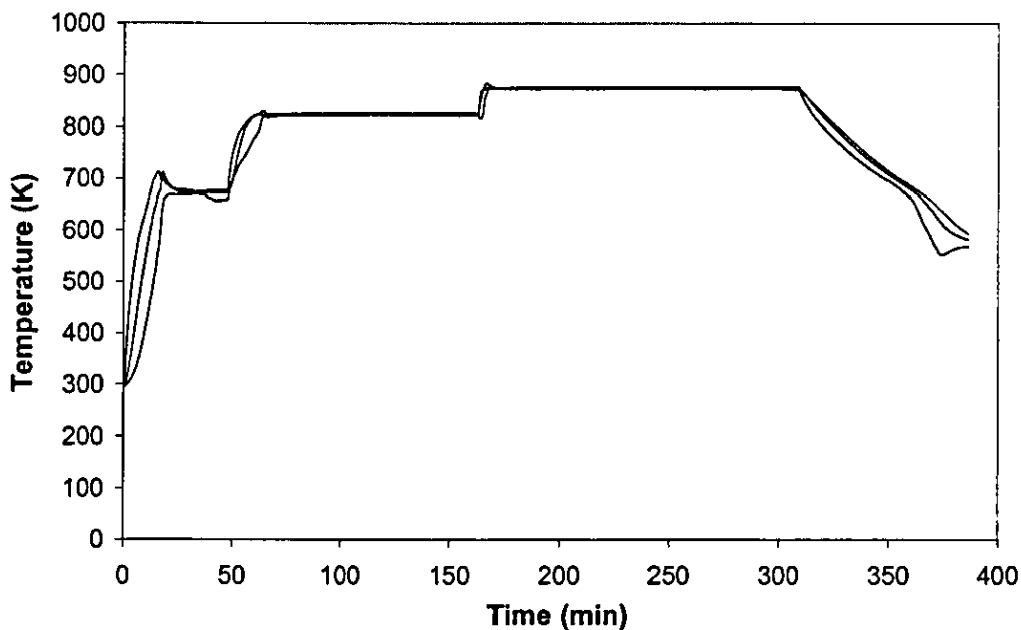


Figure 11: Averaged zone temperatures with dynamically H₂ control

It can be seen that the system provides sufficient controllability to set the reactor temperature longitudinally along the reforming stream.

Figure 12 compares the longitudinal temperature distribution of the multi-zone reformer with that of a more traditional packed bed reformer design [5]. The improvement in temperature control can clearly be seen. The multi-zone approach allows the temperature to be accurately controlled and so by extension the reformate composition.

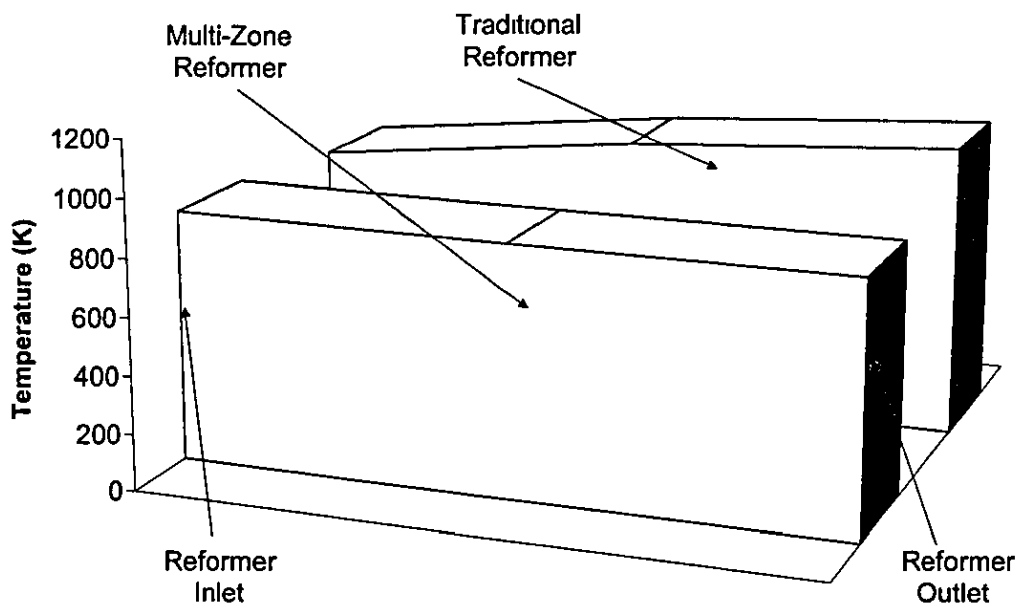


Figure 12: Comparison of longitudinal temperature distribution

3.3 Heat Transfer Performance

The motivation for the following tests was to determine the effectiveness of the micro-channel heat exchanger at distributing heat from the catalytic combustion of the H₂ air mixture, to the reforming reactors on either side of the combustor. During the test, H₂ and air in a ratio of 20% H₂:80% air, was fed to the combustor. The combustor temperature was controlled by varying the amount of H₂ fed to each zone, with the airflow being adjusted accordingly. N₂ was used as a coolant and was passed through the reforming reactors to take up the heat from the combustor. Measurements of the values required to perform a power balance on the reactor were taken once the temperatures of the various flows and the reactor had settled. The measured parameters were as follows.

- 1) Coolant inlet temperature (K)
- 2) Coolant exit temperature (K)
- 3) Air inlet temperature (K)
- 4) Combustor exhaust temperature (K)
- 5) Coolant flow rate (dm³/min (STP))
- 6) Air flow rate (dm³/min (STP))
- 7) H₂ flow rate (dm³/min (STP))
- 8) Combustor temperature (K)
- 9) Ambient temperature (K)
- 10) H₂O (liquid) produced from H₂ combustion (cm³)

With the exception of the H₂O produced from the combustion of the H₂ the above parameters were averaged over a time of 10 min. The amount of H₂O recorded was the total H₂O produced over the 10 min period. By comparing the amount of H₂O produced with that which, would have been produced by complete combustion of the H₂, the percentage of H₂ combusted was calculated and hence the H₂ conversion efficiency. The Figures 13 and 14 show the effects of combustor temperature and coolant flow rate on the H₂ conversion efficiency respectively.

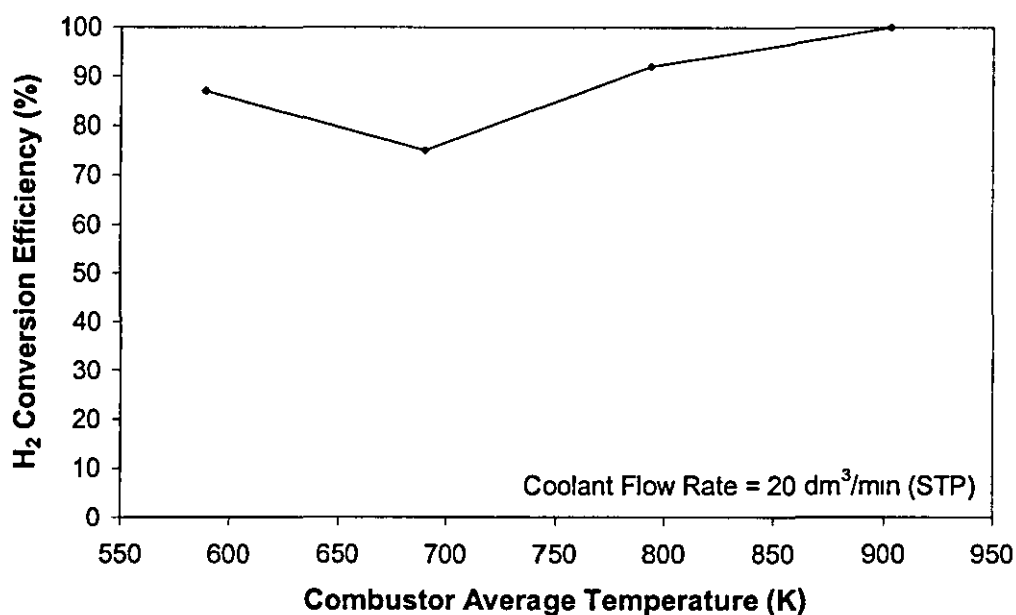


Figure 13: H₂ conversion efficiency at varying combustor temperature

It can be seen there is a trend, which suggests that the greater the combustor temperature the higher the H₂ conversion efficiency becomes. It can be seen that H₂ conversion at 573 K does not follow the observed trend. This is due to experimental error regarding the calculation of H₂ conversion based on the collected H₂O from the combustor exhaust, which can never be exact. On the other hand, the influence of the coolant flow rate on the H₂ conversion is relatively small. There does appear to be a trend of increasing H₂ conversion with N₂ flow rate but this is by no means clear and can be accounted for in the same way that as the anomaly in Figure 13. It can be seen that the averaged H₂ conversion efficiency is in the region of 90%.

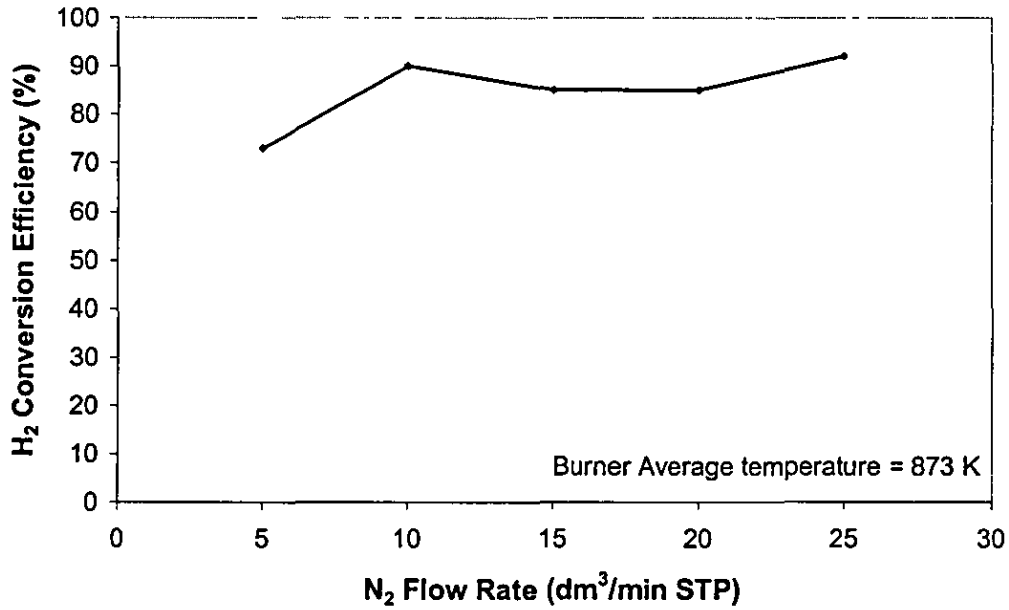


Figure 14 : H₂ conversion efficiency at varying coolant flow rate

To calculate the heat transfer efficiency a thermal power balance of the reactor was performed. The thermal power transferred to the reforming reactor, which is the thermal power obtained by the reforming streams was calculated by

$$P_{reactor} = \dot{m}_R \times \int_{T_1}^{T_2} C_{p,R} dT \quad (3)$$

where \dot{m}_R is the flow rate of the reforming stream, $C_{p,R}$ is the specific heat capacity at constant pressure, T_1 is the reformer inlet temperature, and T_2 is the observed outlet temperature of the reforming stream. The pressure drop across the reactor at the operating flow rates was negligible.

The thermal power produced from the combustion of the H₂ in the combustion layer of the reactor was obtained as

$$P_{burner} = (\dot{m}_{H_2} \eta_b \Delta H_{f_{H_2O}}) + P_{air} - P_{exhaust} \quad (4)$$

where \dot{m}_{H_2} is the flow rate of H₂ in moles per second, η_b is the H₂ conversion efficiency of the combustor, and $\Delta H_{f_{H_2O}}$ is the enthalpy of formation of H₂O at the combustor temperature. P_{air} and $P_{exhaust}$ are the thermal power in the combustor air supply and combustor exhaust respectively. They were calculated using the same

method as $P_{reactor}$ with the appropriate temperatures and specific heats for each stream used.

The heat transfer efficiency was then defined as

$$\eta_{HEX} = \frac{P_{reactor}}{P_{burner}} \quad (5)$$

The heat flux from combustor to reforming streams was calculated as

$$q = \frac{P_{reactor}}{A} \quad (6)$$

where A is the area available for heat transfer.

Figure 15 shows the effect of the temperature of the combustion layer of the reactor on the heat transfer efficiency and heat flux. The reforming stream flow rate was set to 20 dm³/min (STP). It can be seen that the heat transfer efficiency decreases as the average temperature of the combustor increases. At a combustor temperature of 673 K, the heat transfer efficiency peaks at 85%. As temperature increases, it decreases to a level of 65% at 873 K. The decrease in heat transfer efficiency is due to the increase in the H₂ conversion efficiency at high temperatures. Figure 16 shows temperature difference between the reforming stream and the average combustor temperatures, against the average combustor temperature. It can be seen that the temperature difference increases as combustor temperature increases, which means that the temperature increase of the reforming stream is not as high as that of the combustor. This indicates that the increase in temperature of the reforming stream is not sufficient to overcome the effect of the increased H₂ conversion rate. Therefore, the heat transfer efficiency of the reactor decreases.

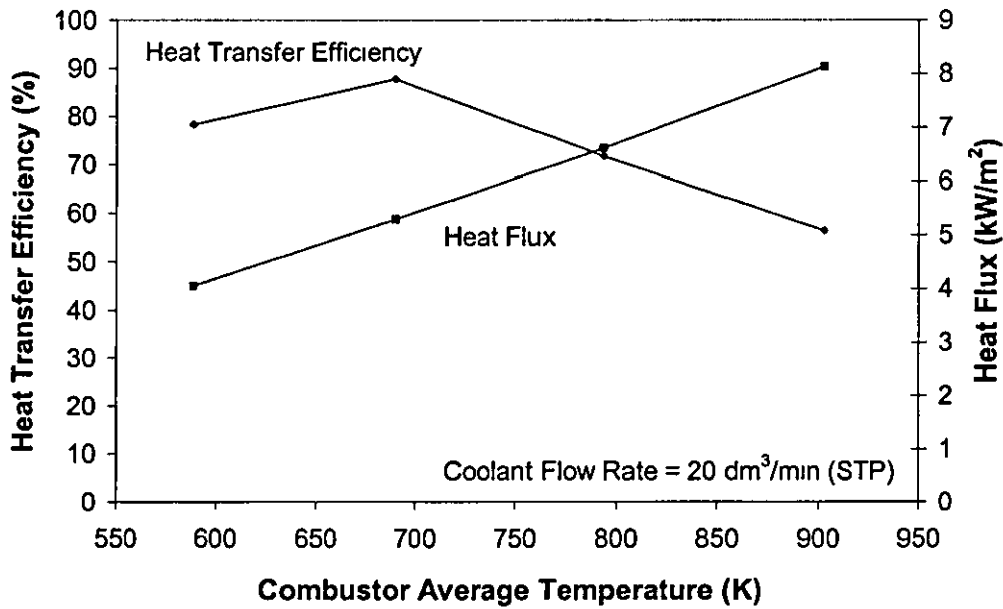


Figure 15: Effect of combustor temperature

The heat flux increase is mainly due to the fact that the H₂ conversion efficiency is generally proportional to the temperature of the combustor as shown in Figure 13. As temperature increases, more heat is generated from the combustor. As a result, both heat flux and the thermal power of the combustor increase.

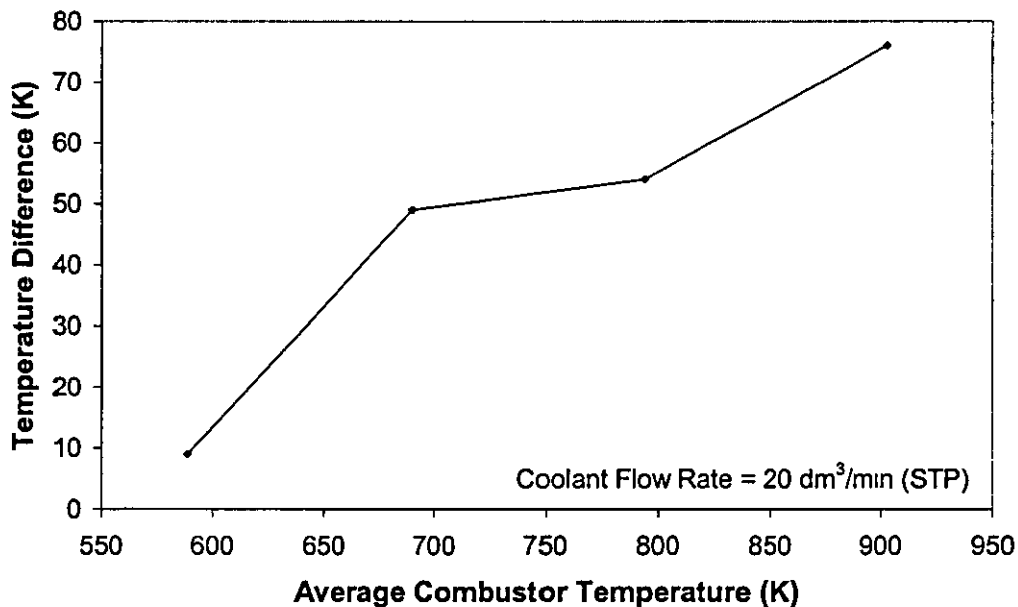


Figure 16: Temperature difference between the reforming stream and the average combustor temperatures.

Figure 17 shows the effect of the reforming stream flow rate on the heat transfer efficiency and the heat flux. The reforming stream was tested using N_2 . The combustor temperature remained constant at 873 K throughout the test by controlling the amount of H_2 supplied to the combustor. It can be seen that as the flow rate of the reforming stream increases so does the heat transfer efficiency and the heat flux. This is due to the fact that the increased reforming flow is able to absorb more heat from the combustor, and the controller responds by increasing the amount of H_2 to the combustor. Since the H_2 conversion efficiency of the combustor is approximately independent of reforming stream flow rate, the thermal power of the combustor increases, and the heat flux rises.

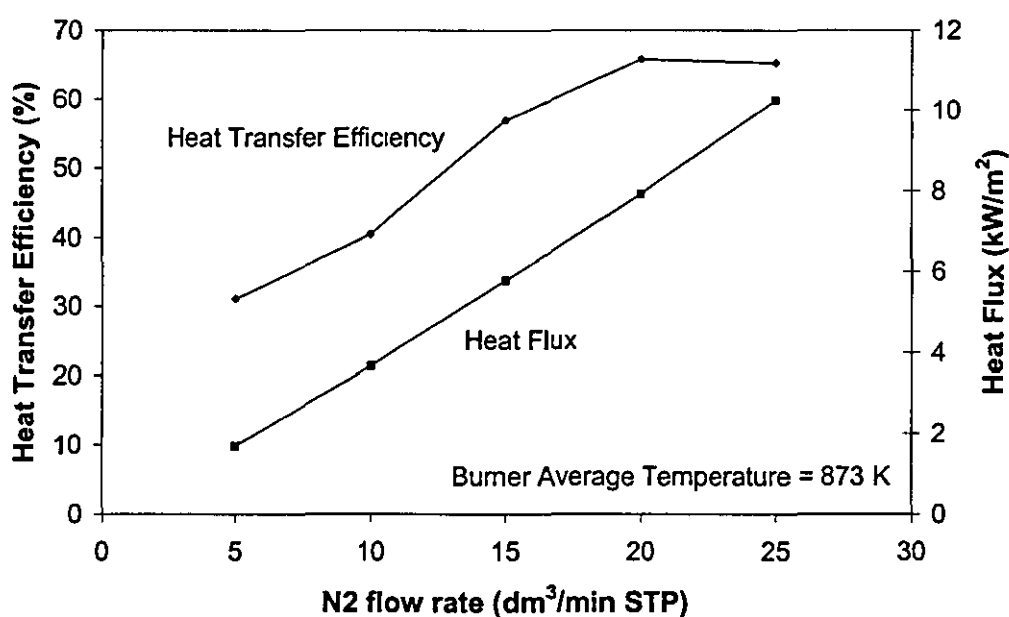


Figure 17: Effect of the reforming stream flow rate

Figure 18 shows temperature difference between the reforming stream and the average combustor temperatures, against the N_2 flow-rate. As the N_2 flow-rate increases, the temperature difference decreases. This is because the higher flow-rates of N_2 enable more energy to be absorbed from the combustor and therefore improves the heat transfer efficiency.

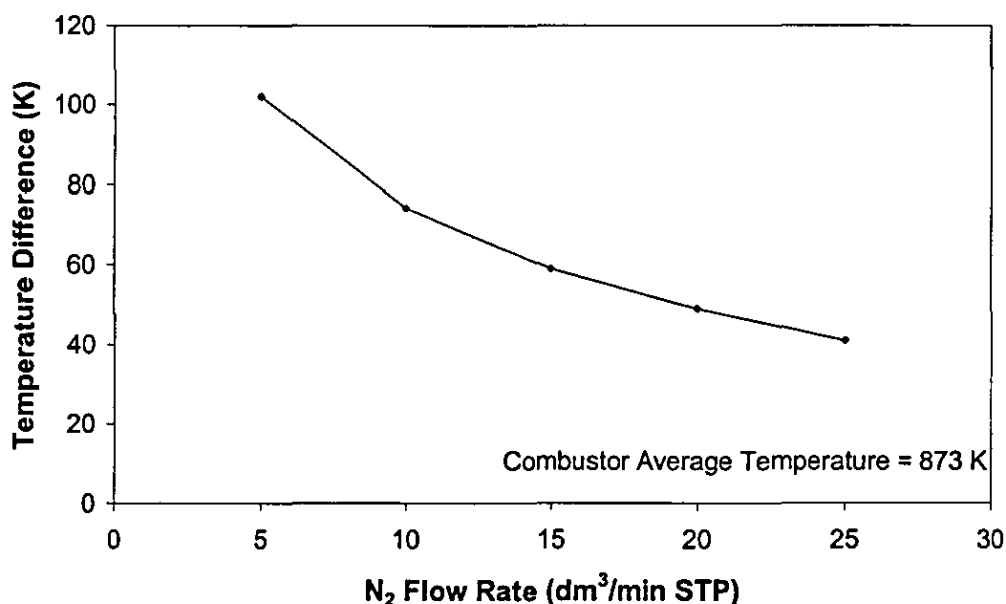


Figure 18: Temperature difference between the reformer stream and the average combustor temperature.

The thermal power transferred to the reforming stream at a combustor average temperature of 873 K and a N₂ flow rate of 25 dm³/min (STP) was approximately 320 W. This is enough thermal power to support the steam reforming of 0.7 dm³/min (STP) propane at a molar steam to carbon ratio of 2 and a temperature of 873 K. Therefore, the reactor is capable of a sufficiently high rate of heat transfer for use as a steam reformer. In addition, as the flow rate of the reforming stream increases the heat flux also increases. This suggests that the reactor is capable of supporting higher flow rates of propane.

4. Conclusions

A micro-channel steam reformer was designed and built. Control and data acquisition software was produced to enable the operation of the steam reformer. Using this software the temperature of each combustor zone can be individually controlled.

It was found that zones 1 and 4, which are positioned at inlet and exit of the reforming stream, respectively, required the most control input. Zones 2 and 3, which are located in the middle of the combustor, could be controlled together without a detrimental effect on the controllers' performance. Additionally, it was found that the flow of the

gases in the combustion layer adversely affects the temperature distribution in the combustor. However, it was shown that the multi-zone combustor layout provides accurate temperature control along the length of the reformer. This improves the traditional reformer designs. The catalytic combustor works effectively with approximately 90% of the H₂ converted. The heat transfer efficiency of the reactor between the combustor and reforming layer was found to be in the region of 65% to 85% at a temperature of 873 K to 673 K, respectively

The reactor is capable of a sufficient rate of heat transfer for use as a steam reformer. In addition, as the flow rate of reforming stream increases the heat flux also increases. This suggests that the reactor is capable of supporting higher flow rates of reforming fuel than demonstrated here.

References

- [1] B. Lindstrom, L. J. Pettersson – Steam Reforming of Methanol over Copper-Based Monoliths. The Effects of Zirconia Doping, *J. Power Sources* 106 (2002) 265-273
- [2] N. Edwards, S.R. Ellis, J.C. Frost, S.E. Golunski, A.N.J. van Keulen, N.G. Lindewald, J.G. Reinkingh – On-board hydrogen generation for transport applications: the HotSpot™ methanol processor, *J. Power Sources* 71 (1998) 123-128
- [3] S. Ahmed, M. Krumpelt - Hydrogen from Hydrocarbon Fuels for Fuel Cells – *Int. J. Hydrogen Energy* 26 (2001) 291-301
- [4] A. Dicks, J. Larminie – Reforming of Fossil Fuels (Status Survey), *Proc Fuel Cell 2000* 0-14/07/2000, Lucerne Switzerland.
- [5] A. Heinzl, B. Vogel, P. Hubner – Reforming of Natural Gas – Hydrogen Generation for Small Scale Stationary Systems, *J. Power Sources* 105 (2002) 202 – 207
- [6] LabVIEW™ software, National Instruments Corporation, Austin, USA.

Appendix 2.2: LPG Steam Reforming in a Compact Microchannel Reactor Using Sulphur Tolerant Catalyst

Draft copy of research paper.

LPG Steam Reforming in a Compact Microchannel Reactor Using Sulphur Tolerant Catalyst

James Reed^{a,*}, Rui Chen^a, Christopher Dudfield^b, Paul Adcock^b

^a*Department of Aeronautical and Automotive Engineering, Loughborough University,
UK*

^b*Intelligent Energy Ltd, The Innovation Centre, Loughborough, UK*

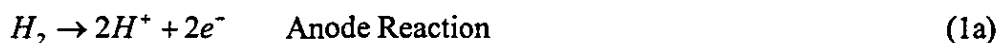
** Corresponding author TEL: (+44) 1509 225860, FAX (+44) 1509 223911, E-mail address: J.P.Reed@Lboro.ac.uk*

Abstract: A multi-function compact chemical reactor designed for hydrocarbon steam reforming was evaluated for use with LPG. The reactor design is based on diffusion bonded laminate, micro-channel heat exchanger technology. The reactor consists of a combustor layer, which is sandwiched between two steam reforming reactor layers. Between the function layers, a temperature monitor and control layer is placed, which is designed to locate the temperature sensors. The combustor layer has four individually controlled combustion zones each connected to a separate fuel supply. The reactor design offers the potential to accurately control the temperature distribution along the length of the reactor using closed loop temperature control. A sulphur tolerant catalyst was washcoated on to the reforming layers. The use of a sulphur tolerant catalyst in the reformer leads to a simpler fuel processor design utilising sulphur tolerant water gas shift catalysts, and sulphur removal taking place before the fuel cell, as part of the H₂ purification process instead of utilising a separate desulphuriser. LPG offers advantages as a fuel over other hydrocarbons because there is already an infrastructure in place for remote areas. The sulphur content of LPG is tolerated by the reformer catalyst to be tested. The reformer was tested over a wide range of reactor temperatures, steam to carbon ratios and fuel flow rates.

Keywords: LPG; Sulphur Tolerant; Microchannel; Steam Reforming

1. Introduction

The fuel cell concept has been around since 1835. William Grove a physics professor at the London Institute based his experiment on reversing the water electrolysis process. The term Fuel Cell was coined in 1889 when an attempt was made to make the first practical model. Fuel cells have since been investigated for use in a number of different applications; automotive, CHP, space flight, aviation, MW scale generators and portable battery sized fuel cells. However, due to the Kyoto agreement and other such national initiatives [Ref.1], there is now a renewed and concentrated interest in technology that can produce a long term, clean and efficient energy solution. Alongside this there is the long term goal of a H₂ economy [Ref.2] A fuel cell can be seen as analogous to a battery. The major difference is that a battery carries its fuel internally, whilst a fuel cell uses external fuel This means that, provided there is a supply of fuel to the cell, electricity will be produced. The solid polymer fuel cell (SPFC) utilises H₂ as its fuel, which it combines electrochemically with oxygen (from air) to produce electricity, heat and water [Ref 3] This can be seen in the equations for the reactions at the anode and cathode below (equation 1a, 1b).



Since H₂ is not naturally occurring in its pure state, it has to be obtained as a secondary fuel from primary sources. This can be done either by the electrolysis of H₂O or by chemically reducing hydrocarbon fuels. Both of these methods require a H₂ network to be set up to facilitate the commercial logistics of fuelling the fuel cell [Ref.4]. In remote areas, particularly where this is economically impractical, the need for small-scale H₂ generators can be argued. The generator needs to have a quick start-up time and follow transients in fuel demand well. Certain applications confer space restraints on the installed system Therefore a compact fuel processor design coupled with the compactness of SPFC technology can be advantageous. Based upon our previous work using microchannel heat exchanger (HEX) technology it is

suggested that using microchannel technology as the basis for a steam reformer could be a way of supplying H₂ to remote areas. LPG was chosen as the primary fuel because of its ready availability in such regions.

1.1 Steam Reforming

Steam reforming of a hydrocarbon fuel is an efficient method to produce a hydrogen rich gaseous fuel. The overall reaction can be described by the following equation [Ref. 5].



Steam reforming is a strongly endothermic reaction and so requires the application of additional heat to sustain it. The necessary extra heat required is usually provided by a combustor coupled to the steam reformer. This design facilitates the use of unused hydrogen from the fuel cell to partially heat the reformer, thus increasing the system efficiency. This is not possible when using partial oxidation (POX) or auto-thermal reaction (ATR) reformers as the POX reaction is exothermic and ATR is thermally neutral. [Ref.5] The composition of the product gas for a given feedstock is dependant on the temperature of the reactor and the steam to carbon ratio.

Carbon monoxide concentrations of between 8 and 15% (Figure 1) are produced as a thermodynamic function of the reaction temperature and steam to carbon ratios required to achieve acceptable levels of hydrocarbon conversion at acceptable reactor temperatures. This has a detrimental effect on the performance of SPFCs due to competition for electro-catalyst sites in the fuel cell between CO and H₂ molecules. This results in the fuel cell efficiency being drastically reduced and introduces the need for a H₂ purification system. [Ref. 6-7]

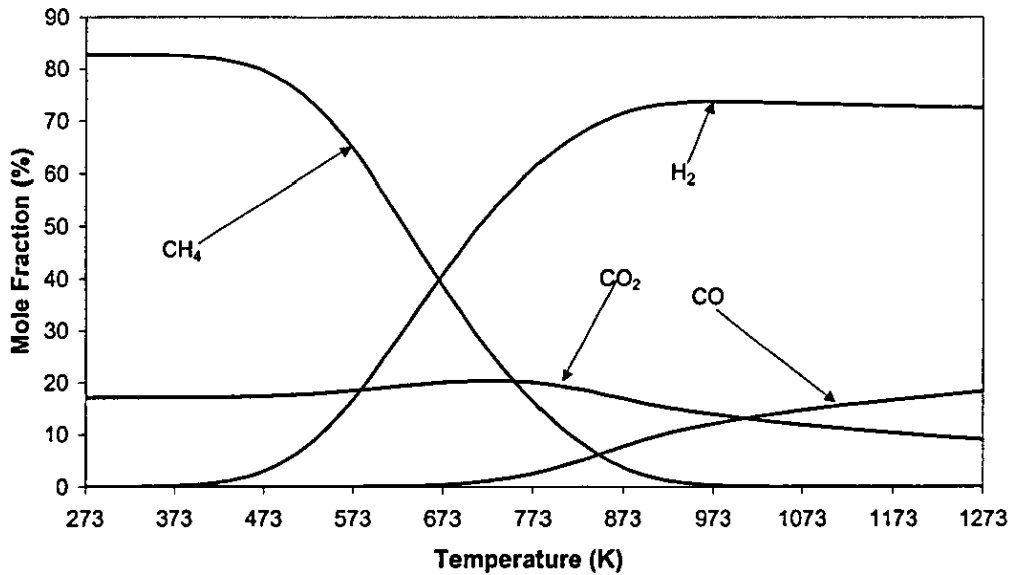


Figure 1: The modelled equilibrium dry products composition of steam reforming LPG at a Steam/Carbon ratio of 3.5 with varying reactor temperature

Most commercial reformers control the temperature at the exit of the reformer by measuring the temperature of the exit gases. This naturally creates a temperature gradient along the length of the reformer [Ref 8](Figure 2) As the temperature of the reactor has a large effect on the reformate composition this has a negative effect on the reformer performance. The reformate composition is highly dependant on the temperature of the reformer. The higher the temperature the greater the percentage of hydrogen produced, but this comes at the cost of increased carbon monoxide production. For LPG at equilibrium, hydrogen production peaks at around 973 K whilst carbon monoxide production continues to increase. This can be seen in Figure 1. Figure 1 shows the dry products of reforming LPG at a steam to carbon ratio of 3.5 with respect to reactor temperature at equilibrium. The thermodynamics of the reaction produces a trade off between the amount of hydrogen produced and the desire to keep carbon monoxide production to a minimum. At lower temperatures complete conversion of the fuel does not take place. This lowers the efficiency of the reformer. For these reasons temperature control of the reformer is critical to the efficient running of the steam reformer.

1.2. Reactor Technology

Existing steam reformer technology has until recently been of the packed bed type with simple thermal control [Ref 8] This method has been widely used at the industrial scale. At small-scale, the residence time of the reactant is limited and without increasing the dimensions of the reactor, the performance of the reactor suffers as a result. [Ref. 9]

Microchannel technology offers benefits for start-up times, transients and thermal management. The nature of microchannel heat exchangers provides a high reaction surface area/volume ratio whilst the pressure drop through the heat exchanger is negligible. The heat exchange properties are such that it makes the technology very attractive in the field of steam reforming where the rate of reaction is limited by the rate of heat transfer to the reactants.

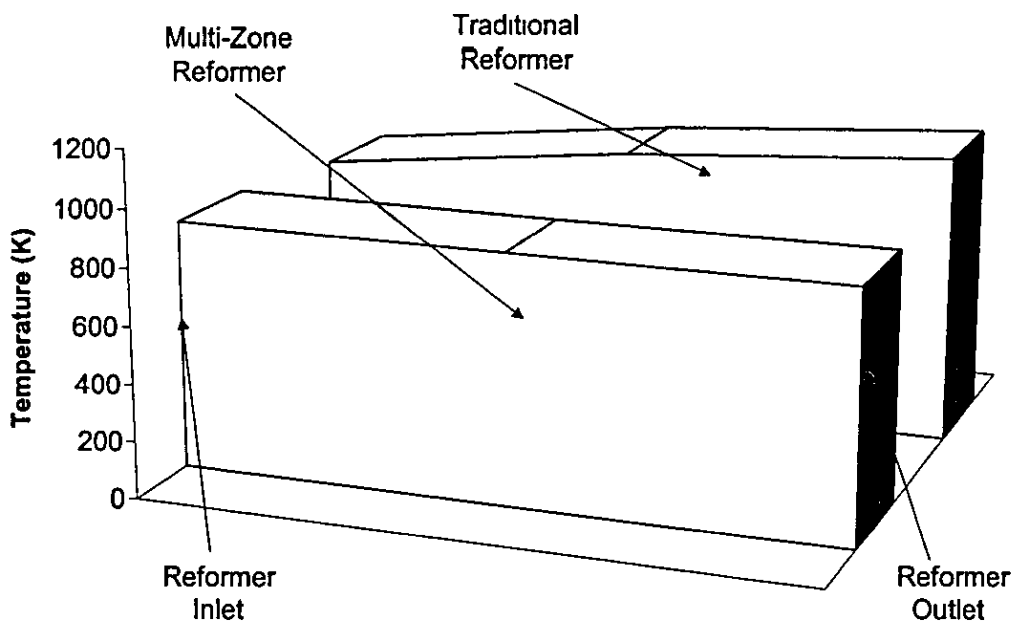


Figure 2: A comparison of the multi-zone reformer and traditional technology temperature profiles.

1.3. Desulphurisation

Sulphur levels in the ppb range will irreversibly damage the platinum catalyst of the fuel cells anode. Also sulphur is a poison for most common nickel based reforming catalysts. Since commercial grade LPG (and other fuels) unavoidably contain sulphur as an odorant, the sulphur needs to be removed from the fuel stream before it reaches the reformer catalyst and fuel cell [Ref. 10]. Typically one of two methods of desulphurisation are used. HydroDesulphurisation (HDS) with zinc oxide beds, or absorption techniques utilising activated carbon [Ref. 3]. HDS is the best suited for SPFC systems as there is an available stream of hydrogen rich gas to promote the hydrogenolysis reaction. The HDS reactor requires heating to around 623 – 673K for the hydrogenolysis reaction to complete. This reduces the efficiency of the fuel processor as well as introducing greater complexity and size. The use of a sulphur tolerant reforming catalyst allows the movement of the desulphuriser reactor downstream, where the reformat is already at the required temperature. Additionally, if sulphur tolerant water gas shift catalysts are used it needs only a H₂ separation membrane (provided the metal membrane is sulphur tolerant) to be used to strip out the sulphur along with the other impurities in the reformat stream before the fuel cell. The sulphur could then be removed by adsorption in the usual way on a zinc oxide bed, or recycled through the steam reformer combustor, without affecting the performance of the fuel processor. This would simplify the fuel processor considerably.

2. Compact Steam Reforming Reactor

Micro-channel reactors are made of a diffusion bonded laminate. Inside the reactor, multi-layers of metal shims create alternating micro-channels and fins. The micro-channel widths are determined by the thickness of the shim material whilst the heights and lengths of the channels are determined by the machined surface. The machining can be either by photochemical or stamping processes. This means that the manufacturing process can be scaled up to produce large production runs. The shims are diffusion bonded together under high temperature and pressure (1173 K, 27 MPa for 4 h) to yield a monolithic metal block that removes the need for gaskets and other seals. A reactor built in this way is effectively a micro-channel heat exchanger.

Experiments at Imperial Chemical Industries. plc. evaluating the heat transfer performance of microchannel type, photochemically etched heat exchangers, found that a heat exchanger containing channels with a depth of 0.3mm, had a volumetric heat transfer performance equivalent to $7 \text{ MW/m}^3\text{K}$ with a water velocity of 0.18m/s . The equivalent shell and tube, and plate heat exchangers had performance listed as $0.21 \text{ MW/m}^3\text{K}$ and $1.25\text{MW/m}^3\text{K}$ respectively. [Ref.11] This makes microchannel technology ideal for the basis of the reactor for a steam reformer as, the heat energy required for the support of the reforming reaction, supplied from a combustor, can be efficiently transferred to the reaction side in a smaller volume than with more traditional technology. The overall reforming system efficiency can then be made more compact.

Based on this micro-channel technology, the authors have developed a new type of catalytic chemical reactor as shown in Figure 3.

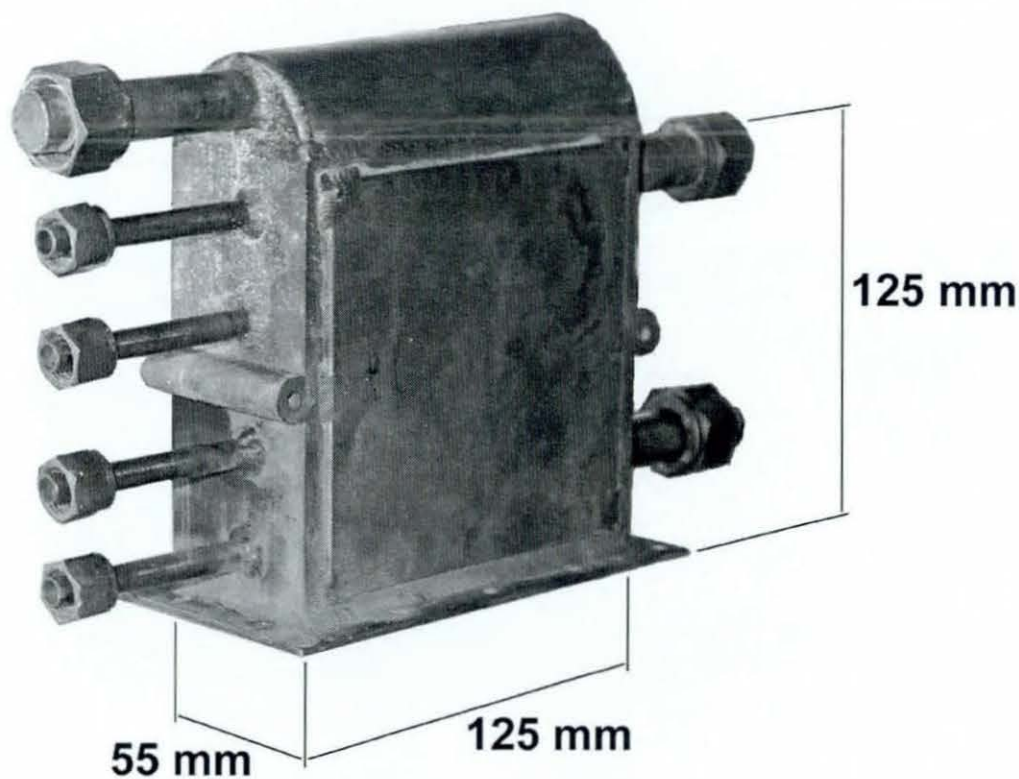


Figure 3: Compact Steam Reforming Reactor

The steam reformer is of microchannel construction and can be visualised as consisting of five main layers. A central combustor layer, two temperature measurement layers and two reforming layers. The combustor layer is itself split into two layers, one for fuel and one for air. These layers are connected via a diffusion layer. The temperature sensing layers are then arranged one on either side of the combustor. The reforming layers are then placed on the side of the temperature sensing layers. This arrangement promotes the efficient transfer of heat from the combustor to the reforming layers. The combustor is divided into 4 zones each with an individual fuel feed and a common air feed. Each fuel feed can be controlled individually and the air feed is controlled accordingly. This arrangement means that the temperature along the length of the reforming layers can be accurately controlled. The reactor is of a stainless steel diffusion bonded laminate construction, which is ideally suited to the high temperatures necessary for the steam reforming of LPG.

Additionally this new micro-channel heat exchanger type steam reforming reactor offers the following advantages:

- Can be more compact than conventional reactors without losing power output.
- Can have a high active area/volume. The reformer detailed in this paper has an active area of 1.35 m^2 in a volume of 175 cm^3 .
- The high rates of heat transfer possible make it ideal for steam reforming where the reaction is limited by the rate of heat transfer to the reformer.

The drawback at this stage of development is the cost of manufacture of the reactor. Economy of scale may offset some of the production costs of the reactor. In particular the area of shim manufacture is one where large scale automation may see costs reduced.

In this research, a novel compact heat and reaction combined reactor, developed for the steam reforming reaction, was experimentally investigated. The reactor is based on micro-channel heat exchanger technology. The reactor has an integrated multi-zoned combustor arranged so that the temperature of the reformer can be controlled along the length of the reformer. A novel precious metal (Pt/Ru) based catalyst was

applied to the reforming side of the reactor using a wash-coating process. The catalyst was designed to be sulphur tolerant and to convert the sulphur into H_2S to be removed at a later stage. The catalyst operating range is limited to 873 K in order to avoid sintering of the catalyst and the accompanying loss of activity. This work represents the first stage in the development of a sulphur tolerant steam reformer. The results gained will be used to assess any additional development the catalyst or reactor might need.

3. Experimental Investigation

3.1. Test Rig

The test rig used to evaluate the steaming reforming reactor performance is shown in Figure 4. The reformer is a multi zoned catalytic microchannel combustor coupled directly to a microchannel reformer. There is a 500W pre-heater for the combustor air supply and a 750W pre-heater for the LPG and de-ionised H_2O supply. There are three pipes inside the pre-heater for the LPG/ H_2O , one is used for the LPG and the other two for the H_2O . The reactants are mixed immediately after the pre-heater and before entering the reformer. The H_2 to each zone of the combustor and the overall air supply to the combustor are controlled using a closed loop control. This allows the reformer temperature to be controlled throughout the reformer. The combustor H_2 /air mixture is controlled so as to mimic the proportion of H_2 and O_2 from typical fuel cell off gases. The excess H_2O is condensed out of the reformat and the remaining gases are passed through online CO and CO_2 (Siemens Ultramat 6) analysers before passing through a Pye gas chromatograph. The water was supplied using a computer controlled continuous flow syringe pump. The flow of LPG is manually controlled via a mass flow controller.

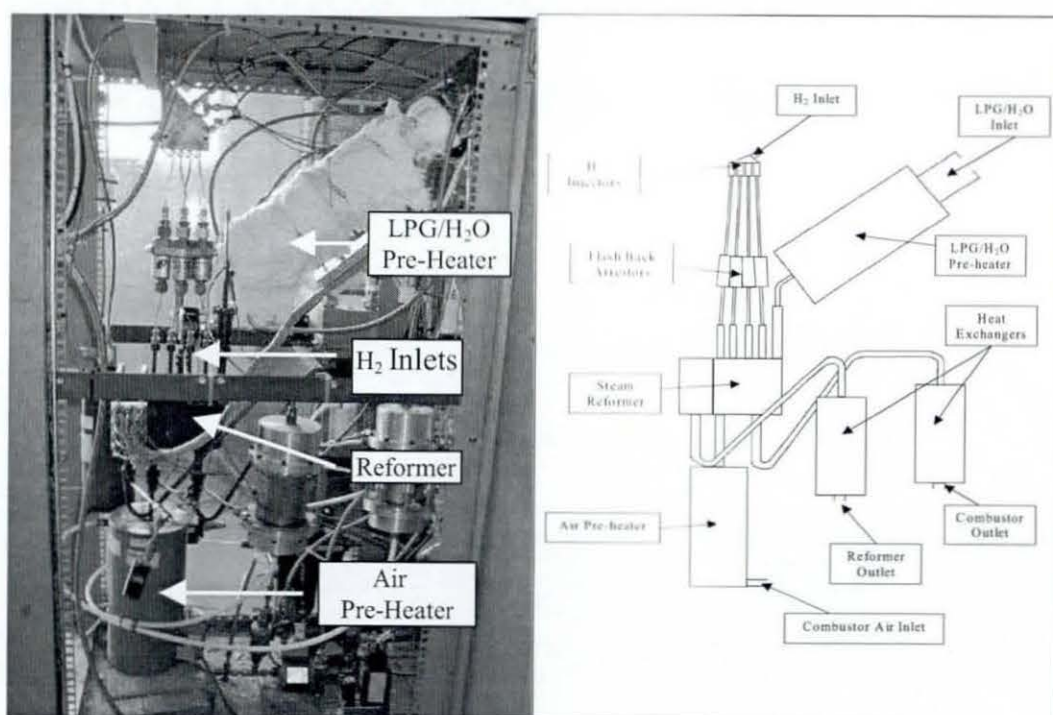


Figure 4: The Test Rig

During the study, the reformer was tested over a range of temperatures, steam to carbon ratios, and reactant flow rates. A commercial grade LPG supplied by Calor Gas [Ref. 12], which contains sulphur compounds, was used as the reactant.

3.2. Test Procedure

The test procedures were as follows:

- The temperature was set to the set-points of 723, 773, 823 and 873 K whilst for each temperature the steam to carbon ratio was set to 2.5, 3, 3.5 and 4.
- The flow rate of LPG was set at $0.75 \text{ dm}^3/\text{min}$ (STP) as this corresponds to approximately 0.5kWe (based on equilibrium data) from a fuel cell, given total conversion of the LPG.
- The set-point with the best performance was then chosen and the LPG flow rate was varied from 0.25 to $1.75 \text{ dm}^3/\text{min}$ (STP) whilst the temperature and S/C ratio were kept constant.

The catalytic combustor lights off at room temperature so no additional heat was required to initiate warm-up. The reformer was then heated to 673 K with only N₂ passing through the reforming side of the reactor. Both of the pre-heats were switched on throughout. This was to make sure that the inlet temperature was sufficiently high and that the H₂O would vaporise on introduction. The reformer was then kept at a constant temperature of 673 K whilst the H₂O was introduced. The amount of H₂O was determined by the steam to carbon (S/C) ratio needed for the test set-point with a flow rate of 0.75 dm³/min (STP) of LPG. The reformer was kept at these running conditions until the temperatures stabilised. LPG was introduced at a S/C ratio of 8 and the temperature of the reformer was then increased to the desired set point. Once the desired temperature had been reached the LPG flow rate was increased gradually until the desired S/C ratio was reached.

The product gas from the reformer (i.e. the reformat mixture) was passed through two on-line analysers one for CO detection and the second for CO₂ detection. A sample of the dry reformat mixture was also injected into the gas chromatograph in order that H₂ and CH₄ content could be determined. The results generated were the percentage composition of the dry reformat.

3.3. Results

The effect of reformer temperature on dry reformat composition can be seen in Figure 5. The LPG supply rate to the reformer was 0.75 dm³/min (STP) and the steam to carbon ratio was 4 during the test. It can be seen that as the reformer temperature increases so does the conversion of LPG. The increased conversion rate can be explained by the increase in energy provided to the reaction at higher temperatures. The increased conversion rate results in increased production of H₂, CO₂ and CO. The production of CH₄ is via methanation. It is interesting to note that the amount of methane decreases when the reactor temperature is above 773 K. This is due to the reformation of the methane. If the results are compared to those found under equilibrium conditions (Figure 1), with the exceptions of LPG conversion and CH₄ production, it can be seen that the same trends occur. The differences here are due to the steam reforming reaction in the real reactor not having sufficient time to reach

equilibrium. The methanation process that produces the CH_4 in the equilibrium model is too slow to do the same in the actual reformer. It is noted that a potential further 10% H_2 can be produced from the LPG.

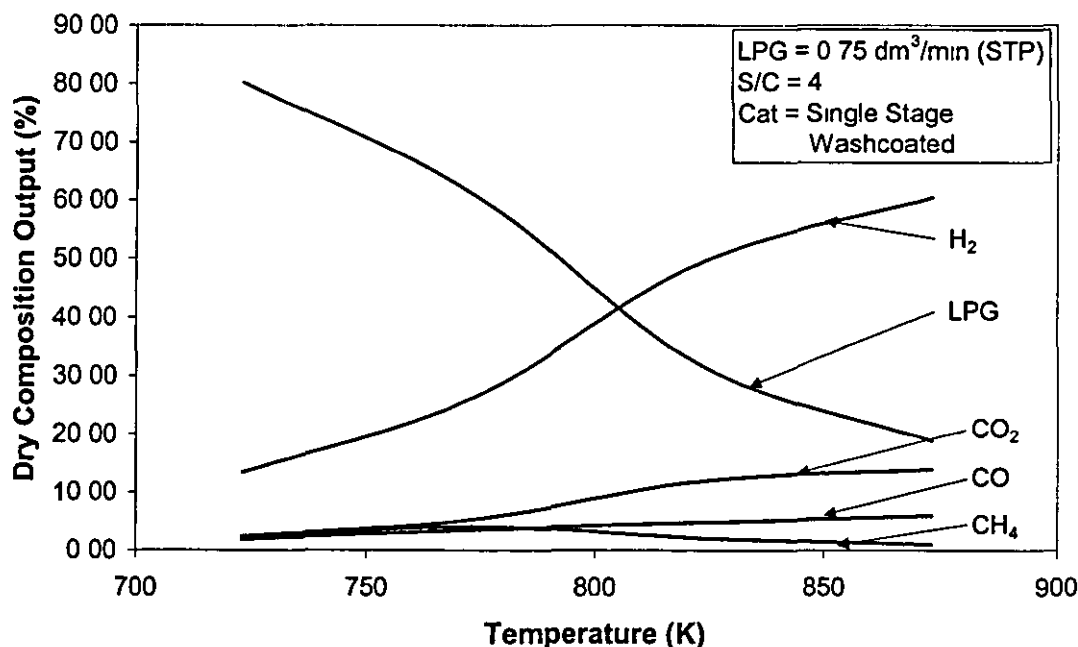


Figure 5: Dry Reformat Composition at Varying Temperature

The effect of the steam to carbon ratio on the dry reformat composition is shown in Figure 6. During the test, the LPG supply rate to the reformer was 0.75 dm³/min (STP), and the reactor temperature was set to 873 K. It can be seen that as the steam to carbon ratio is increased so does the conversion of LPG. It increases the production of H_2 . In addition, the concentration of CO decreases whilst the amount of CO_2 increases. The change in proportion of CO/CO_2 is due to the water shift reaction. Hydrogen from the water is liberated when the water reacts with the CO to produce H_2 and CO_2 . Again, if the results from the experiment are compared to the predicted equilibrium results (Figure 7) it can be seen that with the exception of the percentage conversion of the LPG and the production of CH_4 in the equilibrium results, the spread of values is similar. The maximum steam to carbon ratio investigated was four. This is twice the stoichiometric value. From simulated results it is clear that as long as the steam to carbon ratio increases, the amount of hydrogen produced will increase. However, it is more efficient to liberate this hydrogen, whilst removing carbon

monoxide from the reformat, in a separate lower temperature reactor. In this way the carbon monoxide content can be reduced to approximately 1% without the need for extra heat to be applied to the reformer. Therefore, a steam to carbon ratio maximum limit of 4 was utilised.

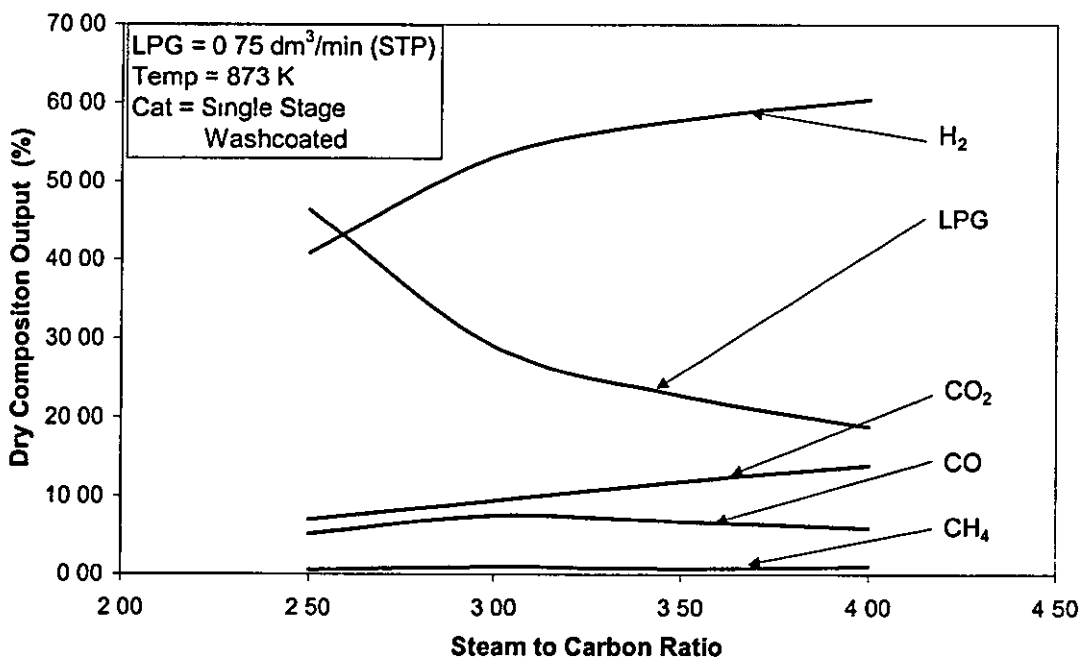


Figure 6: Dry Reformate Composition with Varying Steam to Carbon Ratio

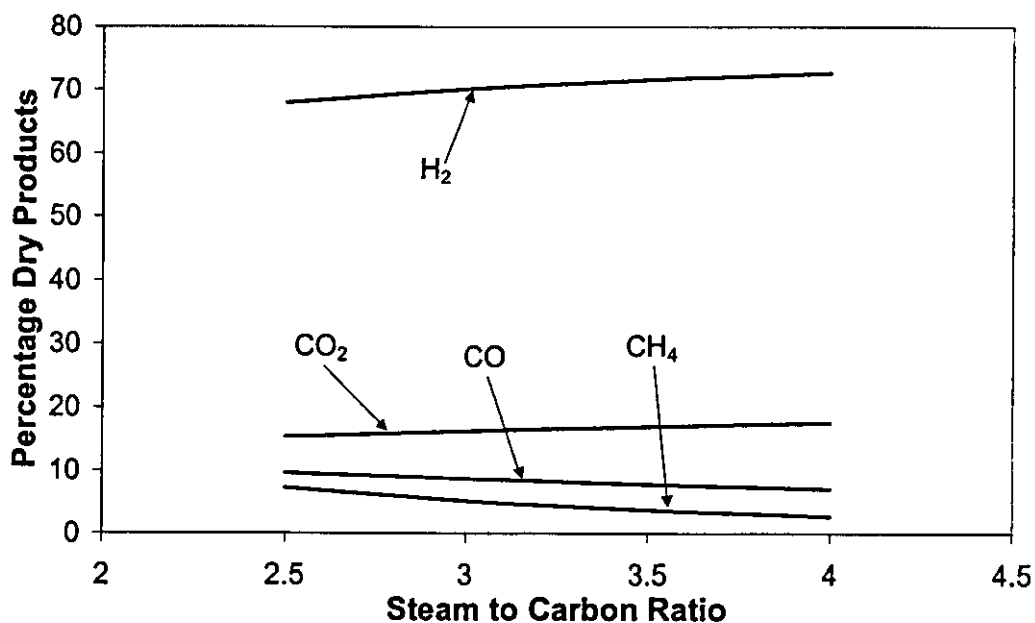


Figure 7: The Modelled Dry reformate composition with varying steam to carbon ratio at equilibrium.

The effect of the flow-rate of the reformer reactants on the dry reformat composition is shown in Figure 8. The steam to carbon ratio during the test was 4, and again the reactor temperature was set at 873 K. It can be seen that as the flow rate of reactants to the reformer was increased the conversion of the LPG decreased. This is due to the reduction of residence time in the reformer itself. It suggests that the activity of the catalyst needs increasing for a reformer of this volume. This will be taken into account during the next stage of work.

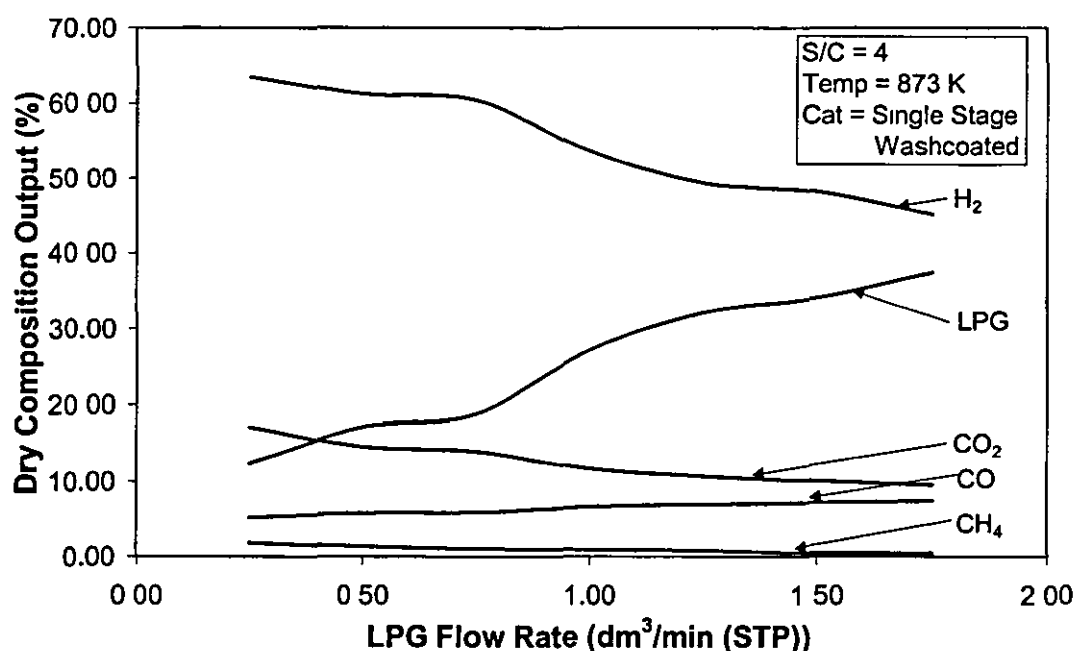


Figure 8: Dry Reformat Composition with Varying Reactant Flow-rate

Space velocity is defined as the volume of gaseous reformat per hour per volume of catalyst which is widely regarded as GHSV. In this study the maximum space velocity was found to be 9420 GHSV. This figure is based on the reformer performance at a LPG flow rate of 1.75 dm³/min (STP) and steam to carbon ratio of 4. The reformer was at a temperature of 873 K. However, this figure is not based on the volume of the catalyst but on the volume of the reformer itself. This is because the catalyst is wash-coated on to the reforming surface, the volume of the catalyst will be much lower than that of the reformer. This would increase the GHSV figure in real term.

The energy conversion efficiency of the reformer can be defined as the ratio between the energy contained by the reformate products and the energy contained by the reactants,

$$\eta = \frac{P_{LHV}}{R_{LHV}} \quad (4)$$

where P_{LHV} is the lower heating value of the products and R_{LHV} is the lower heating value of the reactants.

The products are the hydrogen and carbon monoxide produced. The carbon monoxide is included because after water gas shift reaction, most of the CO has been converted into hydrogen. The reactants are the LPG to the reformer and the hydrogen to the combustor. It has been assumed that any unconverted LPG and any hydrogen in the fuel cell off gas, which is approximately 1/3 of the H₂ to the stack, are burnt in the combustor. The energy used by the electric preheaters is not included in the calculation, as in an ideal fuel processor this energy would be provided by the heat from the reformer and combustor flue gases.

Figure 9 shows the conversion efficiency of the reformer at different reactant flow rates. A steam to carbon ratio of 4 and a reactor temperature of 873 K were used during the test. It can be seen that the average conversion efficiency of the reformer is between 0.5 and 1.5 dm³/min (STP) is 74%. For a reformer of this size 0.25 dm³/min (STP) of LPG is too low. At such low rates, the reformer is too big to operate efficiently. At an LPG flow rate of 1.75 dm³/min (STP), the flow of H₂ to the combustor needs to be increased dramatically (3.50 dm³/min (STP)). This is due to the LPG/H₂O preheat not being powerful enough to heat the reactants sufficiently to vaporise the H₂O before entering the reformer. As a result the reformer's temperature controller has to increase the H₂ flow rate to compensate and vaporise the H₂O at the entry to the reformer. This lowers the efficiency of the reformer.

The energy conversion efficiency of the reactor can be further improved by improving the integration of the reformer with the rest of the test rig/system and by increasing

the activity of the catalyst used to reduce the drop off in performance at higher flow rates of LPG.

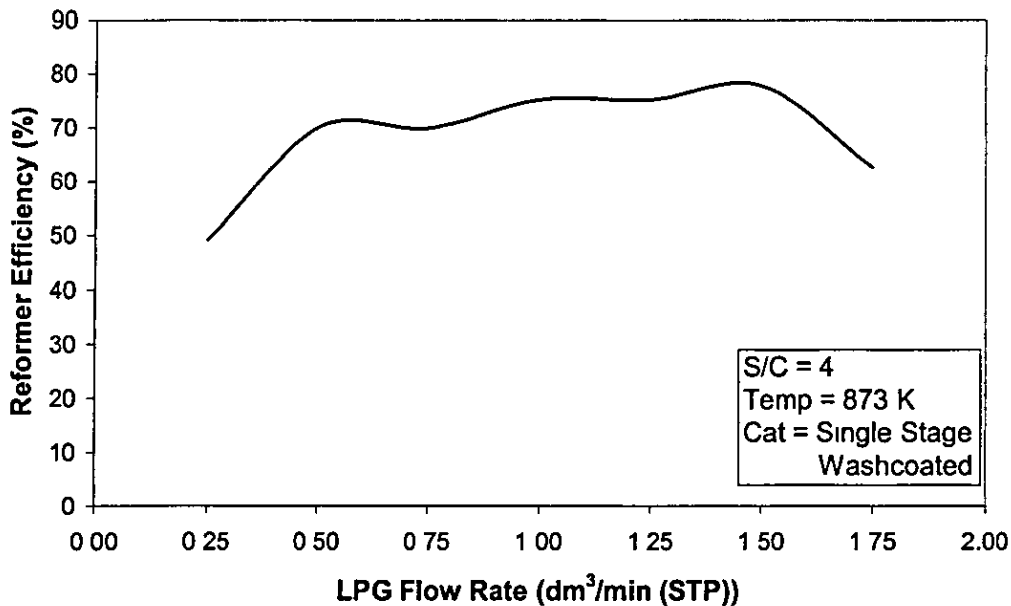


Figure 9: Reformer Efficiency at Varying Reactants Flow-rate

The power output of the reformer is based on calculated equilibrium data which was then modified according to the percentage conversion of the LPG feedstock as follows

$$P_a = \frac{C_a \times H \times 22.41}{F} \quad (5)$$

Where P_a is the predicted power output from the fuel cell in kWe, C_a is the percentage conversion of the LPG, H is the flow rate of hydrogen (mol/min) produced at equilibrium by 1 mol/min of LPG for a given steam to carbon ratio and F is the flow rate of hydrogen (dm³/min (STP)) required to produce 1 kWe output from a fuel cell.

Figure 10 shows the effect of the reactants flow-rate on the predicted power output of a fuel cell. It can be seen that as the LPG flow rate increases the projected power output from the fuel cell increases. The maximum output achieved was 0.86 kWe at

an LPG flow rate of 1.75 dm³/min (STP) and S/C ratio of 4. However, the conversion of LPG decreases with increasing LPG flow rate as shown in Figure 10. When the power output reached 0.86 kWe the conversion of LPG was only 62.5% which, would not be realistic for use in a complete system because of the additional processing required. Using the sulphur tolerant catalyst in this form, complete conversion can not be achieved under any of the operating conditions tested. This will be addressed in future work with variations of the catalyst formulation

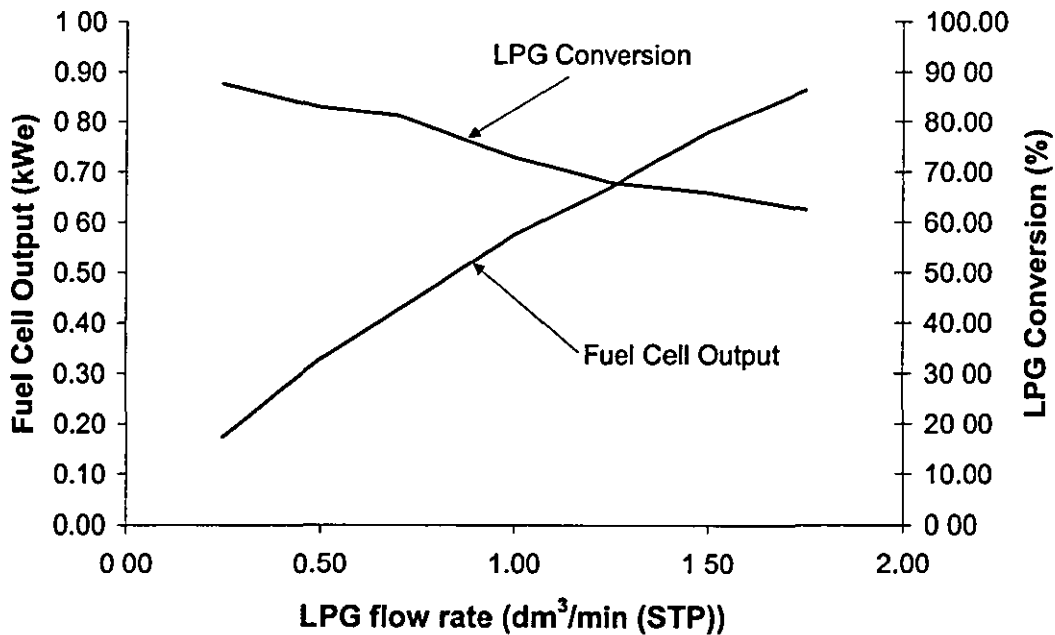


Figure 10: Predicted Fuel Cell Power Output at Varying Reactants Flow-rate

The performance of the controller in keeping the reformer at the desired temperature has been tested and the results are shown (Figure 2) in comparison with traditional reforming technologies. It can be seen that there is only 2-3 K in variation along the reformer length. This is an improvement over traditional single zone combustor designs⁵.

Table 1 outlines the summary of the test results in comparison with the calculated equilibrium results.

	Experimental	Equilibrium
Reformer Temperature	873 K	873 K
LPG Flow Rate	0.75 dm ³ /min (STP)	0.75 dm ³ /min (STP)
Steam to Carbon Ratio	4	4
Power Output	0.45 kWe	0.59 kWe
H ₂	60.4%	72.7%
CH ₄	1%	2.7%
CO ₂	13.9%	17.6%
CO	5.9%	7.1%
Balance (LPG + other HCs)	18.8%	Trace
LPG Conversion %	81.2%	100%
Space Velocity (LPG = 1.75 dm ³ /min (STP))	9450 GHSV	N/A
Reformer Efficiency	74%	N/A

Table 1: Summary of test and calculation results

4. Conclusions

A novel steam reformer was tested. It incorporated a multi-zone combustor. The reformer was wash-coated with a novel sulphur tolerant catalyst. The multi-zone combustor allowed accurate temperature control of the reformer along its length. The performance of the reformer was tested over a range of temperatures, steam to carbon ratios and LPG flow rates.

The results obtained using the sulphur tolerant catalyst suggest that a sulphur tolerant fuel reformer is feasible. However, this work is only the first stage in the development of such a reformer. The sulphur tolerant catalyst allowed for 81% conversion of the LPG and produced results near to that expected by equilibrium modelling, with the overall behaviour of the reformer with respect to temperature and steam to carbon ratio as expected. There is not complete conversion of the LPG even at the lowest flow rate tested. Because of the loss in efficiency of the reformer at this flow rate, it can be inferred that, the sulphur-tolerant catalyst is not sufficient in this form for use

as the basis of a steam reformer for LPG. The maximum usable temperature of the catalyst is 873 K so it would not be possible to improve the performance of the reformer by increasing the operating temperature without extending the thermal range of the catalyst. The next stage of work would be to increase the activity of the catalyst. Possible development routes would be to design a new sulphur tolerant catalyst, or to use a more conventional steam reforming catalyst in combination with the existing sulphur tolerant catalyst to increase the activity in that manner. Because of the temperature control available using this reformer design, the addition of a second catalyst running at a higher temperature than the existing catalyst is feasible. This would create the effect of a dual-stage steam reformer.

The microchannel technology is capable of transferring enough heat to support the steam reforming reaction and offers advantages in size compared to traditional steam reformer reactor designs. Further work using the same microchannel technology will concentrate initially on increasing the activity of the catalyst.

References:

1. Our Energy Future – Creating a Low Carbon Economy, Energy White paper, Department of Trade and Industry, Feb 2003
2. Iceland's Renewable Power Sources, Address delivered by The Minister of Industry and Commerce at "Hyforum 2000" in Muchen, Germany, September 12, 2000
3. J. Larminie, A. Dicks – Fuel Cell Systems Explained, John Wiley and Sons Ltd. ISBN 0 471 49026 1, Copyright 2000
4. J.M.Ogden, M.M.Steinbugler, T.G.Kreutz – A comparison of hydrogen, methanol and gasoline as fuels for fuel cell vehicles: implications for vehicle design and infrastructure development, J. Power Sources 70 (1999) 143 – 168
5. R.A.J Dams, P.R Hayter, S.C. Moore – The Processing of Alcohols, Hydrocarbons and Ethers to Produce Hydrogen for a PEMFC for transport applications, IEEE Electrochemical and Solid-States Letters 97109
6. C D. Dudfield, R. Chen and P.L. Adcock – Evaluation of a CO selective oxidation reactor for solid polymer fuel cell automotive applications, J. Power Sources 85 (2000) 237-244

7. C. Qi, D Pollica, M Hagan, T. Cole, V. Rizzo – Transient CO Preferential Oxidation (PrOx) for PEM Fuel Cell, Society of Automotive Engineers Inc., 2000-01-0378
8. Heinzl, B Vogel, P. Hubner – Reforming of Natural Gas – Hydrogen Generation for Small Scale Stationary Systems, J. Power Sources 105 (2002) 202 –207
- 9 Fuel processing for PEM fuel cells: transport and kinetic issues of system design J M. Zalca, D G. Lofflerb J. Power Sources - 111 (2002) 58–64
10. Desulfurization of Gasoline Feedstocks for Application in Fuel Reforming, D.L King, C. Faz, T. Flynn – Society of Automotive Engineers, Inc. 2000-01-0002
11. E A Foumeny, P.J. Heggs - Heat exchange Engineering Volume 1, design of heat exchangers – Ellis Horwood Ltd, 1991
12. Calor Gas Limited, Warwick, U.K.

Appendix 2.3: A dual-catalyst multi-fuel microchannel steam reformer

Draft copy of research paper.

A dual-catalyst multi-fuel microchannel steam reformer

James Reed^{a,*}, Rui Chen^a, Christopher Dudfield^b, Paul Adcock^b

^a*Department of Aeronautical and Automotive Engineering, Loughborough University,
UK*

^b*Intelligent Energy Ltd., The Innovation Centre, Loughborough, UK*

* *Corresponding author. TEL: (+44) 1509 225860, FAX: (+44) 1509 223911, E-mail
address: J.P.Reed@Lboro.ac.uk*

Abstract: A microchannel steam reformer was evaluated for use with LPG, C₃H₈ and CH₄. The reformer utilised two reforming catalysts, sulphur tolerant at the front of the reformer and nickel based at the rear of the reformer. The reformer was coupled to a multi-zoned catalytic combustor, which enabled the longitudinal temperature profile of the reformer to be set as desired. This enabled the two catalysts to be operated at differing temperatures as required. The reformer was tested over a range of operating temperatures, steam to carbon ratios and feed rates. The performance of the reformer whilst using C₃H₈ and LPG showed good agreement suggesting that the performance of the reformer was not adversely affected by the presence of sulphur in the fuel. 98% conversion of C₃H₈ was achieved at a predicted fuel cell power output of 1.98kWe.

Keywords: Microchannel, LPG, Steam reforming, sulphur tolerant

1. Introduction

Fuel cells as the basis of combined heat and power (CHP) systems are an interesting alternative to the conventional separate natural gas and electricity supplies commonly employed in homes today. The idea being that given a natural gas supply to the house, the CHP system is used to generate any electricity when required. The "waste" heat from the system can be employed to heat water. [Ref 1] It is a short conceptual leap to distributed electricity grids where each user buys from and sells to the grid as required. Small scale electricity generation (<100MWe) in the U.K. is exempt from

having to sell to the national grid under Electricity Regulations 2001 and can distribute electricity directly to its customers using a private grid, making the system more cost effective. This also means that green electricity can compete directly with brown electricity. This is the case in Woking where the Borough Council has set up the first commercial fuel cell CHP system in the U.K. [Ref. 2] Electricity supplies of less than 2MWe are also exempt from the Climate Control Levy.

In hard to reach areas where there is little in the way of a conventional fuel infrastructure (natural gas). There is a need for an efficient method of converting available fuels such as bottled LPG into hydrogen. [Ref. 3] The simplest method available to do this is through the steam reforming process. The steam reforming reaction can be expressed as follows:



The composition of the reformat for a given steam to carbon ratio and feedstock is dependant on the reformer temperature. As such, accurate temperature control is required when steam reforming is used. Because steam reforming is an endothermic process, additional heat is supplied to the reformer by means of a combustor. This supports the reaction and allows the temperature of the reformer to be controlled. The addition of a combustor means that any H_2 not used in the fuel cell can be recycled and burnt in the combustor, thus improving the system efficiency. Because of their nature this is not possible when using partial oxidation (exothermic) or auto-thermal reaction (thermally neutral) reformers.

Unfortunately sulphur is used as an odorant in most hydrocarbon fuels for reasons of safety. Sulphur levels in the ppb range will irreversibly damage the platinum catalyst of a fuel cells anode. Additionally, sulphur is a poison for most common nickel based reforming catalysts. For this reason in conventional systems, the sulphur needs to be removed from the fuel stream before it reaches the reformer catalyst and fuel cell. Some methods of desulphurisation are HydroDesulphurisation (HDS) with zinc oxide beds, or absorption techniques utilising activated carbon [Ref. 4]

However, our previous research has shown that a sulphur tolerant reforming catalyst used for the steam reforming of LPG is viable for low LPG flow-rates.

The sulphur in the fuel is converted to H_2S by reacting over the sulphur tolerant catalyst. This process converts any organic sulphur containing compounds into hydrogen.

This paper details the testing of a dual catalyst microchannel steam reformer shown in Figure 1. The reformer utilises a sulphur tolerant catalyst as well as a more conventional steam reforming catalyst. The reformer will be tested firstly with C_3H_8 and CH_4 before moving on to commercial grade LPG. This is to determine the performance of the reformer firstly, where no sulphur is present and secondly, where sulphur is present. Additionally the use of two catalysts demonstrates the flexibility of the reformers multi-zone combustor.

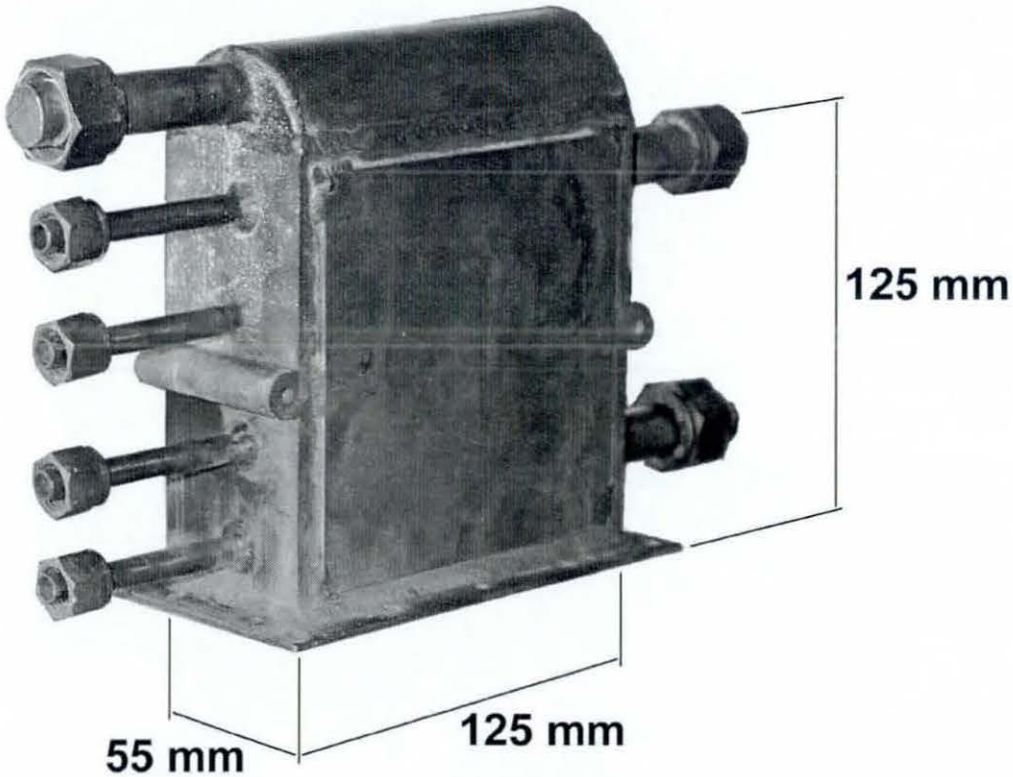


Figure 1: The microchannel reformer.

1.1. Test Rig

The steam reformer is of microchannel construction and can be visualised as consisting of five main layers. A central combustor layer, two temperature

measurement layers and two reforming layers. The combustor layer is itself split into two layers, one for fuel and one for air. These layers are connected via a diffusion layer. The temperature sensing layers are then arranged one on either side of the combustor. The reforming layers are then placed on the side of the temperature sensing layers. This arrangement promotes the efficient transfer of heat from the combustor to the reforming layers. The combustor is divided into 4 zones each with an individual fuel feed and a common air feed as shown in Figure 2

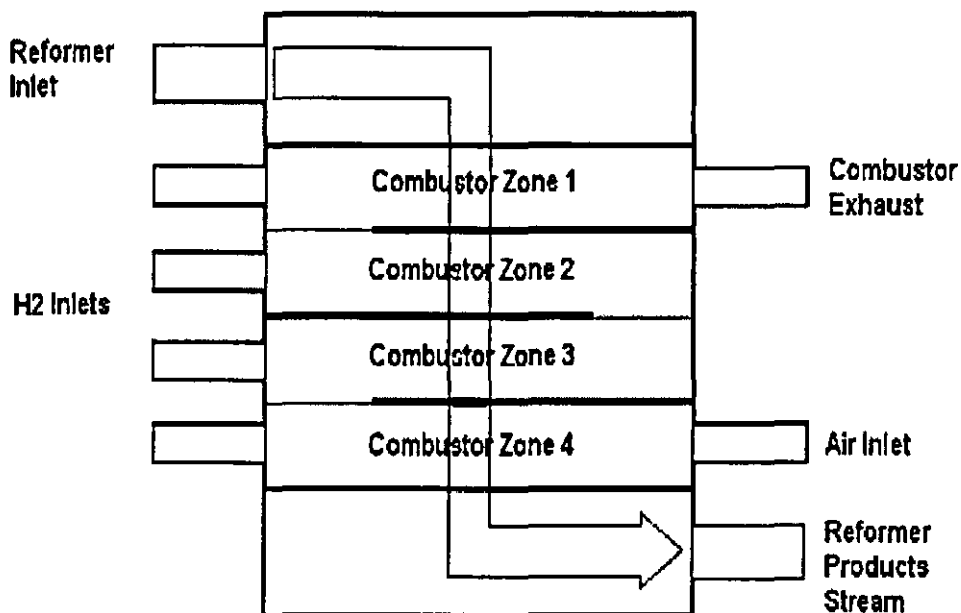


Figure 2: Reformer Internal Layout

Each fuel feed can be controlled individually and the air feed is controlled accordingly. This arrangement means that the temperature along the length of the reforming layers can be accurately controlled. The reforming layers have a total active area of 1.35 m^2 in a volume of 175 cm^3 . The total volume of the reformer is 859 cm^3 (0.86 litres)

The test rig is shown in Figure 3. There is a 500W pre-heater for the combustor air supply and a 750W pre-heater for the LPG and de-ionised H_2O supply. There are three pipes inside the pre-heater for the LPG/ H_2O , one for the LPG and the other two for the H_2O . The reactants are mixed immediately after the pre-heater and before entering the reformer. The H_2 to each zone of the combustor and the overall air supply

to the combustor are controlled using closed loop control in order that the reformer temperature can be set to the desired operating point. The combustor H_2 /air mixture is controlled so as to mimic the proportion of H_2 and O_2 from typical fuel cell off gases. The excess H_2O is condensed out of the reformat and the remaining gases are passed through online CO and CO_2 analysers before being passed through a gas chromatograph. The de-ionised water is supplied using a diaphragm pump. The flow of LPG is manually controlled via a mass flow controller.

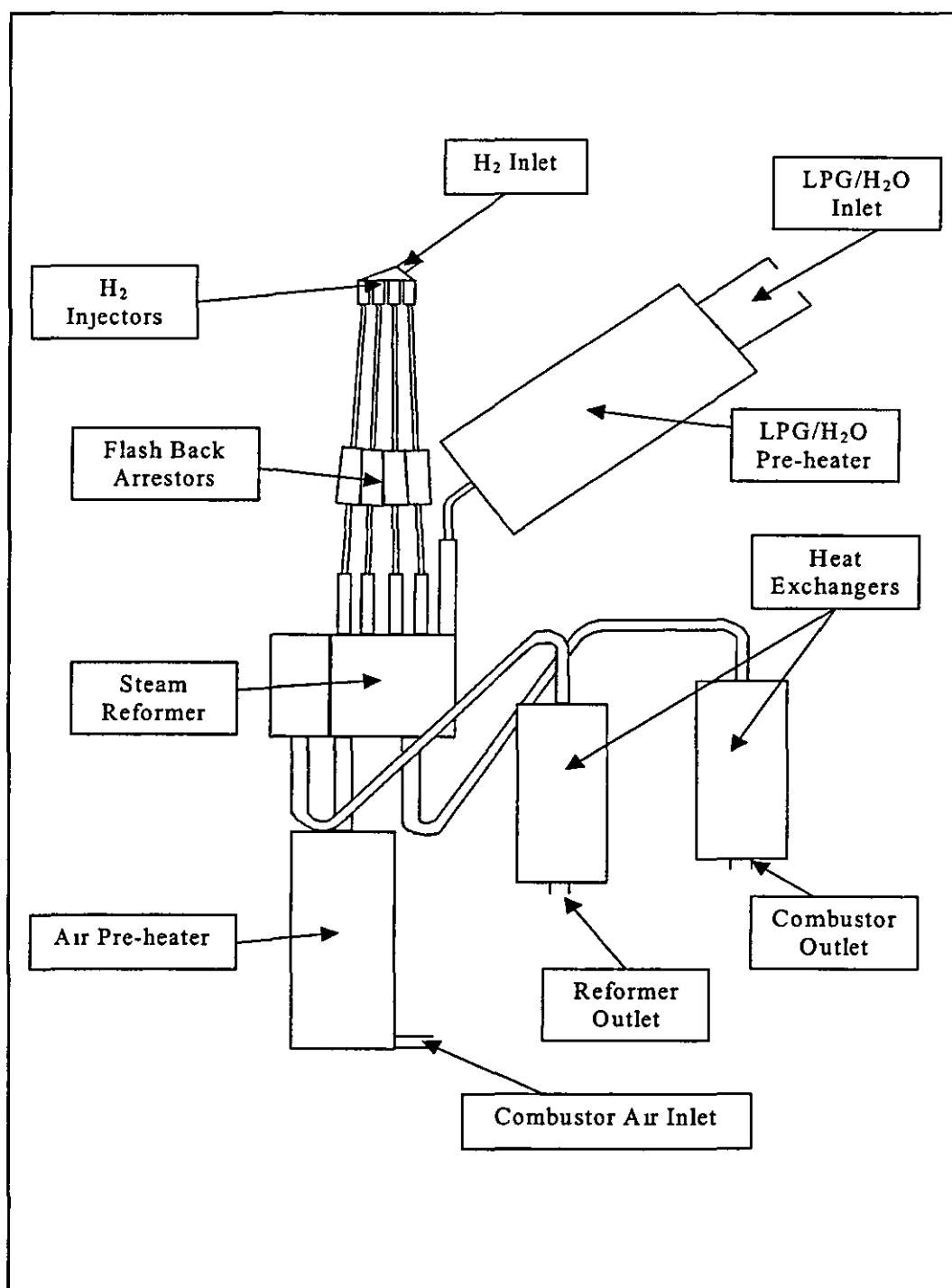


Figure 3: The test rig.

1.2. Catalyst

In our previous work a microchannel reactor was evaluated for LPG steam reforming utilising a novel sulphur tolerant catalyst. The results showed that the sulphur tolerant catalyst on its own was not sufficiently active for a reactor of that size. In this study a

second reforming catalyst was wash-coated over the top of the original catalyst over the second half of the reactor. This can be seen in figure 4. The second catalyst is a standard nickel based reforming catalyst. The multi-zoned combustor allows each catalyst zone to be operated at the temperature best suited to that catalyst. The sulphur tolerant catalyst is limited to 873 K before degradation takes place. The nickel-based catalyst can withstand temperatures of up to 1073 K before the same happens.

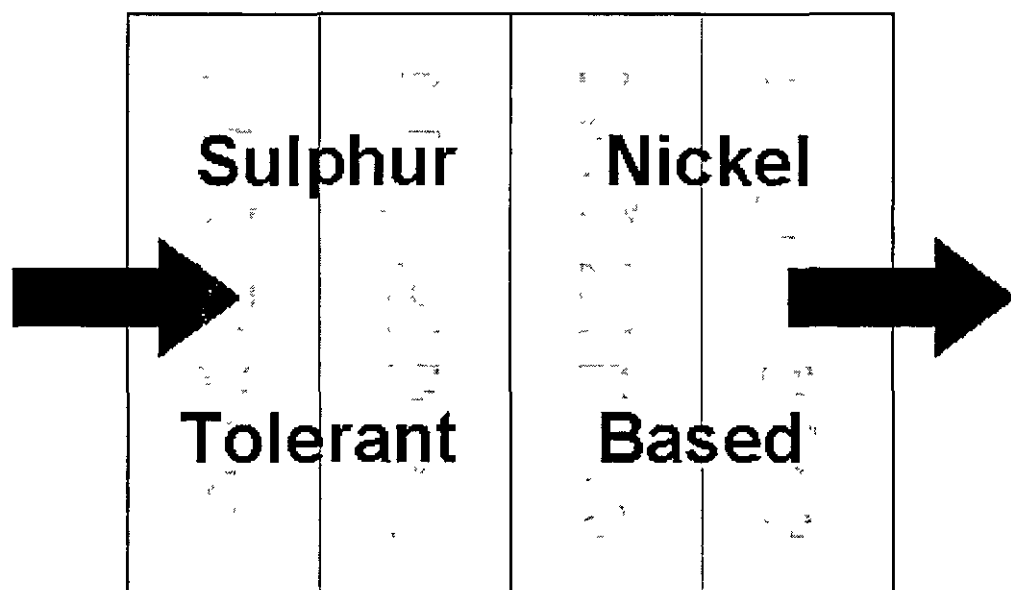


Figure 4: Steam reformer catalyst distribution.

The multi-zoned combustor design allows the temperature of the two catalysts to be operated at different temperatures to each other. This means that the sulphur tolerant catalyst can be operated safely at 873 K whilst the nickel based catalyst can be operated at a different temperature as required. In this way the temperature profile of the reformer can be tailored to suit the optimal operating conditions of the two catalysts.

2. Methodology

During the study, the reformer was tested over a range of temperatures, steam to carbon ratios, and reactant flow rates. The tests were performed with 3 fuels: C_3H_8 , CH_4 and LPG.

The tests performed using C_3H_8 were as follows:

- The temperature in zone 1 was set to 873 K whilst zone 4 was set to the set-points of 873 K, 923 K, 973 K and 1023 K. For each temperature set-point the steam to carbon ratio was set to 2.5, 3, 3.5 and 4.
- The flow rate of C_3H_8 was set at 0.75 SLPM as this corresponds to approximately 0.5 kWe (based on equilibrium data) from a fuel cell which given total conversion of the C_3H_8 .
- The set-point with the best performance was then chosen and the C_3H_8 flow rate was varied from 0.25 to 2.5 SLPM whilst the temperature and S/C ratio were kept constant.

The catalytic combustor lights off at room temperature so no additional heat was required to initiate warm-up. The reformer was then heated to 673 K with only N_2 passing through the reforming side of the reactor. Both of the pre-heats were switched on throughout. This was to make sure that the inlet temperature was sufficiently high and that the H_2O would vaporise on introduction. The reformer was then kept at a constant temperature of 673 K whilst the H_2O was introduced. The amount of H_2O was determined by the steam to carbon (S/C) ratio needed for the test set-point and a flow rate of 0.75 SLPM of C_3H_8 . The reformer was kept at these running conditions for about ten minutes whilst the temperatures stabilised. C_3H_8 was introduced at a S/C ratio of 8 and the temperature of the reformer was then increased to the desired set point. Once the desired temperature had been reached the C_3H_8 flow rate was increased gradually until the desired S/C ratio was reached.

The reformat minus the water, was passed through two on-line analysers one for CO detection and the second for CO_2 detection. The stream was then passed through a gas

chromatograph in order that H₂ and CH₄ content could be determined. The results generated were the percentage composition of the dry reformat. This was repeated for each of the fuels used in the tests.

For the purpose of the results, space velocity is defined as the volume of gaseous reformat per hour per volume of catalyst, which is widely regarded as GHSV. However, this figure is not based on the volume of the catalyst but on the volume of the reformer itself. This is because the catalyst is wash-coated on to the reforming surface, the volume of the catalyst will be much lower than that of the reformer. This would increase the GHSV figure in real term

The energy conversion efficiency of the reformer can be defined as the ratio between the energy contained by the reformat products and the energy contained by the reactants,

$$\eta = \frac{\text{LHV of products}}{\text{LHV of reactants}} \quad (1)$$

The products are the hydrogen and the carbon monoxide produced. The carbon monoxide is included because after water gas shift reaction, most of the CO has been converted into hydrogen. The reactants are the LPG to the reformer and the hydrogen to the combustor. It has been assumed that any unconverted LPG and any hydrogen in the fuel cell off gas, which is approximately 1/3 of the H₂ to the stack, are burnt in the combustor.

The energy used by the pre-heaters is not included in the calculation as this energy would be provided by heat exchangers in a complete fuel processor.

3. Experimental Results

3.1 Evaluation of the Reformer using Propane as a Feedstock

As expected running zone 4 of the reformer at higher temperatures increased the H₂ yield. It also decreased the CO₂% and CH₄% whilst the CO% increased. This can be

seen in Figure 5. As the conversion of the propane remains almost constant through out, the additional H_2 produced is derived from the methane content in the reformat. The CH_4 content decreases as the H_2 content of the reformat increases.

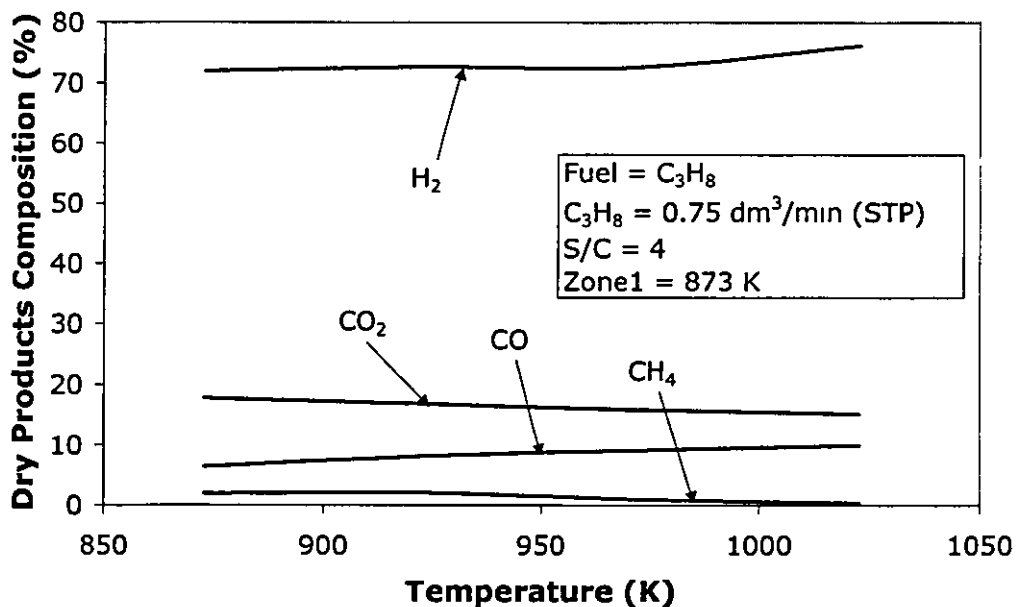


Figure 5: The effect of zone 4 temperature on reformer performance.

As expected increasing the steam to carbon ratio increased the H_2 and CO_2 yield whilst decreasing the CO and CH_4 yield. This is shown in Figure 6. The increase of CO_2 against CO is indicative of some shift reaction activity due to the properties of the addition of the nickel-based catalyst. Some of the CO is combined with H_2O to form CO_2 and H_2 . The maximum S/C ratio tested was 4. This is because it is more efficient to use a specialised water gas shift reactor to liberate H_2 from the excess water and reduce CO levels in the reformat than simply keep increasing the steam to carbon ratio for the reformer. This is due to the fact that the water shift reaction is exothermic and as such is promoted at lower temperatures than those which promote the endothermic steam reforming reaction.

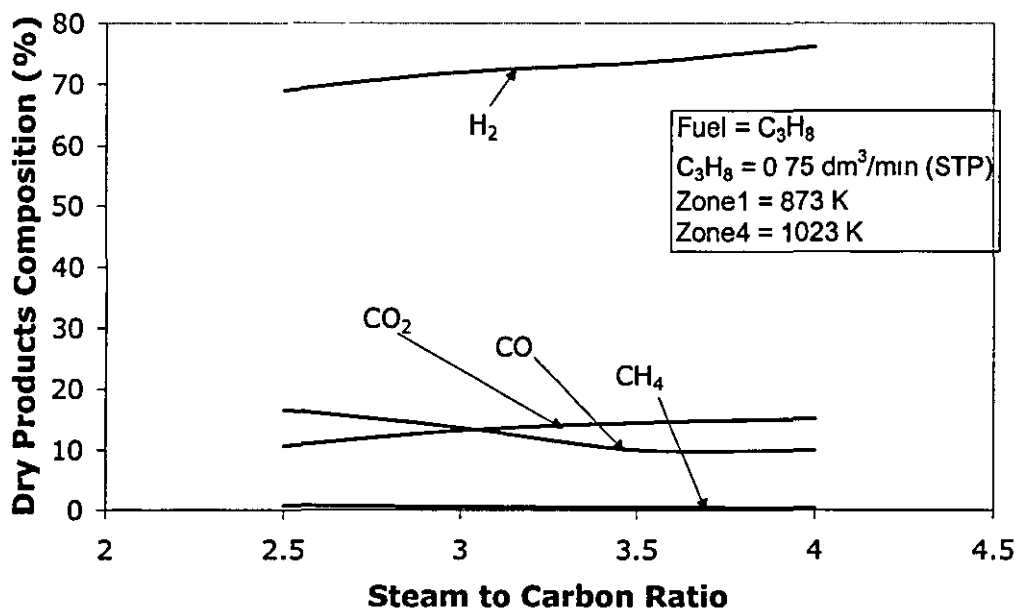


Figure 6: The effect of steam to carbon ratio on the reformer performance.

Figure 7 shows the effect of increasing the flow rate of the C_3H_8 on the reformer performance. Under the test conditions observed the $H_2\%$ output did not decrease even at the higher flow rates tested. This shows that the addition of the nickel based catalyst has had a positive effect on the reformers performance. This was expected due to the higher activity of the new catalyst compared to the sulphur tolerant one. The maximum flow rate used was determined by the peripheral equipment such as the power rating of the reformer inlet electric pre-heat rather than the reformer itself. If the flow rate into the electric pre-heat was too high the pre heat was unable to vaporise the H_2O before it entered the reformer. This lowered the efficiency of the reformer and lowered the temperature of zone 1 below that which the temperature controller could compensate for.

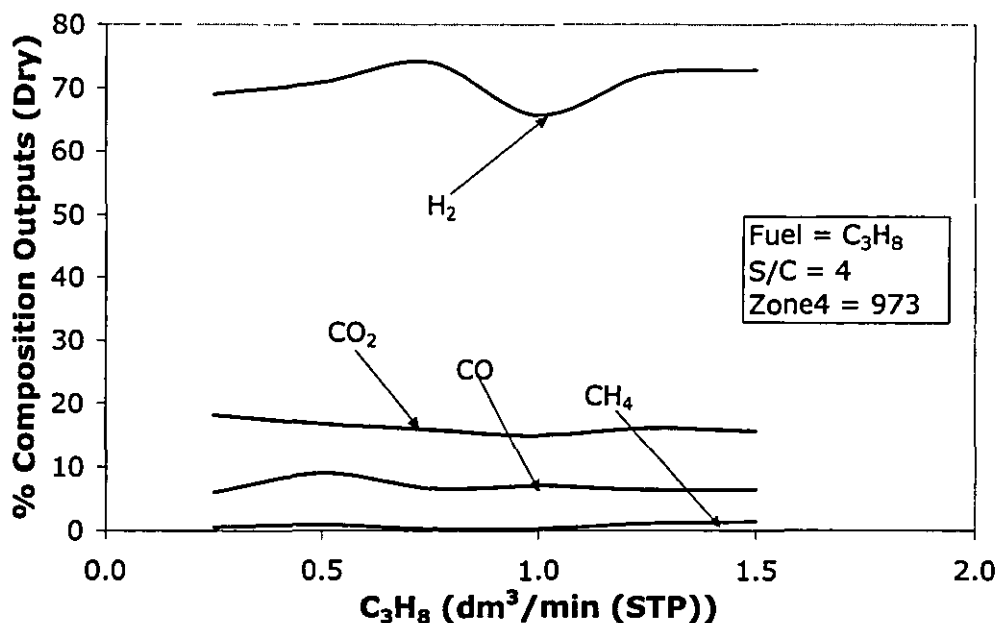


Figure 7: The effect of C₃H₈ flow-rate on the reformer performance.

The average efficiency of the reformer over varied feed flow rates (disregarding the two end points on the chart) is approximately 70% (Figure 8). 0.25 SLPM is a very low LPG flow rate in comparison with the reformer design. At such low rates, the reformer is too big to operate efficiently. At high flow rates the pre heater for the fuel/water mixture was not powerful enough to vaporise the water before it entered the reformer. This meant that the temperature controller would inject extra H₂ into the zone 1 combustor to compensate. This increase in H₂ consumption lowered the reformer efficiency. Because of this it would be possible to improve the reformer efficiency at the higher flow rates by better system integration.

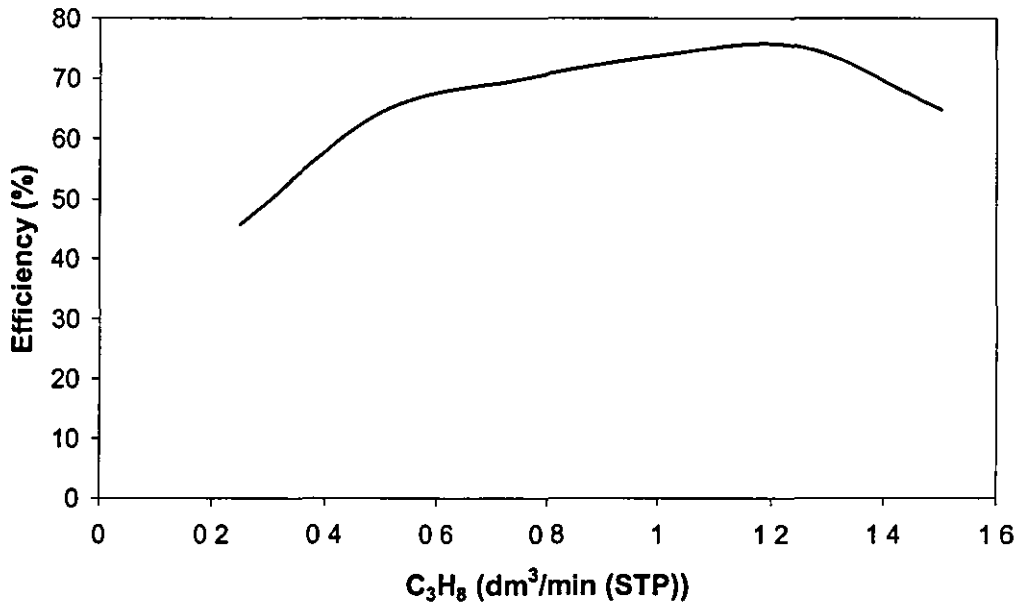


Figure 8: The effect of C₃H₈ flow rate on reformer efficiency.

The maximum power output achieved before the test was stopped due to lack of preheat was 1.98 kWe at LPG = 2.5 SLPM and S/C = 4, Zone 4 temperature 873 K. This can be seen in Figure 9. This value could be improved by increasing the zone 4 temperature and by integrating the system more effectively. It can be seen that there is no drop off in H₂ % volume even at the highest flow rate. Provided that the system integration was improved the power output of the reformer could be above 2 kWe. The gas hourly space velocity at a feed rate of 2.5 SLPM and steam to carbon ratio of 4 was calculated to be 13800 GHSV based on the exit flow.

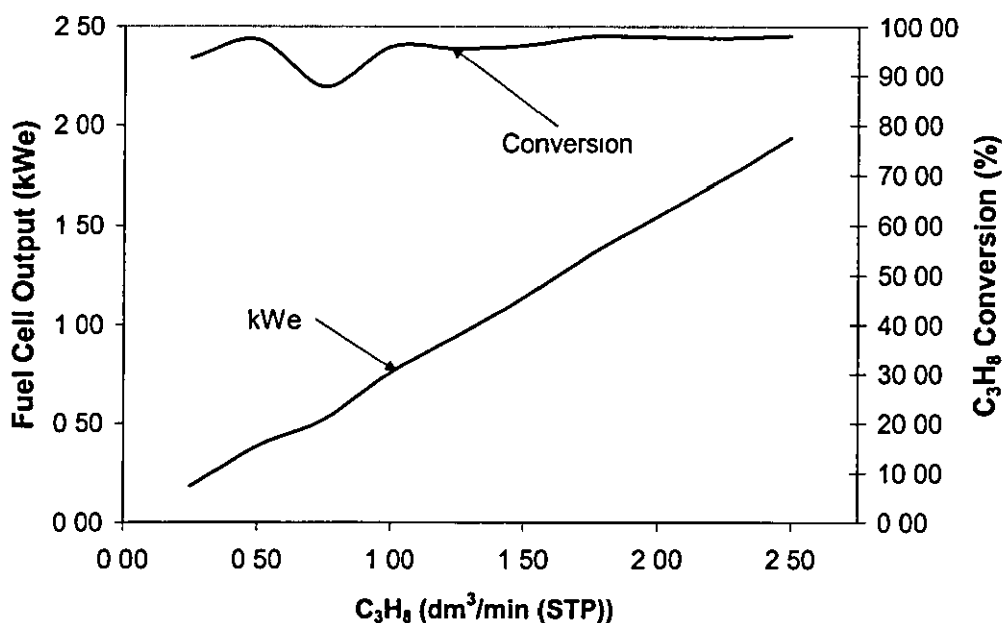


Figure 9: The effect of C_3H_8 flow rate on fuel cell power output.

The maximum flow-rates in the tests were imposed by the pre-heater for the reformer reactants. The tests using C_3H_8 where the flow-rate was increased to 2.5 SLPM were not repeated using LPG or CH_4 to protect the reformer from damage. It was observed that the temperature controller was unable to supply enough heat to the first zone in order to vaporise the incoming water. This was because the flow rate of H_2 requested was so high that the majority of the H_2 passed through the combustor before combusting and in fact burnt in the combustor exhaust. This raised the temperature of the exhaust beyond that which was thought safe. Therefore during the subsequent tests the maximum feedstock flow-rate was limited.

3.2. Evaluation of the Reformer using Methane as a Feedstock

The tests performed with CH_4 were as follows:

- The temperature in zone 1 was set to 873 K whilst zone 4 was set to the set-points of 873 K, 923 K and 973 K. For each temperature set-point the steam to carbon ratio was set to 2.5, 3, 3.5 and 4

- The flow rate of CH₄ was set at 1.88 SLPM as this corresponds to approximately 0.5 kWe (based on equilibrium data) from a fuel cell given total conversion of the CH₄
- The set-point with the best performance was then chosen and the CH₄ flow rate was varied from 0.6 to 2.5 SLPM whilst the temperature and S/C ratio were kept constant.

It can immediately be seen that the performance of the reformer is not as good when CH₄ is used as a feed stock rather than C₃H₈. This is because methane is more endothermic per carbon atom than C₃H₈ [Ref. 3].

It can be seen that the flow rate of the reformer feed stock greatly affects the performance of the reformer (Figure 10). This is due to the shorter residence time of the CH₄ due to the increased flow-rate. This performance drop is also noticeable when the S/C ratio is increased from 2.5 to 4 (Figure 13).

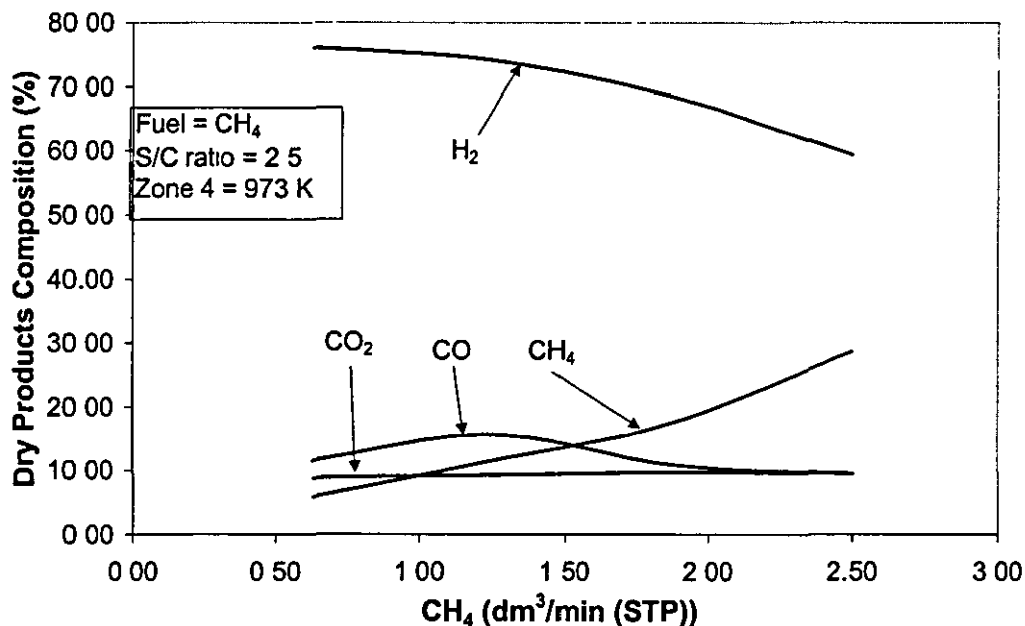


Figure 10: The effect of CH₄ flow rate on the reformer performance.

As expected increasing the temperature of the back end of the reformer increased the H₂% yield whilst also increasing the CO%. The CO₂ and CH₄% decreased. This can be seen in Figure 11. This is due to the increase in energy supplied to the reformer at the higher temperatures.

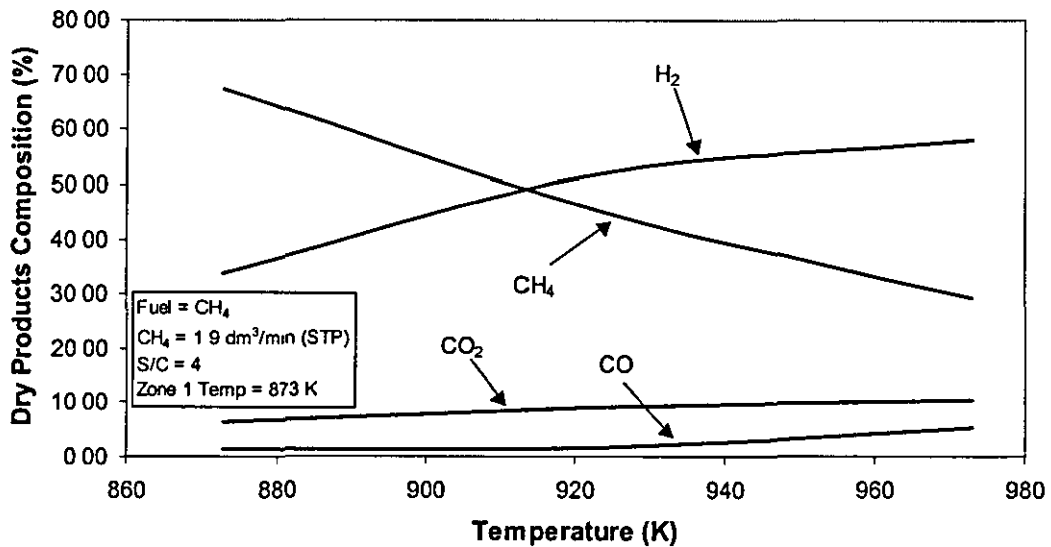


Figure 11: The effect of zone 4 temperature on reformer performance.

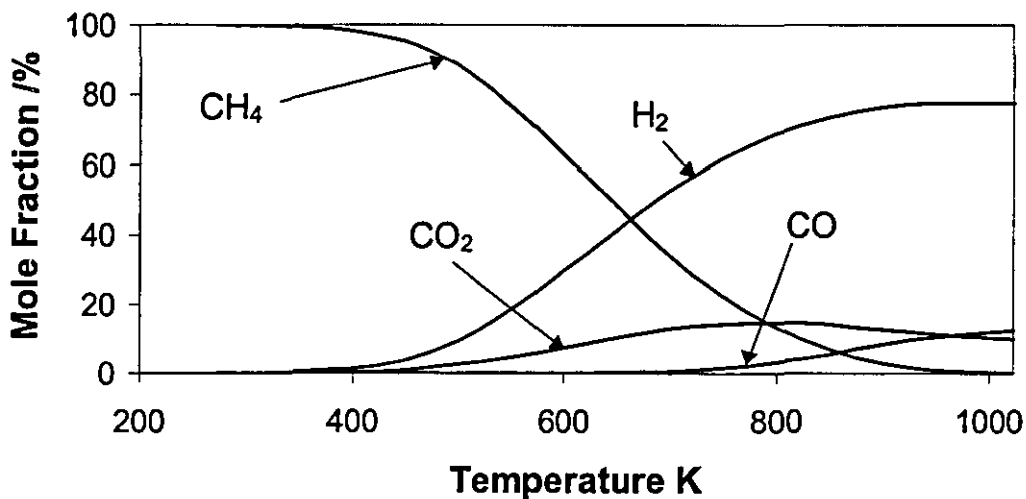


Figure 12: The modelled dry products of methane reforming at equilibrium w.r.t. reformer temperature.

It can be seen that the performance of the reformer whilst using methane is less than that predicted by equilibrium modelling (Figure 12). This is due to incomplete conversion of the methane in the reformer, which indicates that the catalyst activity for the steam reforming of methane is not sufficient for reforming at this scale.

Increasing the S/C ratio caused a drop in CH_4 conversion (Figure 13). This was due to the increase in flow rate through the reformer. As has been seen the reformer

performance is particularly sensitive to changes in CH_4 flow rate but not to changes in the C_3H_8 flow rate. This is due to the reaction kinetics of CH_4 when compared to those of C_3H_8 . However as predicted by equilibrium modelling (Figure 14) the $\text{CO}\%$ decreased whilst the $\text{CO}_2\%$ increased.

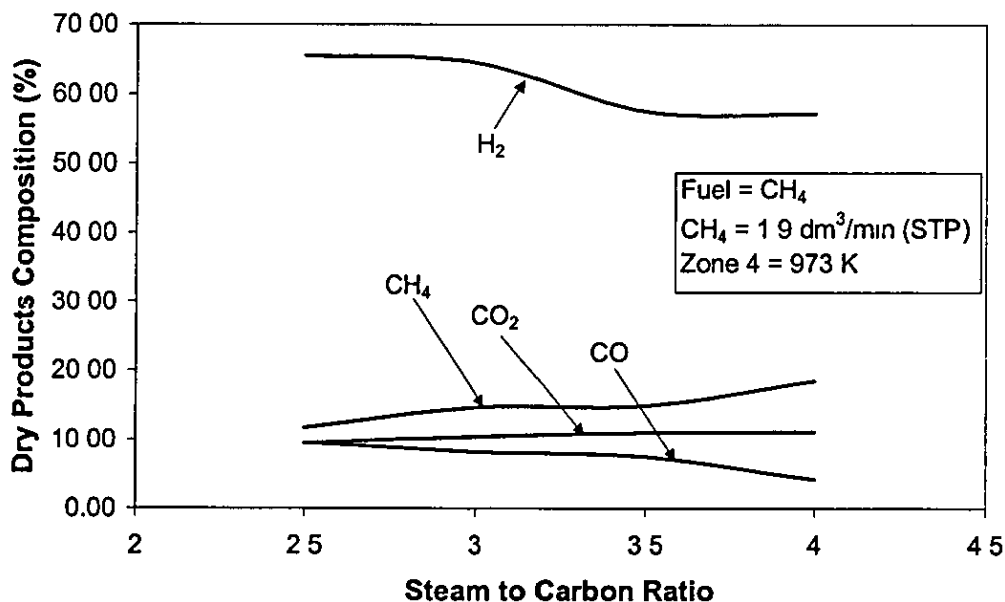


Figure 13: The effect of steam to carbon ratio on reformer performance.

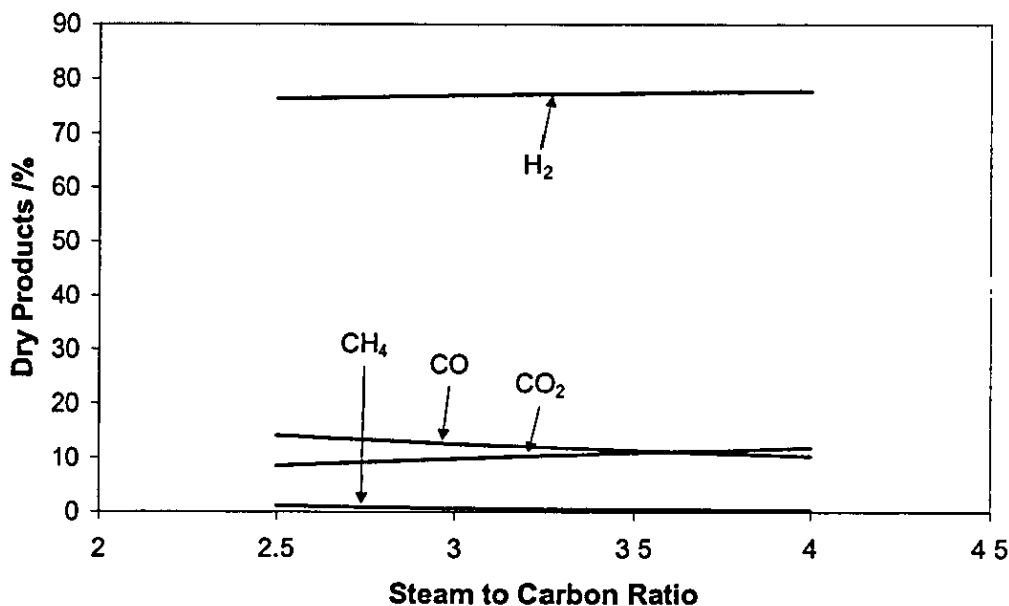


Figure 14: The modelled dry products of methane reforming at equilibrium w.r.t. S/C ratio.

The average efficiency of the reformer over varied feed rates was approximately 60% as shown in Figure 15. It can be seen that unlike the efficiency curves for C_3H_8 and LPG the curve for CH_4 does not drop off at higher flow rates. This is because of the reduced water content (compared to that when using C_3H_8 or LPG) of the flow entering firstly the pre heater and secondly the reformer. The majority of the energy used to heat the feedstock is for the vaporisation of water. This means that despite the decreasing performance of the reformer the efficiency increased. As the conversion drops off so too does the amount of heat required to support the reaction. This combined with the increase in H_2 production due to the higher flow-rates means that the reformer efficiency increases

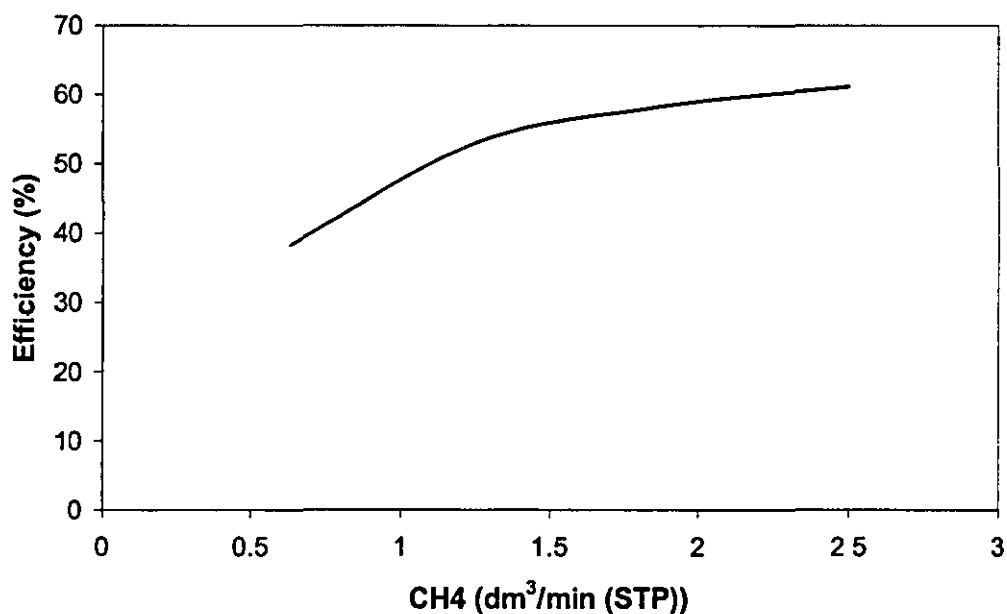


Figure 15: The effect of CH_4 flow rate on reformer efficiency.

It can be seen that despite a loss of conversion at higher flow-rates the H_2 output increases and the predicted power output of a fuel cell improves accordingly (Figure 16). It can be seen that for the same flow rate the power output is lower than that when using C_3H_8 . When an equivalent flow rate is used the performance is still lower than that for C_3H_8 and LPG but the gap is not as large. The gas hourly space velocity at an CH_4 flow rate of 2.5 SLPM and S/C ratio of 4 is 4151 GSHV based on the exit flow.

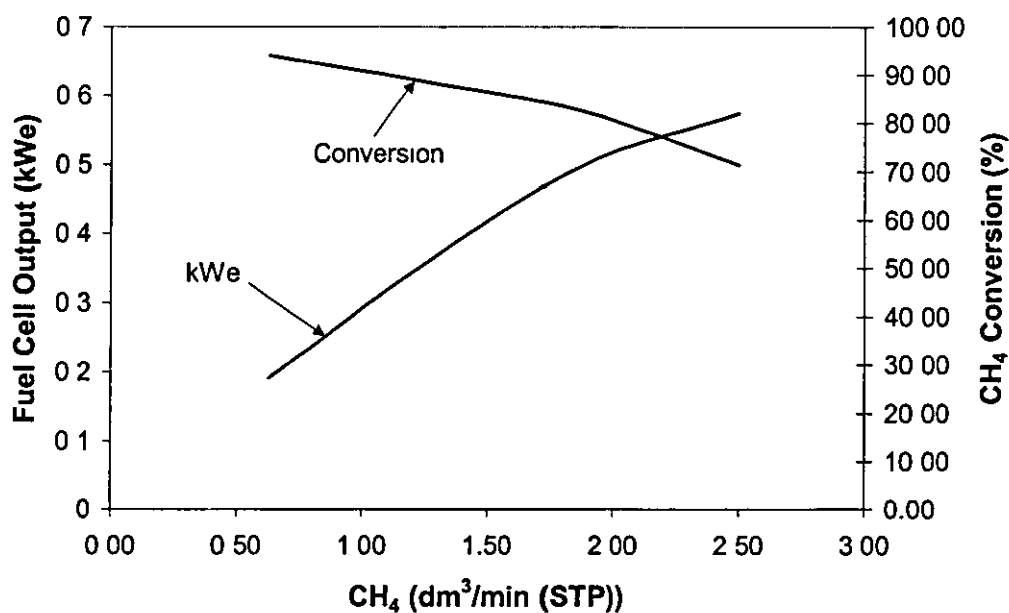


Figure 16: The effect of CH₄ flow rate on fuel cell power output.

3.3 Evaluation of the Reformer using Liquid Petroleum Gas as a Feedstock

For these tests a commercial grade LPG supplied by Calor Gas was used as the reactant. This fuel contains sulphur as an odorant and was chosen to compare the performance with that when using C₃H₈.

The test procedures were as follows

- The temperature in zone 1 was set to 873 K whilst zone 4 was set to the set-points of 873 K, 923 K, and 973 K. For each temperature set-point the steam to carbon ratio was set to 2.5, 3, 3.5 and 4.
- The flow rate of LPG was set at 0.75SLPM as this corresponds to approximately 0.5kWe (based on equilibrium data) from a fuel cell which given total conversion of the LPG.
- The set-point with the best performance was then chosen and the LPG flow rate was varied from 0.25 to 1.25 SLPM whilst the temperature and S/C ratio were kept constant.

It can be seen in Figure 17 that the flow rate of the feedstock does have some effect on the reformer performance. It is possible that the difference between the performance here and when using C_3H_8 is the sulphur in the LPG or just the age of the catalyst. It can be seen that at higher flow rates the conversion of LPG is still above 95% so the effect on the reformer performance is not large.

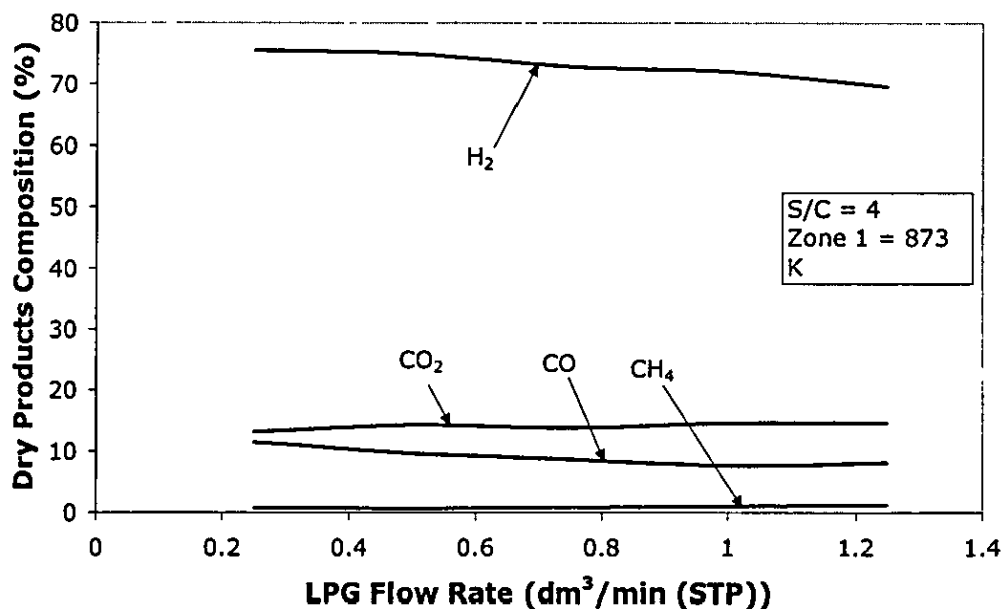


Figure 17: The effect of LPG flow rate on reformer performance.

As seen in Figure 18, increasing the zone 4 temperature increased the H₂ yield. It also increased the CO₂ yield whilst the CO yield decreased. This is the opposite behaviour than predicted by equilibrium modelling (Figure 19) and suggests that the extra H₂ is produced via the water shift reaction. This is at odds with the results gained from equilibrium modelling and those when C₃H₈ was used as a feedstock.

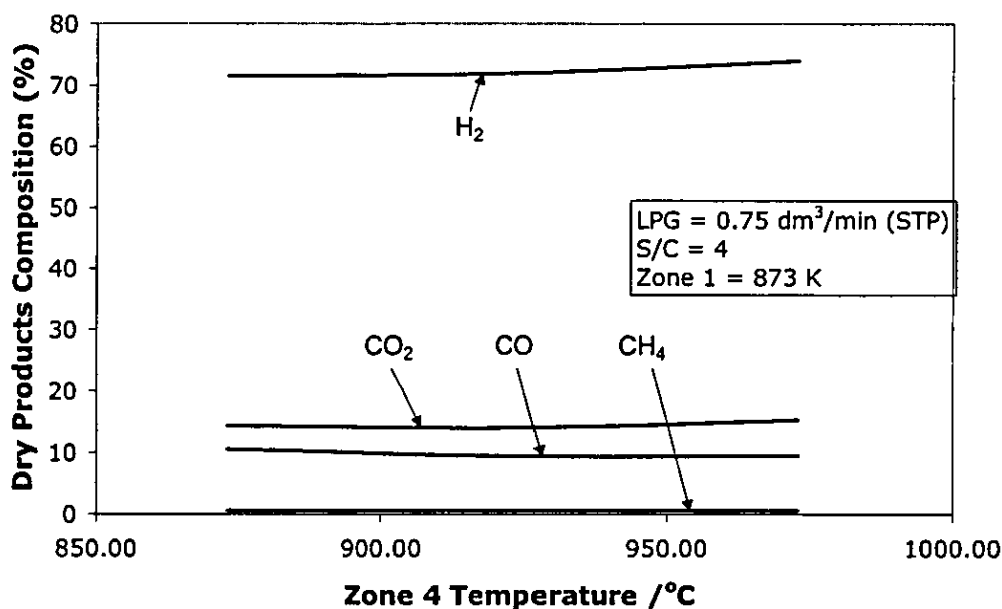


Figure 18: The effect of zone 4 temperature on reformer performance

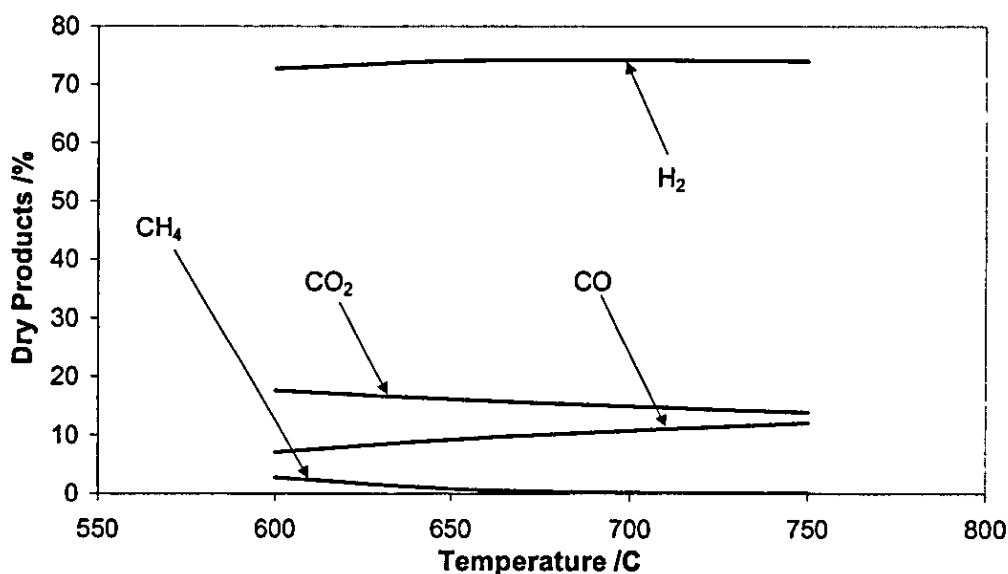


Figure 19: The modelled dry products of LPG reforming at equilibrium w.r.t. reformer temperature.

As can be seen in Figure 20, increasing the S/C ratio increased the H₂ yield. It also increased the CO₂ yield whilst the CO yield decreased. This is due to increased water shift activity caused by the excess water. These results show agreement with the results predicted by equilibrium modelling shown in Figure 21. This shows that the reformer is operating at or near equilibrium conditions demonstrating the effectiveness of the dual catalyst reformer at the steam reforming of LPG.

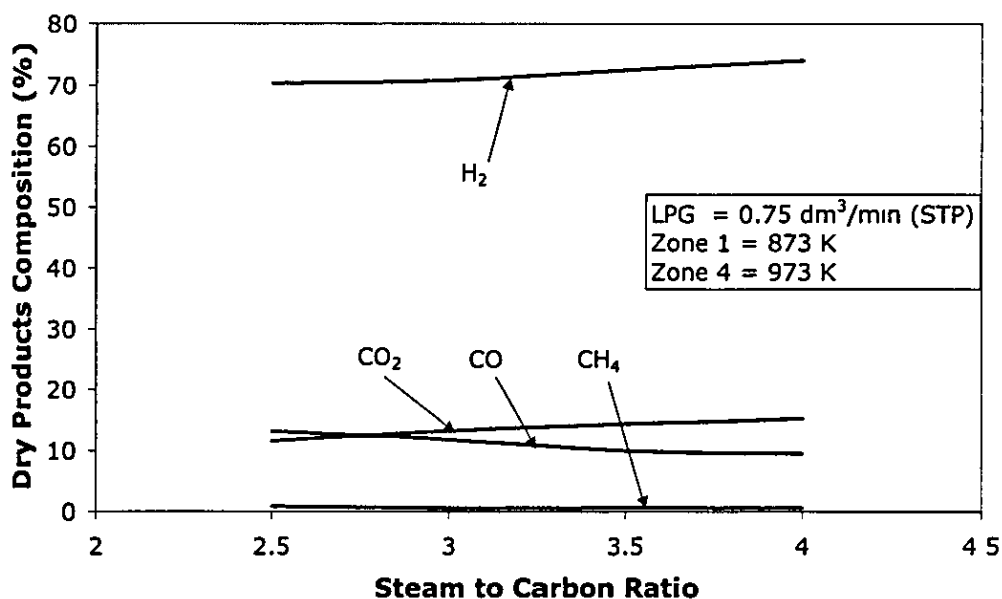


Figure 20: The effect of steam to carbon ratio on reformer performance.

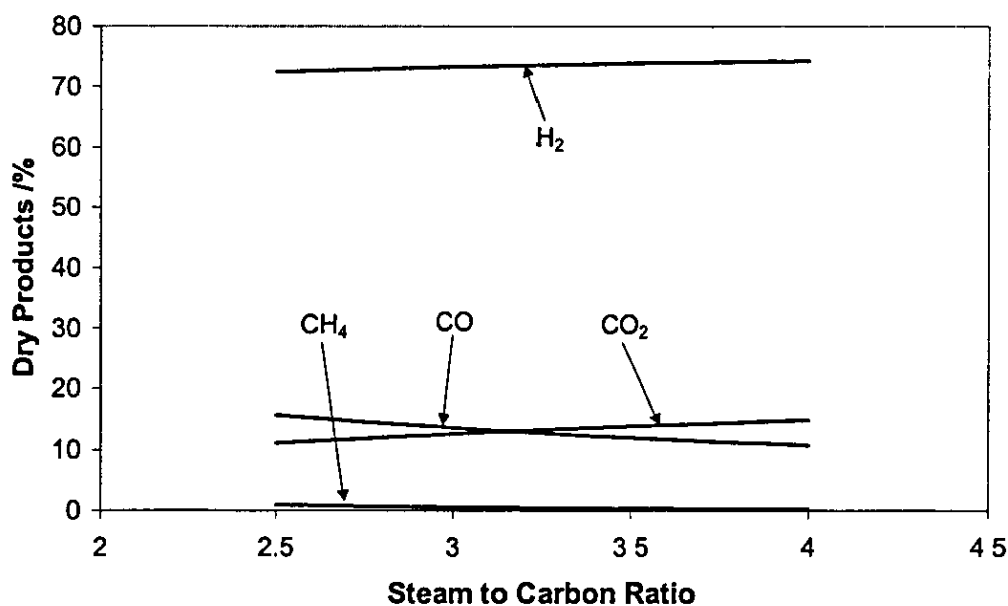


Figure 21: The modelled dry products of LPG reforming at equilibrium w.r.t. S/C ratio.

The average reformer efficiency over varied flow rates was 70% (Figure 22). This is the same as that for C_3H_8 and again shows that due to the sulphur tolerant catalyst in zones 1 and 2 that there is little or no performance loss when using a fuel containing sulphur. Again it can be seen that at low flow rates the reformer is oversized.

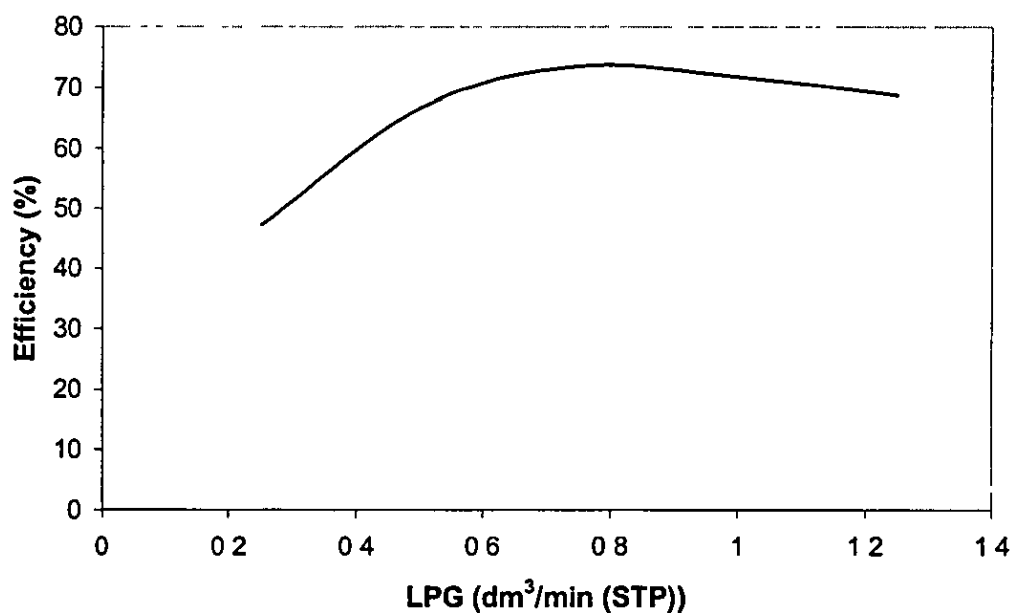


Figure 22: The effect of LPG flow rate on the reformer efficiency.

It can be seen that for the flow-rates tested the power output of the reformer whilst using LPG are very similar to those when the reformer was run using C_3H_8 (Figure 23). This suggests that there may be a synergetic effect when the nickel based catalyst is used on top of the sulphur tolerant catalyst. To confirm or disprove this further durability tests would need to be carried out using the dual catalyst arrangement to rule out poisoning of the nickel based catalyst due to extended sulphur exposure. Because of the slight drop off in reformer performance at the higher flow-rates when using LPG it can be assumed that the power output of the reformer using LPG will be close to that when using C_3H_8 . Further tests will be needed to confirm that that is the case. To do that the test rig will have to be adapted so that the higher flow rates can be used safely. The gas hourly space velocity at an LPG flow rate of 1.25 SLPM and S/C ratio of 4 is 8670 GSHV based on the exit flow.

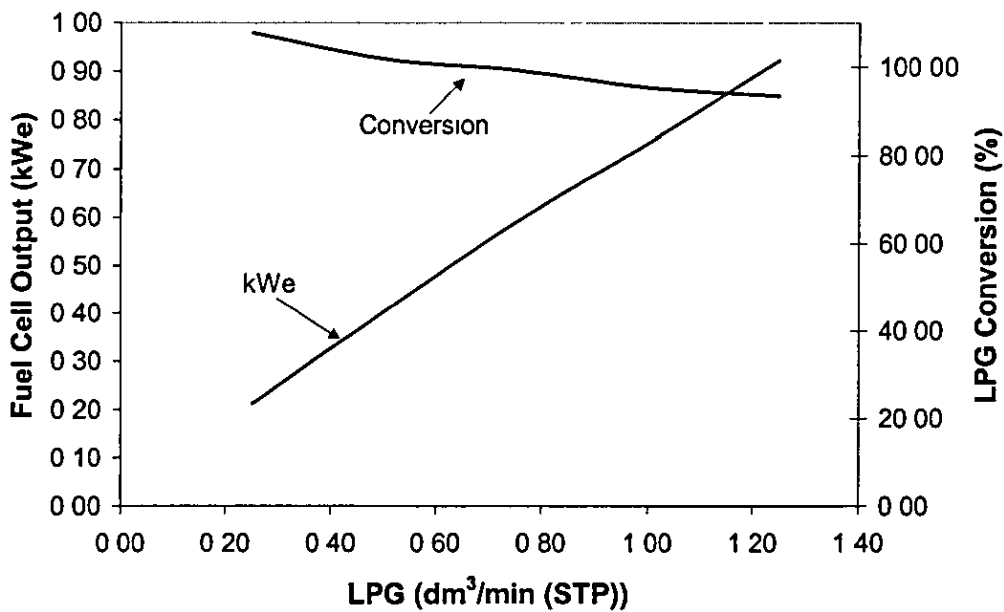


Figure 23: The effect of the LPG flow rate on the fuel cell power output.

	C_3H_8	LPG	CH_4
Operating conditions	Zone 4 973 K, s/c = 4, 0.75 SLPM	Zone 4 973 K, s/c = 4, 0.75 SLPM	Zone 4 973 K, s/c = 4, 1.88 SLPM
H_2 %	72.67	74.01	57.96
CO %	9.11	9.49	4.17
CO_2 %	15.81	15.24	11.09
CH_4 %	0.91	0.55	18.44
Conversion %	98.49	99.29	81.56
kWe	0.58	0.59	0.49
GHSV	6868	6864	4275
Efficiency %	69.81	73.50	58.27

Table 1: A comparison of reformer performance using different fuels.

It can be seen from the results summarised in table 1 that there is very little difference between the performance of the reformer when using C_3H_8 and that when using LPG. This suggests that the sulphur tolerant catalyst is effective at removing the sulphur from the LPG thus stopping or at the least slowing the degradation of the nickel catalyst. As has been noted the performance of the reformer when using CH_4 is lower than that when using the other fuels. This can be explained by the difference in kinetics of steam reforming CH_4 and steam reforming C_3H_8 /LPG.

4. Conclusions

A dual stage steam reformer was tested. The reformer utilised a multi-zone combustor. This enabled the two reforming catalysts to be operated at differing temperatures. The composition of the reformat is dependent on the reformer temperature. The multi-zoned combustor allows accurate control of the reformer temperature and therefore the reformat composition.

The microchannel technology used as the basis of the steam reformer proves itself a viable method of making a compact reformer. The performance of the reformer when using CH_4 is not as good as when using C_3H_8 /LPG. This is due to the reaction kinetics of the respective fuels. Using C_3H_8 as a fuel, at a flow rate of 2.5 SLPM and a steam to carbon ratio of 4, the maximum space velocity attained during the tests was found to be 13800 GHSV. The predicted fuel cell output under these conditions was 1.98kWe. This is a large improvement over more traditional packed bed steam reformers. It produced 1.98kWe from 2.5 SLPM of C_3H_8 in a volume of $0.86m^3$. The performance is very close to that expected at equilibrium, with conversion rates between 95 and 100%. The performance of the reformer when using LPG as a fuel is similar to that of the non-sulphur fuel (C_3H_8). Because of safety concerns the reformer wasn't tested at the high flow rates that were used with C_3H_8 , the results gained show that the presence of sulphur in the fuel had little effect on the performance of the reformer so far. It is anticipated that extended running of the reformer will show some degradation of the nickel catalyst due to the sulphur content of LPG. To further investigate the performance of the reformer using LPG it is necessary to improve the integration of the test rig with the reformer. This would enable higher flow rates of LPG to be tested safely to determine further effects of the sulphur content on the nickel based catalyst.

References:

- [1] Ton van der Does – Fuel cell co-generation: the future of co-generation – Journal of Power Sources 61 (1996) 49-51
- [2] A fuel Cells first – New Review, The Quarterly Newsletter for the UK New & Renewable Energy Industry - Issue 44 May 2000
- [3] Finn Joensen, Jens R. Rostrup-Nielson – Conversion of hydrocarbons and alcohols for fuel cells – Journal of Power Sources 105 (2002) 195-201
- [4] James Larminie, Andrew Dicks – Fuel Cell Systems Explained – John Wiley and Sons Ltd – 2002

